ELECTROFLUIDIZED BEDS IN THE CONTROL OF FLY ASH

by

JEFFREY C. ALEXANDER

B.S., Massachusetts Institute of Technology

(1974)

M.S., Massachusetts Institute of Technology

(1975)

SUBMITTED IN PARTIAL FULFILLMENT OF THE

REQUIREMENT FOR THE DEGREE OF

DOCTOR OF PHILOSOPHY

at the

MASSACHUSETTS INSTITUTE OF TECHNOLOGY

May, 1978

Signature of Author .....

Department of Electrical Engineering and
Computer Science, May, 1978

Certified by .....

Thesis Supervisor

Accepted by .....

Chairman, Departmental Committee on Graduate Students

ELECTROFLUIDIZED BEDS IN THE CONTROL OF FLY ASH

By

Jeffrey C. Alexander

Submitted to the Department of Electrical Engineering and Computer Science, May 26, 1978, in partial fulfillment of the requirements for the degree of Doctor of Philosophy

ABSTRACT

The application of electrofluidized beds to the control of fly ash is studied. The fundamental areas of investigation necessary for this are identified as the understanding of EFB collection of aerosols in the supermicron range and the adhesion of fly ash in fluidized beds. These topics are studied experimentally and theoretically. Two patent applications result.

The major developments of this thesis are:

1) A model for filtration of aerosols by inertial impaction in packed and fluidized granular bed filters is developed and experimentally verified. Filtration efficiency is shown to depend on a modified Stokes number $N_{STK}'=2a^2\rho_p U\beta/9\eta R\varepsilon_v$ where a,ρ_p,U,β,η,R, and ε_v are the aerosol radius, aerosol mass density, gas flow velocity, jetting factor, gas viscosity, granule radius, and bed porosity. The jetting factor is a number varying between 1 and 10 depending upon the flow Reynolds number. As such, it is a measure of increases in local gas flow velocity due to inertial effects of the gas. For Reynolds numbers less than about 150, β has a value of 1. It increases for Reynolds numbers greater than about 150. The single granule collection efficiency, C_{im}, is well modeled by the simple expression $C_{im}\simeq N_{STK}'$ over a wide range of parameter values.

2) It is identified that effective fly ash adhesion in fluidized beds can be achieved by the introduction of a liquid adhesive additive. Other adhesion mechanisms fail because of the large dislodging forces resulting from particle collisions in the bed. From theoretical and basic experimental studies, an adhesion parameter S is defined to be $S=U\rho_p a^{3/2}/\eta d^{1/2}$ where U,ρ_p,a,η, and d are the collision velocity, fly ash mass density, fly ash radius, additive viscosity, and additive thickness on the fly ash. A critical value $S_{crit}\simeq 1.4$ is identified. For $S<S_{crit}$, fly ash is adhered to a substrate while for $S>S_{crit}$ the fly ash is dislodged. These characteristics are observed for fly ash collected in fluidized beds with #6 fuel oil additive introduced as an aerosol.

3) Operation of the EFB as a fly ash collector and fly ash agglomerator is shown in laboratory demonstrations simulating actual conditions. Submicron removal efficiencies above 95% are typical.

Thesis Supervisor: James R. Melcher
Title: Professor of Electrical Engineering

ACKNOWLEDGMENTS

It was an honor to perform this research work under the guidance of Professor James R. Melcher. His scientific expertise, personal concern, and ethical conviction have all uniquely influenced my professional career and personal life. My appreciation will continue in the years to come.

Thanks are due to my thesis readers, Professors J. Beer, D. Staelin, and D. Leith, for their consideration and advice.

Dr. Karim Zahedi's fundamental work in EFB development provided motivation for this thesis. He personally introduced me to the basics of EFB theoretical and experimental work. His friendship and professional competence are appreciated in his role as colleague at MIT and , now, business partner.

Several people greatly influence research such as this. Peter Zieve's friendship and technical knowledge and skills have been especially helpful. Alan Presser assissted in several of the experiments. Paul Warren and Joe Cairns helped build much of the experimental apparatus. All receive my gratitude.

Also much appreciated was the practical guidance given by Tim Driscoll and Bob Burton, the project directors from Empire State Electric Energy Research Corporation (the sponsors of much of the research).

Leida, Terri, Toby, and Anita all deserve as much thanks as I can give for their help in the drawing and typing of this document under difficult circumstances.

Finally, I wish to dedicate this thesis to my family for their constant encouragement and understanding, and for providing me with a strong, happy, and healthy home to grow up in.

Table of Contents

Table of Contents (Continued) Page No.

Table of Contents (Continued) Page No.

LIST OF FIGURES

Page No.

Page No.

LIST OF TABLES

I. Introduction

This thesis concerns itself with the invention and characterization of the Electrofulidized Bed (EFB) particulate air pollution control technology as applied to the control of fly ash such as produced during coal combustion. It is one of a series of studies performed by the MIT Continuum Electromechanics Group on electrostatic particulate control technology which led to the development of the EFB. The point has now been reached where development with particular applications in mind is warranted and desired. As a result, this thesis, as with any practical technology development, deals with a wide range of at first seemingly unrelated disciplines. Where needed, detailed scientific investigations have been performed. Where satisfactory, in depth literature reviews are presented. Non-essential detailed studies have been replaced by appropriate engineering approximations in keeping with the spirit of invention and practical development.

This introductory chapter will be divided into four parts. First will be a discussion of motivation for the thesis, followed by a statement of the objectives of the study at its outset. The third part outlines in detail the major innovative and scientific original contributions of the thesis. Finally, a guide is given as to the organization of the remaining chapters.

A. Motivation for Thesis

The need for effective fly ash control is ever increasing in importance as a result of environmental, economic and even political factors. Because of increasing oil prices and political uncertainties in Mid-East oil producing countries, the present US Administration has placed an enormous emphasis on

coal utilization to reduce dependence on foreign oil and limited domestic gas and oil supplies. This shift in energy producing sources will have a severe detrimental effect on the environment unless adequate pollution control technologies are developed. It is expected that low sulfur Western coals will be used widely to reduce coal combustion sulfur emissions. Conventional electrostatic precipitators are ineffective, though, for the resulting high resistivity fly ash produced.

Coupled with more restrictive environmental laws coming into effect by the early 1980's, the need for new technology development is imperative. It is projected that by 1982, $2 billion annually will be spent for utility plant gas clean up.

As a result, several areas of fly ash development are under active research sponsored by EPA, ERDA, DOE, and private industry. These include the use of fabric filtration, hot-side ESP's, flue gas conditioning, high intensity ionizers, novel devices, reduced rapping reentrainment, electrostatic agglomeration, and high temperature high pressure gas cleanup. Most of this research is centered on the effective control of submicron particulate, that is, particulate with .1 to 1 μm diameters. The concern is well founded since:

1. Submicron particulate is the most difficult to collect by any known collection scheme.
2. Submicron particulate is readily carried long distances in the atmosphere with very little settling.
3. Submicron particulate can carry abnormally large amount of absorbed toxic materials.
4. Submicron particulate are the preferred size for deposition and retention in the human lung.

The Electrofluidized Bed has been identified as a technology which performs with ultra-high submicron collection particulate efficiencies at low capital, operating and maintenance costs. Its development for effective fly ash control would be a major contribution to the national coal utilization effort.

B. Objectives

The principle objective of the thesis is to develope the EFB technology for fly ash control. Thes state of the technology at the outset of this investigation is detailed more in Chapter II -- Background. In short, at that time, the EFB was a proven approach to the control of submicron particles at relatively low loadings and in which the adhesion between pollutant and bed particles was assured (the pollutants were liquid droplets). Fly ash has major components in both the submicron and supermicron ranges and loadings far exceeding those previously tested with the EFB. Further, fly ash is a dry, solid particulate making the adhesion issue of primary importance.

The more detailed objectives of this thesis can be summarized by the following questions.

1. What are the collection properties of an EFB for supermicron particulate and how can the polydispersity of fly ash sizes be most effectively handled?
2. How can stable adhesion between the dry fly ash and the bed particles in the highly agitated EFB be maintained?
3. How can the dynamics of fly ash collection, adhesion, and bed mixing be modeled and optimized?
4. What are the optimum EFB configurations for integration into a large scale coal burning utility plants?

These questions are answered in the thesis.

C. Thesis Accomplishments

The original contributions of this thesis can be closely correlated with the four questions outlined in the previous section and one chapter of the thesis is devoted to each. Each is briefly described in the following subsections.

1. Aerosol Collection Theory in EFB's

The literature was thoroughly reviewed for aerosol collection in packed and fluidized beds. Several different collection mechanisms are identified and studied. The literature satisfactorily treated all the mechanisms except one, inertial impaction. As part of this thesis, a detailed experimental investigation was performed. With the aid of a theoretical development, the expeirmental results could be correlated with a semi-empirical experimentally derived equation.

In further experiments, the superposition of collection mechanisms, especially the electrostatic mechanics is investigated and a simple guideline for determination of polydisperse collection performance of an EFB is put forth.

2. Fly Ash Adhesion to Substrates and Agglomerate Formation

Previously, fly ash adhesive properties have been viewed exclusively from a viewpoint where the dislodging forces have been statically applied. This literature is reviewed. In fluidized beds, dislodging forces tend to be more impulsive in nature due to the interparticle collisions in the bed. The

dynamic response of these force mechanisms are analyzed and an adhesive force resulting from liquid adhesive agent viscosity is identified. The use of liquid adhesive agents for fly ash adhesion constitutes a major invention of the thesis. This adhesion mechanism is modeled theoretically and studied with very fundamental experiments and then with more applied fluidized bed experiments. An adhesion parameter is identified which is useful in predicting adhesion properties.

3. Application of Theories to EFB Fly Ash Collectors -- The Dynamics of Fly Ash Collection and Reentrainment

At this stage of development the tools for invention of an EFB fly ash collector were ready. A basic system was identified for the collection of fly ash in an EFB using liquid adhesive additives. Additives were introduced to the bed as aerosols in the fly ash laden gas stream, and collected with the fly ash. Models were made for the simultaneous aerosol collection, adhesion and bed mixing of the system. Experiments served to verify the models and provide EFB fly ash collection experience and data.

4. Practical Configurations

The basic EFB system was further developed into practical systems with incorporation into utility plants in mind. Several schemes were identified:

1. Fluidized Bed - EFB two stage collector
2. ESP-EFB two stage collector
3. EFB agglomerator

These schemes are individually tested in lab setups simulating actual operating conditions. Successful performance was demonstrated with submicron

collection efficiencies above 95%.

The final choice of a system depends upon characteristics of the specific plant installation.

Directly based on this part of the thesis are two patent applications, now pending, which are presented in the appendices.

D. Organization of Thesis

This thesis consists of the invention and performance analysis for the practical application of a technology. As such it is necessary to first study several pertinent aspects of the complete system in detail, perform modeling of their interrelationships, and finally identify configurations of the technology for the actual application. This outlook determines the organization of the thesis.

The remainder of the thesis begins with a chapter on the background of Electrofluidized Beds and related work. Also reviewed is work in packed and fluidized bed fly ash collectors. This chapter (Chapter II) is presented as a guideline for those unfamiliar with the EFB technology and provides all pertinent references. The uninitiated reader is advised to study it as this ground work is critical for an understanding of the thesis.

Chapters III and IV respectively cover polydisperse aerosol collection and ash adhesion mechanisms. These contain the important original contributions of the thesis as described above. Chapter V covers the modeling of fluidized bed fly ash collection and reentrainement. Experiments to analyze the models and demonstrative effective ash collection and adhesion in fluidized beds are reported.

Chapter VI is probably most important to the casual reader, as it reviews

the findings of Chapters III, IV, and V. Based on these findings, practical system configurations are proposed, discussed and experimentally demonstrated. Economies and large scale utility plant integration are also discussed.

Finally, a brief summary chapter is presented which outlines the importance of this work and where future work should be concentrated.

Several of the appendices are very important and warrant close examination. Appendix A summarizes the experimental equipment and procedures used. As such it is often referenced in the body of the thesis. Appendix B presents experimental results obtained for an Electropacked Bed (EPB) fly ash collector. The EPB is a cousin technology to the EFB. The experimental apparatus used in the primary studies lent itself to convenient EPB study. The results are presented in an appendix to preserve the continuity of the thesis. Appendices C and D present two patent applications which are currently pending. These patents are based on this thesis work. Appendix E shows the derivation of a mathematical formalism for description of agglomerator performance. Appendix F presents a mathematical model for solids mixing in fluidized beds. This model is unverified experimentally, but it does explain many of the phenomena observed in the experiments of this thesis.

II. Background

A. Introduction

An electrofluidized bed (EFB), as now being developed for the collection of pollutant particles, is a shallow bed of millimeter-sized particles immersed in an imposed electric field. The polluted gas passing vertically upward through the bed serves to render the particles in a fluidized state. Because the particulate matter in the gas is charged by ion impact prior to entry into the bed, the imposed field augments or completely dominates its transport to the bed particle surface.

The EFB realizes advantages over conventional electrostatic precipitators (ESP's) by virtue of its immense amount of collection surface area per unit volume. Thus, for collection of submicron particles it can be much smaller and potentially less costly than an ESP. The electric power industry is being forced into current and expected future increases in coal utilization. These increases focus concern on the central problems facing utilities in the collection of particulate emmissions from coal combustion, namely:

1. Economic collection in the submicron range.
2. Collection of highly insulating particles, such as ash from low-sulfur coal.
3. Convenient handling of large quantities of collected pollutant.

ESP's fail in one or all of these catagories for many types of coal burned. Economic collection in the submicron range has already been demonstrated for EFB's and considerable promise is shown in the remaining two categories.

B. Fluidized Beds

1. Mechanics

An understanding of fluidized beds (FB's) is essential to an understanding of EFB's. FB's have found wide applications in various industries and the literature concerning them is abundant. As basic texts, the reader is referred to Davidson[1] or Kunii and Levenspiel[2]. A detailed discussion of FB mechanics is beyond the scope of this report, but the basic aspects believed to be especially pertinent will be discussed.

As gas is passed vertically through a bed of particles at a low-flow rate, the gas merely percolates through the void space between the particles. This type of bed is a fixed bed. As the flow rate is increased, a point is reached where the drag force on the particles is just enough to balance the weight of the bed, and the bed just begins to expand. Such a bed is at minimum fluidization. In typical gas fluidized beds, as the flow rate is increased further, the particles remain in a minimum fluidixed state while excess gas passes through the bed in the form of bubbles.

The phenomenon of bubbles is fascinating and of fundamental importance to bed mechanics. Their size, velocity, and number in a bed depend on the flow conditions. Bubbles are roughly spherical in shape, and typically the lower third carries a wake of particles with it. The wake is continually gaining new particles and losing particles as the bubble goes up through the bed. It is a region of intense agitation and of greatest tendency for agglomerated particles to be broken up. When a bubble reaches the top of the bed, the particles in the wake are thrown violently into the space above the bed. Figure 2.1 shows pictures of bubbles in an experimental two-dimensional bed. Meaningful fluid mechanical theories of bubbles have been proposed by Davidson[3], Jackson[4], and Murray[5].

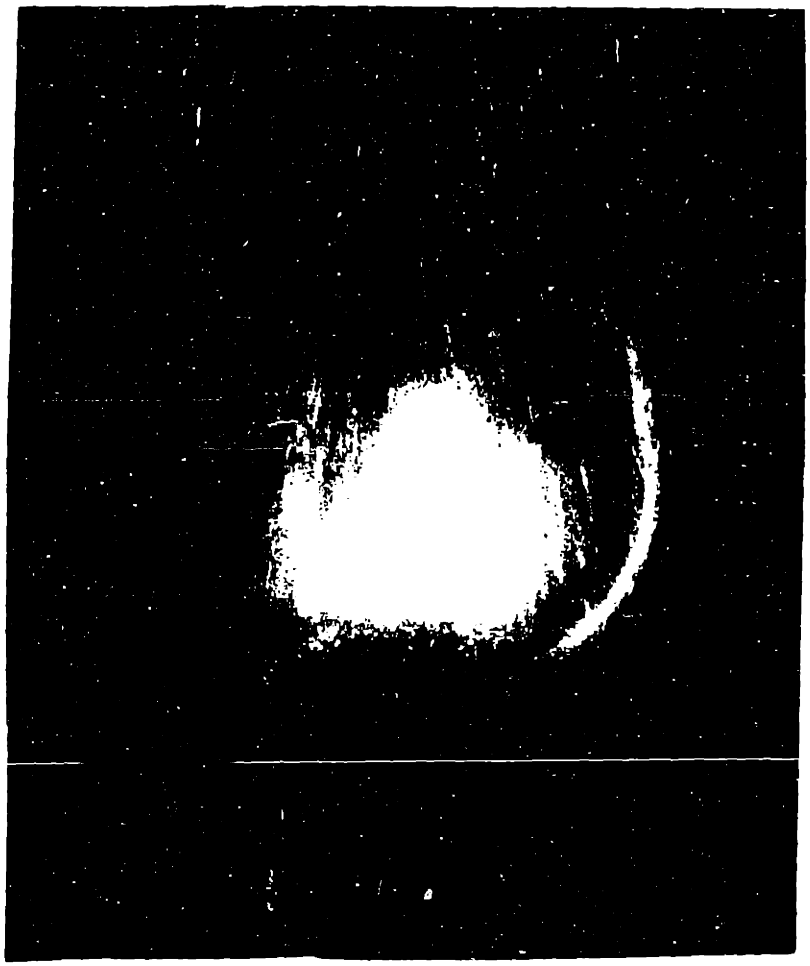

Figure 2.1 Picture of a two-dimensional bubble clearly showing the "classical" bubble shape and particle flow pattern (from P.N. Rowe p. 157). Picture is taken in the frame moving with the bubble.

The carrying of a wake of particles by a bubble is the chief mechanism for axial particle mixing in a typical gas fluidized bed (Rowe[6]). This along with an associated movement of solids in the dense phase has led to diffusion models for axial solids mixing.

Elutriation refers to the selective loss of fine particles from the bed by the process of entrainment. When a particle is small enough that its terminal settling velocity is less than gas velocities above the bed it is a candidate for elutriation. Of course, rates of elutriation also depend on gas flow distribution, the degree to which particles are thrown out of the bed by the explosive action of bubbles erupting, and the length of free space above the bed. Theories are developed in Davidson and Kunii and Levenspiel for elutriation rates given those parameters and the concentration of fine particles in the bed.

The creation of fines in the bed is referred to as attrition. Little more than empirical work has been done on this topic. Particle collision and scraping in spouted beds or bubble wakes are usually believed to be the main attrition mechanism.

2. Aerosol Collection

The collection of aerosols in fluidized beds, as first demonstrated by Meissner and Mickley[7], is summarized by Jackson[8]. In general, four mechanical mechanisms are accountable for the collection:

1. Brownian diffusion - Here particles undergo random motions due to molecular bombardment leading to collection. This mechanism is usually important for particles less than .2 μm diameter.

2. Inertial impaction - Particles with enough inertia cannot follow curves in the fluid streamlines and impact the collecting particles. Effective for particles greater than 1-2 μm diameter.

3. Streamline interception - Some fluid streamlines pass close enough to bed particles that collection occurs due to the aerosol particles finite radius.

4. Gravitational settling - Usually only important for very large particles.

Fixed beds at low-gas flow rates have shown very high (> 99.9%) collection efficiencies while fluidized beds usually do not exceed 90%. Gas bypassing via bubbles is usually blamed for the low efficiencies and various schemes, such as the use of internal baffles of multistage beds, are proposed as remedies. In both fixed and fluidized bed filters tested previous to the work reported here, pollutant loadings have been low, so buildup and eventual entrainment of collected aerosol was avoided.

C. Electrofluidized Beds - A Review of Research at MIT

FUNDAMENTALS OF SUBMICRON PARTICULATE COLLECTION

A major incentive for using the EFB is the extremely short gas residence time required for collection of submicron particulate. A remarkably good model for plug-flow beds pictures the bed particles as being much like the electrodes of an ESP, with the electric field terminating over one side of each particle and originating on the other. Instead of the Deutsch model used for turbulent flow ESP's[9], the "local mixing model" is invoked with the assumption that on the average the fluid mechanics supplies the full surface of a bed particle with the gas-entrained particulate. The electric field simply brings the particulate from the local volume to the bed particle surface. According to this model[2], a bed having unfluidized height ℓ_o, bed particles of mean radius R, a superficial gas velocity U and an imposed electric field E collects particles of mobility b with the efficiency

$$\eta = 1 - \exp(-K_1) \; ; \; K_1 \equiv \frac{3\pi}{8} c \frac{\ell_o}{R} \left(\frac{bE}{U}\right) \qquad (2.1)$$

where c is a coefficient of order unity.

This model is valid provided that bubbling and reentrainment are not substantial. The first of these conditions is promoted by the several screens used to impose the electric field in the co-flow configuration. These tend to prevent the growth of bubbles. The second is not a problem for liquid aerosols such as DOP (used in fundamental studies).

With the objective of testing this model in a way that would separate out less fundamental (but perhaps essential) phenomena, extensive efficiency experiments have been carried out using an apparatus much like that shown in Figure 2.2. For the data shown in Figure 2.3, the cross-flow configuration shown in Figure 2.2 is replaced by a co-flow bed. Efficiencies for DOP aerosols having two different mobilities are represented, the superficial velocity varies from 0.8 to 2.5 m/sec. For all of the measurements, ℓ_o = 6 cm and the bed particles are sand, R = 1 mm. The solid curve is Eq. 2.1 with c = 1.

The residence-time advantage of the EFB is emphasized by recognition the for an ESP having electrode spacing s, the Deutsch equation for the efficiency takes the form of Eq. 2.1, but with the collection coefficient K_1 replaced by $\ell bE/sU$. Because $3\pi c/8$ is essentially unity, this meant that the unfluidized height of an EFB required to give the same efficiency as an ESP of length ℓ is $\ell_o = \ell(R/s)$. Typically, bed particles have a radius R on the order of 1 mm, so that for an electrode spacing of 10 cm the length of the EFB (not counting the charger) is theoretically 100 times less than that of the ESP.

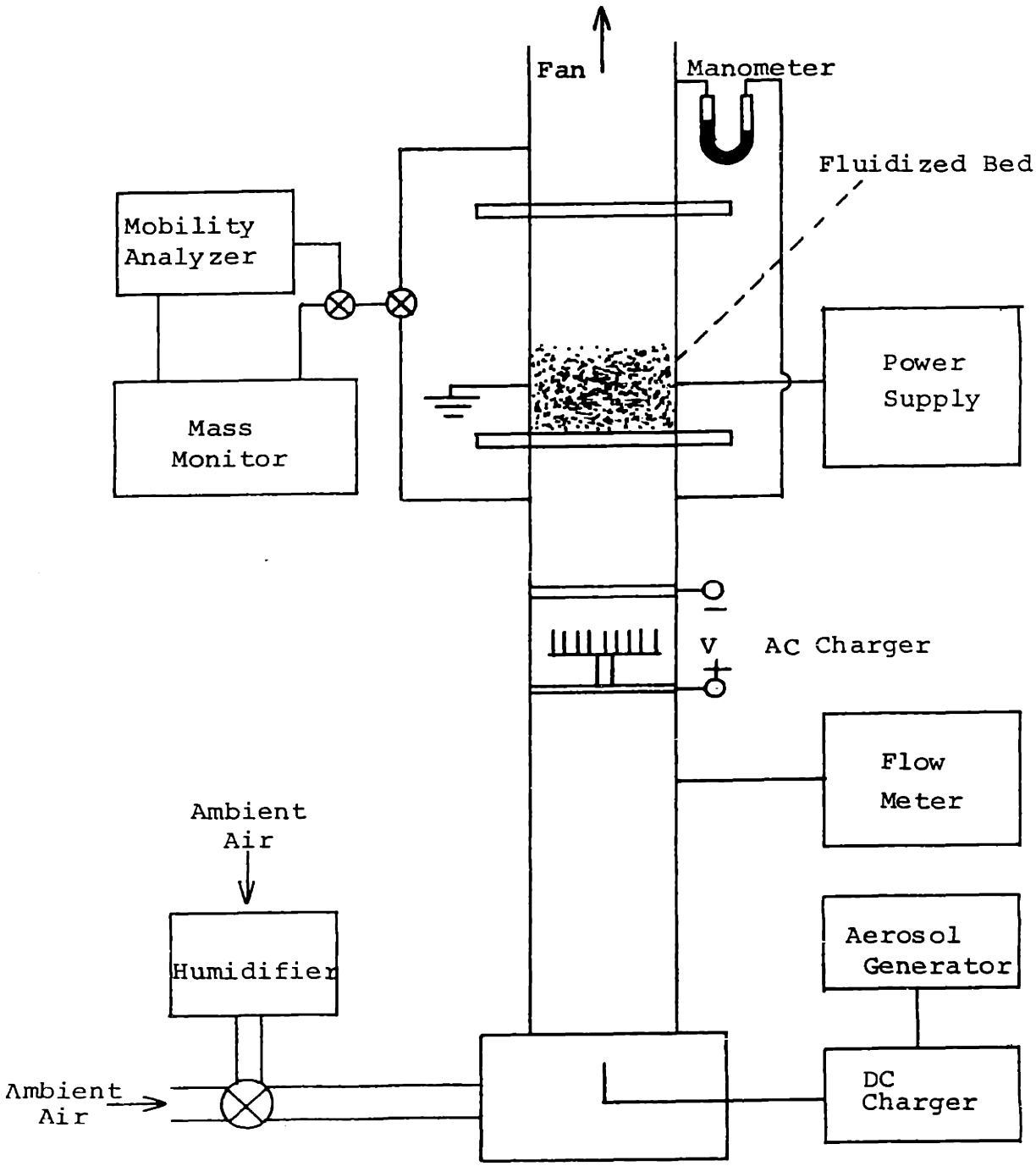

Figure 2.2 Facility for fundamental room termerature tests using di-octyl phthalate aerosol.

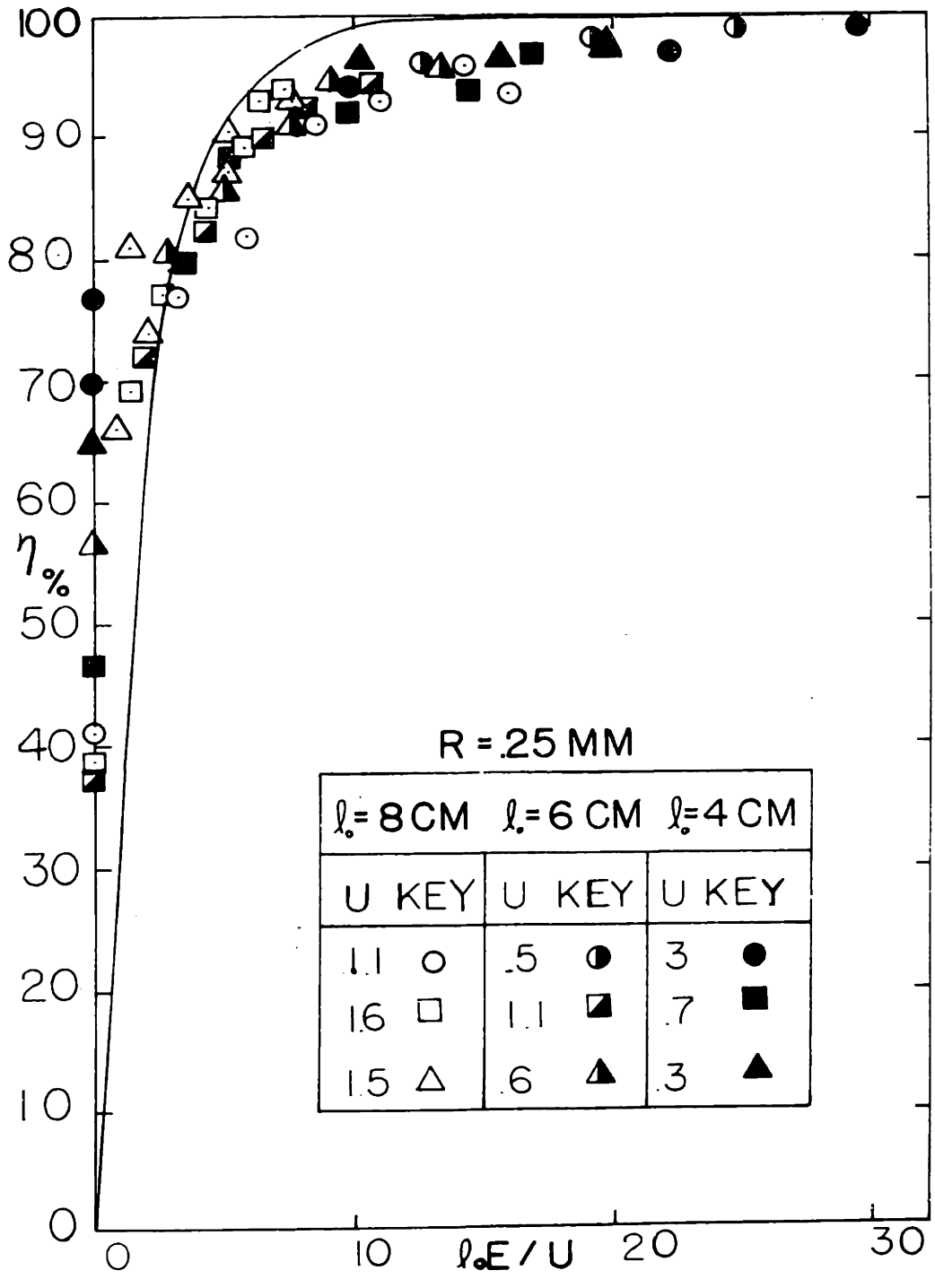

Figure 2.3 Co-flow efficiency as a function of bE/for two different mobilities and sizes of particles.

Initial tests were aimed at establishing this residence-time advantage of the EFB. Subsequently reported results[10] (typified by Figure 2.3) corroborated the model underlying Eq. (2.1) in the submicron range where the electrically induced collection is dominant. Note from Figure 2.3 that without an applied electric field, the bed is between 20 and 30% efficient as a collector. With bubble bypassing minimized and the bed relatively well controlled in a plug-flow mode, these tests are the best available basis for establishing the parameter c. For highly fluidized beds, it is found that $c = 0.9$ with variations of about 15%. For packed or almost packed plug-flow beds, c is about unity and varies with test conditions by 25%. The local mixing model for dilute bed particles perdicts $c = 1$. These tests were performed with sand at relative humidities of 50 - 90%, so that these particles were semi-insulating and hence the collection field placed under control[9.11].

Unless baffled to promote bubble breakup, gas fluidized beds do not expand uniformly as the fluidizing velocity increases and the resulting effects of nonuniformity in the gas-solid distribution is not accounted for in the plug-flow model. This is especially true in the cross-flow beds where the screen electrodes are not used. Models have been developed and correlated with experiments carried out in an apparatus such as that of Figure 2.2. These combine the particle-scale collection model tested in the plug-flow experiments with two-phase models that have been developed for the transfer characteristics of conventional fluidized beds. It is important to recognize that the structure of beds can be strongly influenced by an applied electric field. In what will be termed the "bed electromechanics," particles tend to form "chains" or "strings" while gas flow causes a fluttering motion instead of the typical bubbling one[11]. These effects have important implications for bed mixing and particulate elutriation. However, high sub-

micron collection efficiencies can be obtained at relatively low electric field intensities where electro-mechanical effects are not of significance. Thus, in this work, the Davidson model is adopted for a conventional bubble having the diameter D_b (in which the particle density is low) interacting with the dense phase. Part of the gas passes through a dense region at about the minimum fluidization velocity U_{mf}, while the remainder bypasses the system in the form of bubbles. There is a continual exchange of particles between phases accounted for by the Davidson model.

Two possible extremes can be used to model the penetration of particulate through the bed as a whole. The dense phase can again be viewed as evolving uniformly in the flow direction (the plug-flow model). Because of bubble agitation a complete mixing model is also plausible. Both models have been carried through in this study, with the dense phase plug-flow model clearly found to be more representative of what happens.

The plug-flow bubbling model shows how parameters not represented in the collection coefficient K_1 come into play. The predicted efficiency is

$$\eta = 1 - \frac{1}{m_2 - m_1} \left\{ m_1 e^{m_2 \ell_f} \left[1 + \frac{m_2 \ell_f U_{mf}}{c_q U} \right] - m_2 e^{m_1 \ell_f} \left[1 + \frac{m_1 \ell_f U_{mf}}{c_q U} \right] \right\} \quad (2.2)$$

where m_1 and m_2 are the roots of

$$m^2 + \left[\frac{(c_q + K_1)U}{\ell_f U_{mf}} \right] m + \frac{K_1 c_q U}{\ell_f^2 U_{mf}} = 0$$

and

$$c_q + \frac{9}{2} \frac{(\ell_f - \ell_{mf})}{D_b} \frac{U_{mf}}{U - U_{mf}}$$

The collection coefficient K_1 is the same as defined with Eq. (2.1), U and ℓ_f are respectively the superficial velocity and fluidized bed height under the conditions of interest while U_{mf} and ℓ_{mf} are these quantities under conditions of minimum fluidization. The most important parameter is D_b, the bubble diameter. The quantities necessary to evaluate these expressions are, of course, averages. The bed height is a fluctuating quantity and even in the shallow beds of interest here, bubbles grow significantly as they pass through the bed.

If the rate of gas interchange between the bubbles and the dense phase is large, which according to Davidson's model means that $c_q \to \infty$, the efficiency predicted by Eq. (2.2) reduces to that for the single-phase plug-flow model, Eq. (2.1). The most important aspect of the bubbling model is its prediction of efficiencies less than 100% no matter how large the collection parameter. In the limit $K_1 \to \infty$, the efficiency approaches the limiting value

$$\eta \to 1 - \left[1 - \frac{U_{mf}}{U}\right] e^{-c_q} \qquad (2.3)$$

Using experiments to evaluate c_q, it is found that over a wide range of fluidization states, this parameter is mainly a function of the bubble diameter D_b.

In connection with cross-flow experiments without baffles, the two-phase model has been compared with extensive tests aimed at showing the dependence of collection efficiency on electric field intensity, bed particle size, static bed height, particle mobility and superficial gas velocity, with emphasis on the degree of bypassing through the bubble phase. The bed cross-section was 10 x 10 cm. In order to fix the electrical characteristics of the bed, the relative humidity was controlled at 90%. The fluidized particles were glass beads of 0.5 mm and 1 mm diameter as well as sand with mean diameters of 0.8 and 2 mm. The distributor plate was a 30 mesh plastic screen

sandwiched between two insulating perforated plates with large holes.

Efficiency measurements over a wide range of parameters are summarized in Figure 2.4 where the parameter is K_1 from Eq. (2.1). The solid curve is Eq. (2.1), and hence the limiting efficiency if bubbling is ignorable. A correction is made on the efficiency for mechanical effects. Unfluidized bed heights of ℓ_o= 4, 6 and 8 cm are represented by the data.

That the experimental efficiencies for these bubbling beds do not correlated with the parameter K_1 is evident from Figure (2.4). In effect, the bed height becomes an additional parameter in correlating experiments carried out under different conditions. The data for the 6 cm beds is summarized in Figure (2.5), where the ratio of experimentally observed to theoretically predicted efficiencies is shown as a function of the collection coefficient. The theoretical efficiency is given by Eq. (2.2).

The tendency for the model to predict observations best at high values of K_1 is also seen in results for the other two bed heights. Correlation with the model over the full range of K_1 is best for the deepest bed.

Details of this work on effects of bubble bypassing are given in a forthcoming article[12].

2. SUBMICRON PARTICULATES COLLECTION WITH AC EXCITATIONS

Savings from a reduced need for power conditioning equipment is an obvious advantage of being able to use alternating voltages to excite the EFB. But, perhaps a more important motive comes from the difficulty encountered when conventional ESP's are used to collect highly resistive materials. Poor performance is linked to the dc energization of the ESP. The collection of highly resistive ash results in the buildup of net charge and an attendant

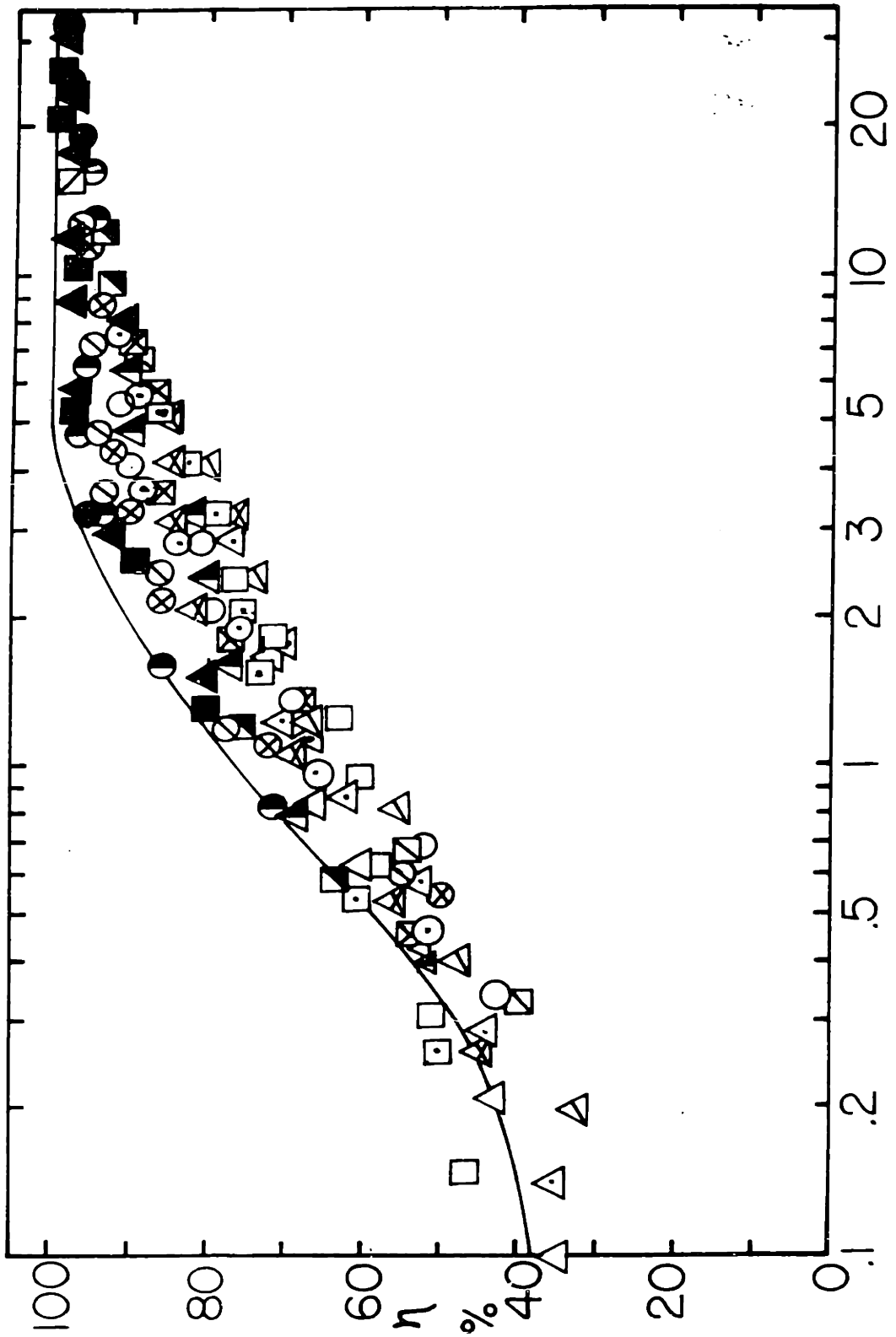

Figure 2.4 Composite of efficiencies for cross-flow beds as a function of collection parameter. Widely varying states of fluidization are represented.

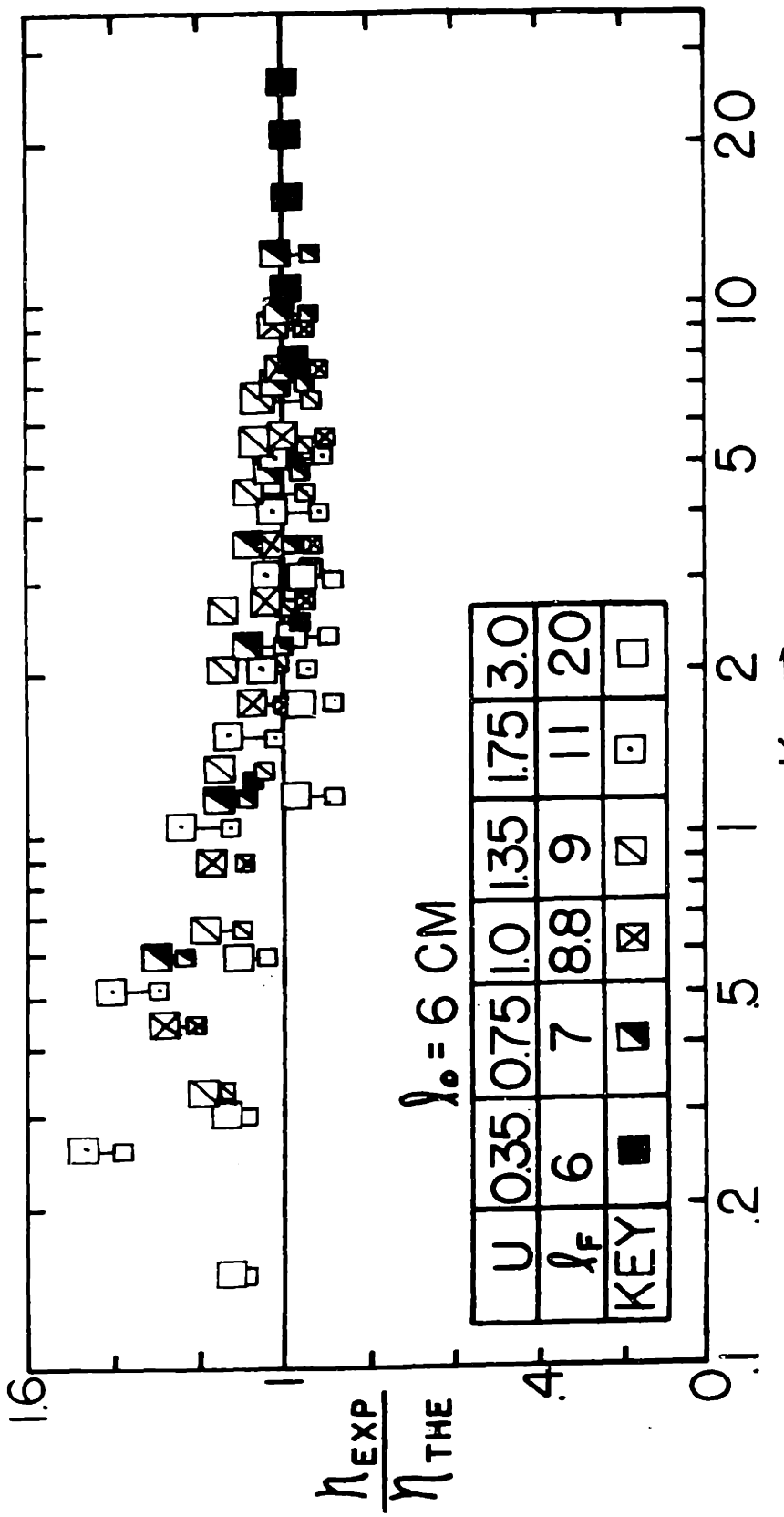

Figure 2.5 Measured efficiency normalized to theoretical efficiency as a function of collection parameter.

interference with the imposed precipitating field. Such effects are not expected in alternating field devices. To be effective with an ESP required to collect submicron particulate alternating fields must have an extremely low frequency (on the order of 1 Hz). (Laminar flow ac ESP performance is worked out in detail by Alexander[13].) Can the EFB operate with 60 Hz excitations? More fundamentally, what are the implications of the frequency dependence of the efficiency for the basic collection process?

With beds of varying particle size and states of fluidization, and with applied fields of different amplitudes, experiments have been carried out using the apparatus of Fig. (2.5). Efficiencies were measured as a function of frequency. Both cross-flow and co-flow configurations were tested over the frequency range of 30 - 5000 Hz.

A correlation of the cross-flow data for the former experiments is given in Fig. (2.6). In order to emphasize the particle-scale collection process to the exclusion of bubble bypassing or bed scale mixing, the beds were tested at low overall efficiencies, in a range where efficiency is proportional to the single particle rate of collection Γ. Thus,

$$\frac{\langle\Gamma\rangle - \Gamma_{nf}}{\Gamma_{dc} - \Gamma_{nf}} = \frac{\langle\eta\rangle - \eta_{nf}}{\eta_{dc} - \eta_{nf}} \qquad 2.4$$

where $\langle\rangle$ indicates the time-average with ac excitation, while nf and dc denote no field and with dc excitation respectively. It is this normalized efficiency that is plotted in correlating the data of Fig. (2.6). To correlate the data, the angular excitation frequency ω is normalized to an angular cutoff frequency $\omega_e = \sqrt{9\pi/8(cs\ bE_o/R)}$, where E_o is the peak applied electric field and s is the velocity gradient adjacent to the equator of a given particle (with the local flow approaching the particle along a polar axis). This parameter can be approximated by $s \equiv 3U_{mf}(1-K^5)/R\ (2-3K+3K^5 - 2K^6)$ where $K = R/R_o$ is the

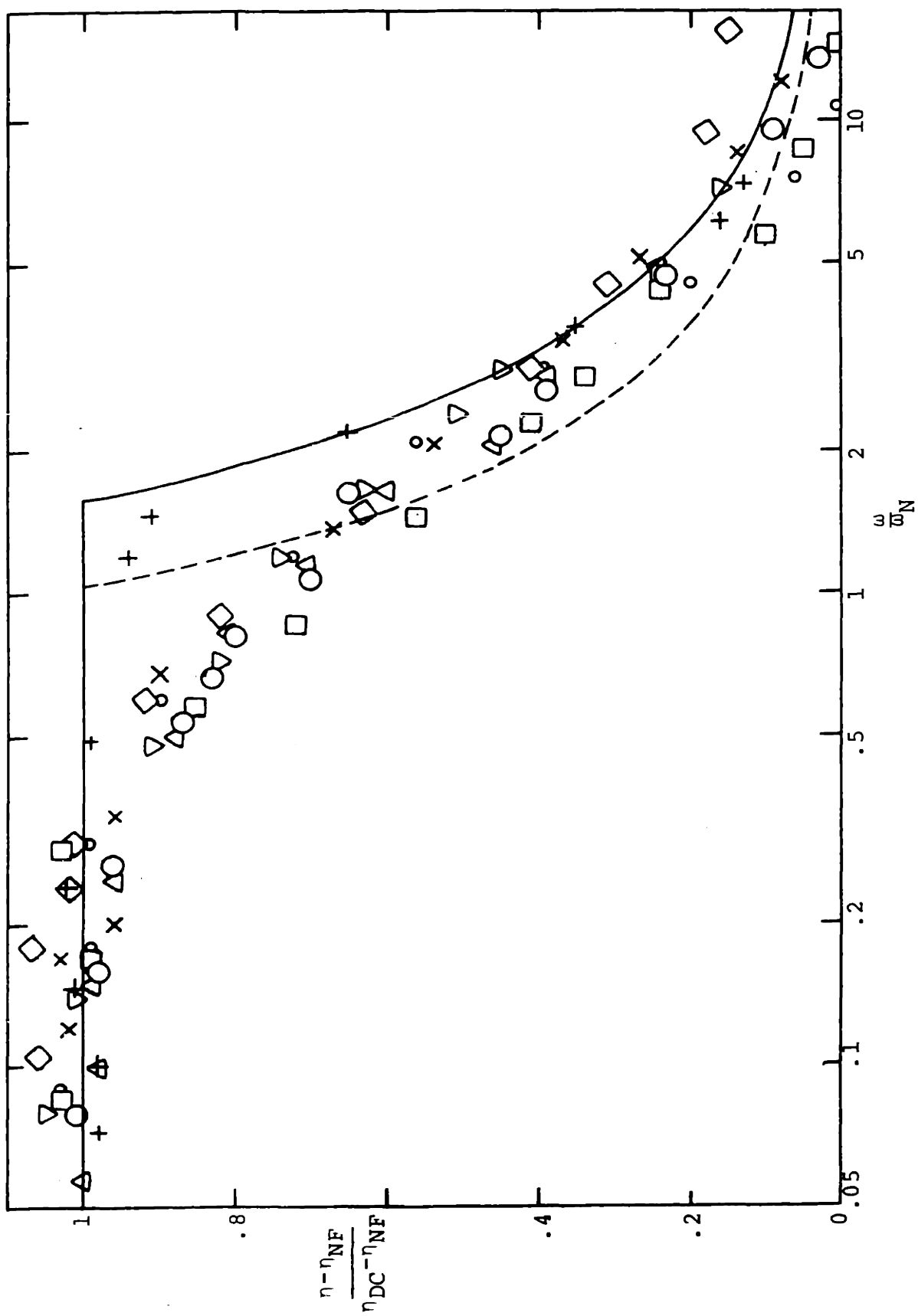

Figure 2.6 Normalized cross-flow EFB collection efficiency as a function of normalized frequency with low and high frequency theoretical

ratio of particle radius to the radius of a unit cell representing the particle voidage. The solid curves represent asymptotic predictions predicated on the period of the applied field either being very low or very high compared to the time required for particulate to traverse a unit cell.

Details of the asymptotic models and specifics of the experiments are available in the literature[14]. It seems clear that such frequency response measurements are a way of probing the mass transfer process at the bed particle scale. From a practical point of view, it is the fact that the 60 Hz efficiency is well below the critical frequency in all of the tests that is most significant. In this low frequency range, the efficiency is as predicted by the models for the dc excitations with $E_{dc} \rightarrow 2E_0/\pi$. As the field reverses, collection occurs first on one side and then on the other side of a collection site. The effective electric field is, therefore, the average of $E_0|\cos \omega t|$ over a full period.

Experiments, correlated with theoretical models, have been carried forward to understand how ac excitations can be used in the corona, ion-impact charging section. The general disposition of the charger is just below the distributor plate is as in Fig. (2.2). At some penalty of power required, the charging can be accomplished at 60 Hz. This makes it possible to operate the entire EFB system, the bed and the charger, from a transformer. As an example, Fig. (2.7) shows the efficiency with the bed in this entirely ac excited type of operation. Details are given elsewhere.

COLLECTION OF OIL ASH

A natural application of the EFB for large-scale gas cleanup is to the products of oil combustion. Experiments have been conducted on a 100

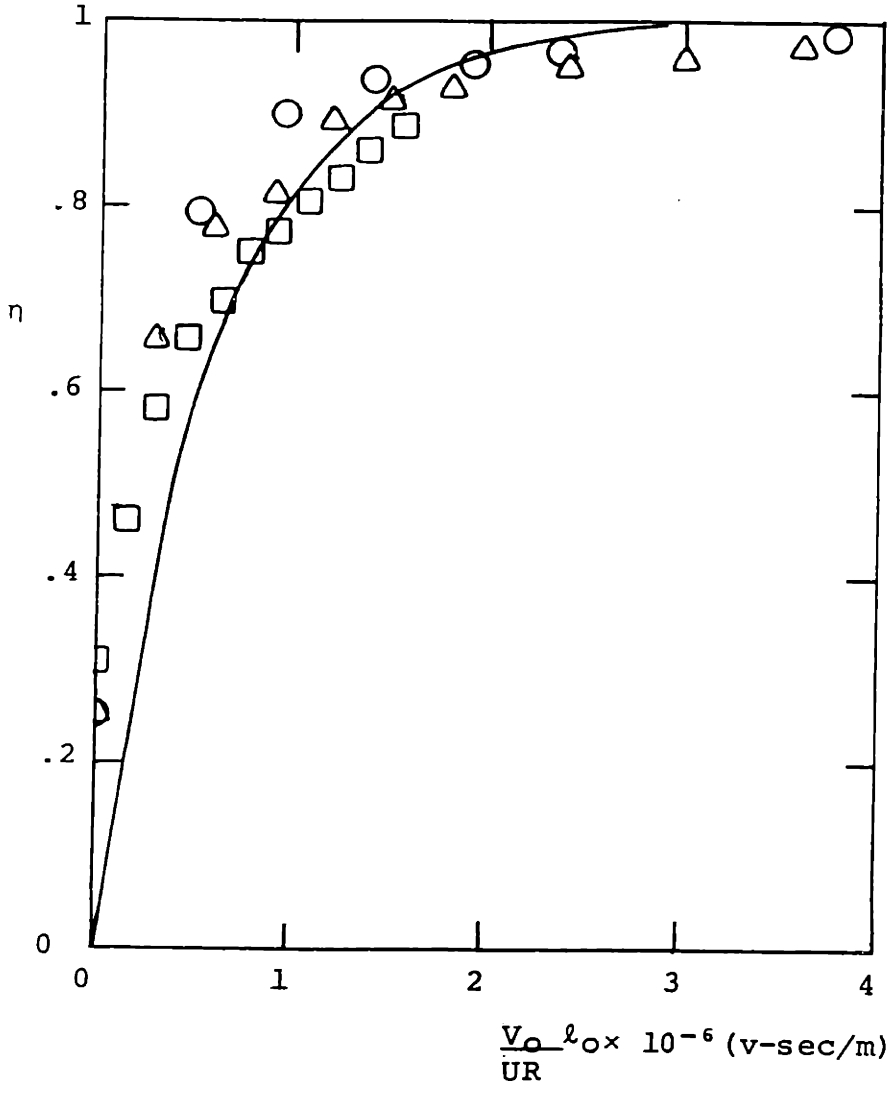

Figure 2.7 Efficiency with 60 Hz on EFB and charger. R =0.5 mm, b = 1.2×10^{-7} (m/sec)/(V/m). Fluidized: ℓ = 10 cm, U = 1.3 m/sec. Packed: ℓ_0 = 7.5 cm, U = 0.5 m/sec.

cfm by-pass on flue gas prior to the economizer in the M.I.T. Central Utility Plant. Loss of heat in the connecting pipes cooled the gas to about 350°F. Tests were conducted in both the co-flow and cross-flow configurations using 1 mm glass beads and 0.8 and 2 mm sand.

The oil ash was entirely in the submicron range with loadings of the order of 0.01 to 0.06 grains/scf. Unlike the DOP, the oil ash is a dry material. Could the EFB be used to collect an essentially dry material and what residence time for the particles was consistent with retaining a reasonable efficiency? A typical test of efficiency as a function of time is shown in Fig. (2.8). For this case, a medium state of fluidization prevailed and the configuration was co-flow. The open circles represent collection with no charging and no applied flied. Because the bed was at a sufficiently high temperature that the humidity did not render the particles semi-insulating, there were appreciable "micro-fields" associated with patches or charge on the particles created by frictional effects. Thus, the open half circles which represent data for collection with charging but without a field applied to the bed, show a considerably higher efficiency than found in experiments such as represented by Figure (2.3). The solid date points are with both charger and applied field on.

It is clear that the bed can operate for substantial periods of time at this mass loading. Either using a once through or a reprocessing system for the sand, the EFB appears to be an economically feasible approach to a utilities scale operation. However, there are questions that must be confronted by a development. The M.I.T. plant is required to use low

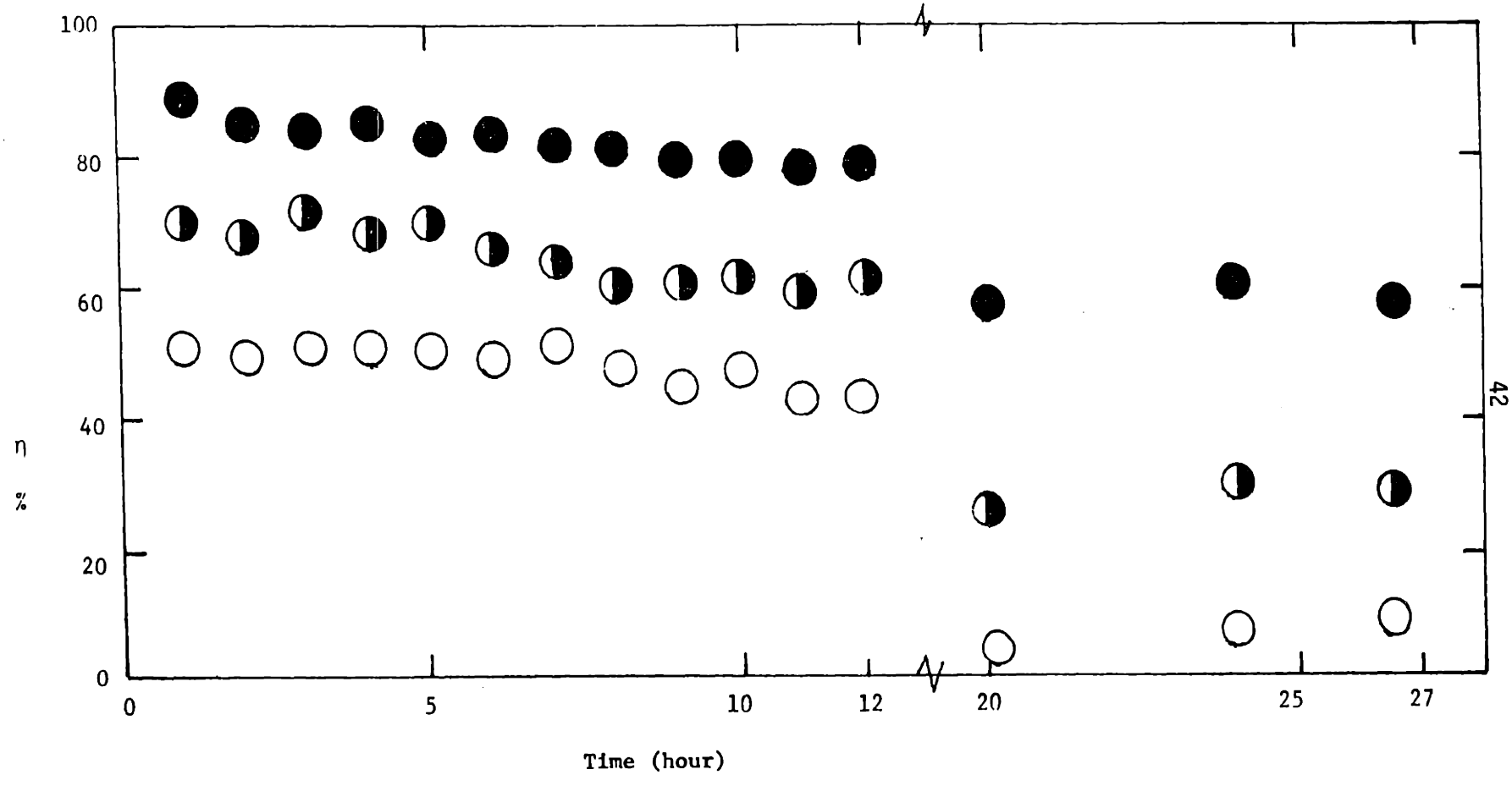

Figure 2.8 Efficiency as a function of time for co-flow EFB on by-pass from MIT Utilities while burning low sulfur oil. Open data points are with charging but no field. Closed circles are for charger and field on.

sulfur oil and considerable excess air, so for the tests conducted, the combustion products were extremely light and free of carbon. What is the effect on bed electrical losses of collecting combustion products of high sulfur oil? Losses with the tests reported here were insignificant.

A sketch of a co-flow EFB incorporated into a stack installation is shown in Fig. (2.9). The top view shows, to scale, the cross-section of a stack, with the EFB constructed around its base. Flue gas is fed into the stack through ducts in the side walls. The dimensions are for a 10^6 cfm unit. A typical pressure drop for 90 - 95% efficiency would be 10 cm H_2O.

4. CONTROL OF ASPHALTIC FUMES IN REPROCESSING OF ASPHALTIC HIGHWAY

Recycling of asphaltic pavement is being developed by the Warren Brothers Company. To be economical, the process should be carried out in adapted conventional plants. A major impediment to the conversion of existing plants is the formation of fine particulate smoke when crushed pavement is processed through the conventional aggregate drier. In the drier, the residual asphalt in the old crushed pavement begins to crack and release hydrocarbon vapor which subsequently condenses into droplets.

Devices currently available for collection of this submicron material are ill suited. The asphaltic by-products are not easily removed from the plates of an ESP. Fabric filters that will catch the submicron particulate subsequently are fouled. Wet wall electrostatic precipitators, charged droplet scrubbers and high energy Venturi scrubbers all create a water pollution problem. The EFB is well suited to this application, not only because of its high efficiency in the submicron ranges, but because the

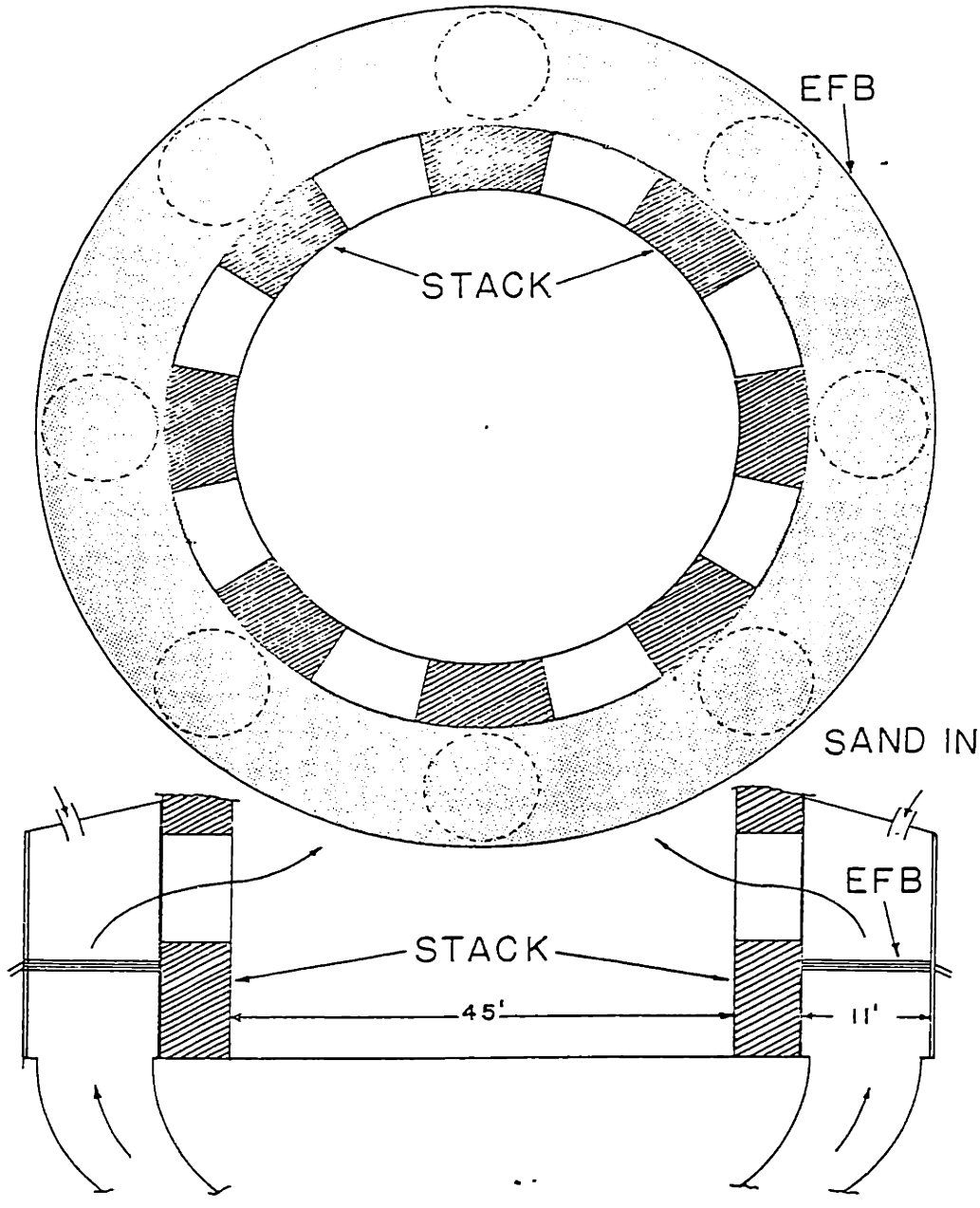

Figure 2.9 Illustration of EFB installation at base of stack.

material used to collect the particulate is easily processed through the EFB and conveniently incorporated into the asphalt hot mix product. In fact, in this and other related operations, oiling of the sand is a desirable step in the plant process.

A prototype EFB of cross-sectional area 1 ft^2 has been tested on both a small-scale prototype asphalt recycling system and on a bypass to a full-scale asphalt plant operating in the recycle mode (Warren Brothers plant #135, Richmond, VA.). In both of the tests reported here, a bag-house was used ahead of the EFB to catch large dust particles from the drier. The submicron material easily penetrated this bag-house. Tests were performed on a batch basis using sand of 2 mm median diameter. The charger was of the plate wire type. Temperatures ranged up to 500°F.

The results of three separate tests of the collection efficiency of the EFB on the small-scale recycling system are reported in Table 2.1. Experimental results are shown along with the theoretical efficiencies predicted by the plug-flow model and by the two-phase bubbling model.

EFB OPERATING PARAMETERS				EFFICIENCY (%)		
Particulate Loading (mg/sm^3)	U (m/sec)	ℓ_o (cm)	E (kv/m)	Experimental	Theoretical	
					Plug-flow Model	Bubbling Model
167	1.7	10	465	96	99	96
82	1.8	10	250	93	94	91
44	1.8	13	500	94	99	92

Table 2.1 Summary of the collection performance of the EFB/ comparison of experimental and predicted efficiencies.

After removal of dust by the bag-filter, the mass median diameter of the smoke ranges from 0.3 to 0.5 μm, with a geometric standard deviation of about 2.

An important parameter is the amount of time that sand can be used before it must be replaced because of a drop in collection efficiency. The mechanisms for this drop seems to be channelling of the gas through spouts in the bed, occuring after the sand becomes viscous due to excessive oil collection. In Table 2.2, tests under similar operating conditions are compared. In the two cases for which the oil loading os 0.7%, the measured efficiency for the oily sand is essentially the same as for the clean sand. In the case of 1.2% oil loading, a drop in efficiency is observed.

EFB OPERATING PARAMETERS			EFFICIENCY (%)				
			Fresh Bed		Oil Coated Bed		
U (m/sec)	E (kv/m)	ℓ_o (cm)	Particulate Loading (mg/cm^3)	Experimental	Particulate Loading	Oil Loading *	Experimental
1.8	500	13	44	94	107	0.7%	94
1.8	500	13	44	94	200	0.7%	95
1.7	465	10	167	96	233	1.2%	85

* Oil loading is defined as the ratio of the weight of collected oil to the bed total weight.

Table 2.2 Comparison of collection performance of fresh and oil coated beds.

Pressure drop usually accounts for the largest share of EFB operating costs. In these tests, the pressure drop across the EFB, including the distributor plate, was less than 18 cm/H_2O. With the bed operating properly, this drop is essentially that across the distributor plate plus what drop is required to support the bed. As spouting occurs because of bed overloading, there is an associated loss of pressure drop that can be taken as an external indication of loss in efficiency.

Results from the Richmond tests are shown in Table 2.3, where 400 cfm is filtered with particulate loadings varying between 4 mg/m 41 mg/m^3. Particulate was observed to have a mass median diameter o μm with a geometric standard deviation of 1.4.

Efficiency Measuring Device	EFB Operating Parameters			Efficie
	E(kv/m)	U(m/sec)	ℓ_o(cm)	(%)
Mass Monitor	400	1.9	10	99.3
Andersen Impactor	400	2.1	11	99.1

Table 2.3 Summary of collection performance in Richmond.

This work is reported in more detail in the literature[16].

ELECTROMECHANICS OF ELECTROFLUIDIZED BEDS

In the application of the EFB to submicron particulates control, is possible to separate the electrical interaction between the bed par and the charged particulate from the electrical interaction between be ticles. It is the latter that is termed the bed "electromechanics." propensity of the field for altering the state of fluidization by indu interparticle stringing is discussed in previous publication[11].

If the bed is to be applied to collection of both submicron and su micron particles, it is necessary to understand the implications of the surprisingly large electrical effects at the bed particle scale. To wh extant can these forces be relied upon to prevent loss of large particl from the bed? Because the field can turn a bubble into a "fritter," th turbulence within the bed is considerably reduced by the field. Each b particle is subjected to a reduced amount of agitation because the "wake mixing" associated with the classical bubble is reduced or eliminated.

what extent are these effects useful in achieving EFB operations in a mode where bed particles are agglomerates of the particulate, the self-agglomerative mode?

Two types of fundamental experiments have been carried out with the objective of having a physical picture of the interparticle force. In the first of these, the EFB (in a cross-flow configuration) is in the annulus between the cylinders of a Couette viscometer, as shown in Fig. (2.10). The shear stress tends to a common asymptote at high field strengths over a range of shear rates. In this high field regime, the electrical force is large enough that the bed is electropacked. Each particle chain transmits its force through friction to the electrodes, so the shear stress can be used as a measure of the interparticle force.

For the particles typical of the EFB applied to air pollution control, polarization forces (associated with the permittivity of the particles) are too small to be responsible for the observed effects. Also, such observations as the dependence of the electromechanical effects on applied voltage negate such polarization forces as the basis for what is observed. A theoretical model has been developed in which the force between particles is accounted for in terms of the concentration of the electric field near the contact caps between particles. In this region there is a strong constriction of the current as it passes between particles. The correlation between theory and experiment supports the contention that it is this field concentration that is responsible for the large electromechanical effects and their dependence on the applied voltage.

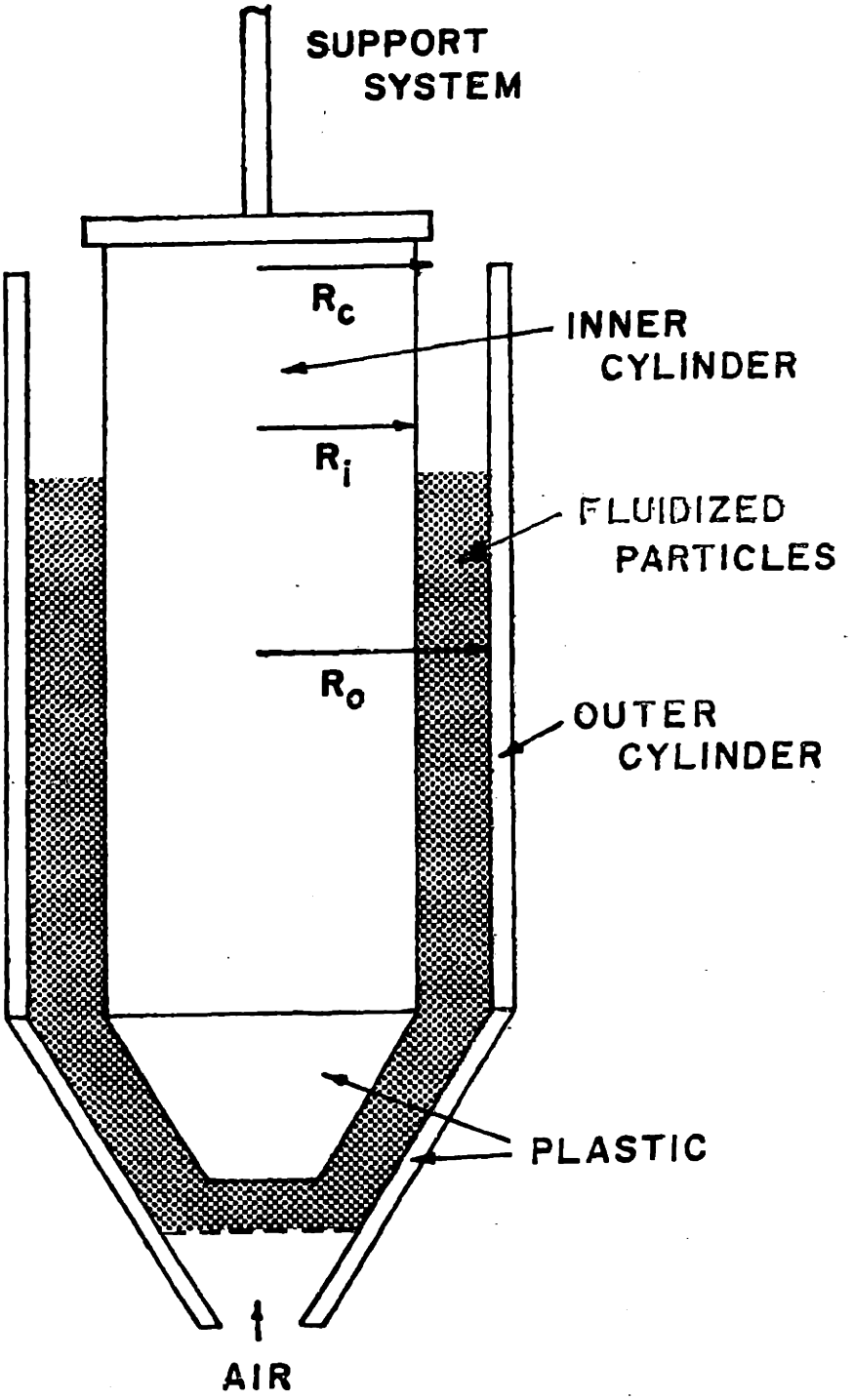

Figure 2.10a Cross flow EFB in viscometer. Outer cylinder rotates and inner one is fixed. Voltage applied between inner and outer cylinders results in shear stress at inner cylinder as shown.

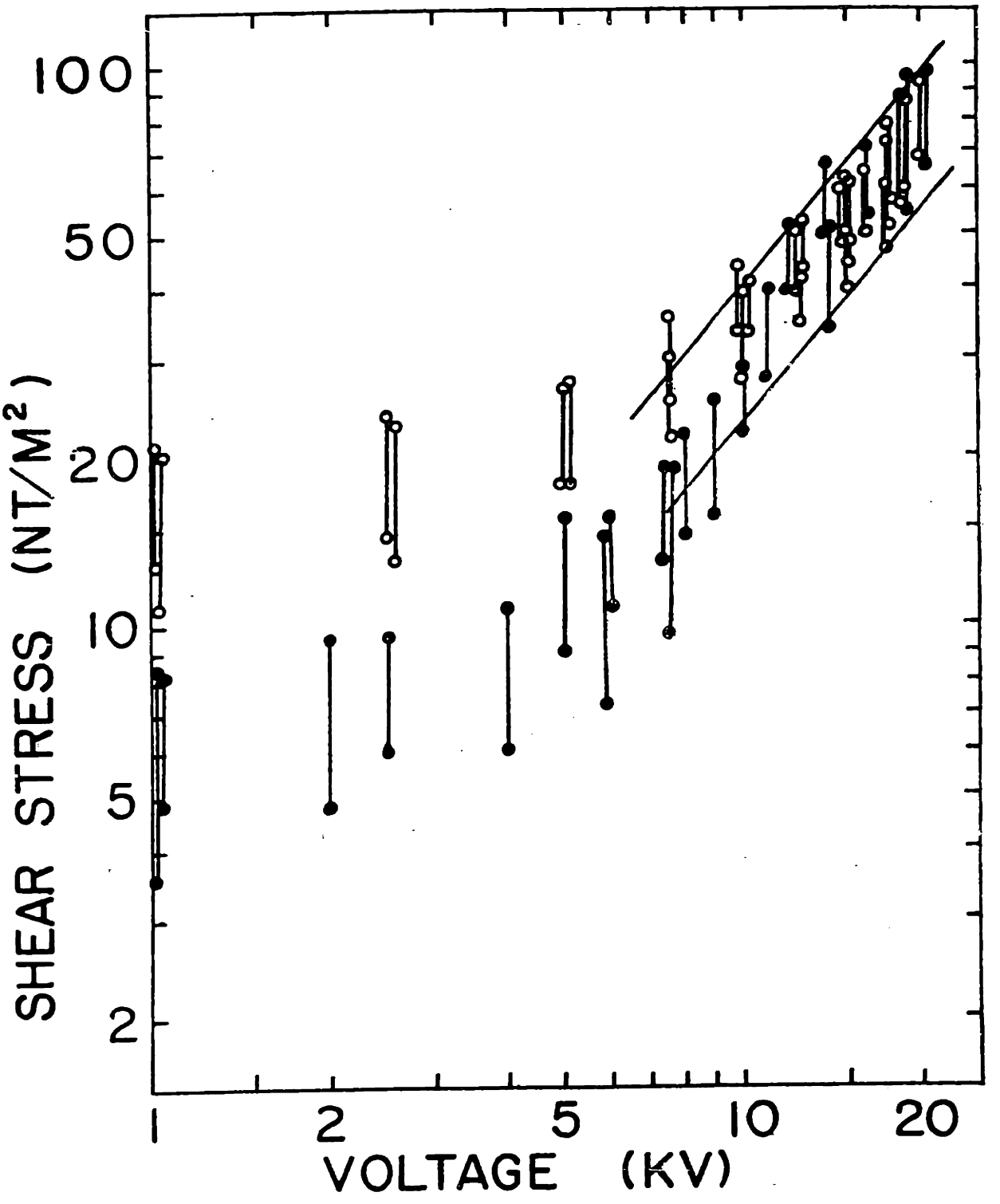

Figure 2.10b Cross flow EFB viscometer data

Further experiments allow deduction of this interparticle force from bed characteristics. In the first of two experiments in this category, the pressure drop at incipient fluidization is measured as a function of the applied voltage. In the second, the minimum voltage required to suspend a bed against an upper screen is measured as a function of the gas-flow rate. Both experiments are performed using the semi-insulating particles typical of the sand at high relative humidities with the cross-flow configuration. Typical results for this latter experiment are shown in Fig. (2.11), which shows the superficial velocity at which particles fall from a pinned position as a function of voltage. The inset shows an idealization of the curves, identifying two regimes. In the low-field regime, the velocity is above U_{mf}, and so there is enough pressure drop to support the bed as a whole. In this regime, failure is because particles at the bottom interface are not held in equilibrium. In the high-field regime, the electric field makes it possible to support the bed as a whole and failure involves the entire bed. Correlations between the bed measurements and a theory based on interparticle forces due to current constriction and a contact cap determined in size by electrical breakdown are not only successful in predicting the dependence of the parameters, but in giving quantitative predictions as well. This work is reported in Appendix B.

D. Fly Ash Collection in Packed and Fluidized Beds

Laboratory moving panel bed filters have been used by Squires and Pfeffer and Zahradnik et al[17, 18] to collect fly ash. At low superficial velocities efficiencies of up to 99% by mass are reported. Simultaneous SO_2 removal up to 100% are realized when alkali alumina is used

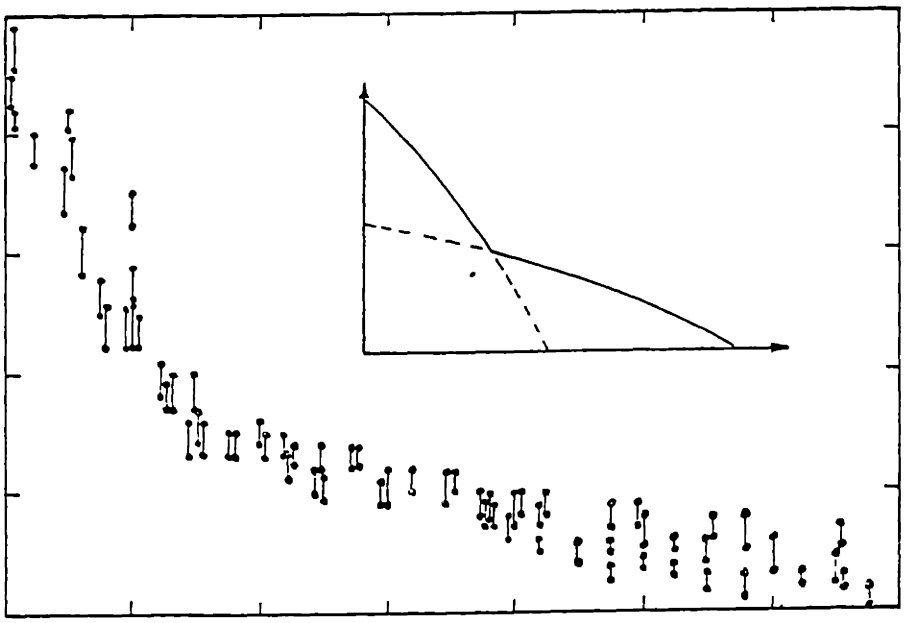

Figure 2.11 EFB support experiment typical data.

as the bed medium. These results are not suprising since the gas face velocities are low and the beds are deep, while the fly ash is probably more than 99% supermicron by mass.

Pilney and Erickson[19] effectively collected fly ash in shallow fluidized beds. Superficial velocities were a fraction of a meter per second, bed depths a few cm, and bed particles submillimeter. The fluidizing air was humidified to promote adhesion, but in general the details of collection, adhesion, and reentrainment were not addressed. In any given bed, the total mass of fly ash collected was small ($\lesssim$100 grains) the reentrainment problem was not important. The importance of adhesion was recognized though and collection on sand, previously formed fly ash agglomerates, porous particles soaked in oil, heated wax particles, and dry polystyrene beads (which, in theory, acquired static electric charge) were tried with varying degrees of success. No meaningful conclusions were drawn from the experimental work. The advantages of the self-agglomerative mode as well as the possibility of simultaneous SO_2 removal were also pointed out. The need to increase gas velocities and bed particle size for practical operation, and the probably resulting detrimental effects on ash retention is recognized.

E. Fluidized Bed Self-Agglomerators

The self-agglomerating mode of fly ash collection is most attractive since in theory such a system would need no steady supply of new bed material, agglomerates of fly ash would simply be removed. Particle growth in fluidized bed dryers has been demonstrated by Metheny and Vance[20] and Markvart et al[21]. In their systems, water solutions or molten solids are

injected into a bed. The excellent heat and mass transfer characteristics of a FB serve to dry the liquid feed on the bed particles resulting in growth of the particles. Langston and Stephens[22] show a self-agglomerating fluidized bed of metallic iron pellets is used as a collector for fine iron oxide particles. Because freshly reduced metallic iron softens and becomes sticky at the temperature of the system operation, the particles adhere. Once collected, the iron oxide is reduced rapidly providing a new sticky surface of metallic iron.

Preliminary experiments performed by the author have shown that ash agglomerates are formed by simultaneous collection of ash and liquid droplets in a fluidized bed. The liquid serves as an adhesive agent and virtually eliminates reentrainment of fly ash. There appeared to be no limit to the size of agglomerates obtainable as bed particles (1 mm radius sand) have been observed to increase their size by several times.

Thus, it appears possible to create surfaces on FB particles "sticky" enough to collect fine particles, yet not so "sticky" as to defluidize the bed, a most encouraging fact for the self-agglomerating fly ash collection mode.

REFERENCES

(1) Davidson, J.F. and D. Harrison, Fluidization (Academic Press, New York, 1971).

(2) Kunii, D. and O. Levenspiel, Fluidization Engineering (Wiley and Sons, New York, 1969).

(3) Davidson, J.F., Trans. Inst. Chem. Eng., 39, 230 (1961).

(4) Jackson, R., Trans. Inst. Chem. Eng., 41, 22 (1963).

(5) Murray, J.D., J. Fluid Mech., 22, 57 (1965).

(6) Rowe, P.N., B.A.Partridge, A.G.Cheney, G.A.Henwood, and E.Lyell, Trans. Inst. Chem. Eng., 43, T271 (1965).

(7) Meissner, H.D. and H.S.Mickley, Ind. Eng. Chem., 41, 1238 (1949).

(8) Jackson, M. AIChE Sym. Series "Fluidization and Fluid Particle Systems," 141, 70, 82 (1975).

(9) White, H.J., Industrial Electrostatic Precipitation, Addison-Wesley, Pub. Co., Reading, MA., p. 164 (1963).

(10) Zahedi, K. and Melcher, J.R., "Electrofluidized Beds in the Filtration of Submicron Aerosols,: APCA Journal, Vol. 26, p. 345 (1976).

(11) Johnson, T.W. and Melcher, J.R., "Electromechanics of Electrofluidized Beds,: I&EC Fund., Vol. 14, p. 146 (1975).

(12) Zahedi, K. and Melcher, J.R. "Collection of Submicron Particulate in Bubbling Electrofluidized Beds," I&EC Fund. (in publication).

(13) Alexander, J.C., "Frequency Characteristics of Electrofluidized Beds in the Collection of Submicron Particulate," M.S. thesis, Oct. (1975).

(14) Alexander, J.C. and Melcher, J.R., "Alternating Field Electrofluidized Beds in the Collection of Submicron Aerosols," I&EC Fund. (in publication).

(15) Final Report to ESEERCO on Electrofluidized Beds in the Filtration of Submicron Particulate, Continuum Electromechanics Group, M.I.T. (1976).

(16) Zieve, P.B., Zahedi, K., Melcher, J.R. and Denton, J.F., "Electrofluidized Beds in the Filtration of Smoke Emissions from an Asphaltic Pavement Recycling Process," Env. Sci. & Tech., submitted for publication.

(17) Squires, A.M. and R. Pfeffer, J. Air Pollution Control Assn., 20, 534 (1970).

(18) Zahradnik, R.L., J.Anyigbo, R.A.Steinberg, and H.L.Toor, Env. Sci. Tech., 4, 66 (1970).

(19) Pilney, J.P. and E.E.Erickson, J. Air Poll. Control Assn., 18, 684 (1968). A detailed report is given in "Final Report on Removal of Fly Ash by Fluidized Bed Techniques," North Star Research Develop. Inst., Minneapolis (1968) (To Dept. of Interior, Bureau of Mines, Contract No. 14-69-0070-375, multilith).

(20) Metheny, D.E. and S.W.Vance, Chem. Eng. Prog., 58, 6, 45 (1962).

(21) Markvart, M., V.Vanecek and R. Drbohlav, Brit. Chem. Eng., 7, 7, 503 (1962).

(22) Langston, B.G. and F.M.Stephens, Jr., J. Metals, 312 (April 1960).

III. Polydisperse Aerosol Collection in Packed and Fluidized Beds

A. Introduction

The first step in the effective control of particulate emissions is the separation of the particulate from the gas stream. In fluidized and packed bed collectors this amounts to the deposition of the particulate onto the bed particles. For now the subsequent fate of the collected particulate is ignored. This important topic will be discussed in later chapters. For the purposes of this chapter, it is assumed that all collisions between particulate and bed particles result in stable adhesion and permanent removal of the particulate from the gas stream.

In general, the collection performance of an entire bed is desired including its dependence on various parameters. The deposition of particulate though, takes place on a scale of the bed particles. Modeling of bed performance typically starts with a treatment of the bed particles as individual deposition sites. Such an approach lends itself to analytical study if the geometries and fluid dynamics are well defined. From these single particle models, or micro-models, overall bed performance is determined by considering the deposition sites as a system of series or parallel collectors, in combinations dictated by the proper macro-model. The proper macro-model must account for the geometrical relations of particles and gas flow on the scale of the entire bed.

As gas entrained particulate travel around bed particles they tend to flow streamlines. Some force must act to cause them to leave the streamline and deposit on the particle. Several forces act on the particulate, with varying degrees of influence. They are listed below as an introduction.

(1) Brownian Diffusion: Particulate is continually bombarded by gas molecules, giving the particulate a certain amount of random motion which may make it collide with the bed particle.

(2) Inertial Impaction: As particulate follows a curved streamline around the bed particle, their inertia makes them deviate from the streamline and can cause collision.

(3) Gravity Settling: The gravitational force on the particulate may be directed toward the bed particle.

(4) Direct Interception: This is not really a force, rather particulate may intercept the bed particle if the streamline it is traveling on passes within a particulate radius of it.

(5) Electrostatic: Electrostatic forces may drive the particulate to the bed particle surface. This category encompasses modes where either the bed particles and particulate may be charged or uncharged and ambient electric fields may or may not be imposed. Usually, though, the particulate must be charged for the forces to be appreciable.

This chapter will begin by discussing the macro-models for bed collection. The plug flow and bubbling bed models will be reviewed there and then the extension of these models to the collection of polydisperse aerosols will be considered. As a precursor to the study of single particle collection models, the several different flow models available in the literature will be presented. Then a concise review is made of previous work in single particle collection modeling and experiments. Criticism is offered to arrive at the most useful models available.

The inertial impaction mechanism is the least well understood in the literature and is the subject of a detailed experimental investigation. A semi-empirical equation for the prediction of inertial impaction is then developed as a result of this program.

Finally, the superposition of various mechanisms is discussed and a detailed experimental demonstration of the importance of the combined effects of inertia, diffusion, and electrostatic collection is presented.

B. Development of Theoretical Framework

1. Bed Collection Macro-models

In this context, the term "macro" is used to connote dynamics on a scale of many bed particles. In other words, the bed is treated as an aggregate without being discretized to the level of its individual particles. The bed macro-collection models are used to extend the single particle collection models to predict quantities which can be directly measured, such as aerosol inlet and outlet concentrations. We will begin by discussing the macro-models because they are generally better understood and accepted. They will then be used to translate experimental results into forms consistent with single particle collection models.

Collection on single particles is characterized by a single particle collection efficiency C. Defined as a ratio of the mass flux Γ (kg/sec) of particulate (with mass density m in the gas) collected by the particle to the flux of particulate carried through a circular "window" of radius R (the bed particle radius) by a flow of velocity U, C is

$$C = \frac{\Gamma}{\pi R^2 U m} \tag{3.1}$$

where m is the mass loading of particulate in the gas.

The actual local flow velocity is not really well defined for all types of beds, so as a matter of definition we will take U to be the superficial velocity U_o as it is usually defined for packed and fluidized beds. The effect of local flow velocity will be accounted for in the single particle efficiency C.

a. Plug-Flow Model

The simplest model to derive is that where the assumptions are made that particles in the bed are uniformly distributed and gas flow is uniform on scales of the bed. The so-called plug-flow model is expected to be

a very good representation of packed beds and a good model for fluidized beds in certain limiting cases.

Fig. 3.1 shows the geometrical configuration appropriate for this model. A supported bed is subjected to a gas flow of superficial velocity U_o containing an aerosol of mass density m_o. The vertical coordinate z is defined as zero at the plane of bed support. In the steady state, then, the mass density will be a function of z with the boundary value

$$m(z = 0) = m_o \tag{3.2}$$

For a slice of the bed in the planes z and $z + \Delta z$ a mass balance requires that the flux of gas entrained aerosol into the slice minus that leaving the slice be equal to the total flux of collected aerosol by bed particles in the slice

$$m(z)AU_o - m(z + \Delta z)AU_o = \left| \frac{\Delta z A(1-\epsilon_f)}{\frac{4}{3}\pi R^3} \right| C_t \pi R^2 U_o m(z) \tag{3.3}$$

where A is the bed cross-sectional area, ϵ_f is the fluidized bed fraction voids, and C_t is the total single particle collection efficiency. In the limit $\Delta z \to 0$ this becomes

$$\frac{dm}{dz} = -\frac{3}{4}\frac{(1-\epsilon_f)}{R} C_t m(z) \tag{3.4}$$

and with the boundary condition on m

$$m = m_o e^{-z/\ell_c} \quad ; \quad \text{for } 0 < z < \ell_f$$
$$; \quad \ell_c = \frac{4}{3}\frac{R}{(1-\epsilon)C_t} \tag{3.5}$$

By noting that the fluidized height ℓ_f is related to the unfluidized height ℓ_o by the unfluidized fraction voids ϵ_o

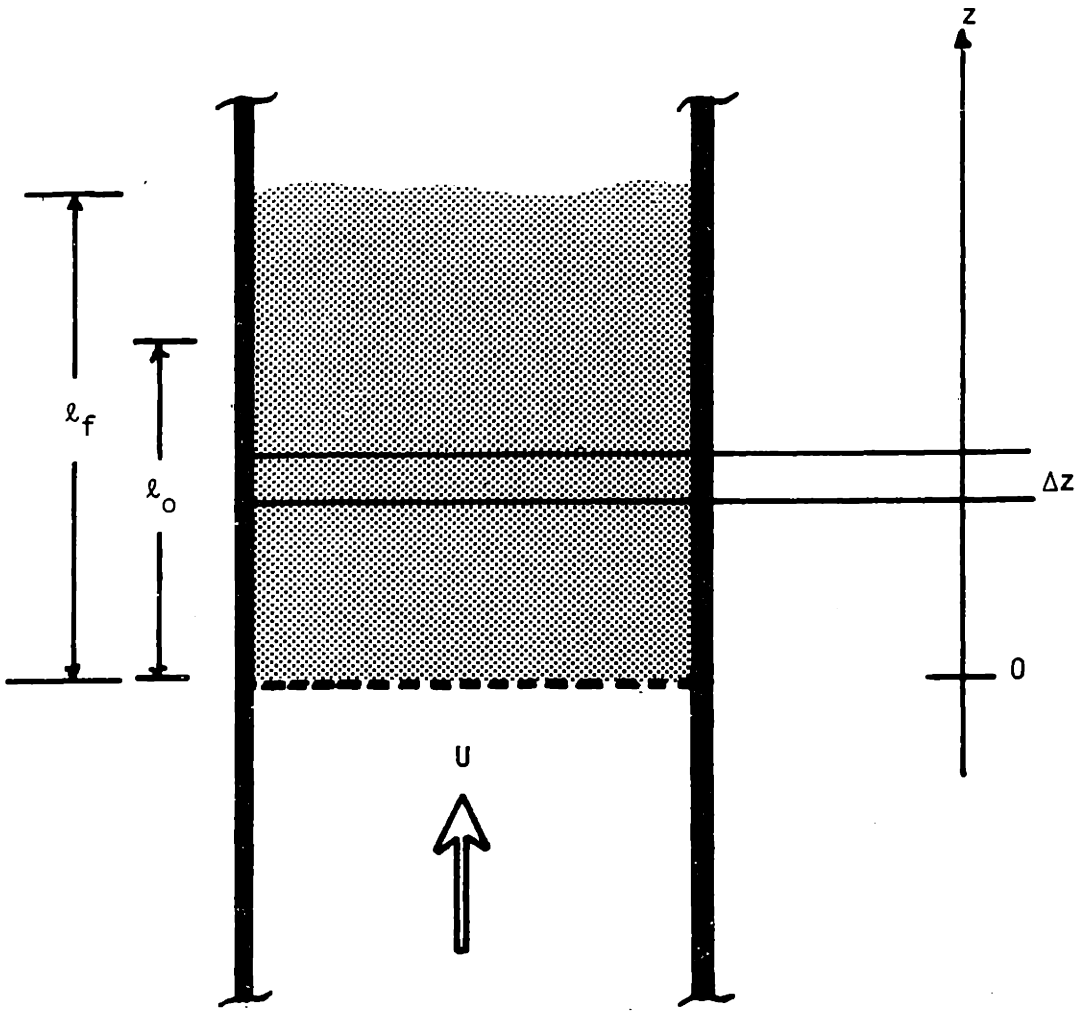

Figure 3.1 Schematic diagram for the development of the plug flow model.

$$\ell_f = \ell_o \left(\frac{1-\varepsilon_o}{1-\varepsilon_f}\right) \tag{3.6}$$

the total collection efficiency, defined as

$$\eta = 1 - \frac{m(z=\ell_f)}{m(z=0)} \tag{3.7}$$

can be solved for;

$$\eta = 1 - \exp\left(-\frac{3}{4}(1-\ell_o)C_t \frac{\ell_o}{R}\right) \tag{3.8}$$

and applies to either packed or fluidized beds.

b. Bubbling Bed Model

Unless overt means are imposed, fluidized bed collectors are not usually well modeled by the plug-flow collection model. Typically, fluidized beds contain bubbles, or regions of very low bed particle densities, which serve to pass packets of gas through the bed without appreciable contact with bed particles. This effect reduces the actual collection efficiency from that predicted by the plug-flow theory. The detrimental effect can be reduced by inserting horizontal baffles into the fluidized bed (or electrode screens in the co-flow bed configuration) which serve to break up the bubbles as they pass. Still, practical efficiencies are limited to about 95%.

An understanding of this phenomenon was developed by Zahedi and Melcher.[1] It is based on the Davidson[2] continuum approach to bubbling fluidized beds and ignores electromechanical effects on bed particles, a good assumption for most practical low-field electrofluidized bed collectors. When the gas flow in the dense phase of the bed is assumed to be plug flow, the collection efficiency is found to be

$$\eta = 1 - \frac{1}{m_2 - m_1} \left[m_1 e^{m_2 \ell_f} \left| 1 + \frac{m_2 \ell_f (1-\beta)}{c_q} \right| - m_2 e^{m_1 \ell_f} \left| 1 + \frac{m_1 \ell_f (1-\beta)}{c_q} \right| \right] \tag{3.9}$$

where m_1 and m_2 are defined as roots of

$$m^2 + \frac{c_q + K_1}{\ell_f (1-\beta)} m + \frac{K_1 + c_q}{\ell_f^{\,2} (1-\beta)} = 0 \tag{3.10}$$

and

$$\beta = 1 - \left(\frac{U_{mf}}{U}\right) \qquad (U_{mf} = \text{minimum fluidization velocity})$$

$$K_1 = \frac{3}{4} (1-\varepsilon_o) C_t \frac{\ell_o}{R}$$

$$c_q = \frac{9}{2} \left(\frac{\ell_f - \ell_o}{D_b}\right) \left(\frac{U_{mf}}{U - U_{mf}}\right) \tag{3.11}$$

U_{mf} = minimum fluidization velocity

D_b = bubble diameter (3.12)

If the gas in the dense phase of the bed is assumed to be completely mixed (i.e., the aerosol mass density is uniform throughout the dense phase of the bed) then

$$\eta = \frac{(1-\beta e^{-c_q}) K_1}{K_1 + (1-\beta e^{-c_q})} \tag{3.13}$$

In very simple terms, the bubbling causes efficiencies to reach asymptotic values for arbitrarily high values of the collection parameter K_1 (or equivalently C_t) which are less than 1. Fig. 3.2[3] shows these

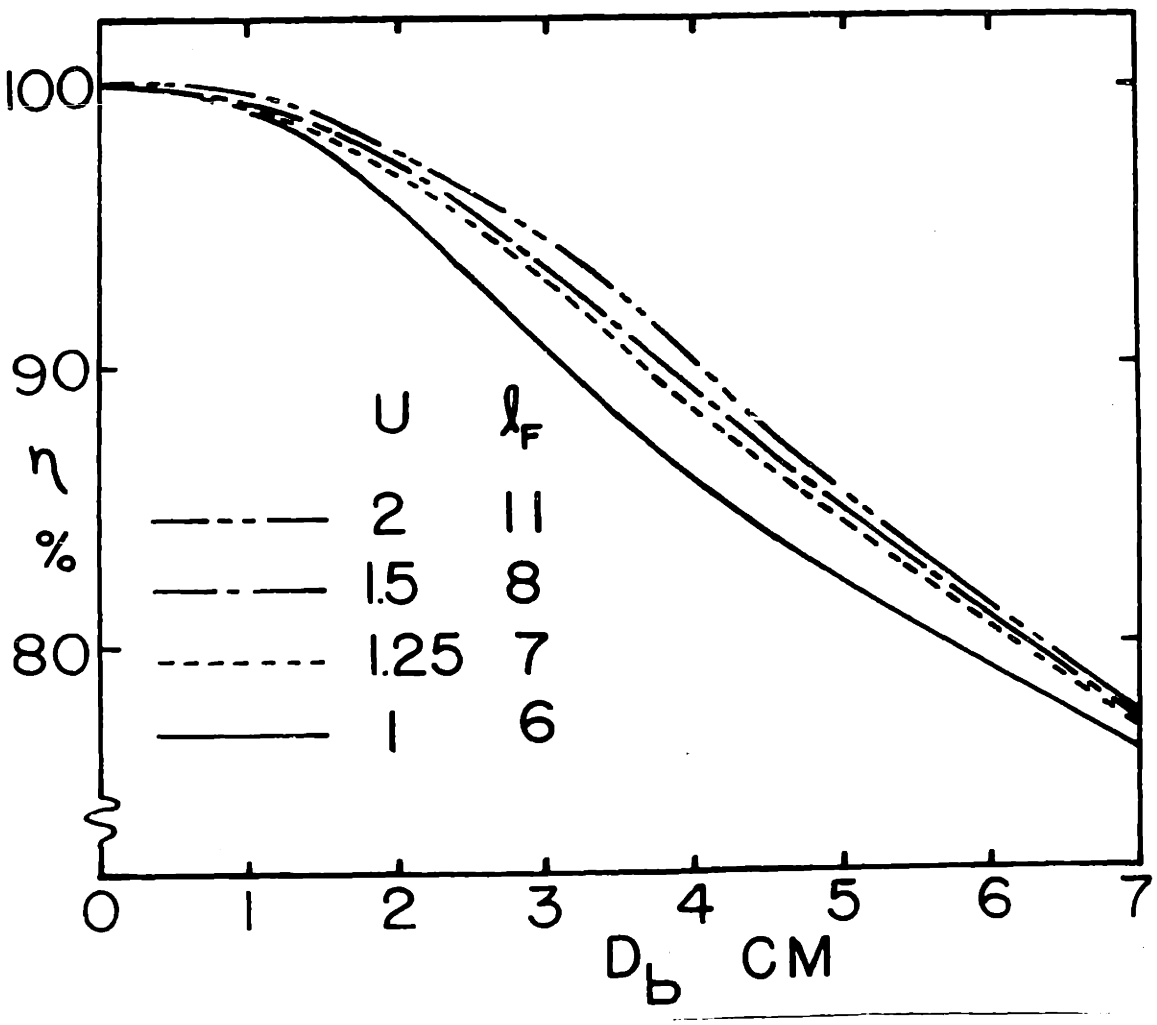

Figure 3.2 Asymptotic efficiency as a function of bubble diameter for a bed of 1 mm diameter glass beads with experimentally determined l_{mf} = 5 cm, U_{mf} = .53 m/sec.

asymptotic values for typical beds as a function of bubble diameter D_b. Large bubbles are seen to have a serious detrimental effect on collection performance.

c. Extension of Models to Include Aerosol Size Polydispersity

The previous models were derived for collection of monodisperse aerosols. They can be simply extended to model the collection of polydisperse aerosols. Polydisperse aerosols are usually characterized by a continuous size distribution function of the mass or number of particles. It is convenient to introduce the size frequency distribution function $\gamma(a)$ where $n\gamma_n(a)da$ or $m\gamma_m(a)da$ is the number or mass of particulate in the size interval a to a + da, respectively. Particle size can be measured in many ways. For present purposes we will take a to be the particle radius for assumed spherical particles. The total number (n) or mass (m) of aerosol particles per unit volume is then used to normalize the distribution function.

$$1 = \int_0^\infty \gamma_n(a)da$$

$$1 = \int_0^\infty \gamma_m(a)da \qquad (3.14)$$

The critical assumption used here in dealing with polydispersity is that individual aerosol particles act independently of each other. For systems where adhesion is guaranteed, this is equivalent to assuming that the spacing between aerosol particles in the gas is very large. As a worst case example consider an aerosol of small 1 μm radius fly ash particles with a rather high mass loading m of 10 gm/m^3. The number density of this aerosol is then

$$\eta = \frac{m}{\frac{4}{3}\pi\rho_p d^3} \tag{3.15}$$

Typically, for fly ash $\rho_p = 2.5 \times 10^3$ kgm/m^3 so

$$\eta \approx 10^{12} \frac{\text{particles}}{m^3} \tag{3.16}$$

and the spacing between particles is about 10^{-4} m or about 100 particle radii. Our assumption of aerosol particle independence appears to be well-founded.

The superposition of collection of a polydisperse aerosol then follows easily since we can now assume that each size particle is collected as if it were the only one present. Extending the application of Eq. (3.8), the collection efficiency as a function of aerosol particle size becomes

$$\eta(a) = 1 - \exp\left(-\frac{3}{4}(1-\varepsilon_o)C_t(a)\frac{\ell_o}{R}\right) \tag{3.17}$$

where $C_t(a)$ is the single particle collection efficiency for particulate of radius a. The assignment of values for $C_t(a)$ will be taken up in a subsequent section.

The overall mass or number efficiency can then be found directly

$$\eta_{\substack{\text{mass}\\\text{overall}}} = 1 - \frac{\int_0^\infty m_o \gamma_{mo}(a)da}{\int_0^\infty m_i \gamma_{mi}(a)da}$$

$$= 1 - \frac{\int_0^\infty m_i \gamma_{mi}(a)(1-\eta(a))da}{m_i} \tag{3.18}$$

$$= 1 - \int_0^\infty \gamma_{mi}(a)da + \int_0^\infty \gamma_{mi}(a)\eta(a)da$$

$$\eta_{\substack{\text{mass}\\\text{overall}}} = \int_0^\infty \gamma_{mi}(a)\eta(a)da$$

Similarly,

$$\eta_{\substack{\text{number}\\\text{overall}}} = \int_0^\infty \gamma_{ni}(a)n(a)da \tag{3.19}$$

2. Single Bed Particle Collection Models

a. Local Gas Flow Models

Micro-collection models can be approached analytically provided the gas flow in the vicinity of the bed particle is well defined. It is likely that no one flow model can account for all conditions to be encountered in a chaotic system like a fluidized bed. Generally though the fluid flow will be governed by the Navier-Stokes equation for a Newtonian fluid of constant density ρ_g and viscosity μ.

$$\rho_g \frac{D\bar{u}}{Dt} = \rho_g\bar{g} - \nabla P + \mu\nabla^2\bar{u} \tag{3.20}$$

where $\bar{u}$ and P are the velocity and pressure field respectively and $\bar{g}$ the gravitational acceleration. Regimes of behavior for incompressible adiabatic flows are usually demarcated by the Reynolds number. For isolated spheres of radius R in a flow with uniform far velocity U and fluid kinematic viscosity $\upsilon = \mu/\rho_g$ this number is defined as

$$Re = \frac{2UR}{\upsilon} \tag{3.21}$$

In general, for low values of the Reynolds number, the flow is laminar and dominated by viscosity, while for high values it is turbulent and dominated by inertia. Transition values however usually depend on the specific geometry of the problem.

For analysis of micro-collection, it is easiest to model the flow as that of an isolated sphere in an infinite uniform flow. With this

geometry two limiting cases give exact analytical solutions. The low Reynolds number regime (Re << 1) implies that the inertial forces are negligible and the simplified form of the Navier-Stokes equation applies

$$\nabla p \cong \mu \nabla^2 \bar{u} \tag{3.22}$$

Then the velocity components are

$$\begin{aligned} u_r &= U_\infty \left[1 - \frac{3}{2}\left(\frac{R}{r}\right) + \frac{1}{2}\left(\frac{R}{r}\right)^3\right] \cos\theta \\ u_\theta &= -U_\infty \left[1 - \frac{3}{4}\left(\frac{R}{r}\right) - \frac{1}{4}\left(\frac{R}{r}\right)^3\right] \sin\theta \\ u_z &= U_\infty \left[1 - \frac{1}{4}\frac{R}{r}\left(3 + \frac{R^2}{r^2}\right) + \frac{3}{4}\left(\frac{R^2}{r^2} - 1\right)\cos^2\theta\right] \end{aligned} \tag{3.23}$$

where U_∞ is the uniform flow far from the sphere. The corresponding stream function defined in the usual way is

$$\Psi = -\frac{1}{2} U_\infty R^2 \left|\left(\frac{r}{R}\right)^2 - \frac{3}{2}\left(\frac{r}{R}\right) + \frac{1}{2}\left(\frac{R}{r}\right)\right| \sin^2\theta \tag{3.24}$$

The coordinate system is shown in Fig. 3.3.

When the Reynolds number is high, viscosity is ignored with respect to inertia and the following solution results.

$$\begin{aligned} u_r &= U_\infty \cos\theta \left[1 - \frac{R^3}{r^3}\right] \\ u_\theta &= -U_\infty \sin\theta \left[1 + \frac{1}{2}\frac{R^3}{r^3}\right] \end{aligned} \tag{3.25}$$

and

$$\Psi = -\frac{1}{2} U_\infty r^2 \sin^2\theta \left(1 - \frac{R^3}{r^3}\right) \tag{3.26}$$

This expression though, does not truly model the high Reynolds number flow because of the onset of turbulence in the form of wakes behind the sphere.

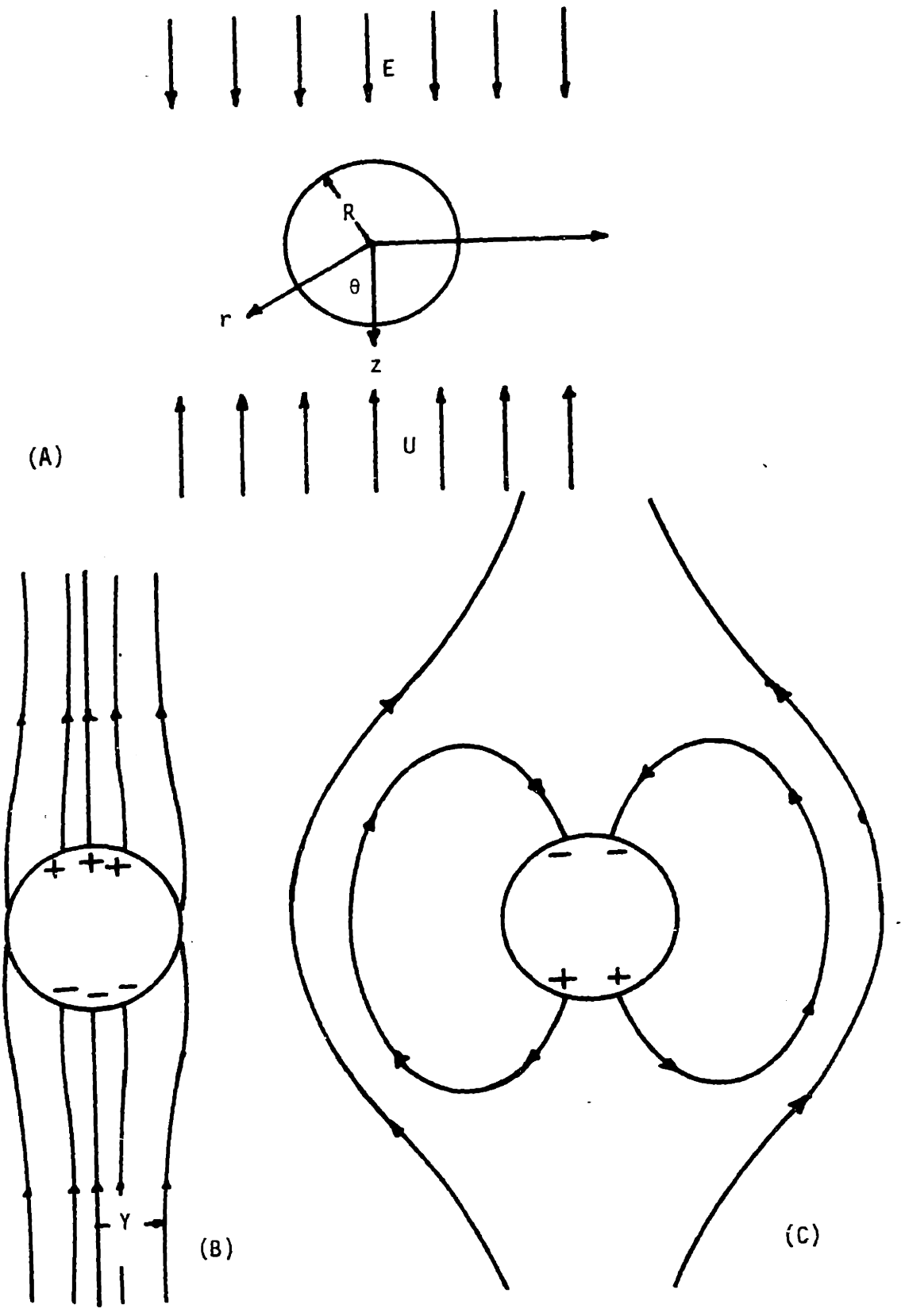

Figure 3.3 Flow model for collection on an isolated bed particle.

However, it is a good model for the flow structure on the incident face of the sphere.

These models must be used carefully if used at all bacause they completely ignore the effect of surrounding bed particles on the flow. Flow models incorporating these effects have been proposed by Happel[4] and Kuwabara.[3] In these the effects of surrounding bed particles were modeled by assuming each sphere in the assemblage of spheres (the bed) to be centered in a spherical unit cell of radius R_o (see Figs. 3.4 and 3.5). The size of the unit cell is determined such that the fraction voids ε in the unit cell is the same as that for the bed ε_b it models. Thus

$$\varepsilon_b = 1 - \left(\frac{R}{R_o}\right)^3 \tag{3.27}$$

The disturbance of the uniform incident flow due to each sphere is contained entirely within that sphere's unit cell. The Navier-Stokes equation then applied in the unit cell region with the assumed boundary conditions of "no slip" at the surface of the particle, continuity of streamlines and no shear stress ($\tau_\theta = 0$) at the unit cell boundary, which are consistent with the assumption of independence of disturbances due to each sphere. A more complete analysis is shown elsewhere[6], where the solution in the limit $Re \to 0$ is

$$\Psi_i = -\frac{1}{2} U_\infty r^2 \sin^2\theta \left| A\left(\frac{R}{r}\right) + B\left(\frac{r}{R}\right) + C\left(\frac{r}{R}\right)^2 + D\left(\frac{r}{R}\right)^4 \right| \tag{3.28}$$

Which is valid inside the unit cell $R \leq r \leq R_o$.

$$A = \frac{1}{\Delta}, \quad B = \frac{-3-2K^5}{\Delta}, \quad C = \frac{2+3K^5}{\Delta}, \quad D = \frac{-K^5}{\Delta} \tag{3.29}$$

$$K = \frac{R}{R_o}; \quad \Delta = 2-3K+3K^5-2K^6$$

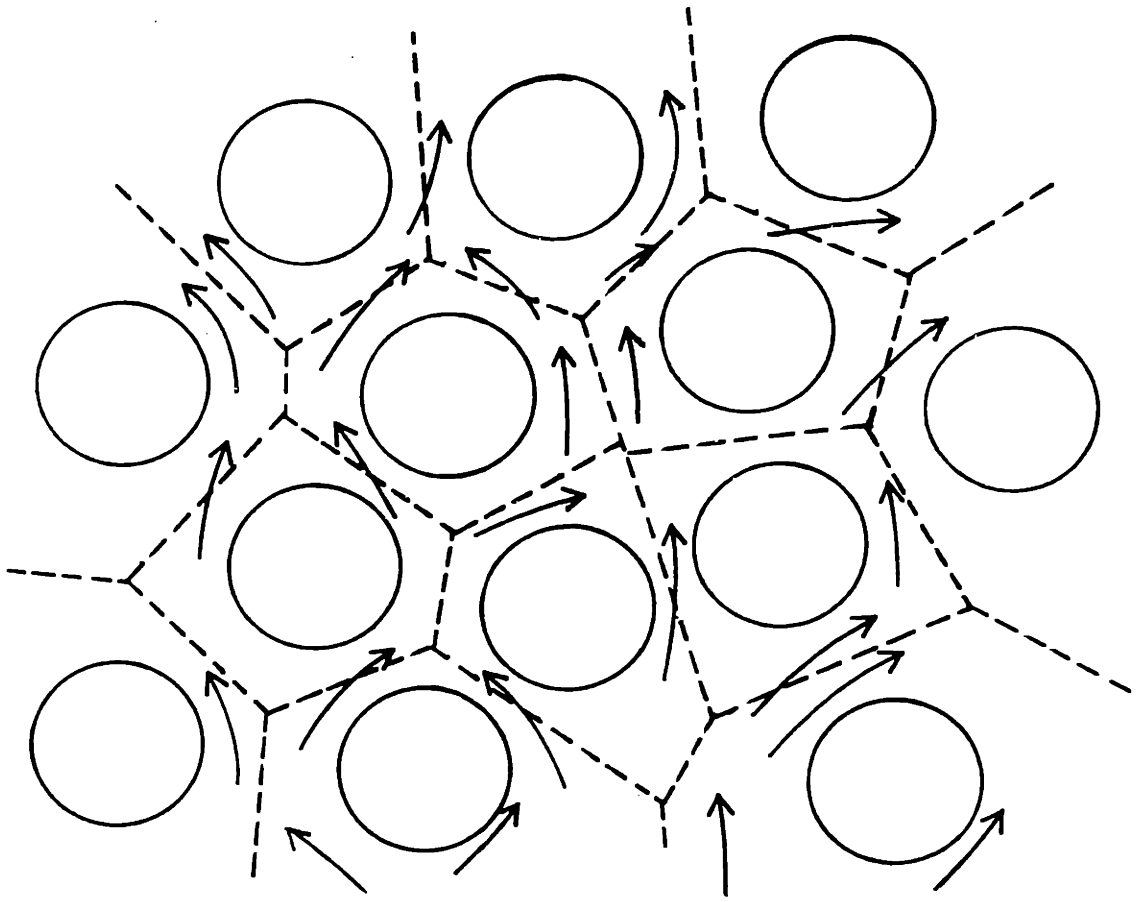

Figure 3.4 Unit cells in fluidized bed.

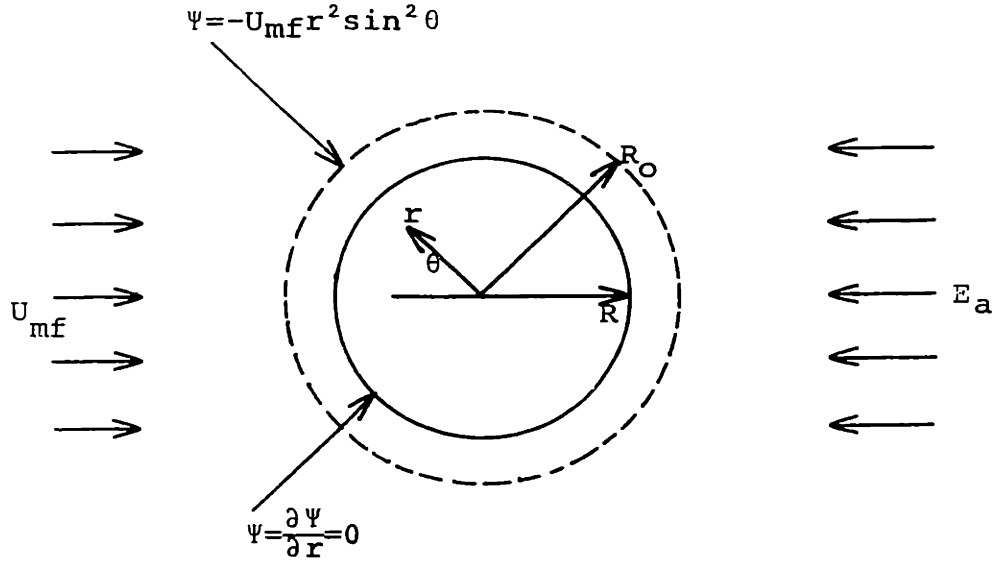

Figure 3.5 Unit cell spherical geometry, field and flow.

For finite Reynolds numbers this model has been solved analytically by Hamielec and LeClair[26], but is difficult to use because it is not a closed form solution.

With these models in hand we can proceed to try to find the one or ones most appropriate for the various collection mechanisms in the bed. At the onset we would expect the flow structure to be determined by the Reynolds number. For beds which may be encountered in any forseeable application, (particle radii of about 0.1 to 3 mm) Reynolds numbers would range from about 10 to 1000. Several workers[7,8,9] have determined experimentally that gas flow in packed and fluidized beds changes from laminar to turbulent for Reynolds numbers of 100-150. How the turbulence manifests itself is another story though. For isolated spheres, as the Reynolds number is increased the formation of vortex wakes and the shedding of these vortex wakes is observed. But in closely packed beds, there is no room for such vortices and turbulence probably appears as the shedding of smaller local wakes which are quickly dissipated. It is also likely that as Reynolds number is increased, the phenomenon of jetting occurs.

Zahedi[3] has postulated, based on work by Ranz and others, that due to the constricted gas flow channels in the bed, actual local gas flow velocities may be as much as 10 times[10] as great as as the superficial velocity. It is now believed that the effect this jetting has on collection mechanisms is a function of the flow Reynolds number. For low Reynolds number flows where viscosity dominates, we expect that the localized jetting would be damped out by the gas viscosity before it "impinges" on the following particle. For high Reynolds numbers, where inertia dominates, we expect the jet to impinge on the following particle as essentially a free jet would. For intermediate ranges of the

Reynolds number we would expect the jet to be damped somewhat and impinge on the following particle with effectively intermediate velocities. In this way, we can see how the effective incident fluid velocity on a bed particle can vary from about 1 to 10 times the superficial velocity.

The proper choice of flow model depends not only on the Reynolds number of the flow, but also on the collection mechanism at work. Different mechanisms effectively impart their forces at different locations about the particle. For example, inertial impaction would be expected to act at the incident face of the bed particle while diffusion would seem to act at the side of the bed particle where fluid flow lines pass closest to the bed particle. These matters will be discussed at greater length in the sections on the individual collection mechanisms.

b. Collection Mechanisms

It only remains now to specify the single particle collection efficiencies $C_t(a)$ to complete our model of packed and fluidized bed collectors. Much work has been done on collection of aerosols by spheres and cylinders assuming the various types of flow models previously presented. This work will be presented as a review with comments as to the applicability of the models proposed. The inertial impaction mechanism is the least well understood in the literature and was the subject of detailed experimental studies here. The experiments and associated model will then be presented.

Diffusion

Particulate is collected on bed particles by their random diffusional motion as is prescribed by its diffusivity D. In general, particulate diffusivities increase as particle size decreases as given by the Stokes-Einstein relation[11]

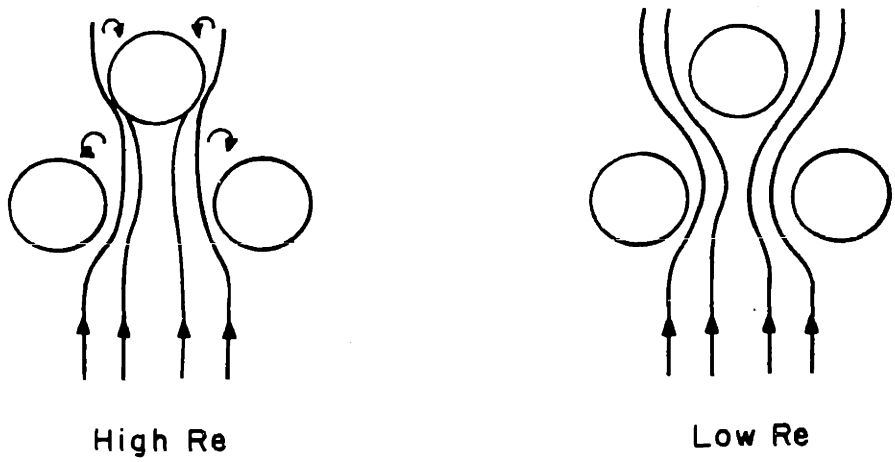

Figure 3.6 Jetting model

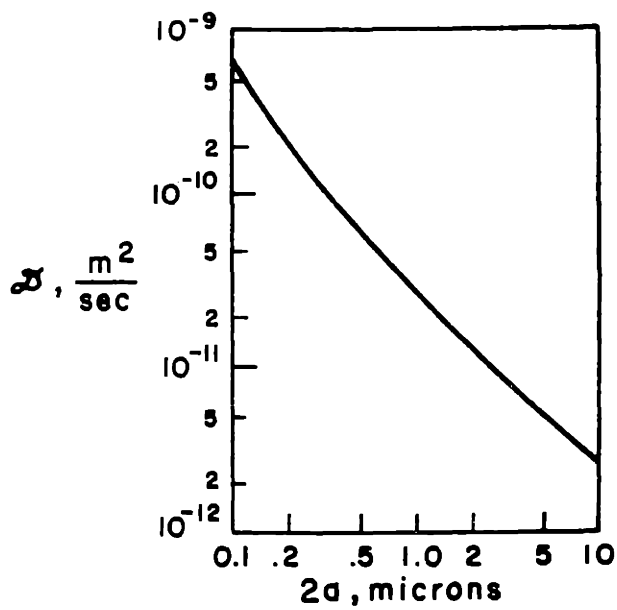

Figure 3.7 Diifusivity of unit density sphere in air.

$$D = \frac{KT}{6\pi \eta_a a} \left[1 + \frac{\lambda}{a}\left[1.26 + 0.4 \exp(-1.10\ a/\lambda)\right]\right] \qquad (3.28)$$

where K is the Boltzman constant, T the absolute temperature and λ the gas molecule mean free path (see Fig. 3.7).

The diffusional collection mechanism can be derived analytically if a representative flow model can be determined. It reduces to solving the convective diffusion equation

$$\frac{\partial n}{\partial t} + \bar{u} \cdot \nabla n = D\nabla^2 n \qquad (3.29)$$

where n is the number density of the particulate. Levich[12] solved for the diffusion to an isolated sphere in an infinite creeping (Re → 0) flow by assuming a thin diffusional boundary layer. This is equivalent to an assumption of Pe >> 1 where the Peclet number is defined as Pe = 2RU/D. He finds for the single particle diffusional collection efficiency

$$C_D = 4.03\ (Pe)^{-2/3} \qquad (3.30)$$

Stairmand[13] found the efficiency for a particle in an infinite ideal inviscid flow to be

$$C_D = (8)^{1/2}\ (Pe)^{-1/2} \qquad (3.31)$$

By assuming the Happel unit cell flow model, Alexander[6] found the creeping flow (Re → 0) diffusional boundary layer (Pe → ∞) approximation to give

$$C_D = 3.54\ (A + C + 6D)^{1/3}\ (Pe)^{-2/3} \qquad (3.32)$$

where A, C, and D are the constants of Eq. (3.29) which result from the flow model. Pfeffer and Happel[14] solve the same problem numerically at finite Reynolds numbers and results are shown in Fig. 3.8. In the limit where Pe → ∞, and Re → 0 the agreement is good with Alexander's analytical result.

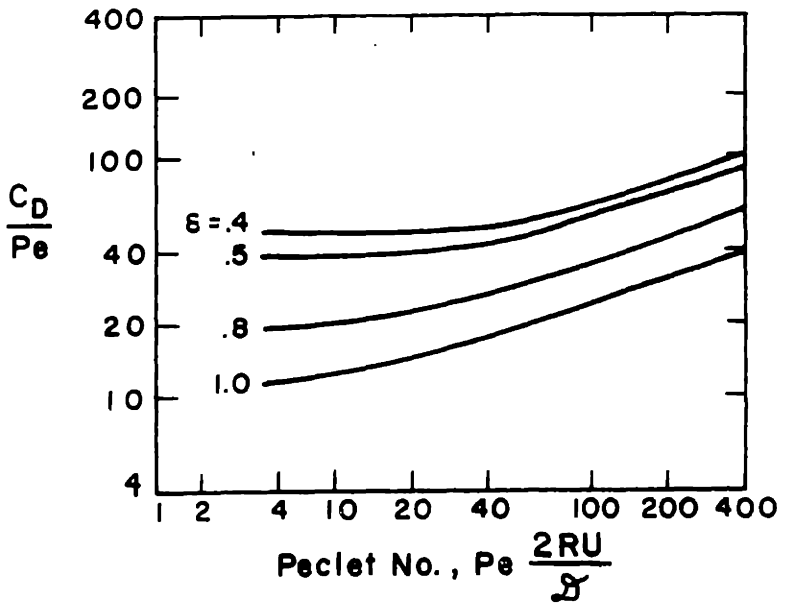

Figure 3.8 Single particle diffusional collection efficiencies vs. Peclet number using Happel flow model at moderate Reynold's numbers, from Pfeffer and Happel.

The choice of appropriate flow model is difficult and probably no one model is completely accurate. The diffusional mechanism would appear to cause particles to be mainly deposited on the sides (with respect to the flow direction) of the bed particles since this is the point of closest approach to the particle for fluid streamlines. This is also the point of highest tangential fluid velocities, so particulate concentration gradients would be greatest, and as a result collection is greatest. Also we only need concern ourselves with streamlines which pass very close to the bed particle in this region. For this mechanism the unit cell model would appear to be most appropriate as it reflects the presence of other particles in the bed. This shows up as an increase in velocity gradient near the particle. Also, this model would not be expected to model the flow well near the outer part of the unit cell where the spherical unit cell is a poor geometrical assumption. Rather the model is generally considered most accurate very near the particle surface where the details of the unit cell boundary geometry are not so important.

The best test of the proper choice of flow models is clearly experimental work. Experiments could be done with gaseous components diffusing to beds of particles, but the very large diffusivities of gaseous species precludes their use in meaningful experiments. As a result, experiments must be done with particulate matter diffusing to beds of particles. These experiments are plagued by lack of sufficient control of the aerosol properties (particularly size) and the confusion in results from the presence of other collection mechanisms. The best experimental results are found in the paper by Gebhart, Roth, and Stahlhofen.[15] They collected monodisperse aerosols of polystyrene spheres in packed beds of glass spheres. Aerosol size ranged from 0.1 to 2 μm, bead diameter from 0.0185 to 0.4 cm, superficial flow velocity from 0.7 to 17 cm/sec and bed depth to 41 cm. As usual, they found the aerosol size dependence of bed collection efficiencies

to have a minimum at typically 0.5 μm. Larger than this size, inertial impaction takes effect as the dominant mechanism, while below this diffusion becomes dominant. In this way they defined regimes where diffusion is dominant. In these diffusion regimes, they found that their data well correlated to the expression

$$\eta = 1 - \exp\left\{ - 6.39 \frac{D^{2/3} \ell_o}{U^{2/3} R^{5/3}} \right\} \tag{3.33}$$

Using our plug-flow macro-collection model, this implies that (with $\epsilon = 0.385$)

$$C_D = 13.85\ (Pe)^{-2/3} \tag{3.34}$$

with the Alexander model, using $\epsilon = 0.385$ to evaluate A + C + 6D we find

$$C_D = 11.4\ (Pe)^{-2/3} \tag{3.35}$$

The agreement is really quite good, considering the assumptions made in the Happel flow model and then the Alexander model. The agreement is certainly better than the uniform infinite flow models. It should be noted that the Gebhart et al. experiments are all in a rather low Reynolds number regime (Re < 75) where laminar flow is usually assumed in packed beds. It is possible that this model would break down at higher Reynolds numbers. Still, it is felt that the diffusion mechanism is fairly well understood and predictable.

Interception

Because aerosol particles have a finite diameter, even if they precisely followed streamlines around the bed particle, some of them would intercept the bed particle if the streamline passed within an aerosol particle radius to its surface. We would expect the effects of this mechanism to depend only on the interception parameter $N_R = a/R$ and the designated flow model.

For infinite potential and creeping flows around isolated spheres, Ranz and Wong[16] derived

$$C_{in} = (1 + N_R)^2 - \left(\frac{1}{1+N_R}\right) \quad \text{(potential flow)}$$
$$C_{in} = \frac{N_R}{2} + N_R^2 - \frac{1}{2}\frac{N_R}{1+N_R} \quad \text{(viscous flow)} \tag{3.36}$$

Using the Happel flow model for $Re \to 0$ we find that

$$C_{in} = N_R^2\left[\frac{A}{N_R} + BN_R + CN_R^2 + DN_R^4\right] \tag{3.37}$$

which for small values of N_R ($N_R << 1$) reduces to

$$C_{in} = (A + C + 6D)N_R^2 \tag{3.38}$$

Interception is not usually dealt with directly in the literature because its effect is small and are always experimentally overwhelmed by other mechanisms. However it is frequently treated as an effect to be considered in combination with other mechanisms.[17,18,19] In these cases it is treated as a modification to the boundary conditions of the solution of other problems; specifically, a theoretically infinitesimal aerosol particle need not intercept the bed particle surface to be collected, but need only pass within its actual radius of the bed particle.

For most of the work we are concerned with here; namely, micron or submicron aerosol collection by millimeter sized bed particles the interception parameter is quite small ($N_R \sim 10^{-3}$). Collection by interception and the augmentation of other mechanisms by interception is quite small for these low values of N_R.

Gravitational Settling

Because of its relative lack of importance gravitational settling is usually not studied in detail. Gravitation settling would be expected to have its greatesteffects on heavy particles be they either large or dense. For unit density 1 μm diameter spheres the settling velocity in still air is about 3×10^{-5} m/sec. If entrained in a gas flow of $U \approx 1$ m/sec flowing past a 1 mm diameter collecting sphere, they would move about 3×10^{-8} m. Clearly interception of the 0.5×10^{-6} m particle would dominate its gravitational settling. Similar comparisons with other mechanisms would show the same result. Only for very dense particles and low gas flow velocities would gravitational settling be important.

Calvert et al.[20] concludes in a summary paper that gravitational settling collection can be predicted by

$$C_G = \frac{U_t}{U_G} A_p \qquad (3.39)$$

where U_t is the terminal settling velocity of the particulate, U_G the gas superficial velocity, and A_p is the fraction of projected area of a single granule which is available for capturing the aerosol by settling. No data correlation is given here and none is available in the literature elsewhere.

Electrostatic

Electrostatic collection mechanisms, especially those pertaining to collection of charged particulate with electric fields imposed in the bed by means of electrodes, have been studied in depth by Zahedi. The details of the electrostatic force mechanisms depend on whether the particulate and or the bed particles are charged or uncharged and whether electric fields are imposed by means of electrodes or net charge buildups in the bed.

The charge on particulate is usually determined by its mechanism of formation. Freshly formed mists or fogs are uncharged. However, in minutes or hours these particles have been found to absorb charge from the atmosphere. Dusts are usually highly charged. These are usually formed by separation or dispersion from a solid or bulk state. Particles initially in contact with each other have small contact potential differences at their contact surfaces. Upon separation these potential differences give rise to particle charges. For fumes and smokes there are no corresponding charging mechanism as they are generally formed by condensation from the vapor phase. Fly ash is generally formed by condensation of the inorganics in coal which were vaporized in the flame region. Thus in its naturally occurring state, fly ash has no appreciable charge.

As will be pointed out, electrostatic collection mechanisms are usually only appreciable when the particulate is charged. As a result, corona charging regions are usually incorporated into electrostatic systems. This topic is discussed in the section on unique problems for EFB fly ash control.

Bed particles may be charged or partially charged through the action of any of several mechanisms. If the particles are sufficiently conducting, particles may become charged when a pair of contacting particles in an imposed electric field are separated. Each of the pair are oppositely charged. By this mechanism any given bed particle will change its amount and sign of charge many times as it collides and separates from other particles in the fluidized bed. Another mechanism results from the collection of the charged particulate. If the particulate is all charged to one sign, it may build up net charge of that sign on the collecting bed particle, provided that the charge relaxation time of the bed is longer than the charge build up time. This mechanism is usually not effective at charging bed particles as relaxation times are usually short compared to charge

build up times. The third mechanism is most prevalent. For highly insulating bed particles, patches of frictionally induced charge can exist on the particle surface. The resulting so-called bed micro-fields can be as large as imposed fields and can as a result be very important in collection. This case is typical of sand, glass, and other insulating bed particles at low temperatures ($T < 400°F$) and low humidities (r.h. < 60%).

Surprisingly, the theoretical determinations of electrically induced collection efficiencies are not sensitive to the flow models chosen. Zahedi[3,21] analyzes the collection efficiencies of charged (charge per particle Q) and uncharged ($Q = 0$) particles for charged (mobility b) and uncharged ($b = 0$) particulate. The results are summarized in Table 3.1. Two flow models were analyzed. The "laminar" flow model assumes either perfect viscous (Stoke's) or potential flow around a single isolated sphere. The locally mixed model recognizes the randomness of fluidized beds. In it, the flow is not really turbulent, but rather is laminar and unsteady in time and space. That is at any two given times or equivalent points in the bed the flow will be laminar but may have utterly different magnitudes and directions. The result of these stochastic processes is similar to a result obtained from modeling the flow as completely turbulent and "perfectly mixed" in terms of particulate concentrations.

Also, the collection of charged particulate on polarized bed particles with a laminar flow model is divided into co-flow - collinear (field and flow in same direction), co-flow - contralinear (field and flow in opposite directions) and cross-flow (field and flow at right angles) orientations (see Table 3.2). Alexander[22] showed that the first and last orientation give identical results and also that all three models give the same result when a Happel unit cell model is employed, rather than an isolated sphere model.

Zahedi[3] (see Fig. 3.9) shows extensive experimental results supporting

Table 3.1 Single particle collection efficiencies for charged and uncharged particulate on charged and uncharged bed particles.

	$Q = 0$	Q
$b = 0$	———	$\frac{a^2Q^2}{6\pi^3\varepsilon_o\mu R^5\eta U_o}$
b	$\frac{\eta q b}{\varepsilon_o \pi R^2 U_o}$	$\frac{Qb}{\varepsilon_o \pi R^2 U_o}$

Table 3.2 Single particle collection efficiencies for charged particulate on polarized bed particles,

Geometric Model	Happel Flow Model	Viscous Laminar Flow-Model	Potential Flow Model	Locally Mixed Model	Turbulent Model
Co-flow -- collinear	C_E	C_E	C_E	C_E	C_E
Co-flow -- contralinear	0	0	0	C_E	C_E
Cross flow	C_E	C_E	C_E	C_E	C_E

$$C_E = \frac{3\left(\frac{\epsilon}{\epsilon+2\epsilon_o}\right)bE}{1+\frac{U_o}{bE}}$$

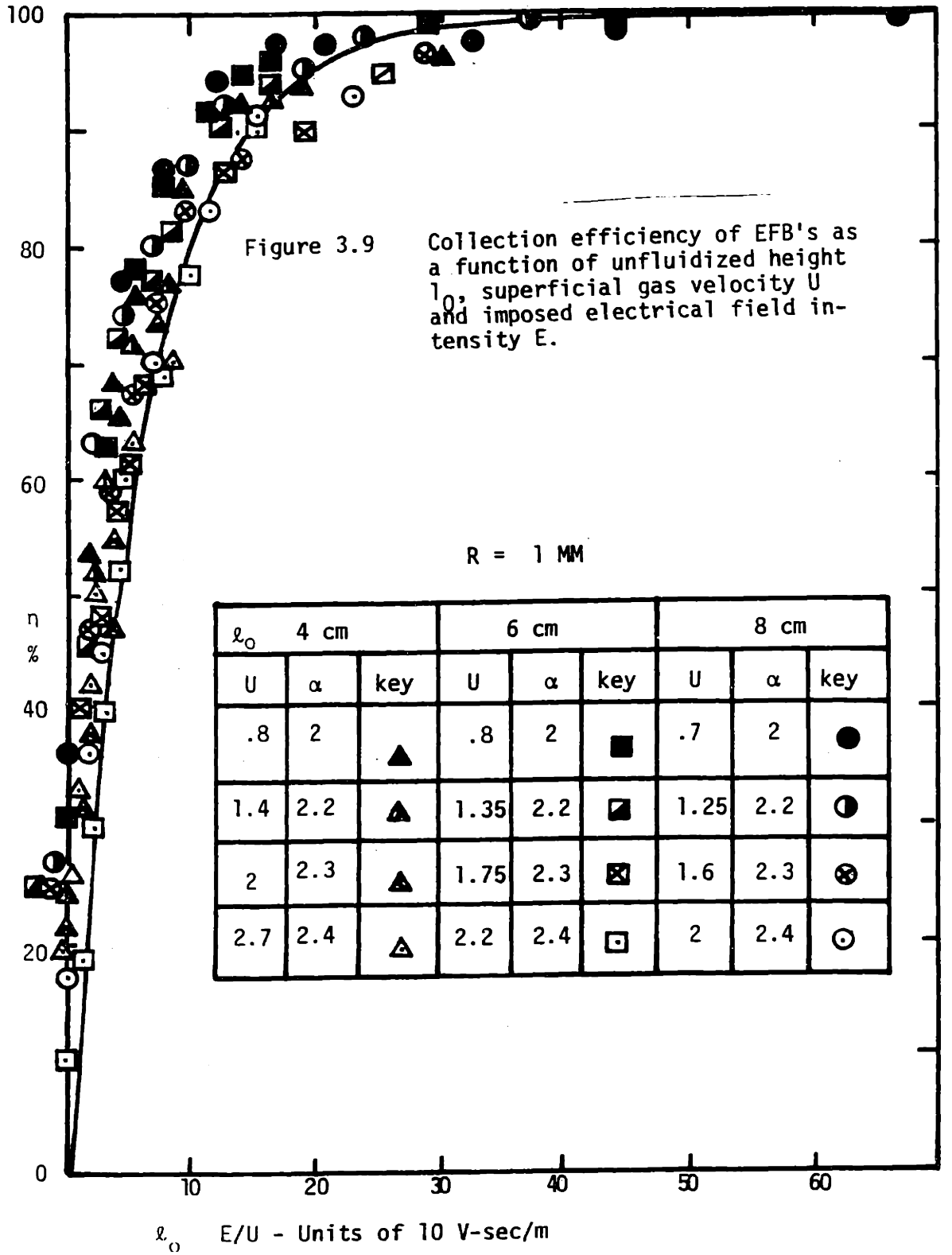

Figure 3.9 Collection efficiency of EFB's as a function of unfluidized height l_o, superficial gas velocity U and imposed electrical field intensity E.

R = 1 MM

ℓ_o	4 cm		6 cm			8 cm		
U	α	key	U	α	key	U	α	key
.8	2	▲	.8	2	■	.7	2	●
1.4	2.2	◭	1.35	2.2	◪	1.25	2.2	◑
2	2.3	▲	1.75	2.3	⊠	1.6	2.3	⊗
2.7	2.4	△	2.2	2.4	⊡	2	2.4	⊙

the locally mixed model for collection of charged particulate on polarized bed particles. Both the bubbling and plug-flow bed models are investigated and verified. Alexander[22] found that these same models apply for beds with alternating fields applied provided that the frequency of alternation is below a certain cutoff frequency f_c defined by the various parameters of the bed and particulate.

$$f_c = \frac{1}{2\pi}\sqrt{\frac{9\pi}{8}\left(\frac{\varepsilon}{\varepsilon+2\varepsilon_o}\right)\frac{sbE_o}{R}} \tag{3.40}$$

Below this frequency, collection is as given in the Zahedi models with E replaced by $2E_o/\pi$. As the frequency increases above this cutoff, the collection reduces monotonically. For beds typically encountered in these applications f_c is about 400 - 500 Hz.

Inertial Impaction

The mechanism of inertial impaction proves to be a dominant mechanism for collection of large or massive particulate. Analysis of inertial impaction usually begins by writing the forces which act on the particulate as it travels around the collecting particle in the fluid. If we ignore gravity, diffusion and electrostatic effects, the only force which acts to divert the particulate from straight line trajectories is viscous drag on it as it moves relative to the fluid. With coordinates as defined in Fig. 3.3 the particle equation of motion is

$$\frac{4}{3}\pi a^3 \rho_p \frac{d^2x}{dt^2} = F_x$$
$$\frac{4}{3}\pi a^3 \rho_p \frac{d^2z}{dt^2} = F_z \tag{3.41}$$

where F_x and F_z are the viscous drag forces given by

$$F_x = \frac{1}{2} C_D \rho_g (u_x - \frac{dx}{dt}) \pi a^2 |\bar{u} - \frac{d\bar{r}}{dt}|$$
$$F_z = \frac{1}{2} C_D \rho_g (u_z - \frac{dz}{dt}) \pi a^2 |\bar{u} - \frac{d\bar{r}}{dt}| \quad (3.42)$$

and where u_x and u_z are the fluid velocities. We have ignored y-directed components because they are equivalent to x components if the problem is cylindrically symmetric about the z axis as is assumed. We also assume that the drag can be described by the steady state Stoke's formulation (suitable for low Reynolds number, $Re_p = 2a[\bar{u} - d\bar{r}/dt]\ \rho_p/\mu_a$). Then the drag coefficient is

$$C_D = \frac{24}{Re_p} \quad (3.43)$$

We then obtain the following equations of motion

$$\frac{d^2x}{dt^2} = \frac{3}{4} \frac{C_D}{\cos \phi} \frac{\rho_p}{2a\rho_p} [u_x - \frac{dx}{dt}] (u_x - \frac{dx}{dt})$$
$$\frac{d^2z}{dt^2} = \frac{3}{4} \frac{C_D}{\sin \phi} \frac{\rho_p}{2a\rho_p} [u_z - \frac{dz}{dt}] (u_z - \frac{dz}{dt}) \quad (3.44)$$

Which reduce in dimensionless form to

$$\frac{d^2X}{dT^2} = \frac{1}{N_{STK}} (U_x - \frac{dX}{dT})$$
$$\frac{d^2Z}{dT^2} = \frac{1}{N_{STK}} (U_z - \frac{dZ}{dT}) \quad (3.45)$$

where

$$X = \frac{x}{R} \qquad U_z = \frac{u_z}{u_o}$$
$$Z = \frac{z}{R} \qquad T = \frac{tU_o}{R} \qquad N_{STK} = \frac{2a^2\rho_p U_o}{9\mu_a R} \quad (3.46)$$
$$U_x = \frac{u_x}{U_o}$$

It should be noted here that we have not specified any particular flow model. Thus, for any flow model the collection can be represented by an equation (Eq. (3.4.5)) which depends only on the Stoke's number N_{STK} defined in Eq. (3.46).

With any given flow model, the inertial impaction collection can be solved analytically. Usually this has been done numerically. Relationships for collection on isolated spheres are found in Green and Lane.[23]

$$C_{im} = \frac{N_{STK}^2}{(N_{STK} + 0.5)^2} \qquad \text{for potential flow}$$

$$C_{im} = \left| 1 + \frac{3}{4} \frac{\log (2N_{STK})}{N_{STK} - 1.214} \right|^2 \qquad \text{for viscous flow} \tag{3.47}$$

These equations are approximately fit to the numerical computations. Ranz and Wong[16] and Walton and Woodcock[24] have correlated many experimental results for single particle collection and find the best fit to closely resemble the potential flow solution

$$C_{im} = \frac{N_{STK}^2}{(N_{STR} + 0.7)^2} \tag{3.48}$$

Further the existence of a critical Stoke's number is predicted by Langmuir.[25] It is expected that below $N_{STR} = 0.083$, inertial impaction simply does not occur (for zero radius particulate).

Tardos, Gutfinder and Abuaf[18] use a numerical solution with the Kuwobara flow model to find the inertial impaction curves shown in Fig. 3.10. They also varied the interception parameter and the effect is seen to be important for large values of N_R. However, for our interests the impaction parameter is practically zero.

Tardos et al. do not show data to support their theory, so their work can only be taken for what it is. It is doubtful that the Kuwobara flow

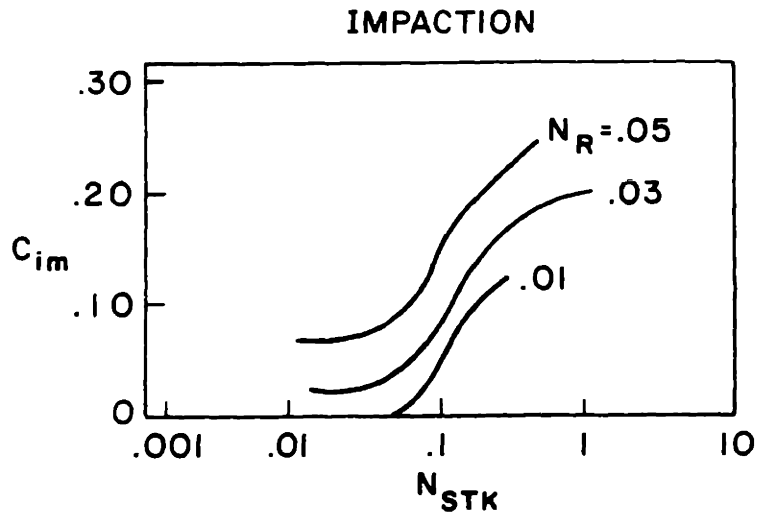

$$N_{STK} = \frac{2R^2 \rho_P U_0}{9\mu a} \; ; \; N_R = \frac{R}{a}$$

Figure 3. 10 Single particle collection efficiency by impaction vs. Stokes number as calculated by Tardos et al.

model will accurately represent the flow in packed and fluidized beds for inertial impacting collection because of the jetting effect. Instead, we would expect the isolated particle collection models to better predict the bed performance. But using theories requires a knowledge of the amount of jetting effects in the beds.

C. Theoretical and Experimental Studies

1. Inertial impaction Development of a Quantitative Model Predictive Capacity

An experimental program was undertaken to study in detail inertial impaction in packed and fluidized beds. Briefly the experiments were run as follows. A polydisperse aerosol of dioctylphthalate (DOP) was generated in an atomizer nebulizer and injected into the test channel where it was carried with its entraining air through a packed or fluidized bed. Fractional collection efficiencies by particle size were measured by an Andersen 2000 cascade impactor. The plots of collection efficiency vs. aerosol size showed regions which could be determined to be dominated by inertial impaction. Experimental points from this region were used for the inertial impaction correlations. By using the appropriate bed macro-collection model, these bed collection efficiencies could be transformed into single particle collection efficiencies (using Eq. 3.17) which could then be correlated with Stokes number.

a. Experimental Results

Several bed materials were tested including glass beads, white silica sand, N.J. #2 yellow sand and crushed bituminous coal. Varying states of fluidization were imposed varying from subfluidization packed beds, to fluidized, to highly fluidized and even to forced packed beds at superfluidization velo-

cities where retaining screen prevented fluidization. The mean sizes of the bed particles, superficial velocities, bed depths, and fluidization state of the tests are run are summarized in Table 3.3. Details of the experimental apparatus and procedures are given in Appendix A.

Fig. 3.11 shows the data in a raw form. Collection efficiency of the bed is plotted vs. aerosol diameter. The characterisitc shape predicted for this polydisperse aerosol in the previous section is well demonstrated. There is no region where diffusion is a strongly dominant mechanism because the test aerosol size distribution did not extend to small enough sizes. But the strong upward trend for larger sized aerosols provides several data points where inertial impaction could be considered dominant. These points will be used in the following discussion of the inertial impaction model.

Of special interest is the low collection efficiencies in the submicron range. It was difficult to correlate the data in these regions because it is likely that diffusion, interception and inertial impaction are all at work, and complicate by the presence or absence of jetting in some of the beds. The important fact is that submicron efficiencies are low. The electrostatic augmentation of submicron efficiency will be demonstrated in the next section.

b. Theoretical Development of the Model

The development of a meaningful model for inertial impaction was felt to be necessarily derived from experimental results. The complexity of the mechanism itself and of the variety of flow models which can be used for the beds in different modes of operation requires this. At the outset, it was expected that the choice of flow models should only depend on Reynolds number. Previous

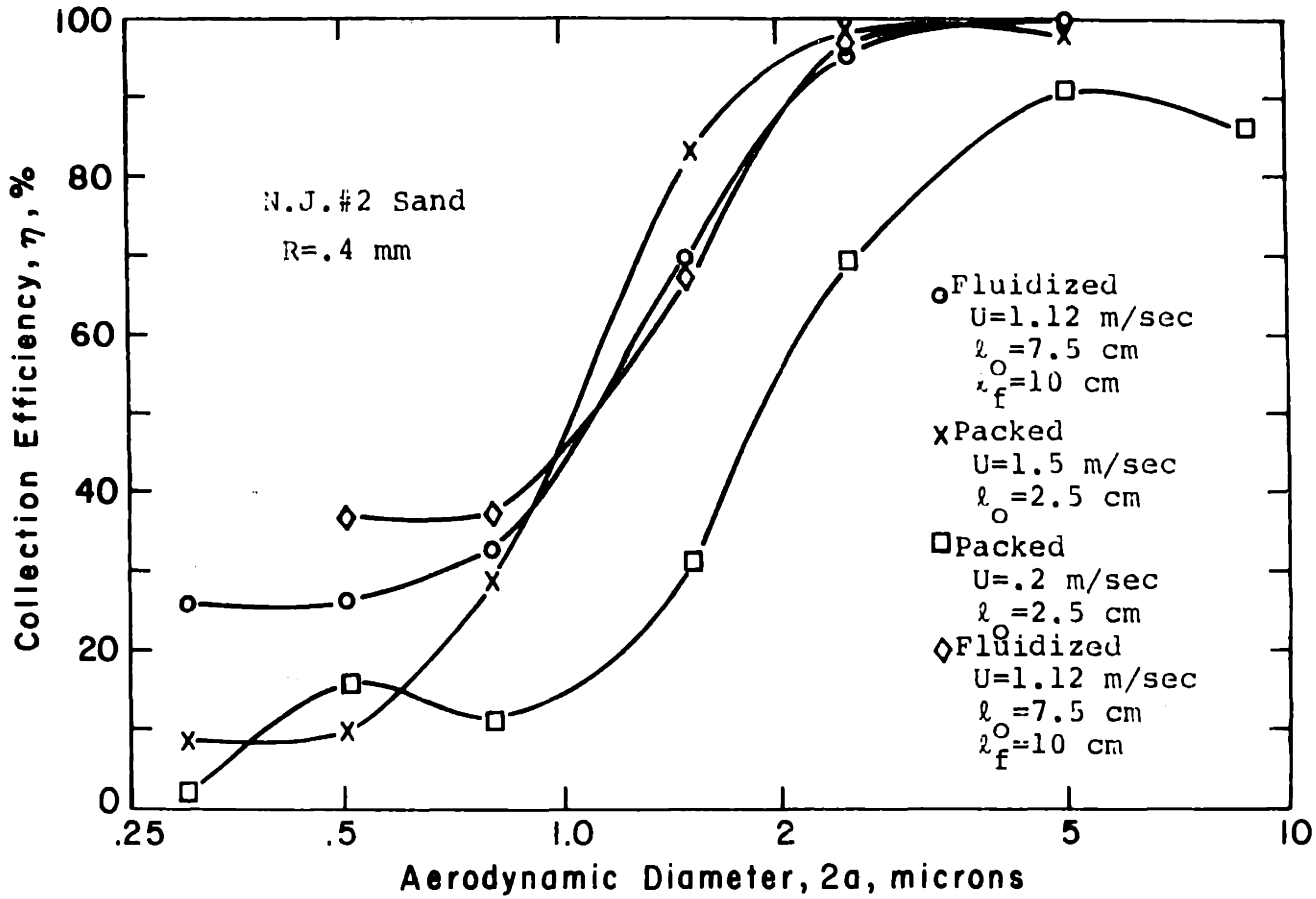

Figure 3.11 Data for fluidized and packed bed collection of polydisperse DOP aerosol. Test conditions as indicated on plots.

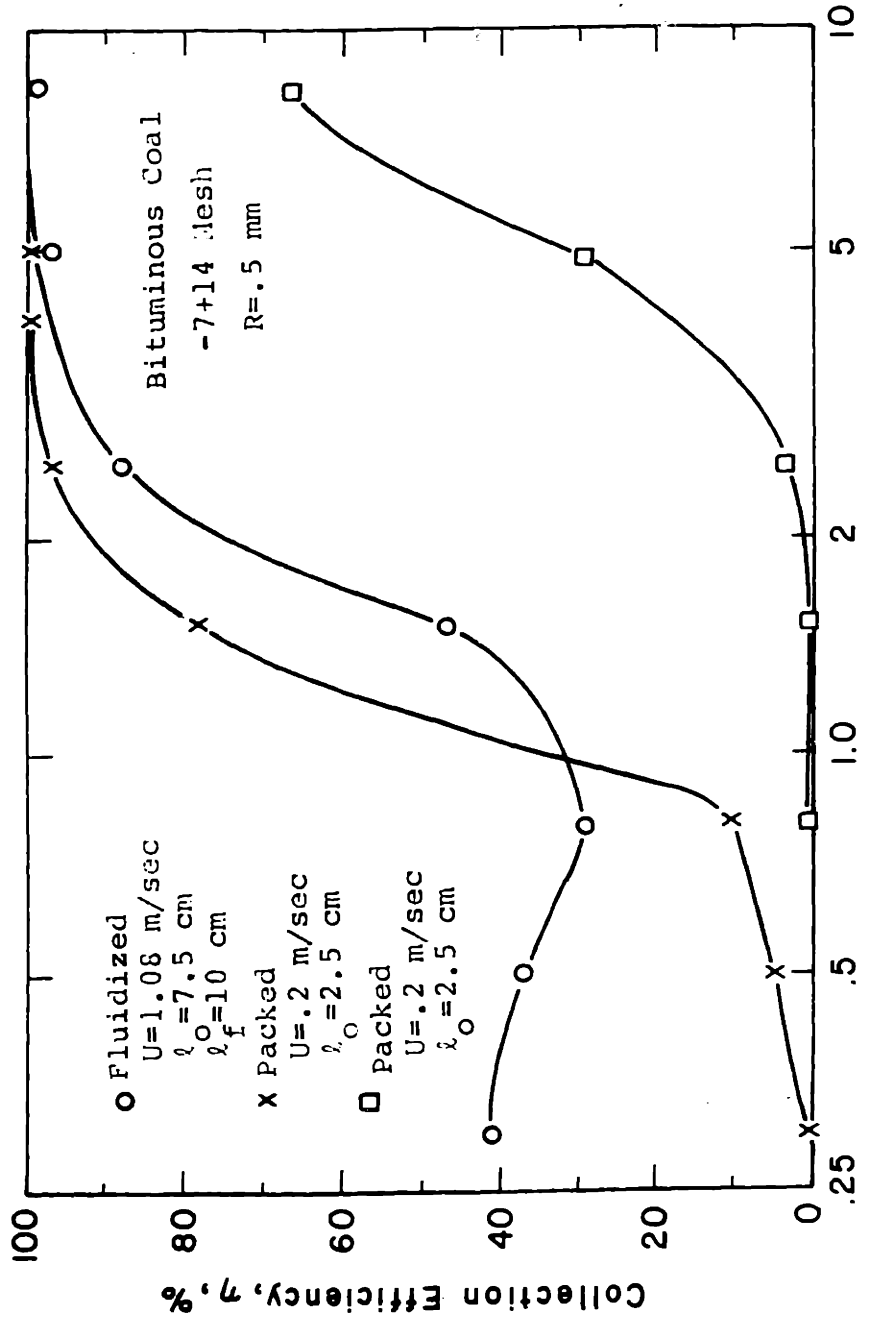
Collection Efficiency, η, %
Aerodynamic Diameter, 2a, microns
Bituminous Coal
-7+14 Mesh
R=.5 mm
o Fluidized
U=1.08 m/sec
ℓo=7.5 cm
ℓf=10 cm
x Packed
U=.2 m/sec
ℓo=2.5 cm
□ Packed
U=.2 m/sec
ℓo=2.5 cm
0
20
40
60
80
100
.25
.5
1.0
2
5
10

Figure 3.11

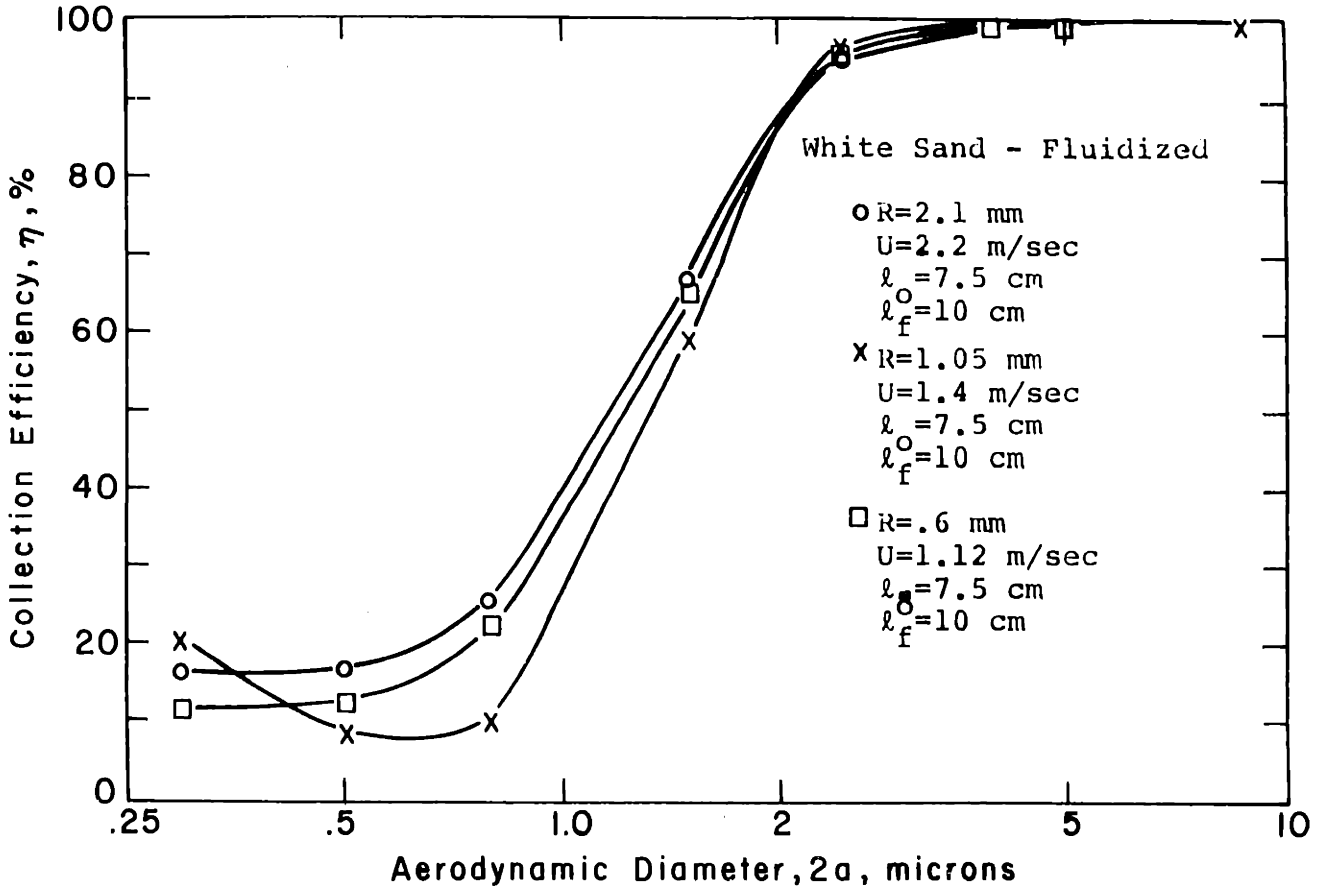
100
80
60
40
20
0
Collection Efficiency, η, %
.25
.5
1.0
2
5
10
Aerodynamic Diameter, 2a, microns
White Sand - Fluidized
o R=2.1 mm
U=2.2 m/sec
ℓo=7.5 cm
ℓf=10 cm
X R=1.05 mm
U=1.4 m/sec
ℓo=7.5 cm
ℓf=10 cm
□ R=.6 mm
U=1.12 m/sec
ℓo=7.5 cm
ℓf=10 cm

Figure 3.11

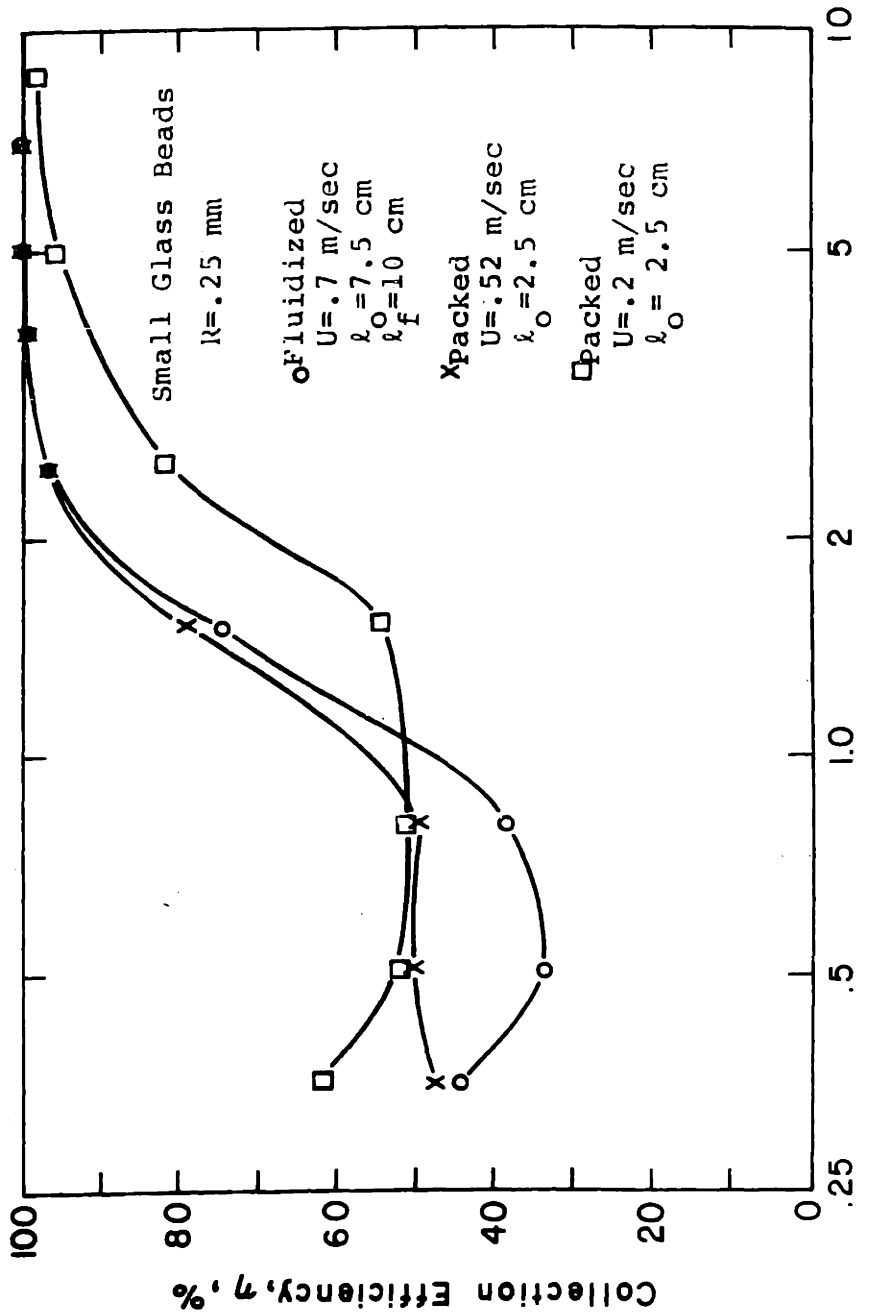
Small Glass Beads
R=.25 mm
Fluidized
U=.7 m/sec
ℓ_o=7.5 cm
ℓ_f=10 cm
Packed
U=.52 m/sec
ℓ_o=2.5 cm
Packed
U=.2 m/sec
ℓ_o= 2.5 cm
Collection Efficiency, η, %
Aerodynamic Diameter, 2a, microns
0
20
40
60
80
100
.25
.5
1.0
2
5
10

Figure 3.11

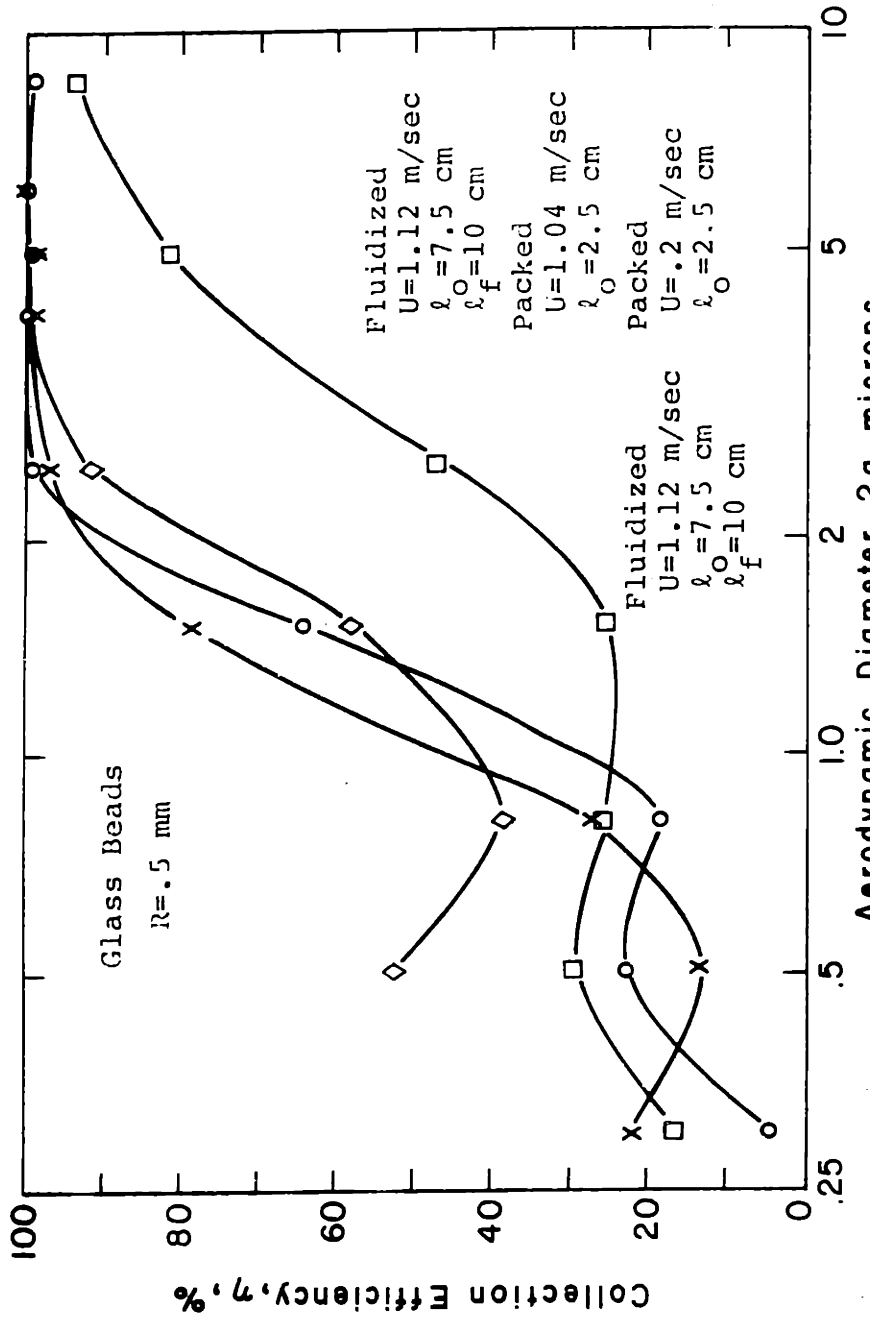
Collection Efficiency, η, %
100
80
60
40
20
0
.25
.5
1.0
2
5
10
Aerodynamic Diameter, 2a, microns
Glass Beads
R=.5 mm
Fluidized
U=1.12 m/sec
ℓ_o=7.5 cm
ℓ_f=10 cm
Packed
U=1.04 m/sec
ℓ_o=2.5 cm
Fluidized
U=1.12 m/sec
ℓ_o=7.5 cm
ℓ_f=10 cm
Packed
U=.2 m/sec
ℓ_o=2.5 cm

Figure 3.11

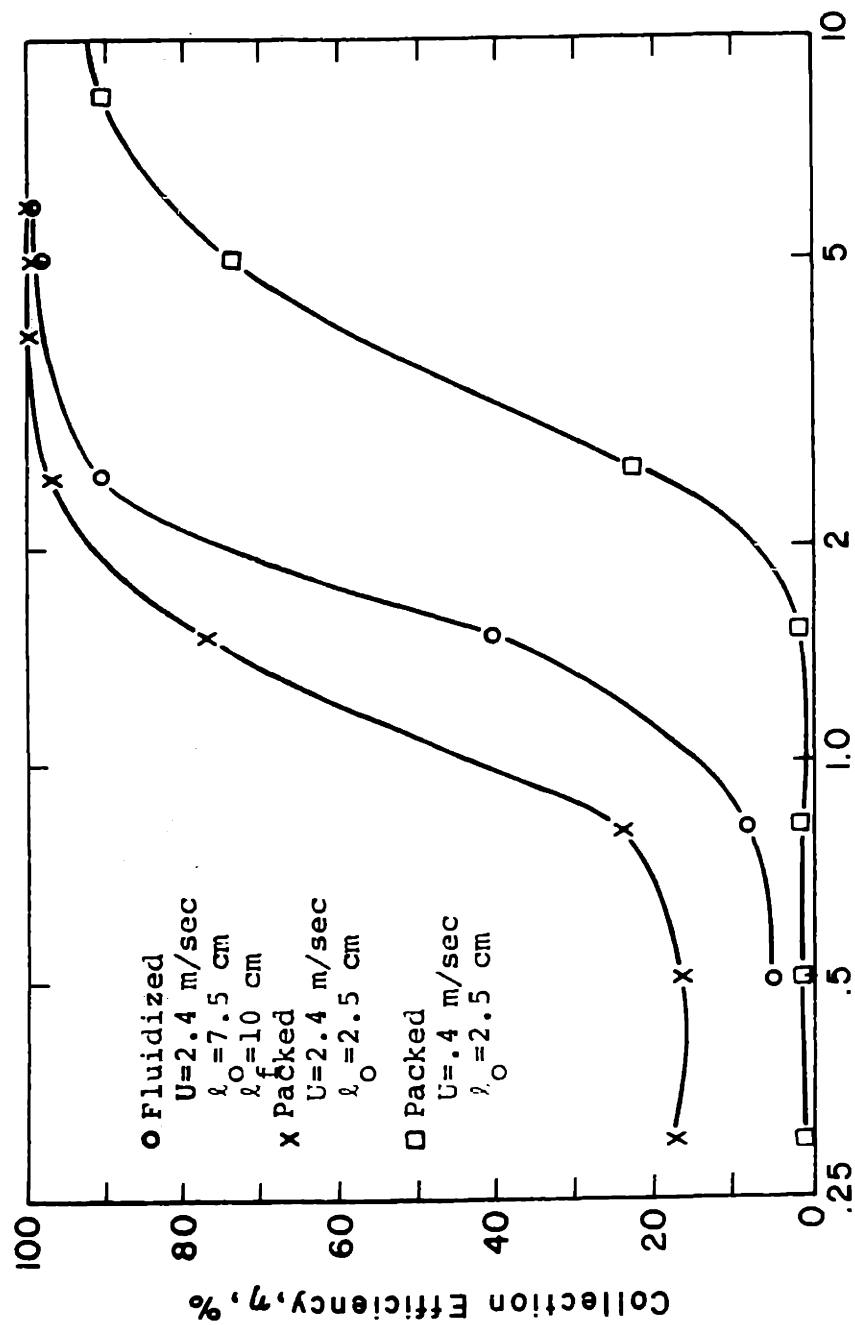
Collection Efficiency, η, %
100
80
60
40
20
0
.25
.5
1.0
2
5
10
Aerodynamic Diameter, 2a, microns
o Fluidized
U=2.4 m/sec
ℓ_o=7.5 cm
ℓ_o=10 cm
x Packed
U=2.4 m/sec
ℓ_o=2.5 cm
□ Packed
U=.4 m/sec
ℓ_o=2.5 cm

Figure 3.11

work [7,8,9] showed that the flow in packed beds became turbulent when the Reynolds number reached about 150. It is then likely that a viscous flow model (most likely the Happel model) would apply for Reynolds numbers below this, while an inertial model (potential flow) would apply for Reynolds numbers above this.

The most widely accepted model for inertial impaction is that of Ranz and Wong[16] for collection of particulate from free jets on isolated spheres. Collection by this mechanism deposits particulate on the forward surface of the collecting sphere. A free jet as it impinges on the sphere's surface is usually described by potential flow models. We propose here a model for inertial impaction in packed and fluidized beds where the single particle efficiency depends only on a Stakes number, in a way similar to the model of Ranz and Wong. Because gas flow patterns vary as the bed Reynolds number varies, we expect to have to modify the Stokes number to account for the jetting effect which we have previously mentioned. The Stokes number is conventionally expressed in terms of the superficial bed velocity U_o as $N_{STK} = \frac{2a^2 \partial P U_o}{9\eta R}$. We expect that as long as we are in the low Reynolds number viscous flow regime, that the flow velocity at any point in the bed is proportional to the imposed superficial velocity U_o. Inertial impaction will occur in a way we will assume to be analogous to that of a free jet on a sphere. Because we wish to assume that impaction depends on the Stokes number, but do not with to assume that the geometry is exactly like that of a free jet impinging on a sphere, we will state that

$$C_{im} = f(N_{STK}) \tag{3.50}$$

in the low Reynolds number regime where $f(N_{STK})$ is a yet to be determined function.

As the Reynolds number is increased, a point is reached where the flow becomes dissimilar. Essentially, jetting between bed particles is occurring as a result of the increasing importance of inertial terms in the Navier-Stokes equation describing the gas flow. Our key assumption in this model is that the function form of C_{im} dependence on N_{STK} is unaltered by the jetting (which really changes the geometry of the flow), except that the jetting causes an increased effective flow velocity. Let us make a hypothetical example to explain this. Suppose we choose some point (a) in the interstices of the bed where the local flow velocity is just equal to the superficial velocity when we are in the low Reynolds number regime.

$$U_a = U_o \qquad \text{for } Re < Re_c \tag{3.51}$$

As we increase the superficial velocity and the Reynolds number increases we expect this relation to hold true because the velocity field remians geometrically similar. Now, as we pass a critical Reynolds number Re_c where jetting begins to occur, our point may begin to experience velocity increases in excess of those that are due to the proportional increase with U_o. These are a result of the jetting and may be expressed as

$$U_a = \beta(Re)\, U_o \qquad \text{for } Re < Re_c \tag{3.52}$$

This "jetting factor" β is a function of Reynolds number. For low Reynolds numbers ($Re < Re_c$) it is defined to be 1 in order to match up with Eq. 3.51. For

higher Reynolds numbers, it is a monotonically increasing function of Re. Ranz[10] has shown from purely a geometrical stand point that for flows through closely packed beds of spheres, the maximum local flow velocity obtainable is 10.28 times the superficial velocity. As a result, we would expect that the jetting factor β would increase to a maximum value of 10.28 at some arbitrarily high Reynolds number where inertia completely dominates the flow.

Since turbulence begins to occur at Reynolds numbers of 150 we might expect this to be the point where β begins to deviate from 1, thus

$$R_e \cong 150 \qquad (3.53)$$

At some higher value of Re we would expect β to "saturate" at a values of about 10.

$$\beta(Re \to \infty) = 10 \qquad (3.54)$$

and we already have a fairly good rough estimate of how the β vs. Re curve should look.

To tie in with inertial impaction, suppose we let the functional form of Eq. (3.50) be sugh that the Stokes number is defined in terms of our flow velocity at point (a), namely U_a. Our assumption that this functional form of C_{im} dependence on N_{STK} does not change as the flow geometry changes allows us to state that the collection is determined by the local flow velocity U_a. Then, we define a "modified" Stokes number, N_{STK}, to include the dependence of U_a on Reynolds number.

$$N_{STK'} = \frac{2a^2 \rho_p U_o \beta(Re)}{9\eta R\ \varepsilon_v} \tag{3.55}$$

and we expect that the collection is

$$C_{im} = f(N_{STK'}) \tag{3.56}$$

where $\beta(Re)$ is some specified function.

The particulate size and mass density, bed particle size and gas viscosity were all well defined. For packed beds and uniformly fluidized (no visually apparent bubbles) the gas velocity was chosen to be U_o (the measured superficial volicity). For bubbling beds, the velocity was chosen to be U_{mf} (the minimum fluidization velcoity). This is in accodance with conventional bubbling bed theory where those values have been shown to be valid in the dense phase of the beds. Conventional Stokes numbers (without the jetting factor) were determined for all of these points.

The raw data of Fig. 3.11 were then analyzed using this general format. First, experimental points were chosen which clearly represented collection by inertial impaction. As explained in the following section of superposition of mechanisms, these points generally lie on the steep part of the collection efficiency curve. For each bed tested about three data points could be used, each representing a different aerosol size. Each data point was reduced from a total bed collection efficiency curve to a single particle efficiency C_{im} using the plug-flow macro-model and eq. 3.17

Stokes numbers were then identified with each point. The particulate size

and mass density, bed particle size and gas viscosity were all well defined. For packed beds and uniformly fluidized (novisually apparent bubbles) the gas velocity was chosen to be U_o (the measured superficial velocity). For bubbling beds, the velocity was chosen to be U_{mf} (the minimum fluidization velocity). This is in accordance with conventional bubbling bed theory where those values have been shown to be valid in the dense phase of the beds. Regular Stokes numbers (without the jetting factor) were determined for all of these points. For points corresponding to beds with Reynolds numbers less than 100, the data was plotted as C_{im} vs. N_{STK} (or equivalently $N_{STK'}$, since $\beta = 1$ for these points).

For points corresponding to beds with Reynolds numbers less than 100, the data was plotted directly as C_{im} vs. $N_{STK'}$. In the determination of $N_{STK'}$ it was assumed that $\beta = 1$ since we are well in the viscous flow regime. These data plotted in a consistent way and are shown by the filled-in symbols in fig. 3.12.

The remaining data, for Reynolds numbers greater than 100 were plotted as C_{im} vs. $N_{STK'}$ as follows. A preliminary plot, fig. 3.14 shows a direct presentation of C_{im} vs. $N_{STK'}$ with the jetting factor β always taken as being taken as being 1. This plot is equivalent to an attempt to correlate our data in a conventional to correlate our data in a conventional way without considering the jetting effect. The scatter is unacceptable for the degree of accuracy required to be useful. As a result, the jetting factor β needed to be incorporated into the modified Stokes number. To do so a best fit curve was numerically calculated for the low Reynolds number data.This curve is shown by the solid line in fig. 3.12. Then each set of data points corresponding to a given bed

Table 3.3 Bed Parameters For Inertial Impaction Experiments

	R(mm)	U(m/sec)	U_{mf}(m/sec)	l_o(cm)	l_f(cm)	ϵ_{vo}	ϵ_{vf}	Re	β
White sand-fluidized	2.1	2.2	-	7.5	10	.45	.59	1560	11
White sand-fluidized	1.05	1.4	-	7.5	10	.42	.56	260	5.0
White sand-fluidized	.6	1.12	.4	7.5	10	.45	-	53	1.0
Glass beads-packed	.25	.2	-	2.5	-	.39	-	13	1.0
Glass beads-packed	.25	.51	-	2.5	-	.39	-	33	1.0
Glass beads-fluidized	.25	.7	.3	7.5	10	.39	-	19	1.0
Glass beads-packed	.5	.2	-	2.5	-	.38	-	26	1.0
Glass beads-packed	.5	1.0	-	2.5	-	.38	-	132	2.2
Glass beads-fluidized	.5	1.12	-	7.5	10	.38	.53	105	1.0
Glass beads-packed	2.0	.4	-	2.5	-	.36	-	222	2.0
Glass beads-packed	2.0	2.4	-	2.5	-	.36	-	1330	10
Glass beads-fluidized	2.0	2.4	-	7.5	10	.36	.52	923	7.0

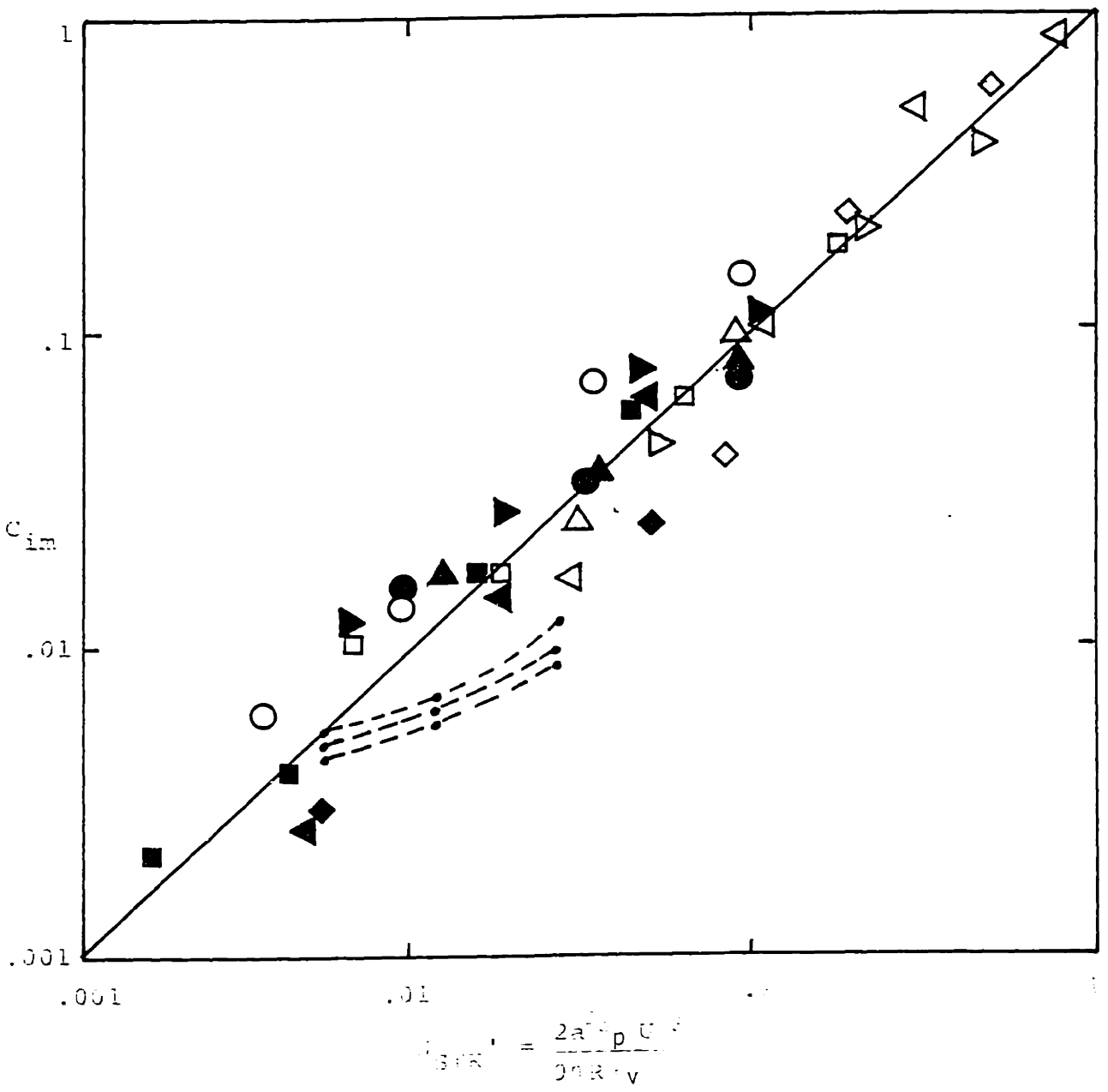

Figure 3.12 Experimental single particle efficiency vs. modified Stokes number.

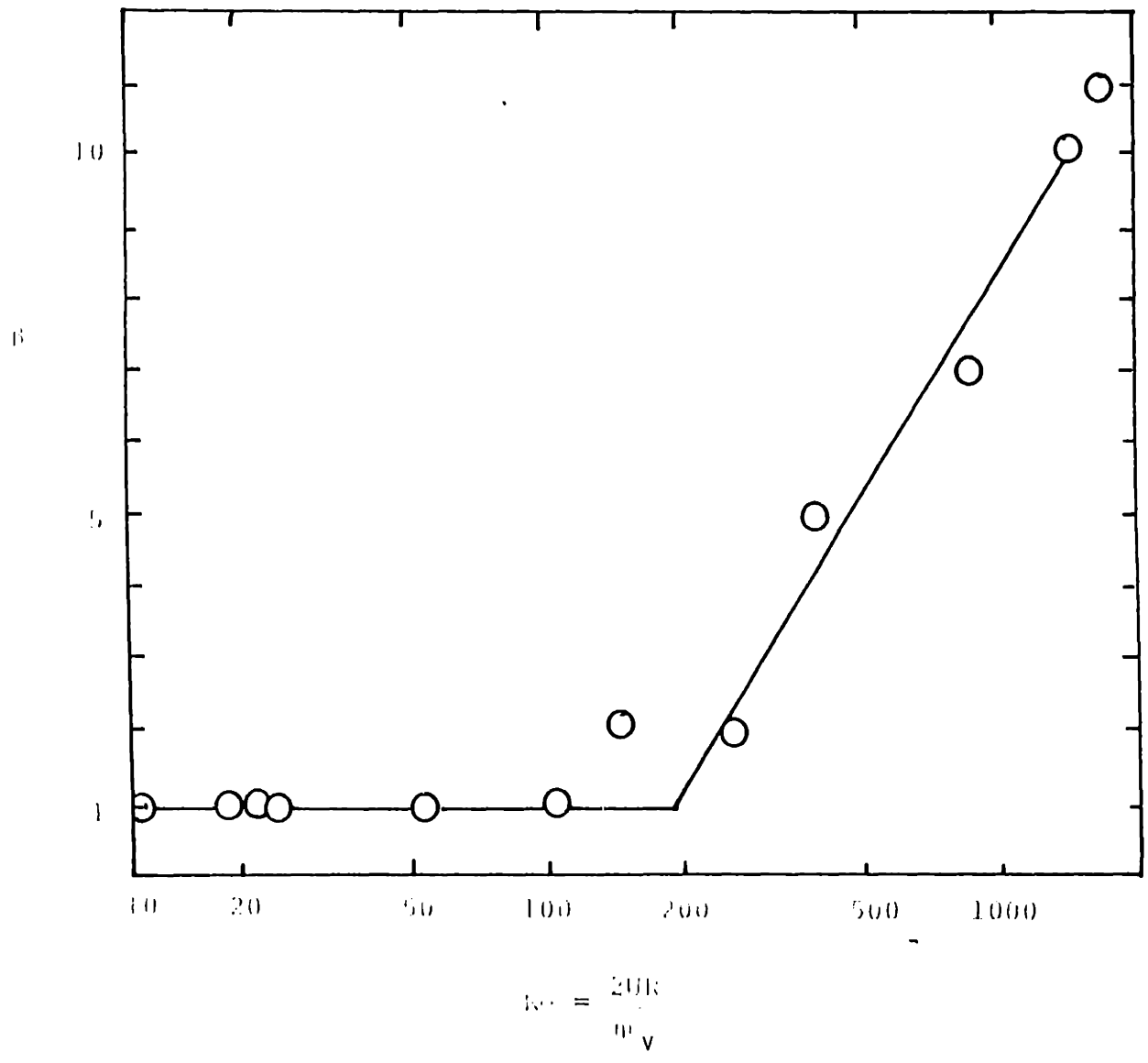

Figure V.1 Experimental jetting factor vs. Reynolds number

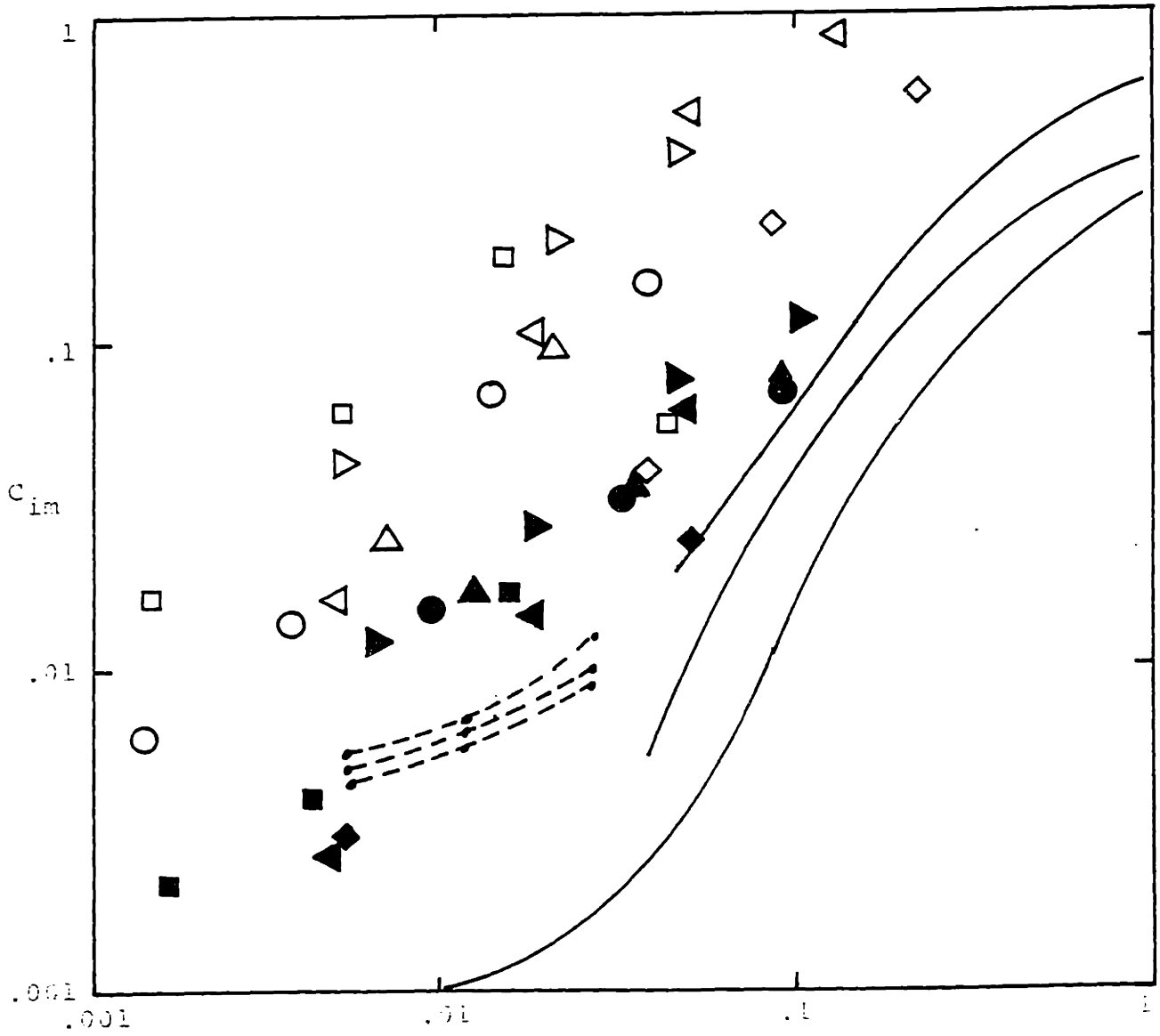

$$\eta_{STK} = \frac{2a^2 \rho}{9 \eta R_c v}$$

Figure 3.14 Experimental single particle efficiency vs. Stokes number.

Reynolds number (i.e. the three data points from each bed tested) were best fitted to the curve. This was done by varying an assumed jetting factor, β, until the sum of the east squares error from the curve was minimized. Table 3.3 is a summary of the pertinent parameters, of all tests, while fig. 3.12 is the resulting plot of the data in the form of C_{im} vs. N_{STK}. Further, fig. 3.13 is the plot of assumed jetting factor β vs. bed Reynolds number Re for the data plotted using the procedure just outlines. The solid line is an approximate curve fit to the data points.

These results are really quite remarkable in light of the complexity of the process they describe. We contend that this experimentally derived theory is applicable (and verified) over a range of modified Stokes numbers of about 10^{-3} to 1. The consistency of the data is good, with scatter in C_{im} being about a factor of 2. This is acceptable for the predictive capacities in which the model is intended to be used.

The jetting factor curve is really where the validity of the theory is more closely scrutinized. It very well fits the limits expected from the previous semi-analytical arguments. It should be noted that this dependence was experimentally derived, but the curve found can now be used as a predictive instrument.

Further credibility is lent to the theory by comparison with other working results. The well accepted theoretical curve for collection from free jets on spherical collectors proposed by Langmuir and Blodgett[25] and experimentally verified by Ranz and Wong[16] is represented by the dotted line in Fig. 3.12. For their isolated sphere we take $U_o = U_a$ (their "far field" flow velocity) and $\beta = 1$. Unfortunately, Langmuir and Blodgett results are hard to interpret and were not intended to be valid for small efficiencies, $C_{im} \leq 1\%$. They were

interested in single sphere collection and any collection less than
negligible and difficult to measure. Because the beds are many sing
collectors in series, very low single sphere collection efficiencies
in significant bed efficiencies. Thus our results extend to a regim
low that considered by many of these previous investigators. Still,
high efficiency region the correlation is good. In addition, Calvert
recently performed a summary and experimental examination of a granul
filters. They concluded that inertial impaction is poorly understood
could not correlate their data with any existing theories. Their data
presented by the dashed lines in Fig. 3.12. Our new theory seems to c
their data acceptably.

For comparison, the theoretical models proposed by Calvert et al a
Trados et al as detailed previously are plotted in figure 3.14 along wi
data. They are seen to approach our model for the low Reynolds number r
but are significantly in error. Scatter is significant and their theori
no mechanism to compensate for the jetting effect.

The model determined here can then be used in the following simple v
Complete specification of bed and particulate parameters is necessary for
determination of the modified Stokes number. The jetting factor β can be
termined from the Reynolds number by using the curve of Fig. 3.13. Then
single particle inertial impaction efficiency can be determined from the c
Fig. 3.12. This entire figure can be roughly approximated by the equation

$$C_{im} \cong N_{STK'} \qquad (3$$

for the region $10^{-3} \lesssim N_{STK'} \lesssim 1$. It should be kept in mind that there is some scatter in the theory, but it is within that necessary for successful use of the model.

2. Polydisperse Aerosol Collection in EFB's

a. Model for Superposition of Collection Mechanisms

The previous sections analyzed all the significant particulate collection mechanisms individually. Without doubt, all of them are acting simultaneously on the particulate. It is doubtful in light of the complexities of even the individual mechanism that any all-inclusive formula for the superposition of the mechanisms can be derived. Attempts at such formulations usually begin from the basic equations of motion including all the force mechanisms (see for example Georege and Poehlein[17]). Typically the results are a large assortment of different parameters and each specific situation (i.e., set of parameters) must be solved numerically on a computer. No attempts are made at experimental correlation.

Rather, for most cases encountered, one mechanisms is dominant over all the others. In any case, it is unlikely that one mechanism could actually decrease the effect of another one unless the mechanisms serves to drive the particulate away from the bed particle. For any one mechanism being dominant it seems reasonable to use that mechanism's single particle efficiency to predict bed performance. If two mechanisms are of comparable importance they must both be considered in a consistent way. One attractive formula is to treat them as if both acted in series. Such a model seems well suited for (say) the combination of inertial impaction and diffusion because inertial impaction collects particulate on the forward face of the collecting sphere while diffusion collects on

the side of the sphere. The net effective single particle C_t efficiency for two combined mechanisms C_1 and C_2 is then

$$C_t = C_1 + C_2 - C_1C_2 \tag{3.58}$$

This expression is satisfying from several standponts. First, if one mechanism is dominant, say $C_1 >> C_2$ then

$$C_t = C_1 \tag{3.59}$$

Second, the superposition of two mechanisms, each with efficiency less than 1, is less than 1 (for C_1, $C_2 < 1$, $C_t < 1$). Third, it presents the superposition as simply a "sum" of the two mechanisms minus a certain amount which accounts for an overlap of the two mechanisms, i.e., a prevention against double counting collected particulate. This formulation should in no way be interpreted as physically based or rigorous. Rather it is a convenience and it is clear that further work needs to be done in this area.

With no electrical effects present, it has been found that bed collection efficiency curves have a characteristic shape when plotted vs. particulate size. It can be seen in Fig. 3.11. The mechanisms responsible for this characteristic shape can be ascertained by analyzing the individual collection mechanisms for a typical bed collector. We take the following values as comprising out typical bed for this analysis.

$R = 1$ mm $\qquad\qquad$ $\varepsilon = 0.385$ (that of a dumped bed of uniform spheres)

$U_o = 1$ m/sec $\qquad\qquad$ $\ell_o = 10$ cm.

In addition we specify the following properties for the gas and aerosol particles

$\eta = 2 \times 10^{-5}$ (air at STP)

$\rho_p = 10^3$ kgm/m^3 (density of water)

For these parameters the Reynolds number is low enough that we may assume

$\beta = 1$

Fig. 3.15 is a plot of the resulting single particle collection efficiencies vs. aerosol particle diamter (for diffusion, inertial impaction and interception). These efficiencies are then combined accorsing to equation 3.58 (using the dominant or tow most dominant mechanisms) to result in Fig. 3.16. This figure shows the collection efficiency of the entire bed as a function of aerosol diameter and the curve is just the characteristic shape found experimentally. What may be concluded is this: For particulate larger than 1 μm diameter, inertial impaction is clearly the dominant mechanism. For particulate smaller than 0.1 μm, diffusion is dominant, with efficiency increasing as diameter decreases (or equivalently diffusivity increasing). The minimum in the submicron size range is a result of neither mechanism being especially effective in this size range.

Since many industrial particulate air pollutants have substantial fractions in the submicron range, a purely "mechanical" bed collector of the type described here is not effective. The bed could be designed differently to achieve collection in this size range; these design changes being aimed at either increasing

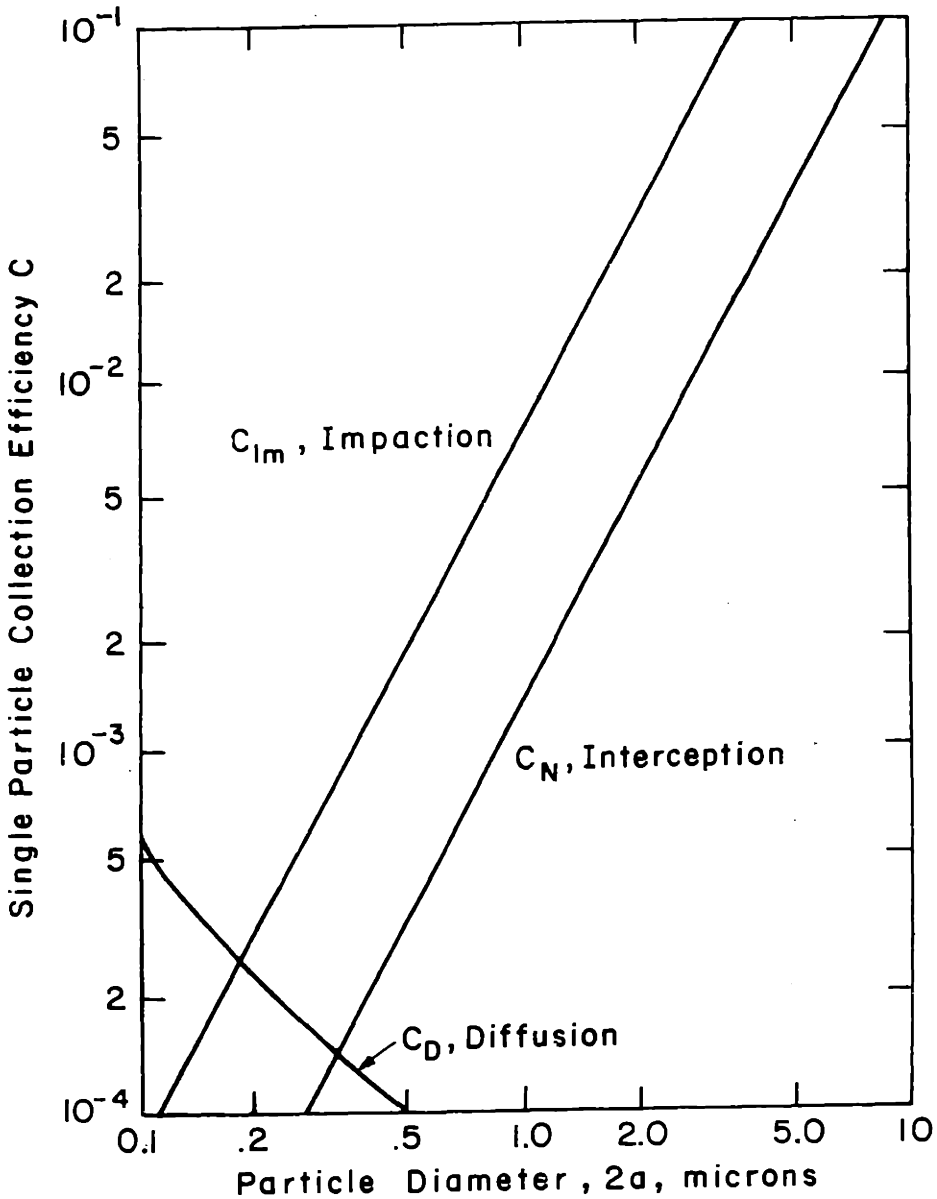

Figure 3.15 Theoretical single particle collection efficiencies of unit density aerosols by diffusion, impaction and interception for a fluidized bed: U=1 m/sec, R=1 mm, ε=0.4.

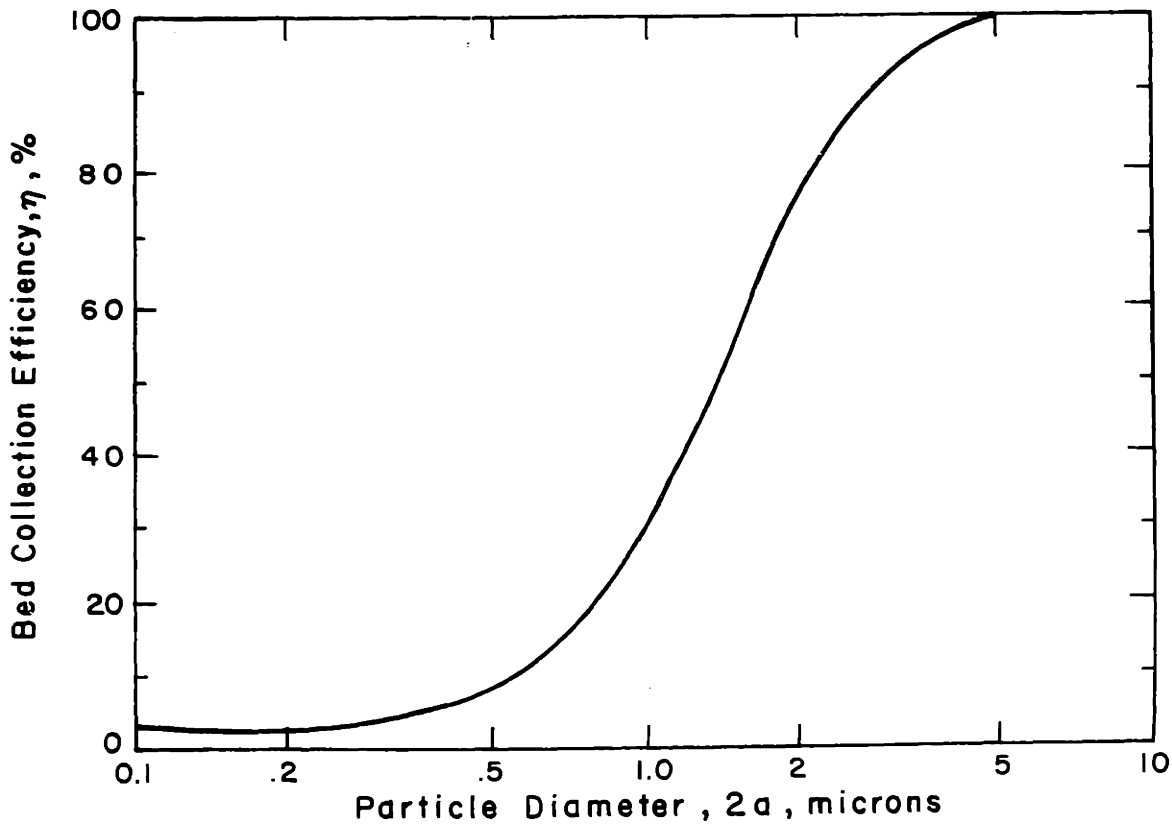

Figure 3.16 Fluidized bed theoretical collection efficiencies for combined single particle mechanisms of Figure 3.15 and bed depth ℓ_0=10 cm.

inertial impaction or diffusion in the submicron range. Looking at our theoretical collection expression, C_{im}, or equivalently the modified Stoke's number, could be increased in two practical way by either increasing the flow velocity U_o or decreasing the collecting particle radius R. To increase C_D (or decrease Pe) we could decrease R or U_o. Or in either case, we could improve bed performance by simply increasing the bed depth ℓ_o. However, to effectively collect submicron particulate, the bed parameters would have to be changed in such a way that the systems would become intolerably large or require excessive pressure drops.

A more effective alternative is to collect submicron particulate with electrostatic forces. As pointed out previously, electrostatic collection is most effective and most dependable when the particulate is charged and electric fields are imposed in the bed. As discussed elsewhere, the particulate charge manifests itself in the electrical mobility of the particulate. Particulate are usually given charge in specific charging regions where free ions and ambient electric field are present. The ambient field serves to drive the free ions to the particulate, and free ions also migrate to the particulate by diffusion. The resulting charge or mobility of the particulate resulting from spending time, τ_{res}, in the charging region has a dependence on particulate diameter not dissimilar from the bed collection curve. Fig. 3.17 shows a mobility curve calcualted for a charge of the following desing. Field and diffusion charging were considered as modeled in White[27].

$E_{chg} = 2 \times 10^5$ v/m (ambient field)

$\tau_{res} = 0.01$ sec (residence time)

$n_i = 7 \times 10^{14}$ ions/m^3 (ion density)

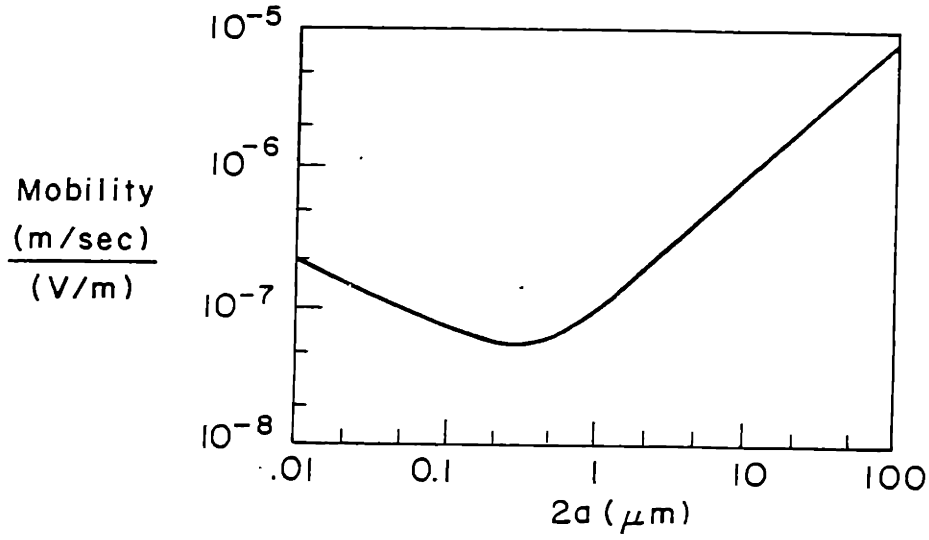

Figure 3.17 Theoretical mobilities of unit density sphere in air subjected to charging conditions given in text.

This distribution was used in the plotting of Fig. 3.18 and 3.19 which show the resulting single particle and entire bed collection efficiencies for our typical case. In these figures, the imposed electric field is varied parametrically. It becomes apparent that submicron pollutants can be effectively controlled with electrostatic collection mechanisms.

b. Experimental Studies

Experiments were performed to demonstrate the importance of electrostatic collection for polydisperse aerosols containing submicron sized components and to examine the model for superposition of collection mechanism. Monodisperse aerosols of DOP were collected in beds of N.J. #2 sand and collection efficiencies measured with the mass monitor. Details of the experiment are given in Appendix A.

A modified version of the Sinclair-LaMer generator produced an aerosol of DOP (dioctylphthalate) droplets of radii uniform enough to be measured by higher order Tyndall spectra. Droplets were charged by ion impact and electrical mobilities measured by a small laminer flow ESP. The resulting distribution is shown in fig. 3.20. The use of a liquid aerosol assures adhesion to the bed particles. To eliminate the effects of space charge on collection and collected aerosol on the state of fluidization, low DOP loadings were imposed.

The data gathered are shown in fig. 3.21 where bed collection efficiency is plotted vs. aerosol diameter with applied electric field as a parameter. This bed is typical of the bed particle sizes, bed depths, and flow velocities expected of practical systems. The importance of electrostatic collection for good submicron collection efficiency is immediately apparent.

As a correlation with theory, Table 3.4 is presented. In it, the single particle collection efficiency by mechanical mechanisms in inferred from the $E = 0$ data in fig. 3.21. The electrical single particle efficiencies are

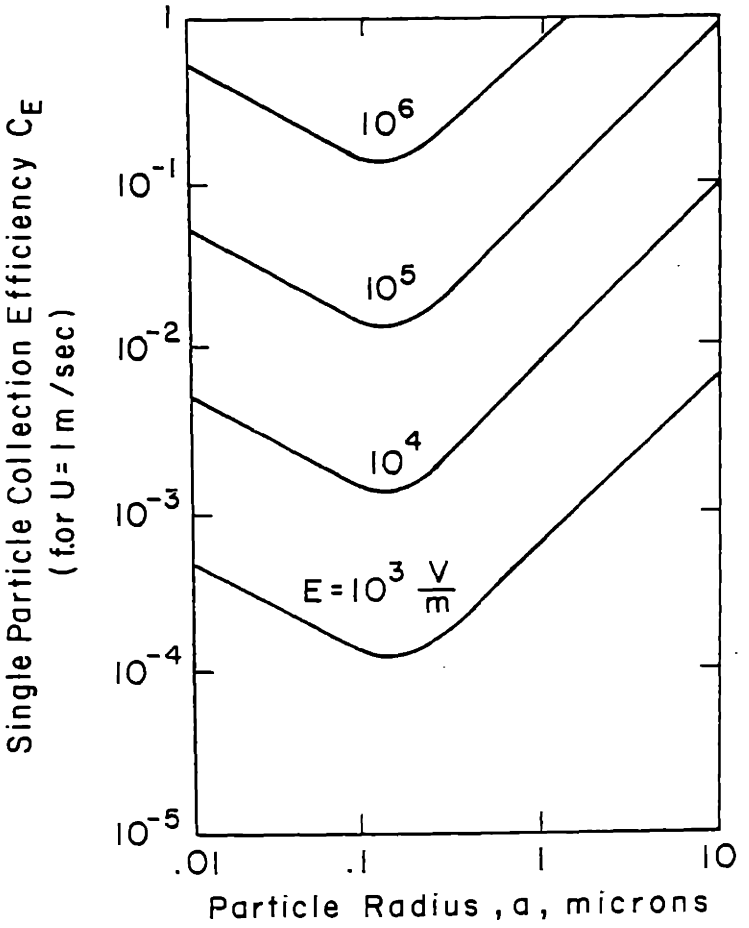

Figure 3.18 Theoretical single particle electrostatic collection efficiencies for aerosol of mobility distribution in Figure 3.17.

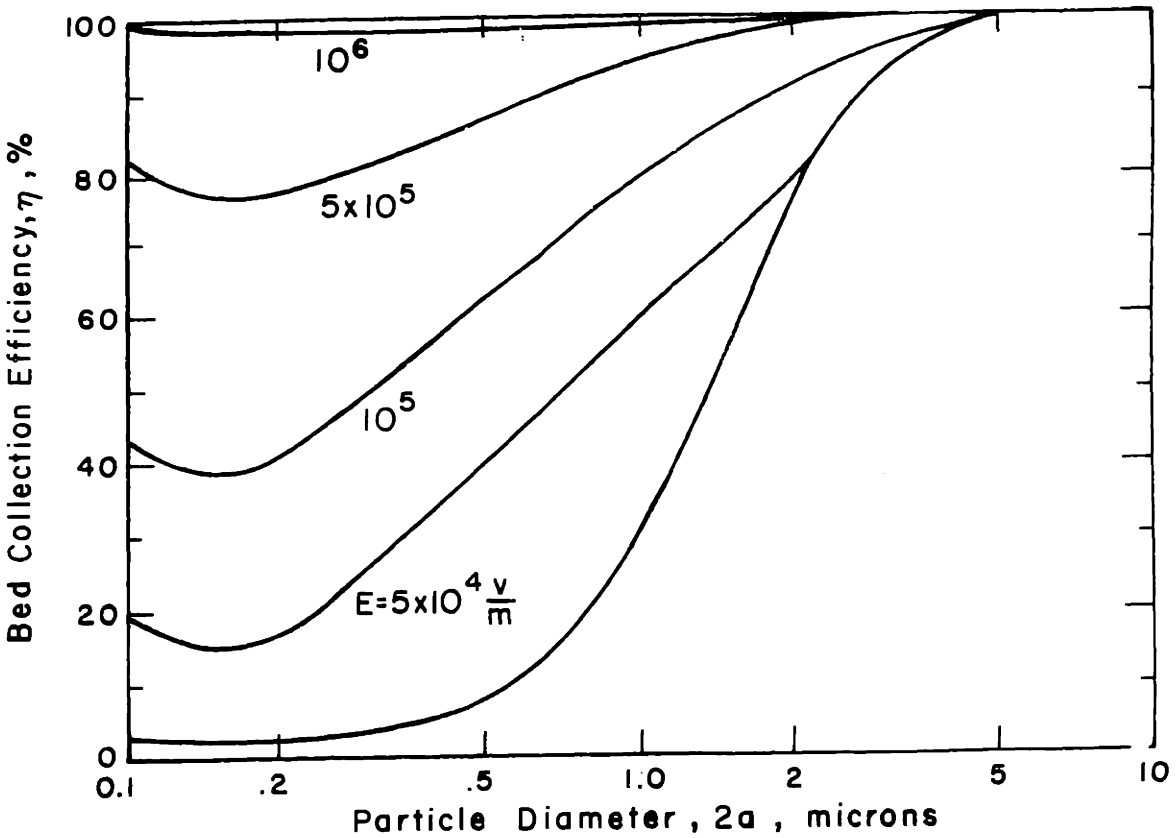

Figure 3.19 Electrofluidized bed theoretical collection efficiencies for combined single particle mechanisms of Figures 3.15 and 3.18 with bed depth ℓ_o=10 cm.

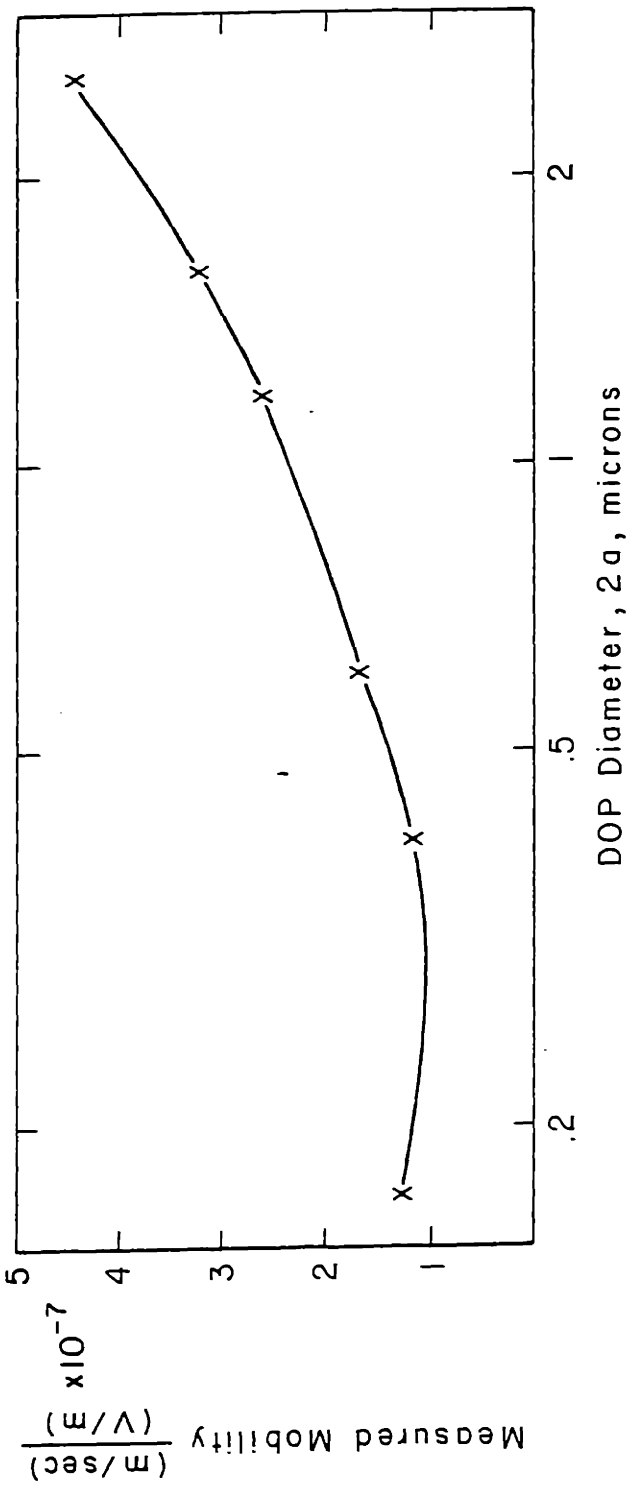

Figure 3.20 Experimentally measured electrical mobilities of monodisperse DOP aerosols.

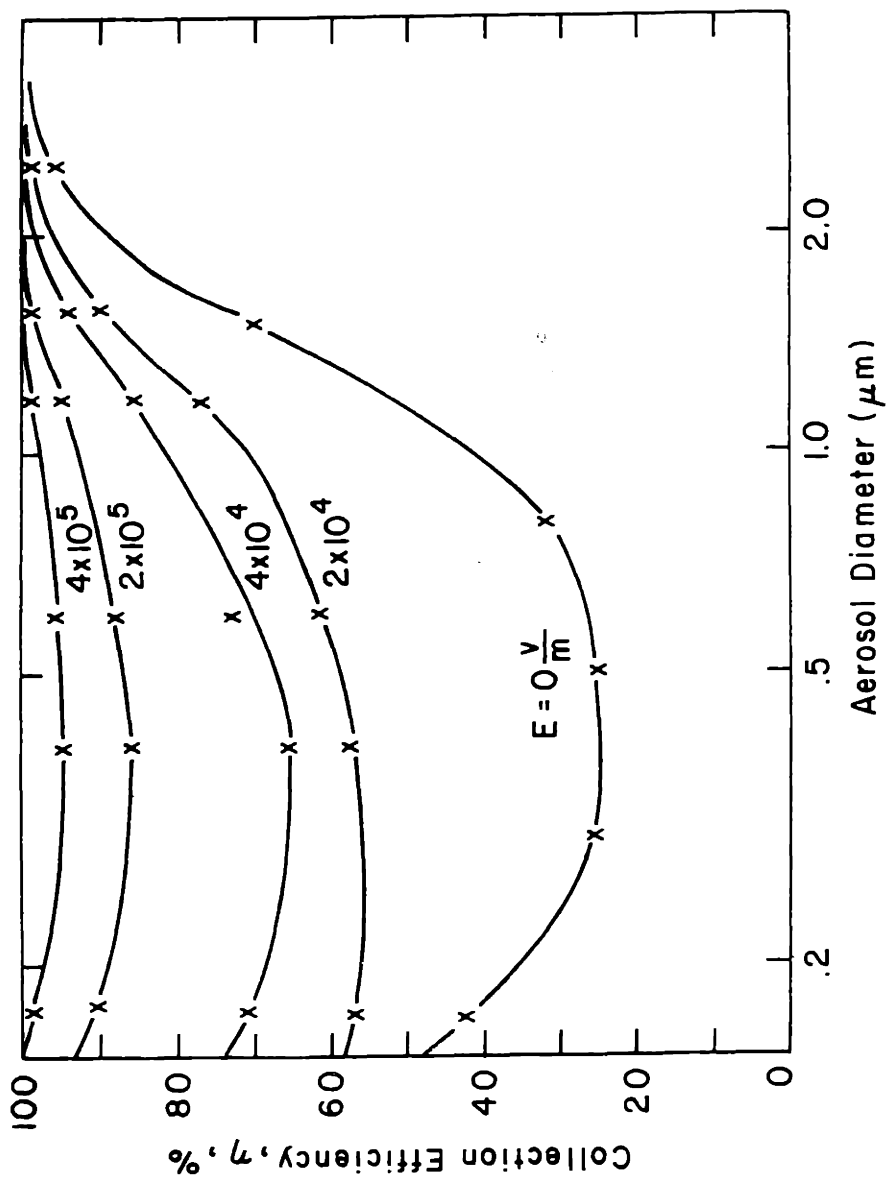

Figure 3.21 Experimental EFB collection efficiencies of monodisperse DOP aerosols. Bed parameters: R=0.5 mm, U=1 m/sec, ℓ_o=7.5 cm.

Table 3.4 Data for polydisperse aerosol collection in the EFB.

$E\ (x10^5\ \frac{V}{m})$

2a(mm)	0	.2	.4	2	4
.17	.44	.66	.71	.99+	.99+
	.44	.57	.78	.91	.99
.4	.26	.53	.65	.99	.99+
	.26	.59	.72	.86	.95
.6	.31	.64	.73	.99+	.99+
	.31	.61	.80	.88	.96
1.2	.52	.82	.86	.99+	.99+
	.52	.77	.94	.95	.99
1.6	.70	.91	.94	.99+	.99+
	.70	.90	.98	.99	.99+
2.5	.96	.99	.99+	.99+	.99+
	.96	.99	.99+	.99	.99+

η_{theory}

$\eta_{exp.}$

theoretically calculated from

$$C_E = \frac{3cbE}{U} \qquad 3.60$$

where c = 1. Finally, the two single particle efficiencies are combined as dictated by Eq. 3. 58. The theoretical and experimental efficiencies can then be compared.

The first column of Table 3.4 data correlate with theory perfectly by definition. The remainder of the data correlate well. It should be kept in mind that the theoretical predictions are based on a plug flow model. Even with the co-flow screen electrodes, the presence of bubbles reduces efficiencies from the ultra high 99+% predicted values. This explains the somewhat lower than predicted values in the high electric field-high efficiency regions.

From this data, it appears reasonable to use Eq. 3.58 to predict the combined effects of different collection mechanisms.

Summary

This chapter is important from several standpoints. It provides a summary of pertinent literature on aerosol collection in granular beds and in the process points out the lack of effective models for inertial impaction. The new model proposed and tested for inertial impaction appears to be satisfactory for the prediction of granular bed filter performance. Finally, by superimposing all the available models granular bed filters are found to be ineffective for the control of submicron aerosols. This problem can be solved by the use of electrostatic collection means. These effects are demonstrated experimentally.

REFERENCES

(1) Zahedi, K. and Melcher, J.R., I.&E.C. Fund., 16, 2, 248 (1977).

(2) Davidson, J.R., Trans. Inst. Chem. Eng., 39, 230 (1961).

(3) Zahedi, K., "Electrofluidized Bed Filtration: Fundamentals and Applications" Ph.D. Thesis, MIT, September 1976.

(4) Happel, J., A.I.Ch.E. Jour., 4, 2 (1971).

(5) Kuwabara, S., J. of the Phys. Soc. of Japan, 14, 4, 527 (1959).

(6) Alexander, J.C., "Frequency Characteristics of Electrofluidized Beds in the Collection of Submicron Particulate", S.M. Thesis, MIT, October 1975.

(7) Kyle, C.R., and R.L. Perrine, Can. J. of Chem. Eng., 49, 19 (1971).

(8) Jolls, K.R. and T.J. Hanratty, Chem. Eng. Sci., 21, 1185 (1966).

(9) Wagner, T.H., A.J. Karabelas, and T.J. Hanratty, Chem. Eng. Sci., 26, 59 (1971).

(10) Ranz, W.E., Chem. Eng. Prog., 48, 5, 247

(11) Friedlander, S.K., J. of Coll. and Int. Sci., 23, 157 (1967).

(12) Levich, V.G., Physicochemical Hydrodynamics, Prentice Hall, Inc. New York, 1962, P. 80.

(13) Stairmand, C.J., Trans. Inst. Chem. Eng., 28, 130 (1950).

(14) Pfeffer, R. and H. Happel, A.I.Ch.E. Journal, 10, 5, 605

(15) Gebhart, J., C. Roth and W. Stalhofen, Aerosol Sci., 4, 355 (1973).

(16) Ranz, W.E., and J.B. Wong, I.&E.C., 44, 6, 1371

(17) George, H.F. and G.W. Poehlin, Env. Sci. and Tech., 8, 1, 46 (1974).

(18) Tardos, G., C. Gutfinder and N. Abuaf, Israel J. of Tech.. 12, 184 (1974).

(19) Tardos, G., N. Abuaf and C. Gutfinder, Atmos. Env., 10, 389 (1976).

(20) Ying, S., R.G. Patterson, S. Calvert, D.C. Drehmed, "Granular Bed Filter Study", 77-32.6, 70th Ann. Mtg. of the APCA, June 1977.

(21) Zahedi, K. and J.R. Melcher, J. of the APCA, 26, 345 (1976).

(22) Alexander, J.C. and Melcher, J.R., I.&.C. Fund., 16, 3, 311 (1977).

(23) Green, H.L. and W.R. Lane, Particulate Clouds -- Dusts, Smokes and Mists, E. and F.N. Spon. Ltd., London, P. 343 (1965).

(24) Walton, W.H. and H.F. Woodcock, Intern. J. Air Poll., 3, 129 (1960)

(25) Langmuir, I. and Blodgett, K.B., Army Air Forces Technical Report, 5418 (1946

(26) Le Clair, B.D. and A.E. Hamielec, I.&E.C. Fund, 7. 4. 542 (1968).

Chapter IV Fly Ash Adhesion in Packed and Fluidized Beds

A. Background

1. Introduction

The second step, after initial collection, in the ultimate removal of particulate pollutants from a gas stream is the retention of the particulate matter on the collecting surface. For liquid particulate pollutants, this adhesion is virtually assured. Primarily though, we are concerned here with the control of fly ash, a dry particulate. As with collection, many adhesion mechanisms exist, and the effectiveness of the different mechanisms varies greatly. We are also primarily concerned with the use of electrofluidized beds, so we will especially focus on an adhesion mechanism most suitable for them.

To begin with, we will briefly discuss fly ash and its properties which pertain to adhesion. Then we will analyze the various adhesion mechanisms individually and try to identify mechanisms which will be dominant and the limitations of those mechanisms, as they apply to packed and fluidized bed collectors.

2. Fly Ash Properties

Fly ash is the solid incombustible residue that is entrained in the effluent gases when coal is burned. Usually, these incombustibles melt in the flame, some even vaporize, but then recondense and solidify as the gas cools. For the most part, they consist of glassy alumino-silicate spheres from submicron to about 50 microns in diameter.

For as many different seams where coal is mined, there are as many different kinds of fly ash. It is just this variation in fly ash properties that has transformed fly ash collector design from a routine engineering

problem into almost an art form. It is an understatement to say that the relation between fly ash chemical properties and collector performance is poorly understood. In general, fly ash can be thought of as consisting of tiny glass-like spheres. Fig. 4.1 is an electron microscope photograph of fly ash obtained from the electrostatic precipitator hoppers of a power plant in Rhode Island. The great range of sizes and spherical shapes are clearly seen.

The chemical composition of fly ash, of course, depends on the composition of the parent coal, specifically its incombustibles. A chemical analysis of a typical fly ash is given in Table 4.1. It is difficult to predict the fly ash properties even from a detailed chemical composition such as this. Fly ash properties are generally believed to be governed by its surface properties, and these result from complex surface reactions that result from contact with the flue gas. It has been postulated that a three layered submicroscopic surface structure is present for fly ash at around 200°C. The innermost layer is basic (predominantly basic calcium chloride compounds) followed by a neutral layer (predominantly calcium sulphate) and an outer acid layer (predominantly sulfuric acid). The development of this layered structure follows from a sequence of reactions of the fly ash with the flue gas constituents, beginning in the high-temperature combustion region and continuing to the relatively low temperatures at the fly ash collector.

Fly ash has several unusual properties that directly relate to adhesion. First of all, when the ash is hot and dry it is very freely flowing and acts almost like a liquid. Upon cooling and adsorption of surface moisture though, it can form clumps and not flow at all. These properties will be seen to directly result from its adsorption of surface moisture. Second, fly ash is a pozzolan, that is without itself being a cement, it has the

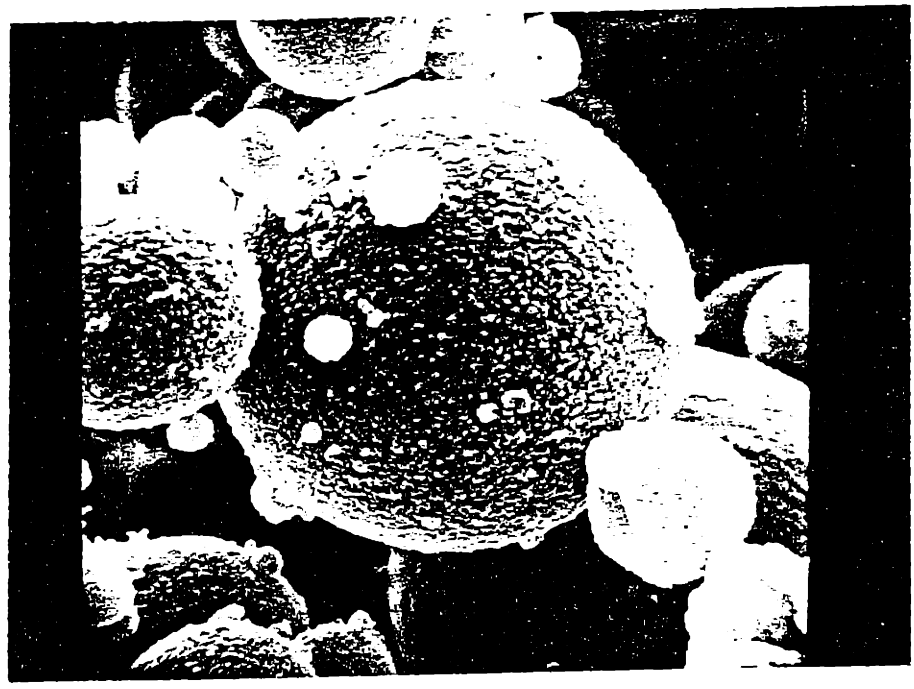

Figure 4.1 Electron microscope picture of fly ash used in reported tests. Magnification 5900x.

Table 4.1 Typical Fly Ash Chemical Analysis

SiO_2	45.9%
Al_2O_3	24.4
Fe_2O_3	12.3
CaO	3.6
MgO	2.5
Na_2O	1.0
K_2O	3.2
TiO_2	0.9
Mn_3O_4	0.1
SO_3	0.9
P_2O_5	0.6
C	4.1
H_2O	0.1
Water solubles	1.8

property of setting hard in the presence of lime and water by reacting with them to form cementitious calcium silicates of low solubility. Very little is known of what physical and chemical factors in the ash determine its activity in this respect.

Fly ash softens and melts at temperatures around 2000° - 2500° F. Fig. 4.2 shows the initial deformation, softening and fluid temperatures of fly ash from several U.S. coals. In addition, many fly ashes have sintering temperatures around 1400-1500° F. Sintering is a process whereby the fly ash is heated to temperatures where plastic deformation occurs at the contact points between fly ash particles. Diffusion of the solid material at these points forms solid bonds between the ash particles upon cooling. The strength of the sintered bonds is aided by increasing compressional forces during sintering.

Fly ash is formed in a wide range of sizes. Because some of it is formed by condensation of gaseous species, a significant portion of the ash is in the submicron range. Fig. 4.3 shows size distributions by mass and by number for several different fly ashes as sampled at actual power plant flues. It is important to note that even though the submicron component may be small on a mass basis, it is large on a number basis. Because detrimental health effects and plume capacities are greatest for submicron sized particles, their removal is imperative. Fig. 4.4 shows the mass density distribution for a typical fly ash from Castle Donington in England.

From an electrostatic standpoint, the most important fly ash property is electrical resistivity. In electrostatic precipitation the fly ash is collected on electrode plates where corona for charging is present. This corona current must penetrate the dust layer to reach the electrode plate. If the fly ash resistivity is too high, the internal fields produced

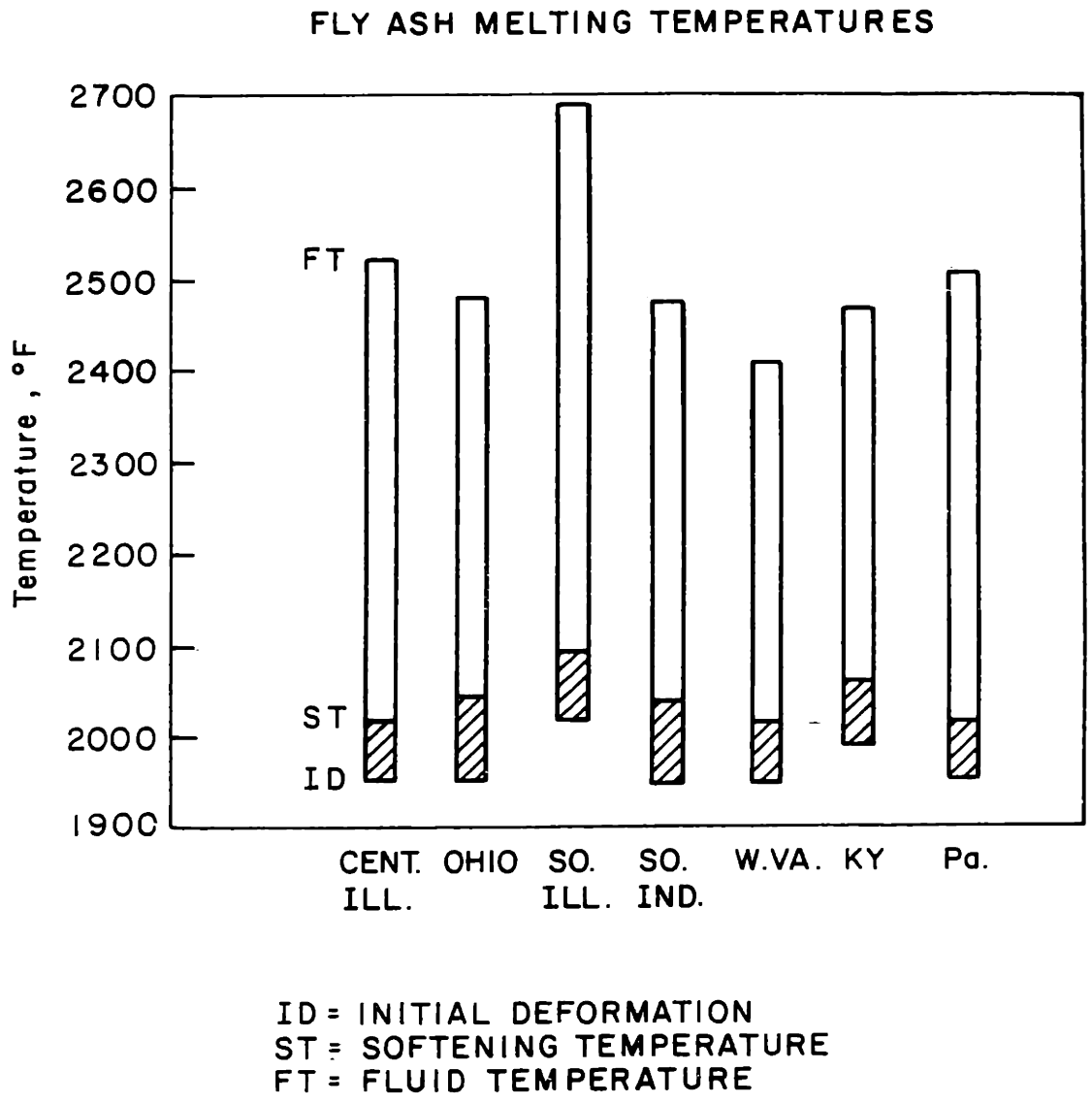

Figure 4.2 Melting temperatures for fly ash from various U.S. coals.

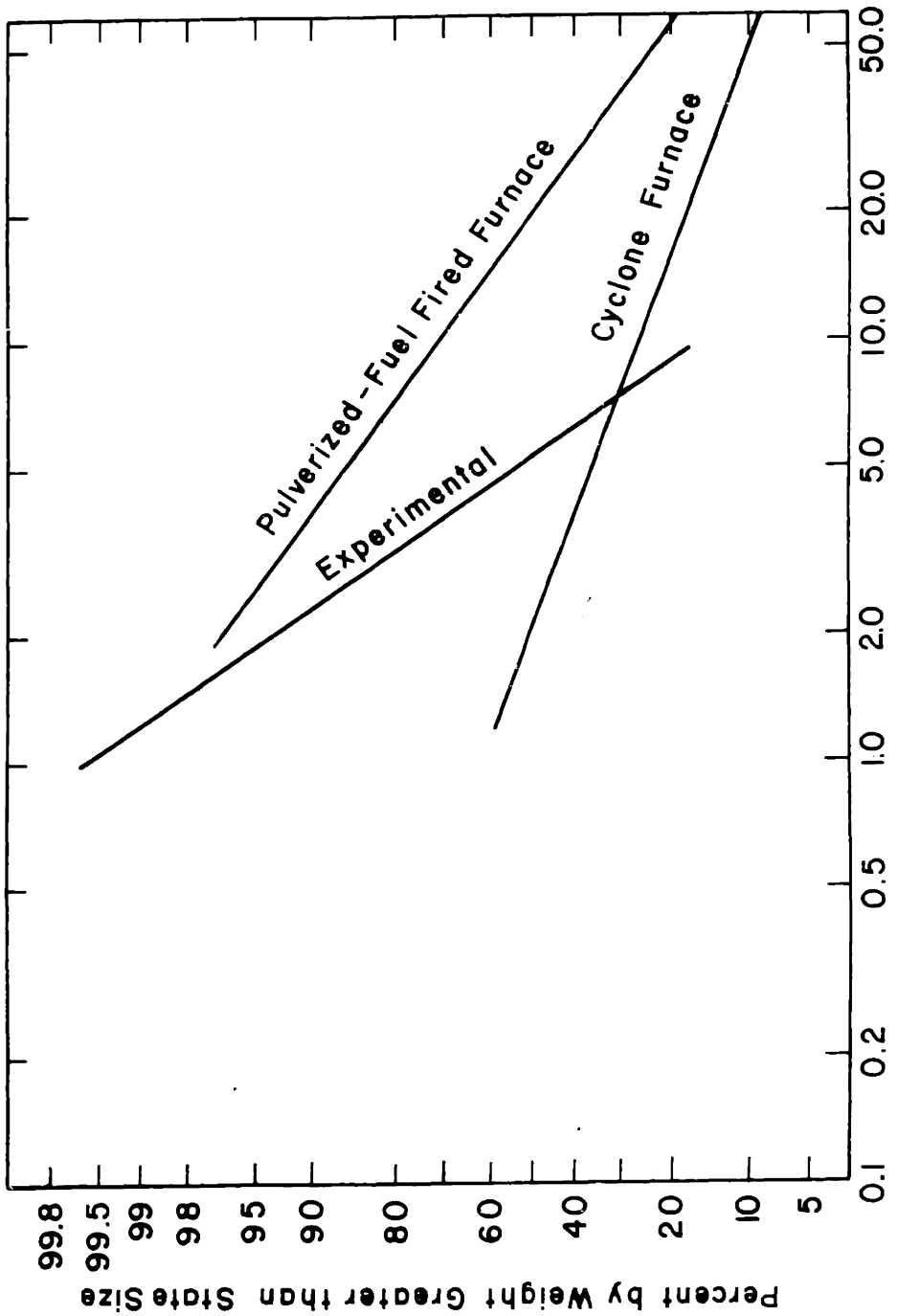

Figure 4.3 Typical size distributions for stack sampled fly ash.

by the current in the dust layer exceed breakdown. The resulting electrical breakdown called back corona seriously hinders precipitator performance because it emits ions (of electrical charge opposite to those of the corona) out into the gas. For practical precipitator operating conditions, problems occur for ash resisitities above about 10^8 Ω-m.

Fly ash exhibits two conduction mechanisms. The intrinsic or volume conduction is basically electronic in nature and as a result has a dependence on temperature which is exponential in nature and increases with increasing temperature. It follows the form

$$\sigma = A \exp(E/kT) \tag{4.1}$$

where A is a constant, E the electron activation energy, k is Boltzman's constant, and T is the temperature.

Surface conduction usually predominates for semi-insulating particles (like fly ash) in the temperature range below 300° F to 400° F. At these low temperatures moisture and chemical films adsorb onto the fly ash surface. Moisture is naturally present in coal combustion flue gases in amounts up to 50%. Adsorption can either be physical or chemical with chemical adsorption providing binding energies much greater than physical adsorption. As a result, the interposition of a chemical binder which is itself strongly bound and in turn strongly adsorbs moisture will result in much greater total adsorption. In all cases, conduction in surface moisture films is electrolytic or ionic in nature.

Typical fly ash resistivities as they vary with temperature are shown in Fig. 4.5. It has been shown that such curves can very roughly be parameterized by sulfur content in the parent coal, but even for coals with the same sulfur content resulting fly ashes can have very different resistivities. The general dependence of ash resistivity on coal sulfur content is believed to result from adsorption of SO_3 from the flue gas. This SO_3 results in a

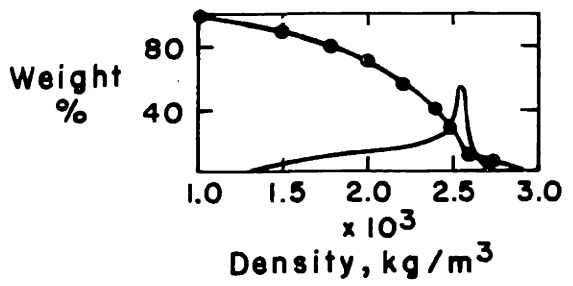

Figure 4.4 Mass density distribution of fly ash from Donington Bay, England.

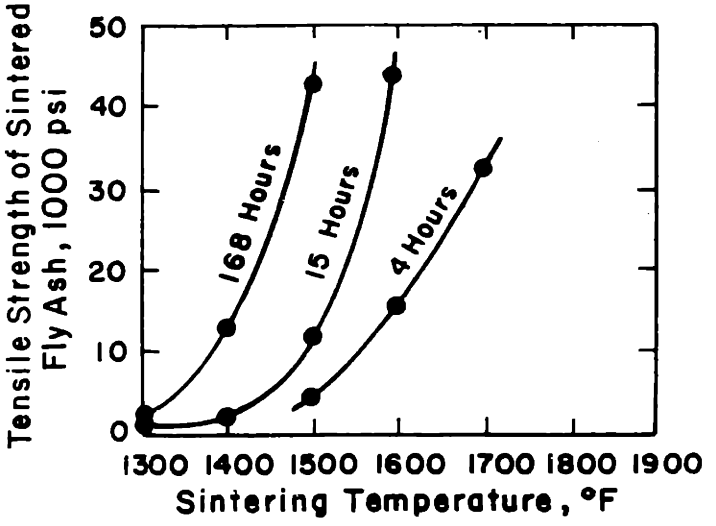

Figure 4.6 Strength of sintered fly ash pellets (from Barnhardt).

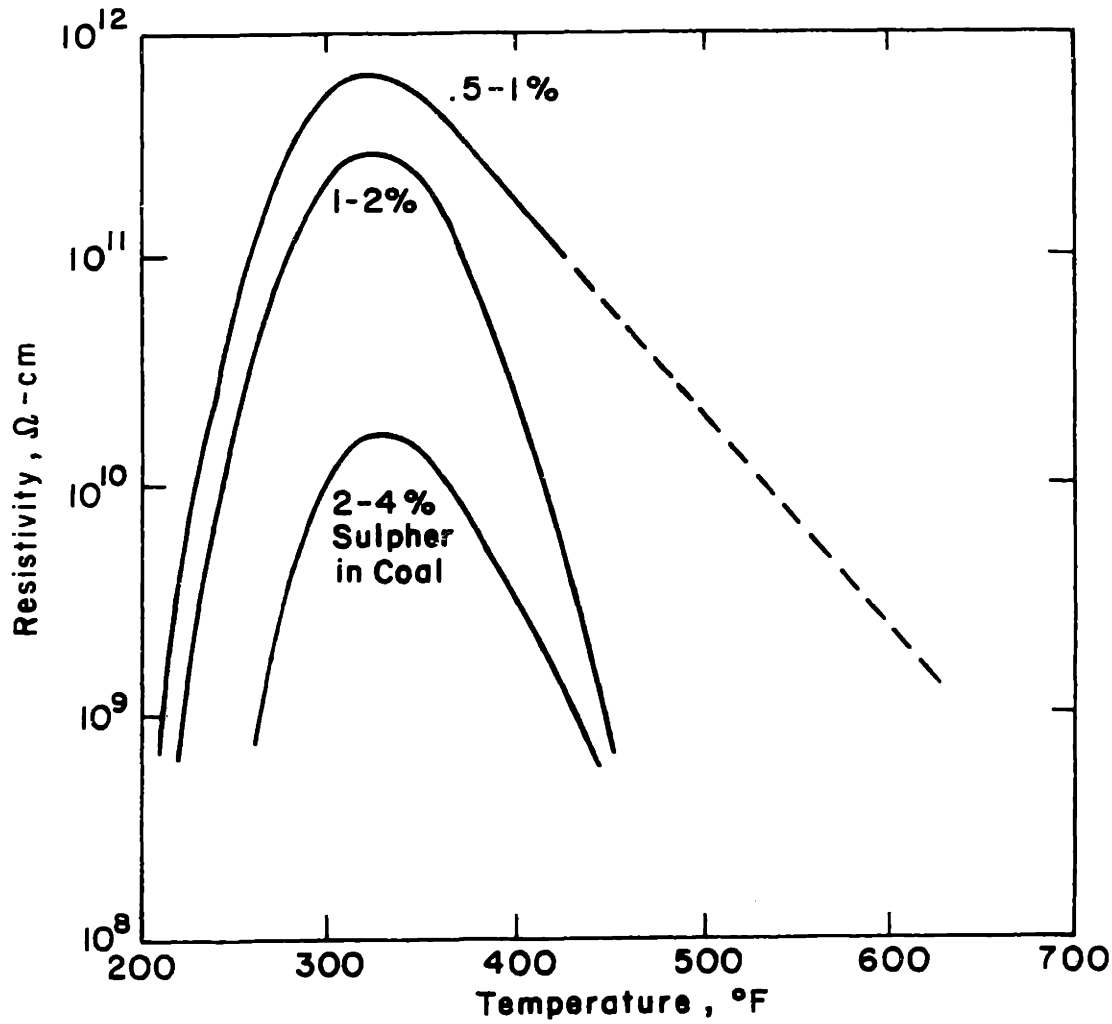

Figure 4.5 Typical resistivities of fly ash from coal of varying sulpher contents.

water soluble sulfate SO_4 on the fly ash surface. This conditions the fly ash surface for strong moisture adsorption. In light of this, SO_3 has been used as an additive to flue gases to reduce the resistivity of hard to precipitate high resistivity fly ashes. This SO_3 adsorption only occurs at low temperatures. This temperature dependence accounts for the increase in resistivity with temperatures up to the point where the volume conduction becomes important. The interplay of these two mechanisms results in the characteristic peak in resistivity at about 300° F. Unfortunately, this is the typical operating temperature of a precipitator or perhaps an electrofluidized bed.

3. Adhesion Mechanisms

The study of adhesion and cohesion mechanisms in fly ash usually centers around its applicability to rapping of electrostatic precipitator plates. As a result, most studies are rather applied in nature and don't delve into the basic mechanisms at work. According to Tassicker[1,2] the component forces are: London-vander Walls, triboelectric, capillary surface dipole, and electric field corona forces. These forces are influenced by the following: particle diameter, porosity, and compaction of the fly ash layer, complex dielectric constant, humidity in the gas, adsorbed surface dipolar molecules, work-function interfaces on the material, and the electric field and current density in the dust layer. The basic building blocks in the development of adhesion models for packed and fluidized bed fly ash collectors are these adhesion mechanisms. In this section we will review previous work done on the analysis of these mechanisms. This review will serve to identify mechanisms felt to be most effective for the engineering problems at hand in this thesis. The next section then, will be the development of the viscous liquid bridge adhesion model, which is the only mechanism considered here as being effective for fluidized

bed collectors.

a. London van der Walls

All molecular and atomic forces, except for gravity which is usually negligible ultimately find their origin in the mutual electrical interactions between the constituent parts of the atom, the nuclei and electrons. It is analytically virtually impossible to approach the problem from this fundamental of a basis. The most basic approximate approach is to begin with adhesion forces based on London van der Walls forces, that is the force by which any atom or molecule is attracted by any other atom or molecule. Bradley[3,4] and Hamaker started from this concept and derived Eq. (4.1) for the attraction between two spherical macroscopic bodies

$$F = \frac{\pi^2 q_o^2 \lambda}{12x^2} \left(\frac{d_1 d_2}{d_1+d_2}\right) \qquad (4.1)$$

where

F = attractive force in dynes.

x = distance of separation in cm.

λ = London van der Walls constant.

q_o = Number of atoms per cm^3 of substance.

$d_1 d_2$ = Diameters of the spherical particles in cm.

$\pi^2 q_o^2 \lambda$ = 10^{-12} according to Hamaker.

The literature contains many conflicting reports concerning the experimental verification of the London van der Walls theories. Generally, these discrepencies are the result of two poorly understood phenomena. The separation distance has never been accurately measured for the small separations required for this force to be appreciable. Surface irregularities make

this task difficult. Also, the experiments were usually performed with poor control of air humidity. This humidity cause adsorption of surface moisture which can vary the interparticle separation, or cause liquid capillary adhesive forces. More will be said on this later.

Casual perusal of Eq. (4.1) reveals that this mechanism should yield significant forces for small particles at small separations. The importance of this mechanism for small particles is further magnified by the dependence of dislodging forces on particle size. Inertial, gravitational, fluid mechanical and electrostatic dislodging forces all decrease dramatically for decreasing particle size. As a result, London van der Walls forces are usually blamed for the tenacity with which small dust particles cling to surfaces.

The actual magnitude of the London van der Walls force depends strongly on the interparticle separation x, which cannot be measured or calculated. The best estimate available at the present time is that of Krupp and Sperling[13] who consider

$$x = 4\ \mathring{A} \pm 30\%$$

Of course, this parameter could be expected to vary greatly depending upon the material and its surface roughness under consideration. In no case would it be less than molecular scale distances, since we assume no molecular bonding.

b. Solid Bridge Forces

Probably the strongest force holding two particles together would occur when a solid bridge exists between the particles. However, the formation of a solid bridge between originally distinct particles involves the occurence of a chemical, physical or thermal reaction which usually

requires special conditions. These conditions do not exist in present technology fly ash containing flue gases. Future technologies, though, such as fluidized bed combustion or MHD combined cycle power generation schemes may involve gas conditions, such as high temperature, which are favorable to the formation of solid bridges. Also, combined fly ash removal and SO_2 scrubbing schemes involving limestone may provide conditions tc utilize the fly ash's pozzolanic properties.

c. Sintering

At about 1/2 to 2/3 of a solids melting temperature, the thermal mobility of the solids molecules becomes so great that diffusion of the molecules will begin to occur from particle to particle at their contact points. At still higher temperatures the material melts at favored points; namely, roughness peaks. Due to surface tension the melt is drawn to the contact points of the particles and form liquid bridges. The adhesive action of these liquid bridges will be analyzed later, but upon cooling, these liquid bridges form solid bridges. Because the required energy for melting decreases with increasing surface curvature, low temperature sintering is more effective for small particles with sharp roughness peaks.

Fly ash sintering has been looked at with two goals in mind. First of all, the sintering characteristics of a fly ash can usefully predict the fouling tendencies in the convection-tube banks of coal fired boilers.[6] Fouling coals have been shown to produce fly ashes that sinter at lower temperatures and shorter times than for nonfouling coals. Fig. 4.6 shows the sintering strength vs. sintering temperature for a typical fouling coal at various sintering times and temperatures.

The second and most important reason for interest in fly ash sintering is that it can transform fly ash from a rather useless (and costly to dispose

of) by product to a valuable building material. Fly ash in its natural state is a freely flowing, dusty material which is even poor as a landfill. A 500 Mw power generating station can produce 600 tons of fly ash every day which after 10 years operation would produce a hill 600 ft. high with a base diameter of one mile. Disposal is not trivial. Sintering of fly ash has been shown to produce a lightweight aggregate that can be used in building and highway construction where it is used as aggregate for concrete and asphalt.

Because sintering is a complicated phenomenon and fly ash properties vary widely, no universal specifications of sintered fly ash tensile strengths are available. It could be assumed that after sintering, the solid bridge formed has the tensile strength of the fly ash material, but the size of the solid bridge is a strong function of fly ash properties and sintering time, temperature and pressure.

d. Chemical Reaction

Depending largely on the environmental conditions, chemical reactions can occur at particle contact points and form solid bridges. This process can usually be aided by the presence of a liquid phase, oxidizing atmosphere or increasing temperatures. The pozzolanic activity of fly ash is an example of this. Because reactions of this sort do not occur naturally in boiler flue gases we will not pursue this adhesive mechanism.

e. Melting Adhesion

This mechanism is similar to sintering, actually it is just the result of raising temperatures high enough to melt the substance at the contact points. This temperature can be produced by friction or plastic deformation at the contact points as well as being externally applied.

f. Electrical Adhesive Forces

The role of electrostatic forces in fly ash adhesion can be a dominant one, in fact it usually is. But until recently, few of the force mechanisms have been studied in detail. The complexity of the electrostatic force mechanisms acting on deposited fly ash layers in electrostatic precipitators result from the multitude of processes occurring. Corona permeates the active regions while charged fly ash particles are being deposited on the layer. Conduction in the layer can be either by volume or surface and particles vary in size and resistivity by orders of magnitude. We can expect many of the same problems in dealing with packed and fluidized bed collectors.

We will begin by analytically looking at force mechanisms in idealized cases of spheres contacting planes or aggregates of uniform spheres. Then, results of controlled experiments will be discussed, and finally more practical experiments.

Spheres in Contact with a Plane

The section on electrostatic collection of particulate covered the collection process up to contact of the particulate with the collecting surface. Much can happen from the time the sphere contacts the surface until steady state is reached. The approach to steady state is on a time scale of the electrical relaxation time of the particulate. If volume conduction is dominant, this time is

$$\tau_{relax} = \rho\varepsilon \tag{4.2}$$

where

ρ = volume resistivity

ε = dielectric constant

of the particulate.

If surface conduction is dominant, Johnson and Melcher[7] show

$$\tau_{relax} = \frac{R(\epsilon + 2\epsilon_o)}{2\sigma_s} \tag{4.3}$$

where

σ_s = surface conductivity.

R = particle radius.

For various fly ash resistivities, this relaxation time can vary from 10^{-1} to 10^{-5} seconds. Clearly, after a short time the fly ash particle behaves like a conducting particle, if applied electric fields are constant in time. It then appears reasonable to model the electrostatic fly ash adhesion as that of conducting spheres on a conducting plane. Lebedev[8] calculated the force on a sphere resting on a plane, see Fig. 4.6, with a normal imposed electric field, to be

$$f_z = - 4\pi\epsilon_o a^2 E_o^2 \ (1.369) \tag{4.4}$$

Notice that this force is negative and implies that this force actually pulls the particle off of the plane it rests on. To call this an adhesive force is to use this term loosely. For small particles, however, this "lift-off" force is much less than the van der Walls or capillary forces that hold the particle to the plane and the electrostatic lift-off force is usually ignorable for fly ash.

A more interesting case arises when current passes through the single particle, Fig. 4.7, or through a layer of such particles, Fig. 4.8. Such cases might include that of an electrostatic precipitator where corona current is continuously deposited on a layer of fly ash on a ground plate, or in an electrofluidized or electrpacked bed the fly ash could be a part of a conduction path or "string" between electrodes. In either case,

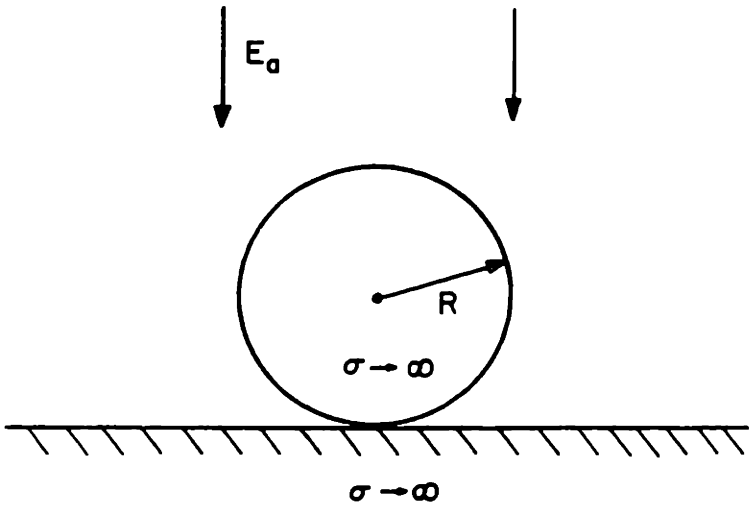

Figure 4.7 Model for electrostatic forces on particle.

the analysis done by Dietz[9] and McLean[10,11] is based on the geometry of Fig. 4.9. The rather large adhesion forces they predict are a result of the very high electric fields near the contact points between the spheres which result from the constriction there of the surface currents. Two assumptions are critical in the analysis

1. The particles are elastic, so the area of contact increases as the interparticle force increases.
2. The electric field which theoretically would grow to very high values near the contact area, is limited to a certain magnitude, E_{max}, by a Schottky type of partial breakdown.

The resulting force between the particles is then

$$f^e = (0.415)\ 4\pi\varepsilon_o a^2 E_{max}^{0.8}\ E_a^{1.2} \tag{4.5}$$

As a result of experiments, (Fig. 4.10) McLean[11] determined that

$$E_{max} \simeq 1\text{-}2 \times 10^7 \text{ v/m} \tag{4.6}$$

In these experiments McLean measured the tensile strength of fly ash layers with imposed electric fields. The solid lines in the plot indicate the theoretical force with various assumed values of E_{max}. Similar results have been obtained by Szirmai and Potter[12]. These results are also interesting from a purely practical standpoint as the cohesive forces in the fly ash layer are shown to increase significantly with imposed electric fields.

Contact Potential Forces

The energy required to remove an electron from a solid is designated by its work function. Even for materials such as copper the work functions of various crystal faces may differ by amounts up to 0.5 volts. For non-homogeneous materials, still larger differences may exist. When two surfaces

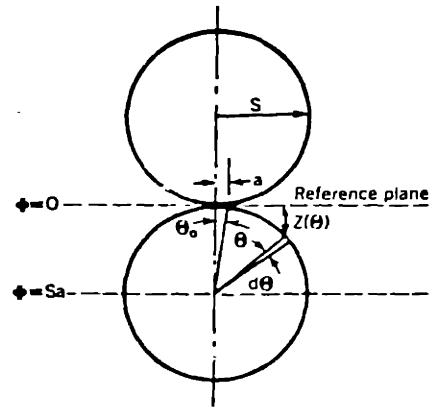

Figure 4.9 Arrangement of ideal particles, two particles in contact.

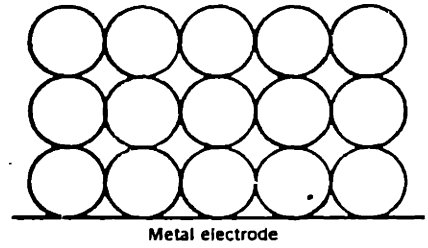

Figure 4.8 Arrangement of ideal particles, simple cubic packing.

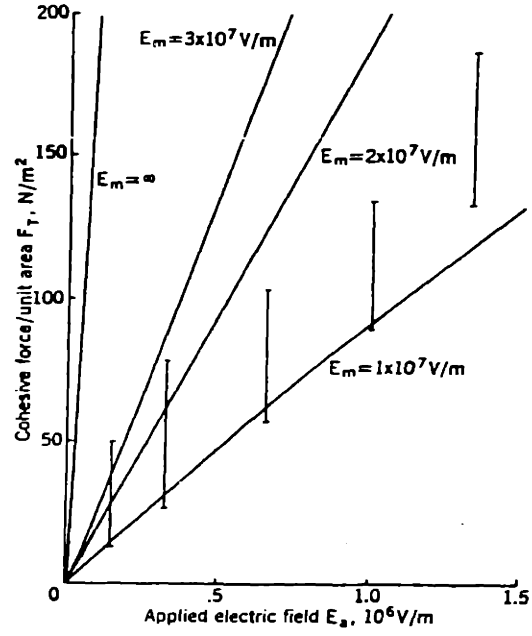

Figure 4.10 Variation of the cohesive force with applied electric field. (-- Calculated values. (1) Experimental values. (from McLean).

of differing work function are brought together, electric fields are created in the interstitial space. If the surface spacing is very small, even a contact potential difference of a fraction of a volt can produce very large electric fields. When actual contact occurs, current flows at the contact point until equilibrium is reached. This results in a net transfer of charge, and is the cause of charging of dusts upon fairly quick separation.

Penney[14,15,16] has shown, through a series of experimental papers, that fly ash particles have numerous patches of alternately intense work function on its surface. If such a particle is allowed to settle on a layer of the same fly ash (such as by electrostatic deposition) the fly ash will orient itself such that there is a significant coulomb attraction between those small patches on adjacent particles. In experiments, adhesive forces some 30 times greater are obtained for freely deposited fly ash layers than for those created by gross mechanical means. It is difficult to correlate those effects with theory because of the nature of the effect. It depends on deviations from regular geometry and inhomogeneities in the crystal structures of the fly ash, but order of magnitude arguments support the possibility of such a mechanism coming into play.

g. Capillary Bridges

In the experimental studies of Van der Walls adhesion forces, the adhesion of particles is usually found to be strongly a function of relative humidity. In fact at high relative humidities, it is usually believed that the Van der Walls forces are overwhelmed by some other mechanism. The mechanism at work is that of capillary forces resulting from liquid bridges formed by the adsorption of water vapor.

When a liquid is present at the contact point between two particles, an adhesive force between them results from the liquid surface tension and the capillary underpressure induced by the curvature of the liquid bridge. The adhesive force can be solved for analytically if the particles are assumed spherical as in the model of Fig. 4.11. Eremenko, Lovrinenko, and Naidich[17] solved for this force with liquid bridge volume as a variable. The results and some of their experimental verification are shown in Fig. 4.12. Their analysis was based on the assumption that the wetting angle at the solid-liquid-air interface was o°. Their interesting result indicates that decreasing the amount of binding liquid increases the contracting force. The limiting contracting force F for arbitrarily small amounts of liquid of surface tension σ between spheres of radius R is the well known formula

$$F = 2\pi R\sigma \tag{4.7}$$

A similar equation

$$F = 4\pi R\sigma \tag{4.8}$$

has been derived by Derjaguin,[18] Bradley[3], and Bowden and Tabor[19] for the adhesion of a sphere to a flat plate by an interposed liquid bridge.

For a non-zero wetting angle, the limiting equations 4.7 and 4.8 are modified to

$$F = 2\pi R\sigma \cos\theta \tag{4.9}$$

$$F = 4\pi R\sigma \cos\theta$$

for sphere to sphere and sphere to plane adhesion forces respectively, where θ is the wetting angle.

The increase of contrasting force with decreasing liquid quantities is

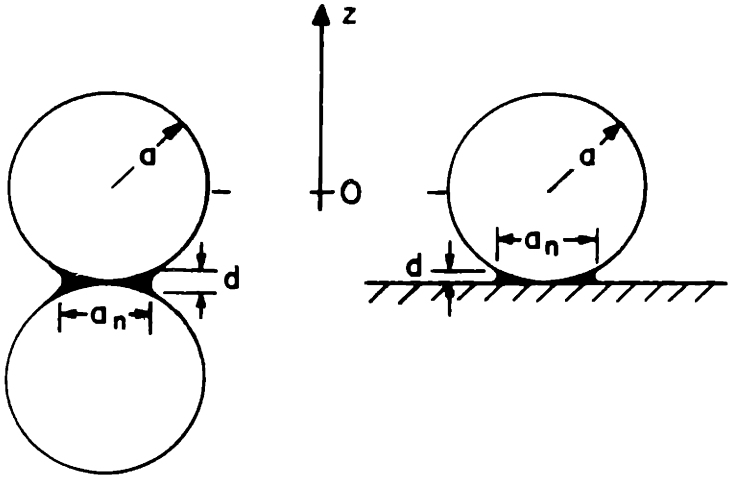

Figure 4.11 Model for capillary bridge and dynamic liquid viscous forces on particles.

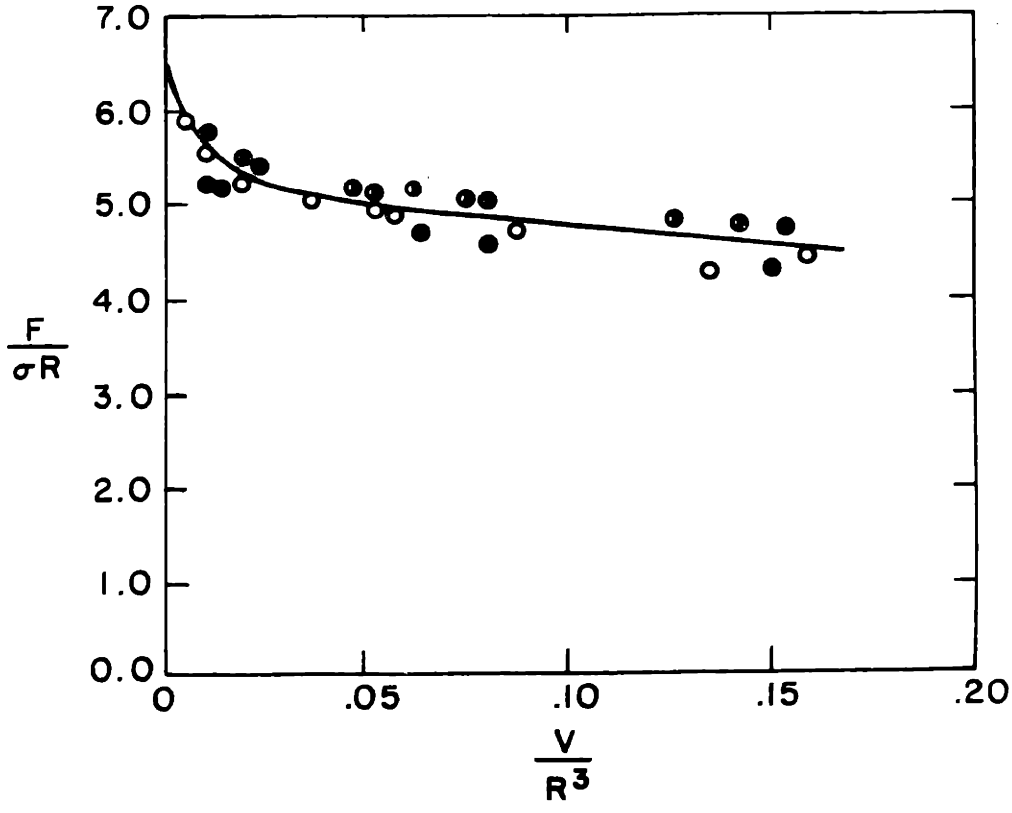

Figure 4.12 Generalized curve of contracting forces vs. amount of liquid.

○ Oil (R = 0.2 cm)
◐ Benzyl alcohol (R = 0.2 cm)
● Oil (R = 0.1 cm)
Solid line is theoretical curve of eq. 4.7.

misleading. It would indicate that even trace amounts of liquid would give maximum adhesion forces. In nature, perfectly smooth surfaces as assumed in the above model are practically non-existent. As a minimum one would expect surface asperities to be on molecular dimensions (around 5 Å). Rayleigh[20] during a study of the cohesion of glass surfaces, noted that except for isolated contact of surface asperities, highly polished silica surfaces remained separated by an average distance of 24.7 Angstroms. Typically, highly polished glass has been shown to have mean height of surface irregularities of about 150 Å.[21] Thus a more accurate model of the adhesion might include these surface asperities which effectively separate the two spheres by a distance x, as indicated in Fig.4. Pietsch[22] derived the resulting contracting force vs. liquid bridge volume with separation x as a parameter. The results are shown in Fig. 4.14. As would be expected, the contracting force decreases with decreasing liquid volume when the liquid volume is small and the sphere to sphere spacing is non-zero. Besides just physically separating the spheres, surface roughness may have other effects on liquid capillary adhesion. It is likely that a certain critical amount of liquid must be present before the liquid bridges would form. This amount would correspond to that required to fill in the crevices formed by the surface asperities. This will be discussed further in the experimental section on viscous adhesion.

In further work, Clark and Mason[24,25] have determined that the contracting force between two liquid bridge bound spheres descreases linearly with sphere separation until a rupture separation, termed x_r, is reached. They propose the equation

$$F = F_{max}\left(1 - \frac{x}{x_r}\right) \qquad (4.11)$$

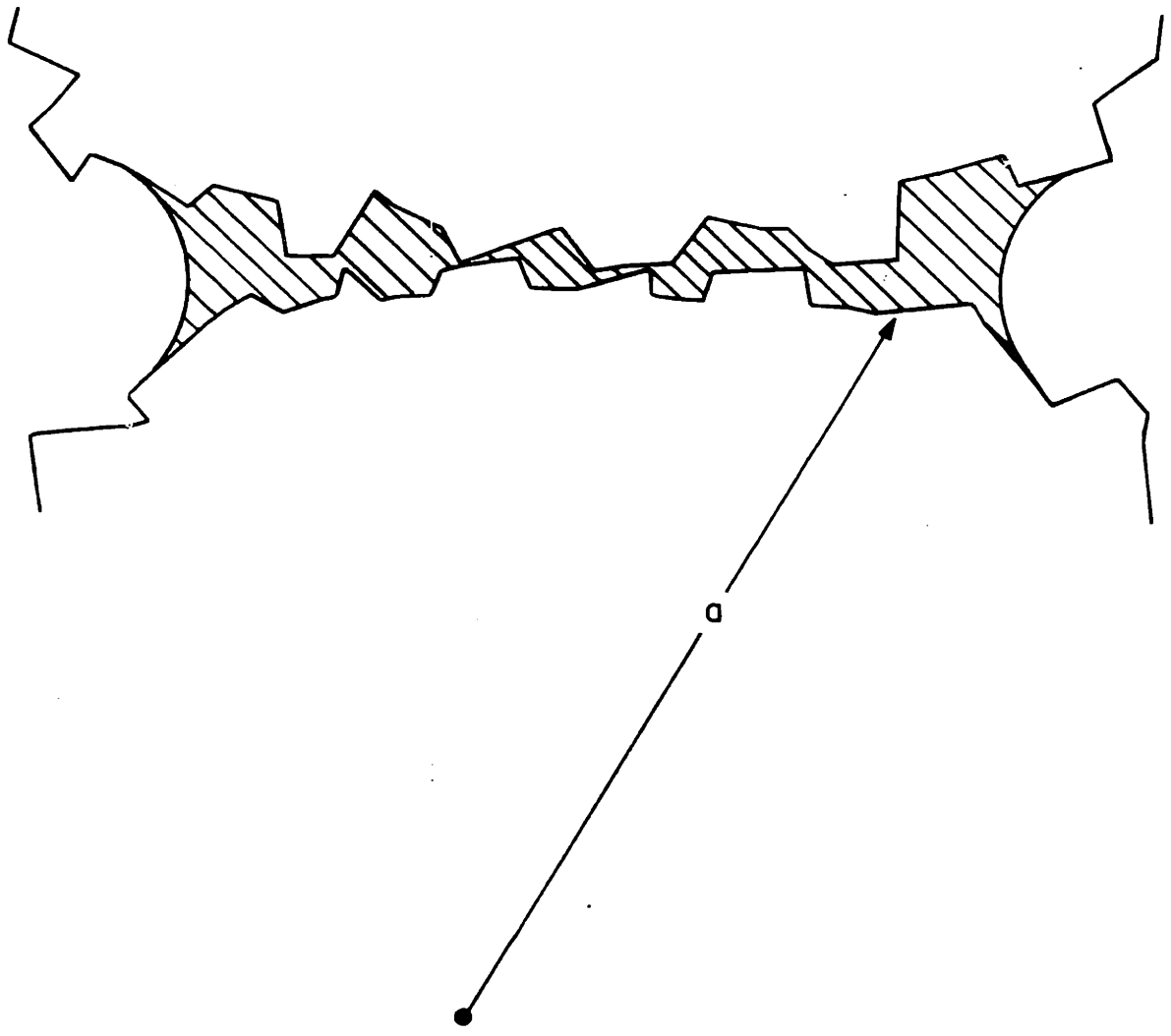

Figure 4.13 Depiction of particle surface asperities and liquid filling.

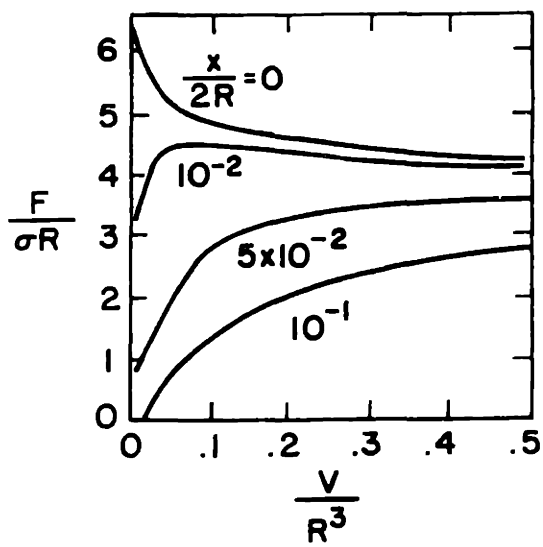

Figure 4.14 Theoretical contracting force vs. amount of liquid at various particle-particle separations. x = particle separation distance. (from Pietsch).

where F_{max} is the contracting force at zero separation.

McFarlane and Tabor[26] were the first to recognize the effect of adsorbed water vapor on adhesion. They found that adhesion in air at 100% relative humidity was as given in Eq. (4.10). Fig. 4.15 shows how their adhesion decreased with decreasing humidity. Simultaneously plotted is the number of molecular layers of water adsorbed from the vapor as reported by McHaffie and Lehner.[27] The correlation is interesting as it shows how the onset of adsorption is associated with the onset of liquid capillary adhesion. However, many discrepancies exist in the literature as to the exact effects of humidity on adhesion. Bowden and Throssel[28] have pointed out that the amount of water adsorbed at a given humidity can vary by orders of magnitude depending on impurities on the surface. This is the probable cause of the discrepancies. As far as the effect of adsorption on adhesion, it is probable that adsorbed water first fills in roughness crevices. This increase the Van der Walls forces by decreasing the effective separation distance between particles. When enough water is adsorbed, liquid bridges are formed and the relatvely large capillary forces come into play.

4. Agglomeration Formation - Tensile Strength

As particles are deposited and retained on a collecting surface, we need to change focus from single particle adhesion to the aggregative behavior of a multitude of such particles. As a model of this behavior we consider a completely random packing of equal spheres with the bonding forces concentrated at the points of contact between spheres. Such a model ignores polydispersity of the particles in the aggregate, be it by size or shape, and non-uniformities of packing characteristics. For the relevant bonding forces (Van der Walls, liquid capillary, solid bridge, contact potential, and electrical current constriction) the localization of

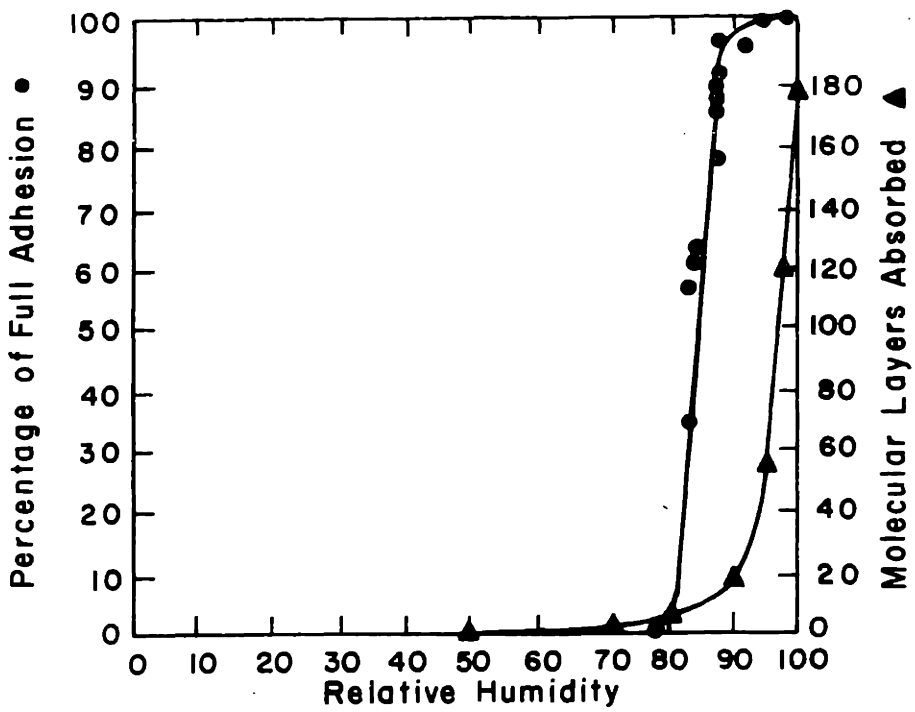

Figure 4.15 Adhesion of glass spheres to glass plane, and molecular layers adsorbed vs. relative humidity (from McFarlane and Tabor and McHaffie and Lehner).

the bonding forces to contact points is representative.

The parameters which should describe the tensile strength of the particle aggregate should be the contact point bonding force, which will term B, the packing density as given by its fraction voids ε_{agg}, the coordination number of the particles, k, that is the number of contacting neighbors to a single particle which form a bonded particle pair, and the particle radius a. When an aggregate is fractured it is assumed that the interparticle bonds are much weaker than the molecular bonds of the particle material, so that individual particles are not ruptured, rather particle pairs become separated at points of contact. The geometry of the surface of split would be somewhat rugged as in Fig. 4.16. It is convenient to define a plane of failure normal to the direction of the tensile force and the particle pairs that make up the actual surface of the split can be referred to as being in the plane.

To determine the tensile strength, we begin by finding the number of contact bonds which must be broken to achieve the postulate fracture. Since the spheres are randomly arranged, any plane of area A passing through the aggregate will intersect P particles,

$$P = (1 - \varepsilon_{agg}) \frac{A}{A_p} \tag{4.12}$$

where A_p is the mean cross-sectional area of a sphere of radius a, which is found to be

$$\begin{aligned} A_p &= \frac{1}{2a} \int_0^a \pi(a^2-y^2)dy \\ &= \frac{2}{3} \pi a^2 \end{aligned} \tag{4.13}$$

Thus P/2 particles are exposed on each face of the actual surface of split of the fracture with plane of failure area A. Any one particle has k/2

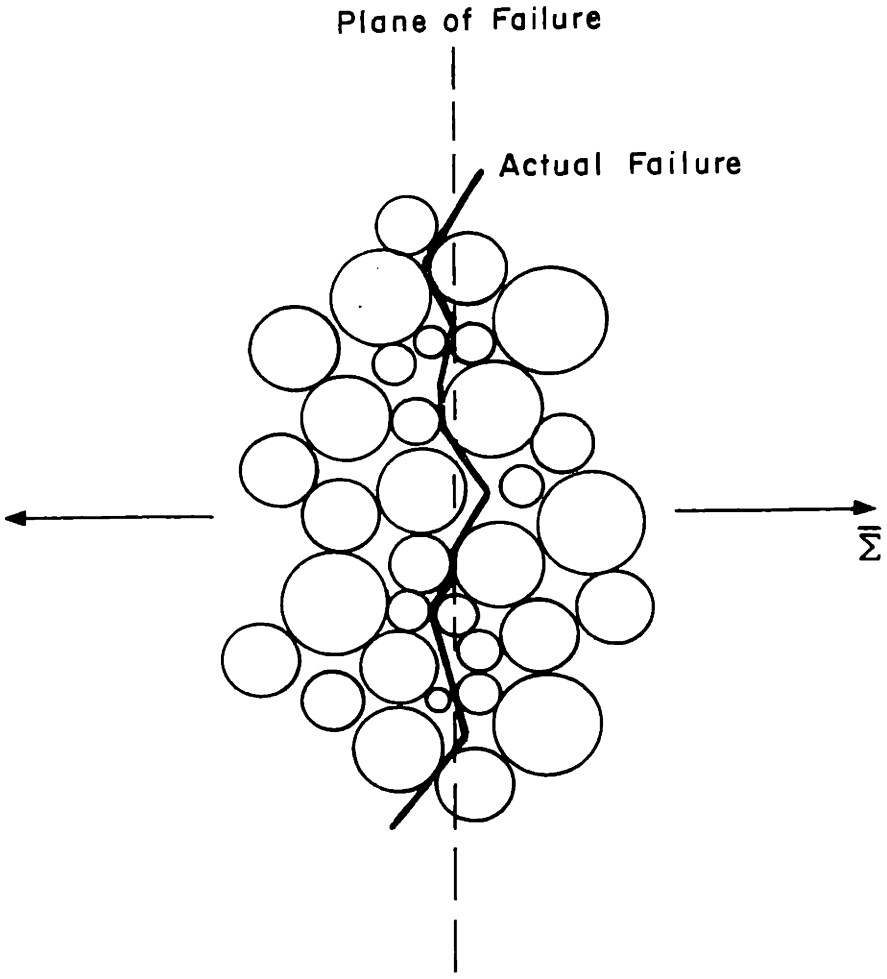

Figure 4.16 Model for calculation of tensile strength of an agglomerate of particles.

bonds in the exposed hemisphere. These bonds are distributed over the entire hemisphere in a random way. Averaging the bonding forces to obtain the normal component is just the average of a sinusoidal over a half period, or 1/2. The tensile force, $\Sigma_t A$, required to break the aggregate along the plane of failure is then just

$$\begin{pmatrix}\text{Force}\end{pmatrix} = \begin{pmatrix}\#\text{ particles in (exposed face of) fracture}\end{pmatrix} \begin{pmatrix}\#\text{ bonds in (one hemisphere) of a particle}\end{pmatrix} \begin{pmatrix}\text{averaging factor (for normal component of force}\end{pmatrix} \begin{pmatrix}\text{force per (contact band)}\end{pmatrix}$$

$$\Sigma_t A = \left(\frac{P}{2}\right)\left(\frac{k}{2}\right)\left(\frac{1}{2}\right)(B) \tag{4.14}$$

or solving for the tensile strength

$$\Sigma_t = \frac{3(1-\varepsilon_{agg})kB}{16\pi a^2} \tag{4.15}$$

For reference, the values of ε_{agg} and k have been studied for randomly close packed uniform spheres to be[23] $\varepsilon_{agg} \cong 0.38$, $k \cong 10$. These numbers do vary, however, depending on the degree of shakedown or pressing on the assemblage.

5. Application to Packed and Fluidized Beds -- Dislodging Mechanisms

The probability of retention or removal of a particle from a surface depends on the interplay of the forces of adhesion reviewed in the previous section with dislodging acting on the particles. The nature of dislodging forces in packed and fluidized beds are very different, in fact the nature of these forces in fluidized beds requires the consideration of aspects of the adhesion forces which have heretofore not been considered in the literature. The development of an understanding of these aspects is a principal contribution of this thesis.

We will begin by identifying the various dislodging forces which may be present in air filtration systems.

Gravity-Acceleration

Depending on the orientation of the surface with respect to gravity or an accelerating frame of reference and mass of the particle adhering to it, gravity or inertia may be sufficient to break the adhesive bonds. This force is

$$\bar{F} = \frac{4}{3}\pi\rho_p a^3 \bar{g} \tag{4.16}$$

where $\bar{g}$ is the acceleration vector, be it imposed by either gravitational or inertial mechanisms. For single particle adhesion, dislodgment occurs if this forces exceeds the adhesive force. Application to aggregate dislodgment is illustrated in the following example. Suppose a layer of particles on a substrate is subjected to a normal acceleration or gravitational field of intensity $\bar{g}$ as shown in Fig. 4.17. The dislodging stress $\bar{\Sigma}_d$ (force per unit area) in the deposited layer is a function of the position or x-coordinate in the layer, it being just $\bar{g}$ times the mass per unit area to the right of the position

$$\bar{\Sigma}_d = (1-\epsilon_{agg})\rho_p\,(D-x)\bar{g} \tag{4.17}$$

where D is the layer thickness. The tensile strength of the layer as given by Eq. (4.15) is a constant throughout. Figure 4.17 depicts the dynamics of the dislodgement of the layer. The plots below the figure show the tensile strength Σ_t and the dislodging stress Σ_d vs. x-coordinate. For thin layers, the tensile strength exceeds the dislodging stress for all x. As the layer thickens with further particle deposition the point is reached where Σ_d just exceeds Σ_t near the substrate. The aggregate will fracture along this plane when this critical layer thickness is reached

$$D = \frac{\Sigma_t}{(1-\epsilon_{agg})\rho_p g} \tag{4.18}$$

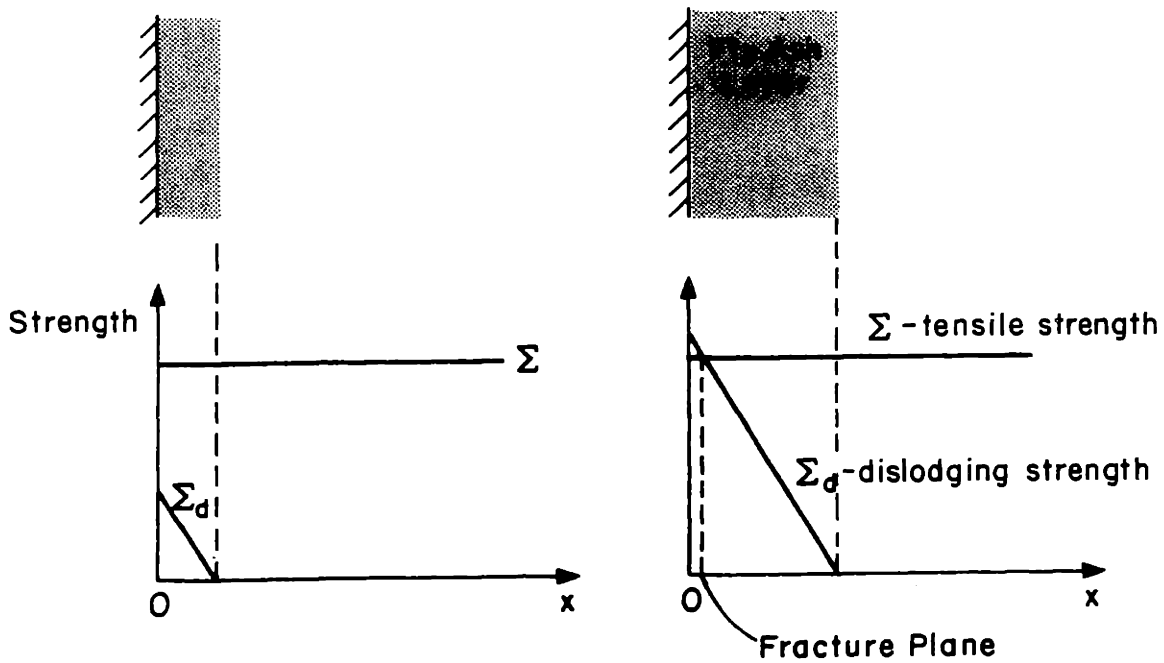

Figure 4.17 Dislodgement of a fly ash layer by acceleration.

Dislodgement by gravity is probably quite rare in filtration technology, but dislodgement by acceleration is the principal mechanism for removing collected dusts from electrostatic precipitator plates. The so-called "rapping" intensities are usually optimized in the field to be around 20-30 g's.

One might expect fluidized bed collectors to exhibit acceleration dislodgement resulting from the motion of bed particles in the fluidized state. This is indeed the case; in fact, the accelerations are so intense that our adhesion force models are no longer applicable. Particles in fluidized beds are suspended by the vertical gas flow and are thus relatively free to move. Fluidized beds for air pollution control typically require particle sizes in the millimeter range. Uniformly fluidized beds of such particles exhibit bubbling, and the associated high rates of particle mixing and particle agitation. This results in frequent and energetic particle-particle collisions. The collisions of such hard particles results in accelerations or equivalently, dislodging forces which are impulsive in nature and of magnitude far exceeding any adhesion forces which may attach dust particles to them. Witness the attrition of fluidized bed particles whereby the dislodging forces from collisions and scraping are so large as to even break the molecular chemical bonds of the solid bed particles. It would indeed appear futile to expect fluidized beds to retain appreciable amounts of collected dust based on the state of the art knowledge of adhesion mechanisms. The solution of this problem is the subject of the remaining sections of this chapter.

b. Blow-Off

The other principle dislodging mechanism encountered is blow-off. The literature is vague on this subject and quantification difficult. Formulations forproduction are usually only valid for the specific experimental configurations studies (see for example Larsen[30]). Difficulties arise because of the lack of understanding of local flow patterns near the small particle being

blown off of the surface. For lack of a better formulation we will assume that dislodging forces by blow-off are of the order of the air drag on an isolated particle in a flow of a suitable effective velocity. This force is;

$$F_D' = C_D \frac{\rho U^2}{2}$$

where C_D is the coefficient of drag, A the bodies (in this case the sphere's) projected area in the direction of the gas flow, ρ the gas density and U the gas velocity. Figure 4.17a is a plot of the drag coefficient vs. Reynolds for the case of a sphere. For Reynold's numbers less than about 1 (or in other words for particles of radius less tham 10mm in a gas of velocity 1m/sec), the coefficient of drag C_D can be week approximated by

$$C_D \approx \frac{24}{R_e}$$

which reduces equation to the familiar Stokes drag form

$$F_D = 6\pi\eta\, a\, U$$

c. Comparison of Forces

It is now instructive to compare some of the various adhesion and dislodging forces for particles on flat surfaces. These are shown in Figure 4.17a, plotted vs. particle radius a. Assumptions for each force are:

London-Van der Walls: Separation distance is about 4Å.

Electrostatic: Plotted is $4\pi\varepsilon_o\, a^2\, E^2$ which is the typical force magnitude for those analyzed. E is taken as being the breakdown strength of air at STP, thus those are the maximum obtainable forces.

Capillary: These are the forces for a bridge of water at STP as the bridge volume goes to zero and particle separation is zero.

Gravity: The gravitational force for a unit density sphere.

Stokes drag: The drag force for small particles in a 1 m/sec gas flow velocity. The Cunningham correction factor is not included.

The plot shows that for micron and submicron sized particles capillary forces, if present, are dominant. For dry systems, Van der Walls forces are substantial and dominant. Blow-off and gravity are not important. This analysis is useful for packed bed collectors, but it should be remembered that in fluidized beds, the impulsive collision forces are completely dominant over all those studies here.

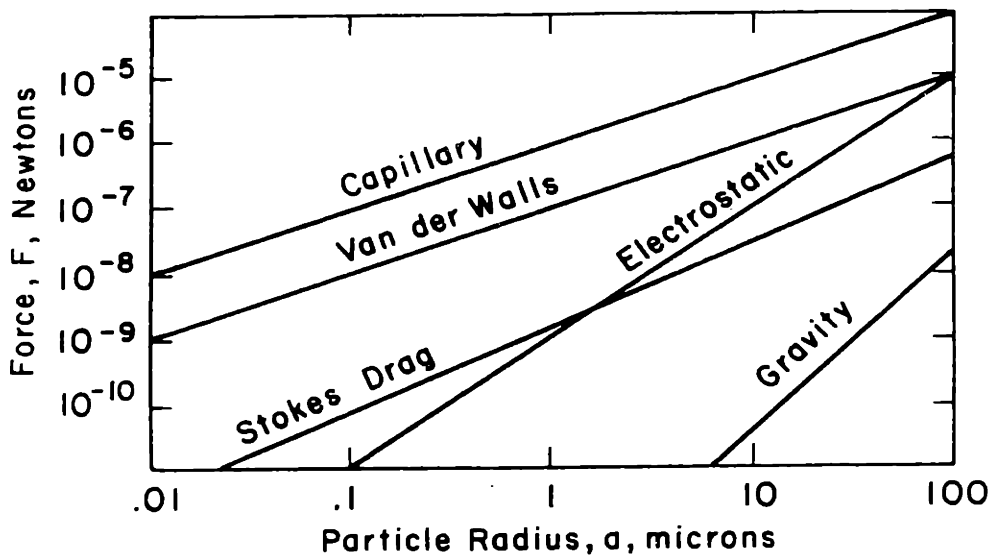

Figure 4.17a Force magnitudes of various adhesion and adhesion disloding forces.

B. Fluidized Bed Dynamic Adhesion Model -- Theoretical and Experimental Studies

The adhesion mechanisms detailed previously were determined for statically applied forces, but the removal of particles attached to a surface is really a dynamic process. Most dislodging forces considered in previous literature

were essentially statically applied, i.e., gravity, aerodynamic drag, or even rapping, that is the time during which the dislodging force is applied is longer than that needed to remove the particle. As we have pointed out, disloding forces in fluidized beds are very large in magnitude, but are applied impulsively, i.e. for very short durations. Because of their intended applications previous authors have ignored the dynamics aspects of the particle removal process.

The dynamics of removing a particle from the surface involves two considerations in addition to the static adhesive force; namely, the magnitude of theseforces as a function of the particle distance from the surface and the appearance of any new forces resulting from the relative motion of the particle and the surface. The dependence of adhesive force on separation has been dealt with already. For Van der Walls, and electrical forces, no additional forces can be foreseen to be the result of motion. For the liquid capillary adhesion mechanism, however, the rupturing of the bond involves motion of the liquid. Because of the very small physical dimensions dealt with, it is very likely that fluid viscosity may prove significant in retarding the motion of the sphere; in fact, we will find viscosity to be dominant.

a. Viscous Liquid Bridge Model

The model we will now consider is based on the geometry of Fig. 4.11. In it two identical spheres are bound by a liquid bridge at their contact point. Important dimensions are the sphere radius a, the sphere to sphere separation x, the liquid bridge neck radius a_n, and the liquid bridge thickness d. Because of the complexity of the geometry and fluid motion the model will be derived dimensionally. In this way it is equally valid for the sphere-sphere or sphere-plane cases and the liquid bridge thickness d is that for each case respectively.

We wish to derive an equation of motion for the upper sphere assuming the lower sphere to be fixed in space. As the upper sphere moves, two forces act on it resulting from the liquid bridge. First, the capillary contracting force given in Eq. (4.11) with F_{max} as in Eq. (4.9) acts in the negative x-direction. Second, motion of the sphere is accompanied by motion of the liquid in the bridge. Viscosity of the liquid dissipates energy and retards the motion. Because of the viscosity, pressure gradients are required to move the liquid. These pressures result in retarding forces on the sphere. We will ignore the inertia of the liquid as it is much less than the inertia of the sphere for small liquid bridge volumes.

The liquid disc has two fundamental size scales, d, the disc edge thickness, and a_n, the neck radius. As the spheres move apart the geometry of liquid motion is very complex. We will assume that as the motion occurs, the fluid mechanics can be characterized by a length scale that is the geometric mean of the two available dimensions.

Pressure gradients to drive the liquid motion are then of the order

$$\frac{\partial P}{\partial r} \sim \frac{P}{\sqrt{a_n d}} \qquad (4.19)$$

where $\sqrt{a_n d}$ is the above mentioned geometric mean and P is some measure of characteristic pressure in the disc. If the flow of the liquid is laminar as we postulate and expect, considering the small dimensions, high viscosities, and moderate velocities encountered, we expect the pressure gradient to drive the liquid roughly according to the conventional viscous channel flow relations where the channel is of width $\sqrt{a_n d}$, η is the liquid viscosity and u_ℓ the characteristic liquid velocity.

$$\frac{\partial P}{\partial r} \sim \eta \frac{u_\ell}{a_n d} \qquad (4.20)$$

Equating Eqs. 4.19 and 4.20 we find the relation between pressures and liquid velocities developed in the liquid bridge.

$$P \sim \frac{\eta u_e}{\sqrt{a_n d}} \tag{4.21}$$

To relate these pressures and velocities to those of the sphere, whose motion we are primarily concerned about, we need to consider the geometry of an ideal liquid bridge. The liquid bridge forms a disc of thickness d and width a_n, as in Fig. 4.18. The edges of the disc are exposed to the air while the top and bottom of the disc touch the spheres. Upward motion of the upper sphere requires radially inward motion of the liquid at its edges; in fact, conservation of mass requires

$$u_r (2\pi a_n d) = u_s(\pi a_n^2) \tag{4.22}$$

where u_s is the vertical (x-directed) velocity of the sphere.

Because liquid velocity is largest at the disc edge, they are representative of thevelocities responsible for the greatest viscous retarding forces. To achieve such liquid motion the pressure must be a maximum at the disc edge and decay radially inward in the disc. The decay distance is characterized by length $\sqrt{a_n d}$, Eq. (4.19). Thus force on the upper sphere results from pressure acting in a ring of diameter a_n (the neck radius) and width $a_n d$ or effective area $2\pi a_n \sqrt{a_n d}$. The under pressure in this ring is characterized by P, so the force on the upper sphere is

$$F_s \sim -P(2\pi a_n \sqrt{a_n d}) \tag{4.23}$$

Combining Eqs. (4.21), (4.22), and (4.23), while disregarding the numerical constants and noting that for small liquid quantities $a_n^2 = 2da$ we find the force-velocity relation.

$$F_s \sim -\eta a u_s$$

or

$$F_s = -\gamma_v u_s \tag{4.24}$$

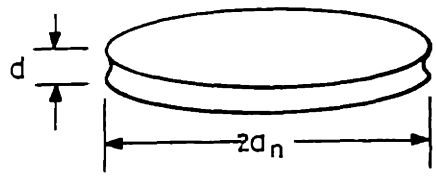

Figure 4.18 Geometry of liquid disc for viscous adhesion model.

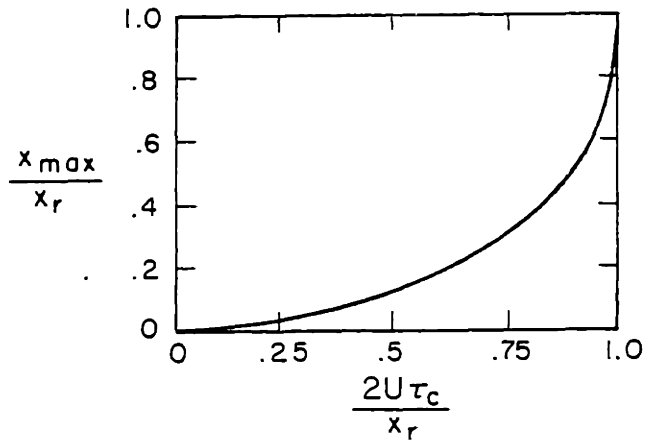

Figure 4.19 Normalized maximum particle excursion vs. normalized impulse strength for capillary force dominated case of liquid adhesion model.

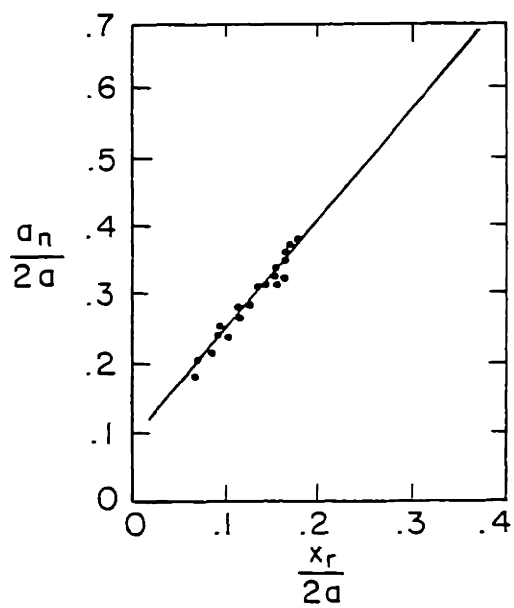

Figure 4.20 Liquid bridge neck radius vs. particle rupture separation (from Fisher).

where $\gamma_v \sim na$.

The equation of motion of the upper sphere when not subjected to any externally applied forces is then

$$m\frac{d^2x}{dt^2} = -F_{max}\left(1-\frac{x}{x_r}\right) - \gamma_v \frac{dx}{dt} \tag{4.25}$$

where $m = 4/3\pi\rho_p a^3$ = mass of the sphere.

We can non-dimensionalize this equation by introducing the normalized variables

$$\underline{x} = \frac{x}{x_r}$$
$$\underline{t} = \frac{t}{\tau} \tag{4.26}$$

and Eq. (4.25) becomes

$$\frac{d^2\underline{x}}{d\underline{t}^2} + \frac{\tau}{\tau_v}\frac{d\underline{x}}{d\underline{t}} - \frac{\tau^2}{\tau_c^2}\underline{x} = -\frac{\tau^2}{\tau_c^2} \tag{4.27}$$

where

$\tau_v = \frac{m}{\gamma_v}$ = viscous damping time constant

$$\tau_c = \sqrt{\frac{mx_r}{F_{max}}} \tag{4.28}$$

$= \frac{1}{\omega_n}$; ω_n = undamped natural frequency of the system

b. Viscous Liquid Bridge Impulse Response

Dislodging forces in fluidized beds are impulsive in nature, resulting from collisions of bed particles. It is the springlike nature of the liquid bonds that allows dust particles to be retained on the bed particle surfaces. The dynamics of dust particle adhesion can be modeled by the equation of motion derived in the previous section. The instant after the impulse force is applied to the sphere the equations derived are valid. The effect of the impulse force is to impose initial conditions on the problem. Consider a dust particle attached to a bed particle in the fluidized bed. The bed particle is traveling with a velocity U. Suddenly, it impacts another bed particle causing it to stop. In the frame of reference of the bed particle, this event is equivalent to suddenly giving the attached dust particle a velocity U. The impulsive force serves to instantaneously accelerate the dust particle to this velocity. Defining time t = 0 as just after the collision, the initial conditions in the frame of reference of the bed particle are

$$x(t=0) = 0$$
$$\frac{dx}{dt}(t=0) = U \tag{4.29}$$

or

$$\underline{x}(\underline{t}=0) = 0$$
$$\frac{d\underline{x}}{d\underline{t}}(\underline{t}=0) = \frac{U\tau}{x_r} \tag{4.30}$$

The solution to Eq. (4.27) is then

$$\underline{x} = 1 + Ae^{s_1\underline{t}} + Be^{s_2\underline{t}} \tag{4.31}$$

where

$$s_1, s_2 = \frac{\tau}{2\tau_v}\left[-1 \pm \sqrt{1 + 4\frac{\tau_v^2}{\tau_c^2}}\right]$$

$$A = \left(\frac{u_o\tau}{x_r} + s_2\right)/s_1 - s_2 \qquad (4.32)$$

$$B = \left(-\frac{u_o\tau}{x_r} - s_1\right)/s_1 - s_2$$

Physically, what happens after the impact is that the dust particle begins moving away from its substrate. Its inertia keeps it moving while the capillary contracting force and viscous retarding force act to slow its motion. If its motion is stopped before the liquid bond ruptures (if $x < x_r$ when dx/dt becomes zero), the capillary force then acts to restore the system to its initial state (x = 0). All we really care about is whether x ever exceeds x_r, or whether the liquid bond ruptures.

It is useful to look at two simpler limiting cases, one where the capillary contracting forces are much greater than the viscous retarding forces, and the other vice versa. These limiting cases are defined mathematically by comparing τ_v and τ_c. The first case is

$$F_{max} >> F_s$$

or

$$F_{max} >> \frac{\gamma_v x_r}{\tau} \qquad (4.33)$$

and is equivalent to

$$\tau_c^2 << \tau_v\tau \qquad (4.34)$$

which is also equivalent to the third term of Eq. 4.27 dominating the second. Because the system natural response time as characterized by τ cannot be smaller than the least of τ_c or τ_v, then Eq. 4.34 implies

$$\tau_c << \tau_v$$

Thus, the solution, Eq. 4.31, in this capillary dominated case is then given

by Eq. 4.31 with

$$S_1 = \frac{\tau}{\tau_c}$$

$$S_2 = \frac{-\tau}{\tau_c} \qquad (4.35)$$

The maximum excursion $\underline{x}_{max}$ can be found by noting that it occurs for the first time after $\underline{t} = 0$ when $d\underline{x}/d\underline{t} = 0$. Figure 4.19 shows the calculated $\underline{x}_{max}$ vs. initial velocity U (in the non-dimensional form $2U\tau_c/xr$. For $\underline{x}_{max} < 1$ the liquid bond is not ruptured. It can be seen that this is the case for all

$$U < \frac{2\tau_c}{x_r} \qquad (4.36)$$

When the viscous retarding forces are much greater than the capillary contracting forces,

$$\frac{\gamma_v x_r}{\tau} >> F_{max} \qquad (4.37)$$

or

$$\tau\tau_v << \tau_c^2 \qquad (4.38)$$

In this case

$$\tau_v << \tau_c$$

$$S_1 = 0, \quad S_2 = \frac{\tau}{\tau_v}$$

$$\underline{x} = \underline{x}_{max}\left|1 - e^{-t/\tau_v}\right| \qquad (4.39)$$

where

$$\underline{x}_{max} = \frac{U\tau_v}{x_r} = \frac{Um}{\gamma_v x_r} \qquad (4.40)$$

The damping constant, γ_v, has not yet been determined exactly, only dimensionally. If we assume that the constant of proportionality in that equation for γ_v is of order 1, we can compare τ_v and τ_c quantitatively. As a typical case we consider the adhesion of fly ash by a water film. For water at room temperature

$$\sigma = 7.3 \times 10^{-10} \frac{\text{kgm-m}}{\text{sec}^2}$$
$$\eta = 1.3 \times 10^{-3} \frac{\text{kgm}}{\text{m-sec}} \tag{4.41}$$

For fly ash with a small water additive quantity

$$a \simeq 1 \times 10^{-6} \text{ m}$$
$$d \simeq 1 \times 10^{-7} \text{ m} \tag{4.42}$$
$$\rho_p = 2.5 \times 10^{3} \text{ kgm/m}^3$$

A relationship for the rupture separation x_r has been developed experimentally by Fisher.[29] He found that

$$x_r \propto a_n \tag{4.43}$$

(his plot is given in Fig. 4.20) with the constant of proportionality being about 1.25. Using these results, Eq. 4.7 for F_{max}, and our typical values, we find

$$\frac{\tau_v}{\tau_c} \simeq 8 \times 10^{-3} \tag{4.44}$$

The viscous dominated case appears to be applicable for problems we will be dealing with.

The relation predicting γ_v was only dimensional in nature as in Eq. 4.24 and the constant of proportionality remains to be determined. Equation 4.40

specified the criterion for detachment of a particle. Restated, a particle is dislodged if

$$\frac{Um}{\gamma_v x_r} > 1 \tag{4.45}$$

We can use Eq. 4.24 for γ_v,

$$m = \frac{4}{3}\pi\rho_p a^3 \tag{4.46}$$

and Eq. 4.43 to determine that dislodgement is governed by the adhesion parameter S,

$$S = \frac{U\rho_p a^{3/2}}{\eta d^{1/2}} \tag{4.47}$$

Some critical value of S exists, S_{crit}, such that for $S > S_{crit}$ the particle is dislodged. The value of S_{crit} cannot be determined analytically because γ_v is only dimensionally specified.

The following section describes a set of fundamental experiments which were undertaken to determine the validity of the above theory and to measure the value of S_{crit}.

c. Fundamental Viscous Adhesion Experiments

In this set of experiments the dislodgement of isolated particles is measured. These are initially attached to a substrate by the liquid and subjected to impulsive dislodging forces of the type previously described. The particles were laboratory grade glass beads of radii .25 and .5 mm. They were attached to aluminum foil substrates by thin films of 10 W and 20 W motor oil.

The oil coating thickness was controlled and determined in the following way. A fine mist of the specified oil was produced in an atomizer-nebulizer. The mist was directed into a chamber in which the 1 cm^2 foil piece was placed on a grounded plate. A set of sharp needles above the grounded plate was

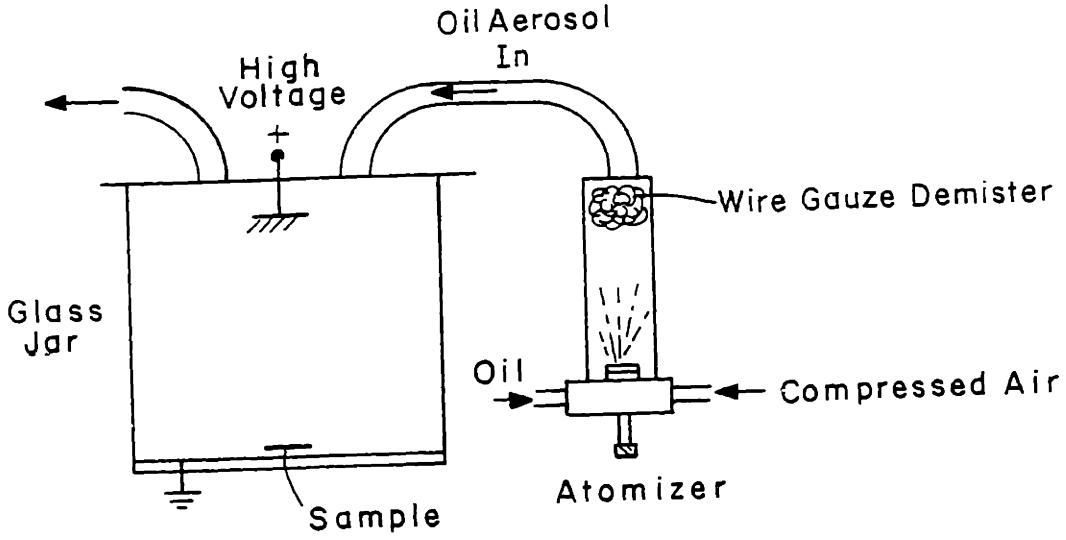

Figure 4.21 Schematic of apparatus for depositing uniform known amounts of oil on $1cm^2$ foil piece.

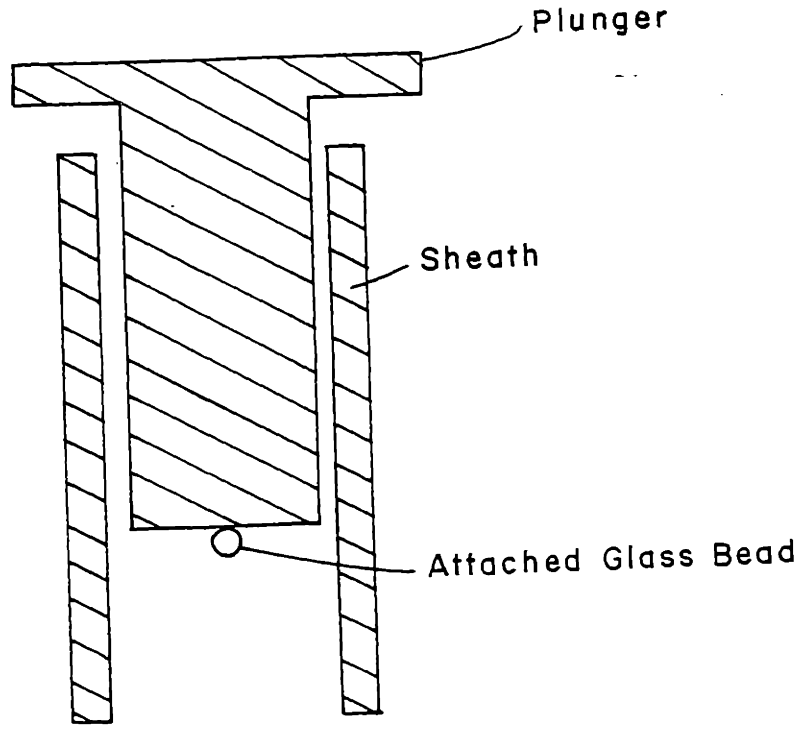

Figure 4.22 Schematic of plunger apparatus for fundamental study of adhesion of spheres by viscous liquids.

held at a high potential, producing corona and electrostatically depositing the oil mist on the ground plate and foil piece. The foil piece was much smaller than the deposition area, so that the foil received uniform mist deposition over its entire surface. After sufficient deposition, the foil was removed. The thickness of the oil coating was determined by weighing it before and after mist deposition, with the added weight considered to be oil uniformly spread on its surface.

A number of glass beads were then placed on the foil, sufficiently spaced such that no interaction between beads was possible.

Impulsive dislodging forces were applied to the beads via the plunger assembly shown in Fig. 4.22. The foil was attached securely to the bottom of the plunger with the attached beads hanging from it. The plunger was then dropped from successively higher distances. Upon dropping, the plunger accelerated under the action of gravity until it struck the supporting frame. At this point its motion was suddenly stopped, thus imparting an impulsive force to the suspended glass beads. Our theory, though, does not require us to calculate the magnitude or duration of the impulse, only its time integral which can be equivalently expressed by the imparted change in velocity. The velocity of the plunger and glass beads before impact is given by

$$U = \sqrt{2g\ell} \tag{4.48}$$

where g is the gravitational acceleration constant and ℓ is the distance that the plunger falls before being stopped. After impact the velocity of the plunger (and foil) is zero, while the glass beads still have velocity U. Thus the conditions for which the previous section's analysis is formulated are achieved.

As the plunger was dropped from successively greater heights, more

glass beads were dislodged. At each drop height, the number of beads dislodged was recorded. Then the average dislodging velocity U_d was determined for each run. Numerous runs were performed in which the bead size a, oil viscosity η, and oil thickness d were varied. The results of the experiments are summarized in Fig. 4.23. In it the average dislodging velocity U_d is plotted vs. the parameter $\eta d^{1/2}/\rho_p a^{3/2}$. Our viscous adhesion theory predicts that the critical adhesion parameter which we have now experimentally determined,

$$S_{crit} = \frac{U_d \rho_p a^{3/2}}{\eta d^{1/2}}, \tag{4.49}$$

should be invariant. This is equivalent to our data in Fig. 4.23 all falling in a straight line. Further, the slope of the straight line should be the numerical value of S_{crit}. Our data is seen to reasonably fit a straight line and its slope gives us an experimentally determined value of S_{crit},

$$S_{crit} \simeq 1.4 \tag{4.50}$$

This number can be traced back through the derivation leading to Eq. 4.47 to determine that

$$\gamma_v \simeq 3.3\, \eta a \tag{4.51}$$

2. Use of the Model for Fluidized Beds -- Fly Ash Breakthrough Experiments

The applicability of the viscous adhesion theory, as verified by the fundamental experiments, to adhesion in fluidized beds remains to be studied, The fundamental experiments were for particle sizes and oil coating thicknesses much greater than we expect to encounter in fluidized beds. Also, the impulse force model is just that for fluidized beds, a model, and its validity needs to be tested.

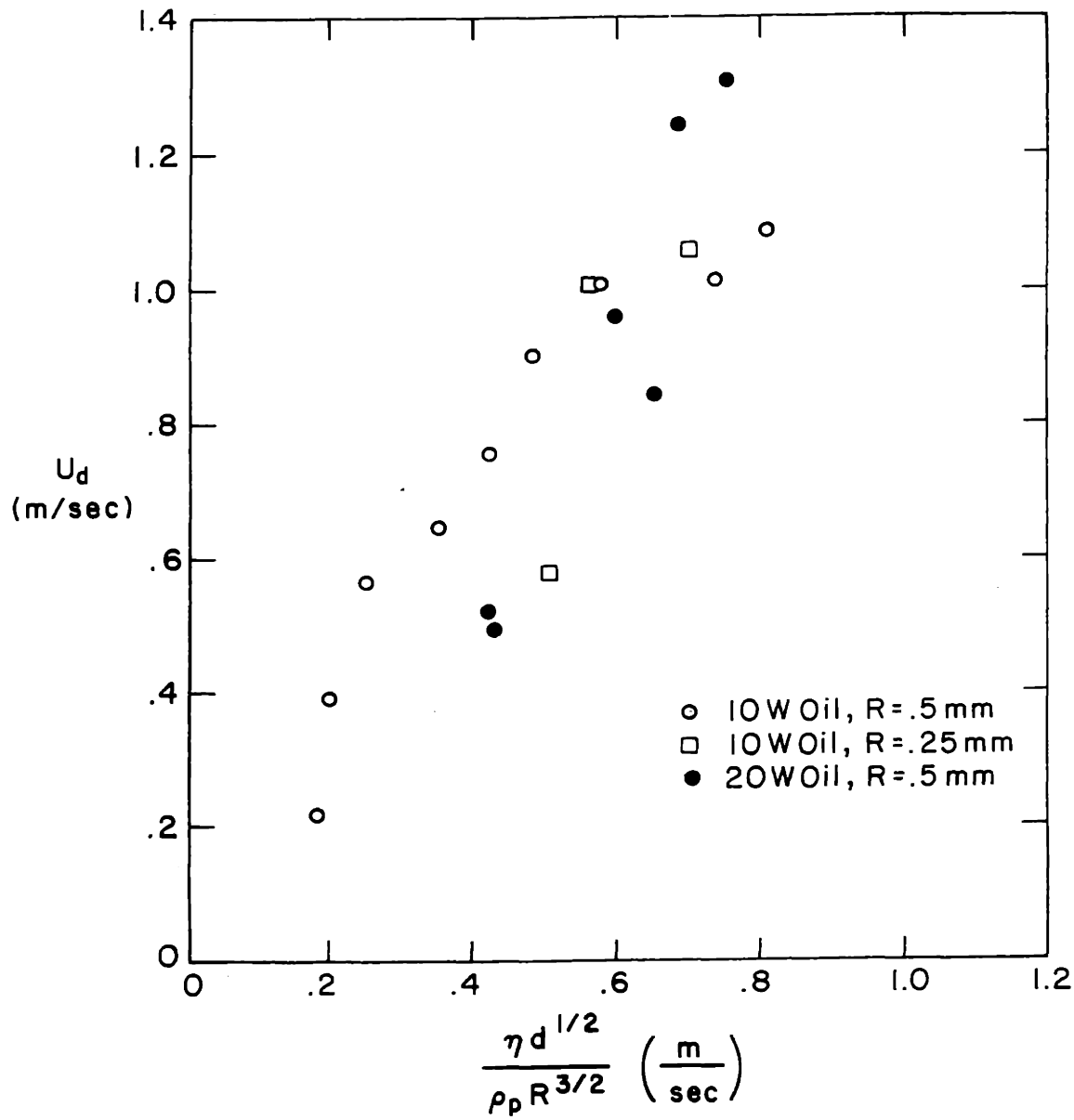

Figure 4.23 Experimental results of fundamental experiment on adhesion of spheres by viscous liquids. Experimental dislodging velocity plotted vs. theoretical dislodgement velocity parameter.

The simplest test of these models was envisioned to be the following experiment. Fluidized beds of uniform glass beads were set up and precoated with known quantities of oil. A fly ash of known size distribution was then injected into the inlet air stream of the bed. The feed rate of the fly ash was held constant while the outlet fly ash concentration was monitored continuously, thus giving a collection efficiency function vs. time. Fortunately the experiments yielded results where the fluidized beds showed high collection efficiency (η = 95%) for an initial time period, then showed a rapid drop in efficiency until $\eta \approx 0$ (see Fig. 4.24). This motivated naming the experiments as "breakthrough" and defining a "breakthrough time" t_b as the time when the collection efficiency has dropped to 50% of its initial high value.

a. Oil Mixing Models

Additional modeling of mass transfer processes in the bed is required for meaningful analysis of the breakthrough experimental results. Specifically, the behavior of the oil in the bed as fly ash is collected is unknown at the outset. It is expected that initially the oil in the bed uniformly coats all the bed particles by the good particle-particle contacting provided by the rapid solids mixing in the fluidized bed. In other words, every exposed surface in the bed is covered with the same thickness T of oil. As fly ash is collected, this oil coating becomes covered and may spread to cover the new surfaces introduced to the bed by the collected fly ash. The nature of the oil spreading or oil mixing is the subject of two models presented in this section, namely the limited mixing and complete mixing models. It is left to experiment to determine which is most appropriate.

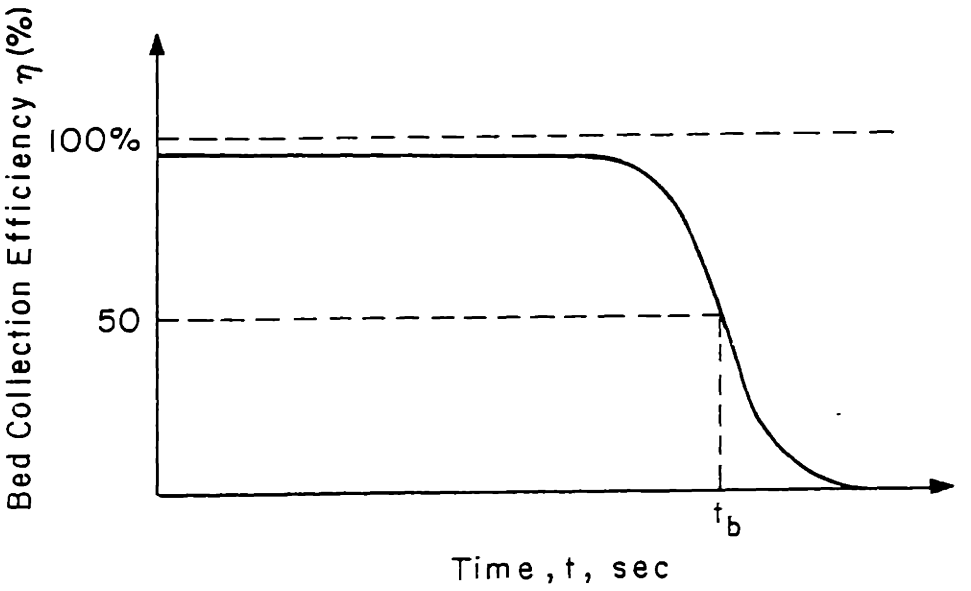

Figure 4.24 Expected collection efficiency vs. time plot for an oil coated fluidized bed collecting fly ash.

Limited mixing model. Consider the deposition of fly ash particles on the oil coated bed particles of a fluidized bed. This model assumes that when a fly ash particle is deposited on the oil coated bed particle surface it covers a certain amount of oil. This covered oil is used to adhere the fly ash particle and is forever lost to the system for adherence of other fly ash particles, that is, this oil is frozen beneath the fly ash particle. The other side of the fly ash particle is initially dry, but is exposed to the bed. By contact with the rest of the bed, though, it will become oil coated, in fact it can be assumed that the remaining oil in the bed will cover this new surface such that the oil thickness is uniform over the exposed surface of the bed. As subsequent fly ash particles are collected, this process is repeated.

To treat this process quantitatively, we make the assumption that the bed has an essentially constant amount of exposed surface area S_o. That is, as fly ash particles are deposited, they cover the same amount of surface area as they create. The thickness of the oil coating T on the exposed surface is, however, not constant as oil is being covered by deposited fly ash. Thus the oil coating thickness on the exposed bed surface is a function of time, T(t). Further, let us define t_m as the time required to cover the bed with a single layer of fly ash particles. Thus, t_m is a function of the fly ash deposition rate, fly ash size, and exposed bed surface area.

A conservation of mass equation for the oil can be used to arrive at an equation for T(t). The volume of oil on the exposed bed surface at time t is $S_oT(t)$. This volume must equal the oil on the exposed bed surface at time $t + \Delta t$ (or $S_oT(t + \Delta t)$) plus the amount of oil covered by fly ash deposition during Δt. Since the whole bed surface area is covered in time t_m, then $S_o(\Delta t/t_m)$ is covered in time Δt, and $T(t)S_o(\Delta t/t_m)$ is the volume of oil covered

in Δt. Equation 4.52 results:

$$S_o T(t) = S_o T(t + \Delta t) + S_o T(t) \frac{\Delta t}{t_m} \tag{4.52}$$

Rearranging terms, dividing by Δt and taking the limit $\Delta t \to 0$ gives

$$\frac{dT}{dt} = - \frac{T}{t_m} \tag{4.53}$$

If we let T_o be the initial oil thickness in the clean bed and define $t = 0$ to be when the fly ash collection begins, then

$$T(t = 0) = T_o \tag{4.54}$$

and Eq. 4.53 is solved for

$$T = T_o \exp(- \frac{t}{t_m}) \tag{4.55}$$

Equation 4.55 can now be used to predict breakthrough times t_b given the viscous adhesion model as dictated by Eqs. 4.49 and 4.50. We expect breakthrough to occur when the oil thickness is so thin that it is not sufficient to adhere fly ash to the bed particles. This critical thickness is d in Eq. 4.49. Other parameters in Eq. 4.49 as applied to our fluidized bed model are the bed particle velocity U, oil viscosity η, fly ash mass density ρ_p, and fly ash radius a.

When oil thickness reaches this critical thickness, breakthrough occurs, mathematically this is stated

$$T(t_b) = d \tag{4.56}$$

Using Eq. 4.55

$$T_o \exp (- \frac{t_b}{t_m}) = d \tag{4.56}$$

or

$$\frac{t_b}{t_m} = - \ln(\frac{d}{T_o}) \tag{4.57}$$

This result is plotted in Fig. 4.25a. The relation between breakthrough time t_b and initial oil thickness T_o is not linear according to this model..

Complete Mixing Model. This model is much simpler in concept and derivation than the limited mixing model. Basically it is this. The initial oil in the bed is uniformly spread over all available surface in the bed. This surface consists of the initial clean surface of the bed S_o and any addition surface added by depositing fly ash $S_A(t)$. Thus, S_A is a function of time because fly ash is continually being deposited. This model appears attractive in light of the success of fluidized bed models in predicting completely mixed behavior. Several mechanisms exist which could account for the mixing of oil that is covered by fly ash.

First, the fly ash particles are free to roll about on the surface of the bed particle and in this way could act like ball point pens to uniformly spread the covered oil. This rolling and oil spreading action is promoted by the particle-particle collisions and contact in the bed. Second, through bed particle collisions, adhered fly ash particles can be transferred from bed particle to bed particle, thus exposing once covered oil for mixing in the bed. Because those mechanisms are most likely present in fluidized beds, this model appears attractive.

Suppose the bed is covered with a monolayer of fly ash in the time t_m (as we defined earlier). Also suppose that this monolayer of ash carries along a surface area S_A. Then an oil layer of initial thickness T_o is spread to thickness $T(t)$ at a time t due to the increase in surface area $S_A(t/t_m)$ by the addition of fly ash. So

$$T(t) = \frac{T_o S_o}{S_o + S_A \frac{t}{t_m}} \tag{4.57}$$

At the breakthrough time $t = t_b$, then $T(t = t_b) = d$. So

$$\frac{T_o}{d} = 1 + \frac{S_A}{S_o}\frac{t_b}{t_m} \tag{4.58}$$

and a plot of t_b/t_m vs. T_o/d would look like Fig.4.25b. This model predicts that t_b is essentially linear with initial oil quantity.

Both of these oil mixing models are based on the postulate that the oil has enough time to mix during the continual deposition of the fly ash. Put another way, it is assumed that the oil mixing time is much less the characteristic fly ash deposition time t_m. Because oil mixing is achieved by bed particle contact and bed particle mixing, it should be characterized by at most the solids mixing time of the bed. This time is typically on the order of 1 second. Compared to $t_m \approx 100$ for even the highest fly ash loadings, this assumption appears valid.

b. Fly Ash Breakthrough Experimental Results

A more detailed explanation of the breakthrough experimental procedure is now given. Experiments were performed in the fluidized bed experimental channels described in Appendix A and shown in Figs. A.1 and A.B Bed particles were again laboratory quality glass beads. Runs were made for particle radii varying from .1 mm to 2 mm. Before a run was made, the beds were precoated with one of two types of No. 6 fuel oil, a low viscosity oil and a high viscosity oil. Oil coating was achieved in one of two ways. In the first, a measured amount of oil was poured directly into the bed, manually mixed, and then fluidized to achieve full mixing. In the second method, the fuel oil was atomized (in the nebulizer of Fig. 3.13) and injected into the inlet fluidizing gas of the bed. The bed collected the atomizing oil, and the collection of the bed was measured by filter paper

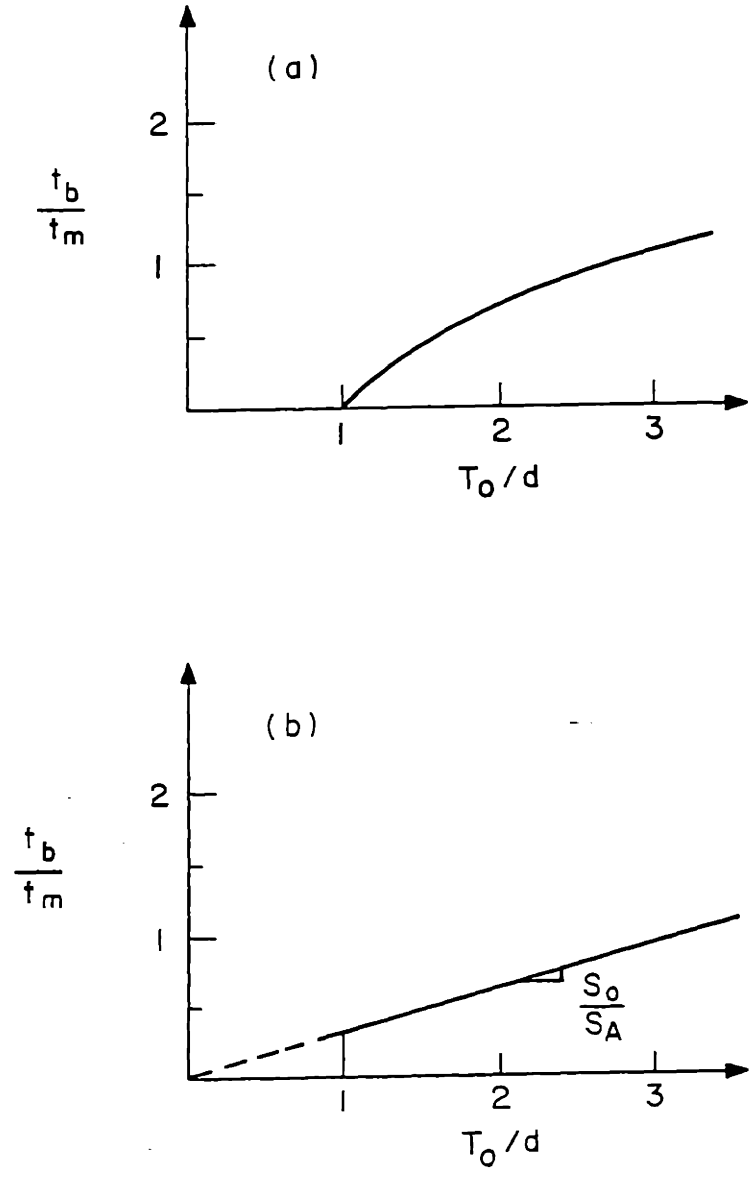

Figure 4.25 Oil mixing model theoretical plots of normalized breakthrough time to normalized initial oil thickness. a) Limited Mixing. b) Complete Mixing.

samples of the inlet and outlet gas. Thus the total amount of oil deposited in the bed was deduced. The two methods showed no noticeable differences in results.

Fly ash injection was achieved using a "turn-table" feeder shown schematically in Fig. A.9.

Fly ash mass loadings in the fluidized bed outlet gas stream were monitored continuously in real time using the following sampling system as shown schematically in Fig. A.13. An isokinetic probe mounted in the channel above the bed drew the gas sample which then was passed through the dilution system shown in Fig. A.11. With this system dilutions of 10:1 were obtainable and controllable. Dilution was necessary so that the mass monitor, the next step of the sampling train, could be used.

The response time of the mass monitor is related to the crystal resonant frequency which is in the MHz range. That of the D/A converter is related to the crystal difference frequency whose smallest value is 300 Hz. The longest response time is the gas residence time in the sampling tubes, which was minimized to be about 0.1 sec.

The experiments were run as follows. After oil coating the clean dry bed of glass beads, the proper fluidization conditions were set up and

measured. The fly ash injector, sampling system, and strip chart recorder were then turned on simultaneously. The experiment was then allowed to run until well after breakthrough. The strip chart was a record of events. A typical strip chart is shown in Fig. 4.29. It should be noted that by the sampling system constructed here, it is the slope of the strip chart plot that is proportional to the fly ash mass loading. Thus the small initial slope of the curve corresponds to a small fly ash loading in the outlet gas, and thus a high bed efficiency. The steep final slope similarly implies a very low final collection efficiency. Figure 4.30 shows the calculated curve for collection efficiency vs. time for the strip chart of Fig. 4.29.

Tests were run for many bed particle sizes, oil quantities, and fluidization velocities. The test conditions are summarized in Table 4.2.

The first use of the test results was to determine the proper oil mixing model. Experimental results were reduced to a plot of t_b/t_m vs. T_o/d. t_b was the experimentally measured breakthrough time, d was the theoretical oil critical thickness from Eq. 4.49, t_m and T_o were calculated from the experimental conditions using the following relations:

$$S_o = \frac{3\ell_o A(1 - \varepsilon_o)}{R}$$

$$t_m = \frac{\pi S_o \rho_p a}{3 m_o \eta_b U A} \qquad (4.59)$$

$$T_o = \frac{V_o}{S_o}$$

where ℓ_o = unfluidized bed height

ε_o = " " fraction voids

R = bed particle radius

m_o = incident fly ash mass loading

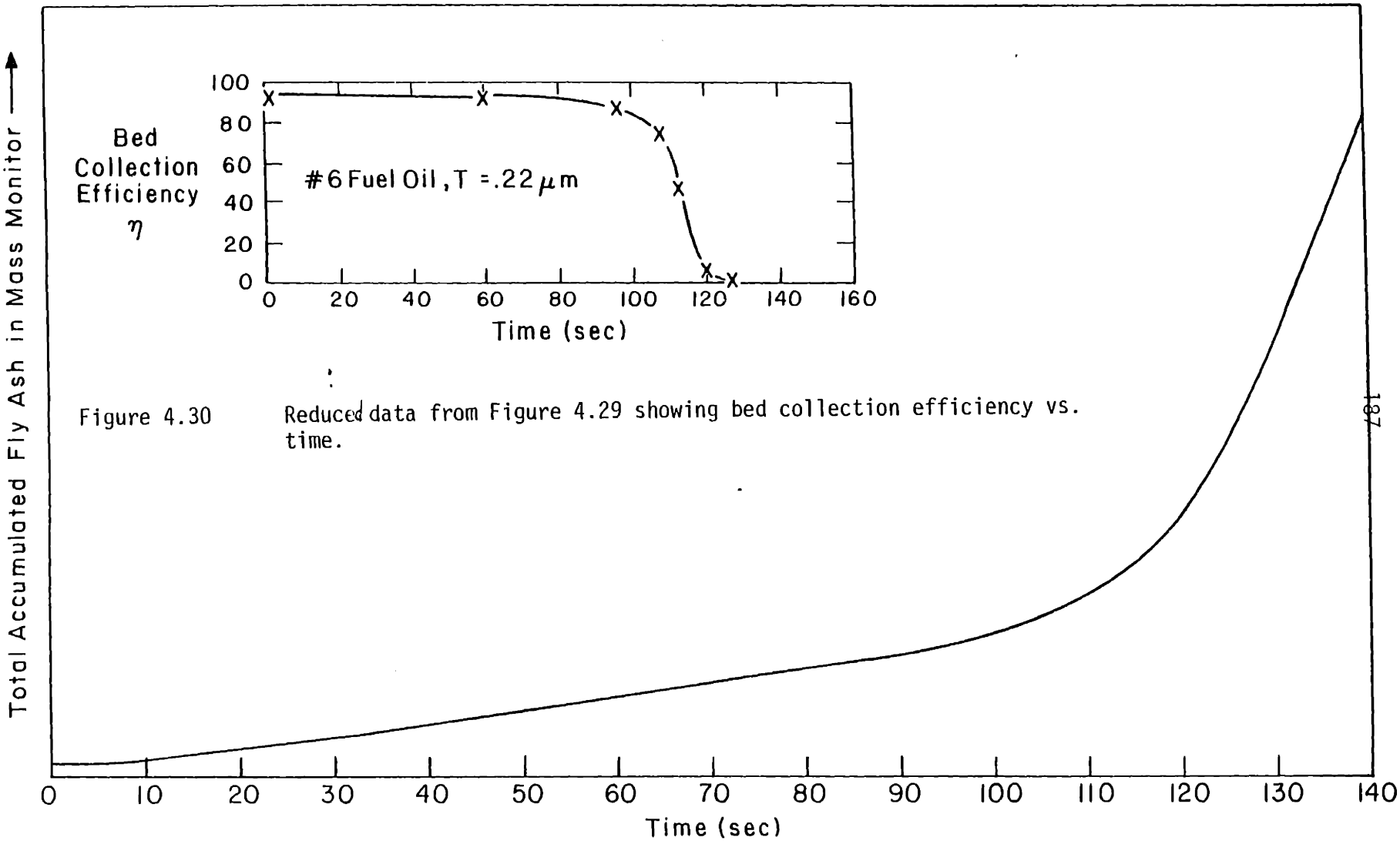

Figure 4.30 Reduced data from Figure 4.29 showing bed collection efficiency vs. time.

Figure 4.29 Strip chart for typical experimental run, measuring total accumulative sampled fly ash vs. time. 10 sec. equals 1 inch.

a = incident fly ash mean radius

η_b = initial bed collection efficiency

A = bed cross sectional area

V_o = added oil volume

Several experimental points from runs with three different bed types are shown in Fig. 4.31, which cover a wide range of initial oil thicknesses. The results apparently support the complete oil mixing model which is characterized by a linear relation between the plotted quantities.

We now use the complete oil mixing model to analyze our experimental results. Our experimental results and conditions give us T_o, t_m and t_b from which we can calculate an experimentally determined d using the complete oil mixing model

$$d_{exp} = \pi T_o \frac{t_m}{t_b} \qquad (4.60)$$

Our theoretical predictions of d are summarized as

$$d_{theory} = \left[\frac{U\rho_p a^{3/2}}{(1.4)\eta}\right]^2 \qquad (4.61)$$

All of the test results are summarized in Fig. 4.32 where d_{theory} is plotted vs. d_{exp}. If the theory is accurate, we would expect the points to lie on the slope 1 solid line shown. Our choice of presentation of the results reduces them to a form in which the individual bed parameters are all normalized out. The bracketed bars in the plot represent the range in d_{exp} which were observed for any one set of bed parameters as the initial oil quantity was varied. For each set of bed parameters d_{theory} is a single value.

Table 4.2 Breakthrough Experiment Bed Parameters

Run Number	Bead Diameter	Oil Viscosity	Fly Ash Loading	Mass Oil Added (gm)	Mass Ash Collected (gm)	Breakthrough Time (sec)	U_o (m/sec)
α - 1	1	--	high	0	0	0	.7
α - 2	1	low	high	.178	7.332	73	.7
α - 3	1	low	high	.473	11.836	115	.7
α - 4	1	low	high	.585	19.162	170	.7
α - 5	1	low	high	.869	25.145	245	.7
α - 6	1	low	high	1.875	60.66	657	.7
α - 7	1	low	high	2.300	59.053	660	.7
β - 1	1	low	low	0	0	0	.7
β - 2	1	low	low	.209	5.284	245	.7
β - 3	1	low	low	.552	13.447	630	.7
β - 5	1	low	low	1.692	39.080	1800	.7
β - 6	1	low	low	1.474	39.816	1600	.7
γ - 1	1	low	low	1.1	36.20	1750	.7
δ - 1	2	high	low	.216	7.59	335	1.1
δ - 2	2	high	low	.825	25.24	1000	1.1
δ - 4	2	high	low	.08644	1.776	75	1.1
δ - 5	2	low	low	.259	7.148	321	1.1
δ - 6	2	low	low	.658	20.179	860	1.1
ε - 1	2	low	low	0	0	0	1.1
ε - 2	2	low	low	.42	11.55	525	1.1
ε - 3	2	low	low	1.55	33.22	1510	1.1
ε - 5	2	low	low	.76	19.36	880	1.1
ι - 1	4	low	low	1.246	17.57	800	2.3
ι - 2	4	low	low	2.530	33.00	1500	2.3
ι - 3	4	low	low	.279	5.87	267	2.3
ι - 4	4	low	low	.476	8.69	395	2.3
ι - 6	4	high	low	.467	7.26	220	2.3

Oil Viscosities

low 8×10^{-2} $\frac{kg}{m/se}$

high 1.6×10^{-1} $\frac{kg}{m/s}$

Fly Ash Loading

low ≈ 2 gm/m^3

high ≈ 10 gm/m^3

All Cases

$\ell_o = 7.5$ cm

$\ell_f = 10$ cm

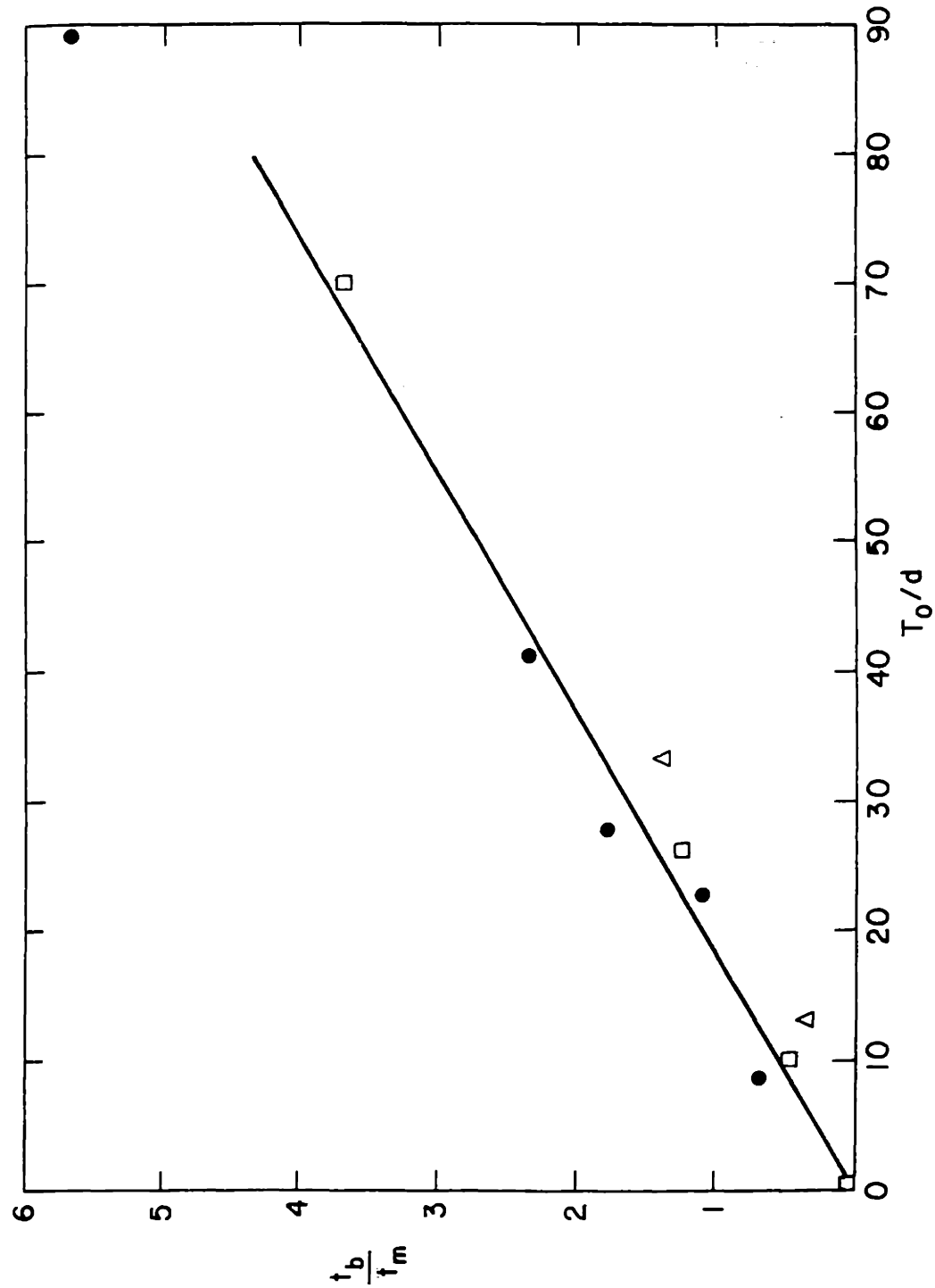

Figure 4.31 Experimentally measured normalized breakthrough time vs. normalized initial oil thickness for several runs.

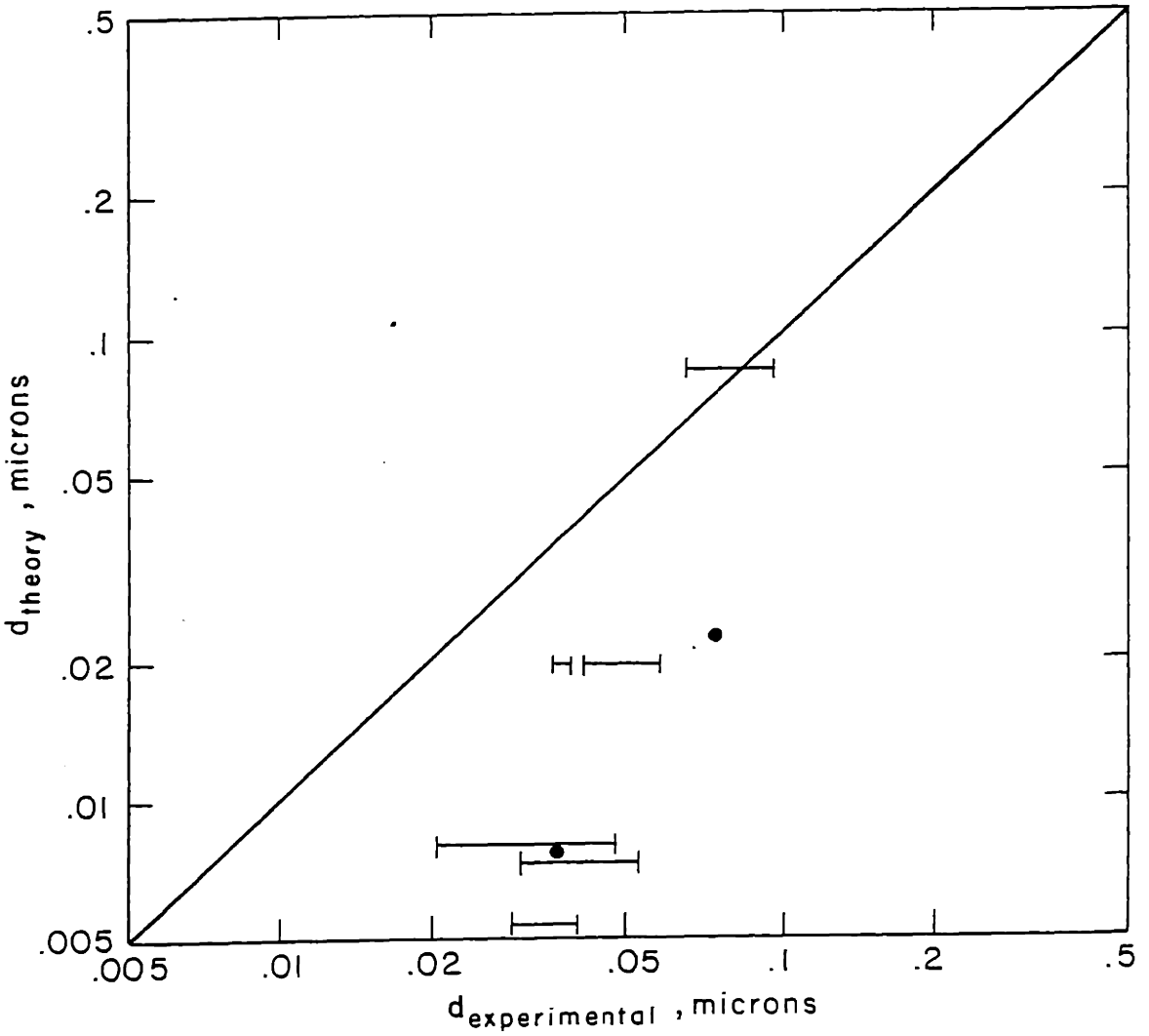

Figure 4.32 Comparison of experimentally determined critical oil thicknesses for particle dislodgement to those predicted theoretically.

A very interesting and important result is observed from the experimental results. Apparently there is an absolute minimum oil thickness required to adhere the fly ash, and this minimum is independent of bed parameters such as U, R, a, η, etc. The results appear to be approaching the theoretical values for larger oil thicknesses, but the available experimental equipment prevented the establishment of bed conditions which would provide theoretical oil thicknesses greater than about .1 μm.

The explanation of this absolute oil thickness minimum behavior derives from an examination of the effects of surface asperities. Surface asperities were discussed earlier in the section on capillary adhesion forces. It was pointed out that even polished glass surfaces show surface asperities of about 150 Å. It does not seem unreasonable then that naturally formed fly ash particles would exhibit surface asperities of at least this much. Our experimental results show the minimum required oil thickness to be in the range of 200 to 500 Å. This correlation is no coincidence.

To summarize this effect, it is apparent that the crevices formed by fly ash surface asperities must be filled with oil before the viscous (or for that matter capillary) adhesion mechanisms can take effect. The amount of oil necessary to do this was found to be equivalent to a 200-500 Å uniform coating on the fly ash tested. The theoretically predicted oil quantities (based on a perfectly smooth surface model) are much less than the amounts required to fill the asperities. For envisioned practical fluidized bed systems, even those with the most intense collisions, the theoretical oil qunatities just approach those required by the asperity limit.

These experiments point out a very useful fact. Because of asperities, the smallest oil quantity which can ever be used to effectively adhere fly

ash in fluidized beds is 2 to 3% of the mass of the fly ash being collected. This results from a simple geometrical calculation of the mass of a 200 to 500 Å layer of oil on the surface of a typically sized (5 μm diameter) fly ash sphere.

REFERENCES

(1) Tassicker, O.J., J. of the APCA, 25, 122 (1975)

(2) Tassicker, O.J., "Aspects of Forces on Charged Particles in Electrostatic Precipitators", Dissertation, Wollongong University College, Univ. of New South Wales, Australia, 1972.

(3) Bradley, R.S., Phil. Mag., 13, 853 (1932).

(4) Bradley, R.S., Trans. Far. Soc., 32, 1088 (1936).

(5) Hamaker, H.C., Physics, 4, 1058 (1937).

(6) Barnhart, D.H., and P.C. Williams, Trans. of the ASME, August 1956, p. 1229.

(7) Johnson, T.W., and J.R. Melcher, I & EC Fun., 14, 146, (1975).

(8) Lebedev, N.N., and I.D. Skal'skaya, Russian Physics: Technical Physics, 7, 3, 268 (1962), translated from Zhurnd Tekhnicheskoi Fisiki, 32, 3, 375 (1962

(9) Dietz, P.W., "Electrofuildized Bed Mechanics", Ph.D. Thesis, MIT, Spetember 19

(10) McLean, K.J., J. of the APCA, J. of the APCAm 26, 9, 866 (1976).

(11) McLean, K.J., J. of the APCA, 27, 11, 1100 (1977).

(12) Szirmai, S.G. and E.C. Potter, Journal of Physics EL Scientific Instruments. 1976, Vol. 9.

(13) Krupp, H. and G. Sperling, J. appl. Phys., 37, 11, 4176 (1966).

(14) Penney, G.W., Archives of Environmental Health, 4, 91 (1962).

(15) Penney, G.W. and E.H. Klinger, AIEE Trans. (Communications and Electronics), 81, 200 (1962).

(16) Niedra, J.M. and G.W. Penney, AIEE Trans. (Communications and Electronics), 12, 2, 46 (1965).

(17) Eremenko, V.N., Y.V. Naidech, and I.A. Lavirnenko, "Liquid Phase Sintering", 55, (Consultants Bureau, NewYork-London, 1970).

(18) Derjaguin, B., Koll. Zeit,. 69, 155 (1934).

(19) Bowden, F.P. and D. Tabor, "The Friction and Lubrication of Solids", Clarendon Press, Oxford, 302 (1950).

(20) Rayleigh, Lord, Proc. Roy. Soc., A156:326 (1936).

(21) Corn, M., J. of the APCA, 11, 11, 523 (1961).

(22) Pietsch, W.B., Nature, 217, 736 (1968).

(23) Bernal, J.D. and J. Mason, Nature, 188, 910 (1960).

(24) Mason, G. and W.C. Clark, Chem. Eng. Sci., 20, 859 (1965).

(25) Mason, G. and W.C. Clark Nature, 216, 826 (1967).

(26) McFarlane, J.S. and D. Tabor, Proc. Royal Soc., A202, 224 (1950).

(27) McHaffie, I.E. and S. Lenher, J. Chem. Soc., 127, 1559 (1925).

(28) Bowden, F.D. and W.R. Throssel, Proc. Royal Soc., A209, 297 (1951).

(29) Fisher, R.A., J. Agric. Sci., 16, 492 (1926).

(30) Larsen, R.I., American Ind. Hyg. A.J. 19: 265 - 270, August 1958.

V. Fluidized Bed Fly Ash Collection and Agglomeration

This chapter serves as the assembly point of the more fundamental processes modeled in the previous chapters into a theory that describes the steady-state behavior of a fluidized bed as a fly ash collector or agglomerator. We have separately modeled the mechanisms of fly ash deposition on and adhesion to fluidized bed particles. In this chapter we will incorporate these models into a collection and reentrainment model for the entire bed. First we will model a fluidized bed in the collection and reentrainment of a monodisperse aerosol, then extend the model to incorporate polydispersity. The application of the models to fluidized beds designed for collection or agglomeration will be discussed, and experimental results of fundamental studies and demonstration systems will be presented. Finally, the implications of these results for practical system design will be covered.

A. Models for Collection and Reentrainment in Fluidized Beds

1. Monodisperse Aerosol Model

Modeling of the collection and reentrainment of a monodisperse aerosol serves as a good vehicle for the definition of some new concepts useful for the description of more complicated systems and as a building block for the development of the polydisperse model and agglomerator models. We begin by considering a plug flow fluidized bed as in Fig. 5.1 and consisting of bed particles of radius R. The inlet gas is carrying a monodisperse aerosol of mass loading m_0 and aerosol particle radius a.

In the bed, we envision two processes occurring. Aerosol particles are deposited onto the bed particles by any of the mechanisms described in Chapter 3. For now we will simply say that the deposition of aerosol is

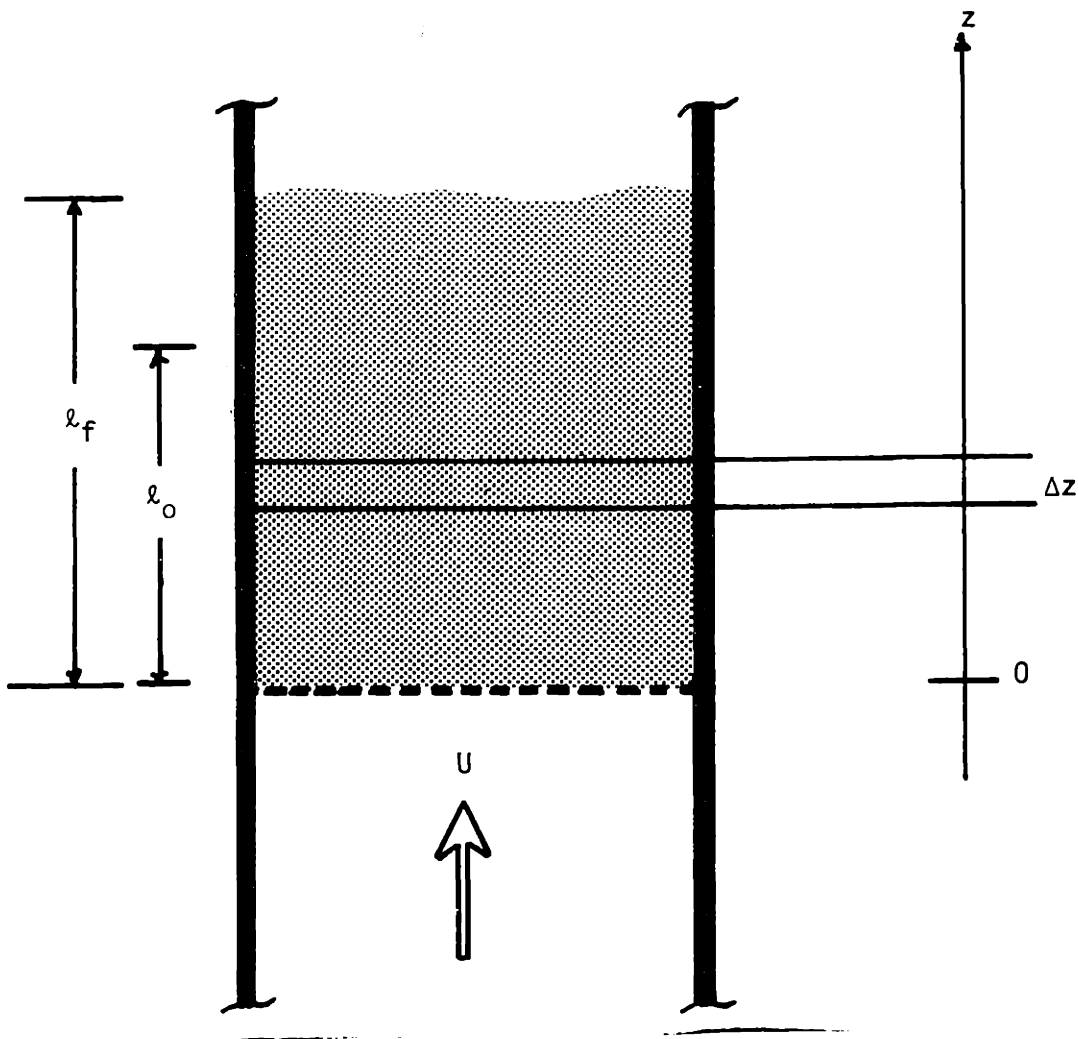

Figure 5.1 Schematic diagram for development of plug flow collection and reentrainment model.

determined by the overall single particle collection efficiency C_t which accounts for the superposition of all the mechanisms. Then we have a deposition rate Γ_c which depends on the gas superficial velocity U of bed particle radius R, the single particle efficiency C_t, and the local aerosol mass loading in the bed m(z):

$$\Gamma_c(z) = \pi R^2 U C_t m(z) \tag{5.1}$$

The units of Γ_c are kg/sec and it measures the rate of deposition of aerosol particles from the gas stream onto a single bed particle.

Once aerosol particles are deposited on the bed particle, there is a chance that they will be dislodged due to the interplay of adhesion and dislodging mechanisms described in Chapter 4. The retention of an aerosol particle will depend on several parameters, such as quantities of adhesive additives, aerosol size, bed agitation, etc. For now, we wish to keep this development as general as possible and we define a reentrainment rate Γ_e with units of kg/sec that measures the rate at which aerosol particles are reentrained into the gas flow from a single bed particle. The reentrainment rate Γ_e is expected at the outset to depend strongly on the amount of aerosol particulate that is on the surface of the bed particle. Clearly, nothing can be reentrained if there is nothing there, also some maximum reentrainment rate might be expected for arbitrarily large amounts of aerosol particulate on the bed particle surface. If we let M represent the amount of aerosol particulate on a single bed particle, Γ_e might have a dependence on M as shown in Fig. 5.2. In the figure, Γ_e saturates to a value of Γ_{es} for all $M > M_o$. M_o is the value of M above which the reentrainment rate is independent of M. Thus M_o might typically be the mass of aerosol required to entirely cover the bed particle, or some multiple of it. The saturation level Γ_{es}

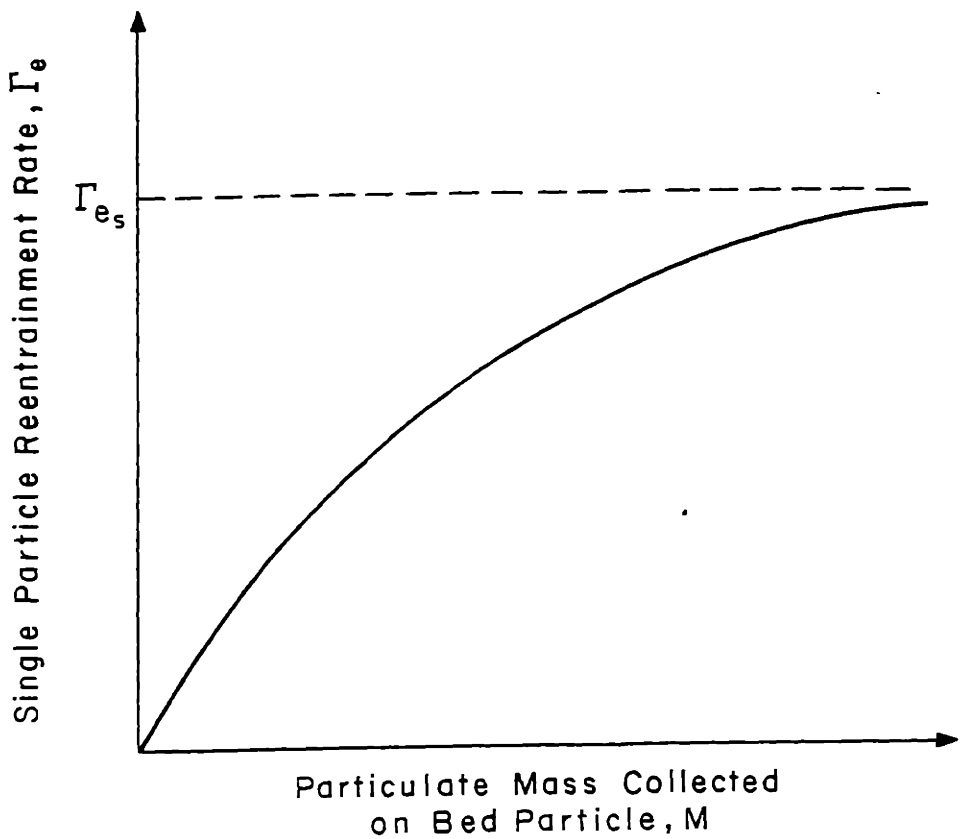

Figure 5.2 Assumed functional dependence of single particle reentrainment rate on mass of collected particulate.

of the reentrainment rate would be expected to depend on the interplay of adhesive and dislodging forces. As such, it is left to experimentation to clarify the dependence of τ_{es} on the adhesion models proposed in Chapter 4.

Another assumption now made is that of perfect particle mixing in the fluidized bed. That is, all of the bed particles are identical regardless of their location in the bed. Specifically, this is saying that the amount of aerosol on any bed particle is the same as on any other bed particle. To achieve this the time characterizing particle mixing in the bed must be much less than the time characterizing aerosol deposition. In general, this is a very good assumption as fluidized beds are known for their high rates of particle mixing.

With these assumptions and models we are now prepared for the dynamics of the combined collection and reentrainment processes. We envision the bed as being in a quasi-steady state which directly results from the high solids mixing rate in the bed. The build-up rate of the aerosol on the bed particles is the slowest dynamical time of the system. Given a reentrainment rate τ_e resulting from a given value of M, all other quantities are at steady-state values. They are only functions of time as they are related to the slowly varying $\tau_e(t)$.

For the thin (Δz thick) slice in the bed shown in Fig. 5.1, we write a steady-state conservation of mass equation

$$UAm(z) - UAm(z + \Delta z) = \frac{\Delta z A(1 - \varepsilon_f)}{\frac{4}{3}\pi R^3}\left[\tau_c - \tau_e\right] \qquad (5.2)$$

where the difference in mass flux into and out of this slice is equal to the

difference in collection and reentrainment from all the bed particles in the slice. Taking the limit of $\Delta z \to 0$, we arrive at the differential equation

$$\frac{dm}{dz} = \left[T_e - \pi R^2 U C_t m(z) \right] \frac{(1 - \varepsilon_f)}{\frac{4}{3} \pi R^3 U} \tag{5.3}$$

The boundary condition imposed on this equation results from the inlet aerosol mass loading:

$$m(z = 0) = m_o \tag{5.4}$$

Defining

$$\ell_c = \frac{4}{3} \frac{R}{C_t(1 - \varepsilon_f)} \tag{5.5}$$

We find the collection efficiency of the bed defined as

$$\eta_b = 1 - \frac{m(\ell_f)}{m(o)} \tag{5.6}$$

to be

$$\eta_b = \left(1 - \exp(- \frac{\ell_f}{\ell_c}) \right) \left(1 - \frac{T_e}{\pi R^2 U C_t m_o} \right) \tag{5.7}$$

As aerosol particulate builds up on the bed particles, T_e increases. It is useful to now assume a relationship between T_e and M so that we may study the dynamics of the bed collection performance. Let us assume a simplified approximation to the general dependence shown in Fig. 5.2, now shown in Fig. 5.3. Further, we can relate the amount of deposited aerosol M to the collection characteristics of the bed:

$$\frac{dM}{dt} = \left[m_o - m(\ell_f) \right] UA \quad \frac{\frac{4}{3} \pi R^3}{\ell_f A (1 - \varepsilon_f)} \tag{5.8}$$

Initially, the relation between M and T_e is (from Fig. 5.3)

$$T_e = \frac{T_{es}}{M_o} M \tag{5.9}$$

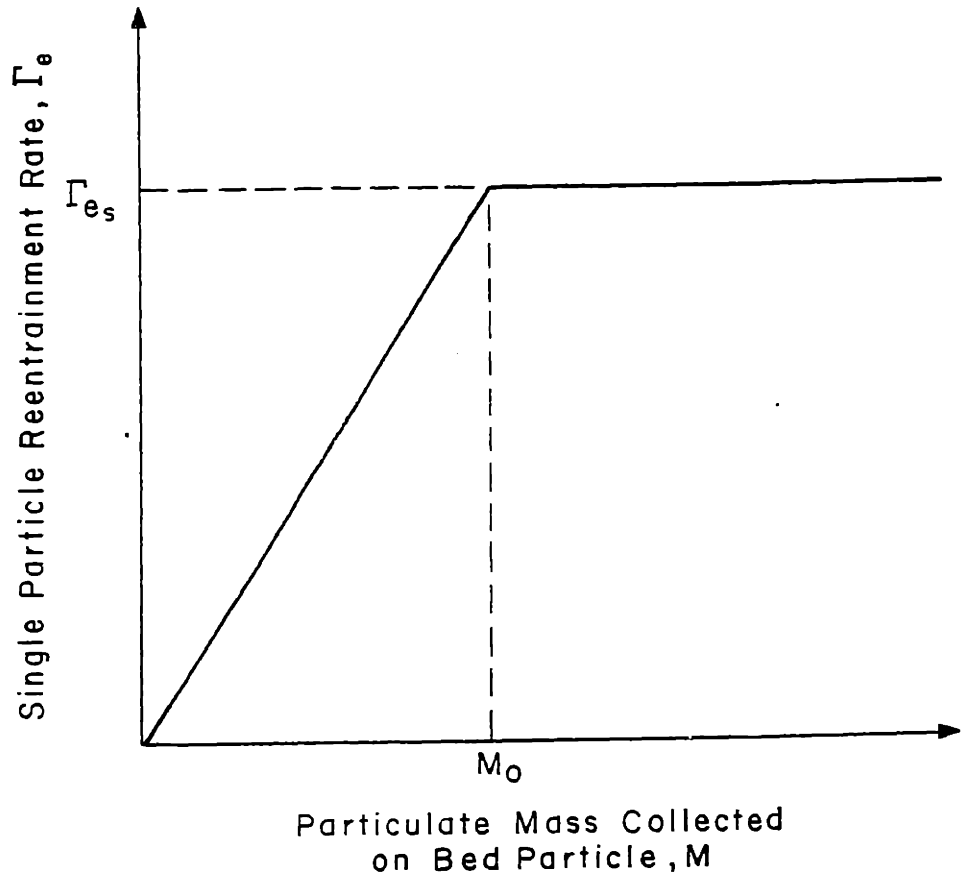

Figure 5.3 .. Idealized assumed functional dependence of single particle reentrainment rate on mass of collected particulate.

This relation holds for $M < M_o$ (or equivalently $T_e < T_{es}$). Then by noting that

$$m_o - m(\ell_f) = m_o \eta_b \tag{5.10}$$

Eq. 5.8 becomes

$$\frac{dT_e}{dt} + \frac{T_{es}}{M_o}\left(1-e^{-\ell_f/\ell_c}\right)\frac{4R}{3\ell_f(1-\varepsilon_f)C_t}T_e = \frac{T_{es}}{M_o}\left(1-e^{-\ell_f/\ell_c}\right)\frac{\frac{4}{3}R^3 U m_o}{\ell_f(1-\varepsilon_f)} \tag{5.11}$$

Initially the bed is clean, or $M = 0$, so

$$T_e(t = 0) = 0 \tag{5.12}$$

The solution to Eq. 5.11 is then

$$T_e = m_o \pi R^2 U C_t \left[1 - \exp(-\frac{t}{\tau_e})\right] \tag{5.13}$$

where

$$\tau_e = \frac{3M_o\,\ell_f(1-\varepsilon_f)C_t}{4T_{es}(1-e^{-\ell_f/\ell_c})R} \tag{5.14}$$

is the time characteristic of the build-up of collected aerosol particulate in the bed. The bed collection efficiency is then found to be

$$\eta_b = \left[1 - \exp(-\frac{\ell_f}{\ell_c})\right]\exp(-\frac{t}{\tau_e}) \tag{5.15}$$

These equations are applicable for $M < M_o$. When M increases enough, such that $M > M_o$, then

$$T_e = T_{es} \tag{5.16}$$

and

$$\eta_b = \left[1 - \exp(-\frac{\ell_f}{\ell_c})\right]\left[1 - \frac{T_{es}}{R^2 U C_t m_o}\right] \tag{5.17}$$

and the bed collection efficiency is specified for all time. Two distinct modes of operation become apparent upon close examination of these solutions.

If

$$\pi R^2 U C_t m_o < \Gamma_{es} \tag{5.18}$$

then the saturation level $\Gamma_e = \Gamma_{es}$ is never realized, rather

$$\Gamma_e(t \to \infty) = m_o \pi R^2 U C_t \tag{5.19}$$

and

$$\eta_b(t \to \infty) = 0 \tag{5.20}$$

Thus, depending on the relationship between Γ_{es} and $m_o \pi R^2 U C_t$ the bed will have steady-state efficiencies of

$$\begin{aligned} \eta_b &= 0 && \text{for } m_o \pi R^2 U C_t < \Gamma_{es} \\ \eta_b &= (1 - e^{-\ell_f/\ell_c}) \left(1 - \frac{\Gamma_{es}}{m_o \pi R^2 U C_t}\right) && \text{for } m_o \pi R^2 U C_t > \Gamma_{es} \end{aligned} \tag{5.21}$$

These two cases are summarized in the graphs of Fig. 5.4.

When adhesion is assured, we may write

$$\Gamma_{es} = 0 \tag{5.22}$$

and the steady-state bed collection efficiency reduces to its familiar form

$$\eta_b = 1 - e^{-\ell_f/\ell_c} \tag{5.23}$$

This limit points out the interesting fact that the bed collection efficiency is the product of two terms. The first is the bed collection efficiency with assured adhesion which we will call η_c. The second is a relation between the single particle collection and reentrainment rates which we will call the adhesion efficiency η_a. Thus,

$$\eta_b = \eta_c \eta_a \tag{5.24}$$

where

$$\eta_c = 1 - e^{-\ell_f/\ell_c} \tag{5.25}$$

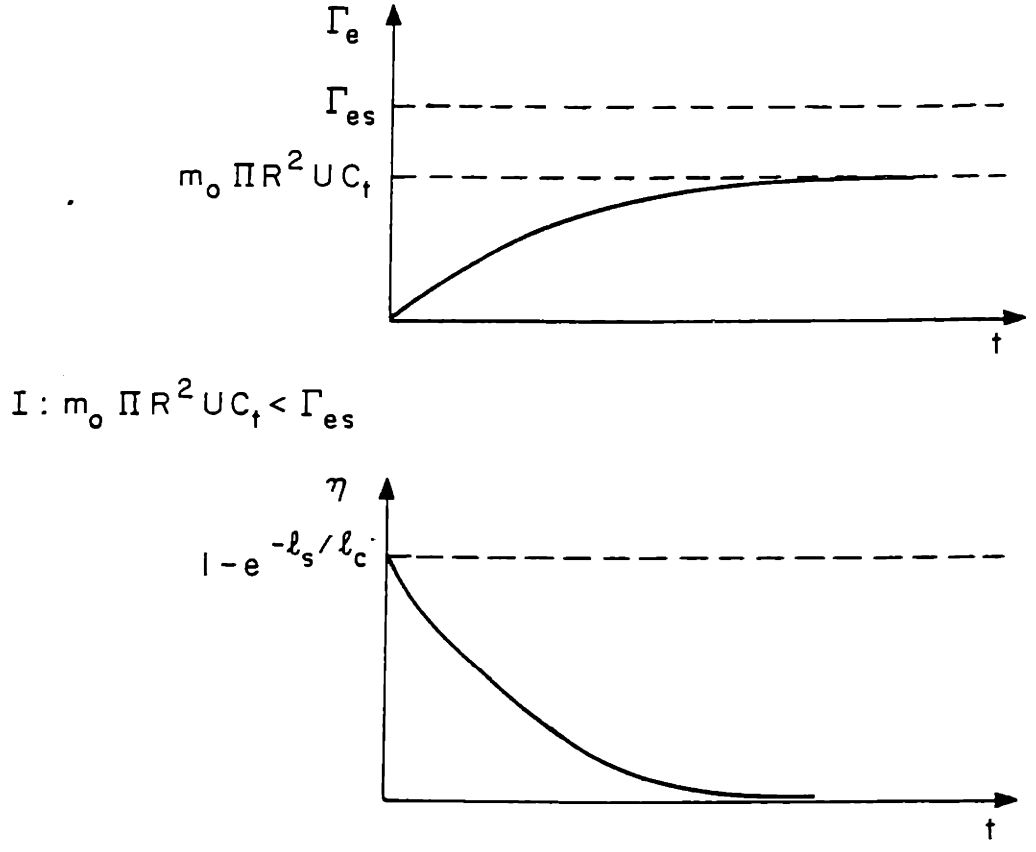

Figure 5.4 Time dependence of reentrainment rates at bed collection efficiencies for two regimes of operation.

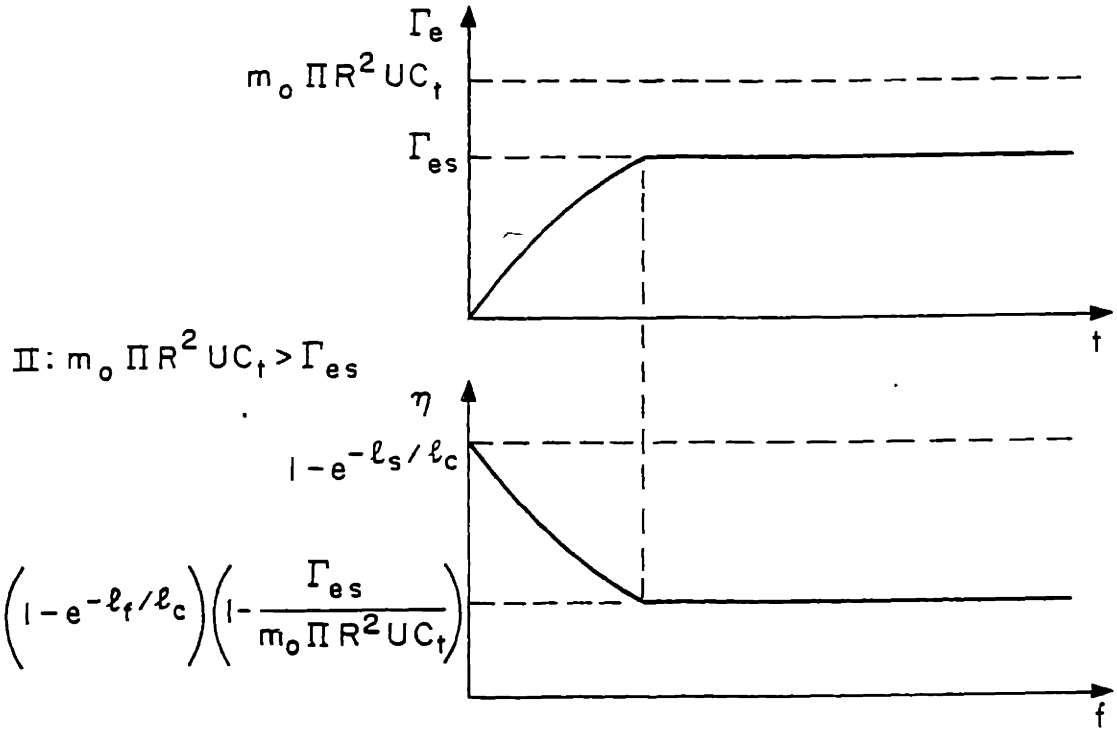

Figure 5.4 Time dependence of reentrainment rates at bed collection efficiencies for two regimes of operation.

$$n_a = 0 \qquad \text{for } m_o \pi R^2 U C_t < \tau_{es}$$

$$= 1 - \frac{\tau_{es}}{m_o \pi R^2 U C_t} \qquad \text{for } m_o \pi R^2 U C_t > \tau_{es}$$

Of course we must be concerned with the time characterizing the approach to this steady state. By rearranging terms in Eq. 5.14, we find

$$\tau_e = \left(\frac{m_o \pi R^2 U C_t}{\tau_{es}} \right) \left(\frac{A \ell_f (1 - \varepsilon_f)}{1 - e^{-\ell_f / \ell_c} \, m_o A U \frac{4}{3} \pi R^3} \right) M_o \tag{5.26}$$

The first term on the right-hand side of Eq. 5.26 is the ratio of the single particle collection rate (at z = 0) to the single particle saturation re-entrainment rate. The second term is the reciprocal of the average aerosol mass flux to a single particle and the third term is just M_o. Thus the product of the second and the third term is the time T_M to build up collected fly ash of mass M_o on each bed particle if adhesion were assured or

$$\tau_e = \left(\frac{m_o \pi R^2 U C_t}{\tau_{es}} \right) T_M \tag{5.27}$$

As of now we can only guess as to what T_M would be by making an assumption as to the magnitude of M_o. Typically, we might expect M_o to correspond to a coating on the bed particle of a few layers of the particulate. If we assume the following typical values for a fly ash collection system

$$\begin{aligned}
&a \simeq 2.5 \times 10^{-6} \text{ m} \\
&U \approx 1 \text{ m/sec} \\
&m_o \approx 10 \text{ gm/m}^3 \\
&\ell_f \approx 10 \text{ cm} \\
&R \approx 1 \text{ mm} \\
&1 - e^{-\ell_f / \ell_c} \cdot 1 \\
&\varepsilon_f \approx .4 \\
&M_o \approx 1.5 \times 10^{-10} \text{ gm}
\end{aligned} \tag{5.28}$$

then

$$T_m \simeq 400 \text{ sec} \tag{5.29}$$

is a measure of the transient times involved.

The monodisperse model presented here is useful for its simplicity. It should not be expected to rigorously describe a real system, but it does introduce useful concepts such as reentrainment rate dependence on total collected particulate, the transient and steady-state collection characteristics, and the adhesion efficiency concept. These concepts will carry over directly to the polydisperse extension of the model which will be used to analyze experimental results.

2. Polydisperse Aerosol

The extension of the monodisperse collection and reentrainment model to include polydispersity of the particulate size distribution is a straightforward exercise. Again we assume perfectly mixed bed particles and plug gas flow. A bubbling gas flow model could be applied but it would add complexity that we feel does not warrant itsuse. Further, the experiments performed and all useful practical schemes now envisioned include the use of baffles or electrode screens to approximate plug flow conditions in the bed.

As in Chapter III, we represent the size distribution of the particulate aerosol by the distribution function $\gamma(a)$, where

$m\gamma_m(a)da$ = mass of aerosol in size range a to a+da

(the distribution may also be on a number basis)

with m being the total aerosol mass loading. This function is normalized by

$$\int_0^\infty \gamma_m(a)da = 1 \tag{5.30}$$

This aerosol is collected and reentrained in the fluidized bed collector. Thus both the total aerosol mass loading m and the size distribution are functions of z, the vertical coordinate in the fluidized bed. Further, the reentrainment rate is size selective to a certain extent as adhesion mechanisms are size selective, and as in the monodisperse case, the reentrainment rate is dependent upon the total mass of collected aerosol on the bed particles. The dynamics of the build-up to steady-state reentrainment rates could be carried through as done for the monodisperse case, but we feel that the additional complexity is not warranted. Instead we will assume that steady-state conditions have been reached. Further, we are assuming here that the reentrained particulate does not consist of agglomerates, but rather of individual particles. The possibility of agglomeration does exist and will be covered in a succeeding section of this chapter.

Single particle collection and reentrainment rates can then be expressed on a size fractional basis:

$$\mathcal{T}_c(a) = \pi R^2 U C_t(a) \gamma_m(a,z) m(z) da = \begin{array}{l}\text{mass of particles in size range}\\ \text{a to a+da collected per unit}\\ \text{time per bed particle}\end{array} \tag{5.31}$$

$$\mathcal{T}_e(a) = \mathcal{T}_{es} \gamma_{me}(a) da = \begin{array}{l}\text{mass of particles in size range a to}\\ \text{a+da reentrained per unit time per bed}\\ \text{particle}\end{array}$$

The true dependence of fractional reentrainment rate upon size and adhesion mechanisms is now left unspecified. We have merely characterized it by the total single particle reentrainment rate $\mathcal{T}_{es}$ and its size distribution function γ_{me}.

The resulting steady-state conservation of mass for a single aerosol size in a slice Δz of the bed as in Fig. 5.1 is

$$UA[m(z)\gamma_m(a,z)da - m(z+\Delta z)\gamma_m(z+\Delta z,a)da] \tag{5.32}$$

$$= \frac{\Delta z A(1-\varepsilon_f)}{\frac{4}{3}\pi R^3}\left[\pi R^2 U C_t(a)\gamma_m(a,z)m(z)da - \mathcal{T}_{es}\gamma_{me}(a)da\right]$$

or taking the limit $\Delta z \to 0$ this becomes

$$\frac{d}{dz}\left[m(z)\gamma(a,z)\right] = \left[\frac{\bar{T}_{es}\gamma_{me}(a)}{\pi R^2 U C_t(a)} - \gamma_m(a,z)m(z)\right]\frac{1}{\ell_c(a)} \tag{5.33}$$

where

$$\ell_c(a) = \frac{4R}{3C_t(a)(1-\varepsilon_f)}$$

The boundary condition at $z = 0$ is given by the inlet aerosol characteristics:

$$m(z=0)\gamma_m(a,z=0) = m_o\gamma_{mi}(a) \tag{5.34}$$

where

m_o = total inlet aerosol mass loading

$\gamma_{mi}(a)$ = inlet aerosol size distribution function

Then

$$m(a)\gamma(a,z) = \frac{\bar{T}_{es}\gamma_{me}(a)}{\pi R^2 U C_t(a)}\left[1 - e^{-z/\ell_c(a)}\right] + m_o\gamma_1(a)e^{-z/\ell_c(a)} \tag{5.35}$$

and the size fractional bed collection efficiency is found from

$$\eta_b(a) \triangleq 1 - \frac{m(z=\ell_f)\gamma_m(a,z=\ell_f)}{m_o\gamma_{mi}(a)} \tag{5.36}$$

to be

$$\eta_b(a) = \left[1 - e^{-\ell_f/\ell_c(a)}\right]\left[1 - \frac{\bar{T}_{es}\gamma_{me}(a)}{m_o\pi R^2 U C_t(a)\gamma_1(a)}\right] \tag{5.37}$$

As for the monodisperse case, it is useful to define the fractional bed collection efficiency as the product of an adhesion assured fractional collection efficiency $\eta_c(a)$ and a so-called fractional adhesion efficiency $\eta_a(a)$

$$\eta_b(a) = \eta_c(a) \times \eta_a(a) \tag{5.38}$$

where

$$\eta_c(a) = 1 - e^{-\ell_c/\ell_c(a)}$$

$$\eta_a(a) = 1 - \frac{T_{es}\gamma_{me}(a)}{m_o\pi R^2 U C_t(a)\gamma_i(a)}$$

The fractional adhesion efficiency is seen to be one minus the ratio of the single particle reentrainment rate (for aerosol of eadius a) to the single particle collection rate (at z = 0) of that same sized aerosol. Thus $\eta_a(a) = 0$ implies that radius a aerosol is being reentrained just as fast as it is collected, while $\eta_a(a) = 1$ implies that the aerosol is perfectly adhered to the bed particle.

As done in Chapter III, the overall bed mass collection efficiency can be expressed as an integral of the size fractioned efficiencies (see Eqs. 3.18, 3.19 for derivation)

$$\eta_b = \int_o^\infty \gamma_{mi}(a)\eta_c(a)\eta_{a(a)}da \qquad (5.39)$$

B. Experimental Collection and Reentrainment in Fluidized Beds

1. Discussion

The modeling in the previous two sections was presented mainly as an analytical formalism for discussing the collection, adhesion, and reentrainment dynamics in the bed. Fluidized beds are very complex in nature and volumes of books are filled with attempts to describe their gas and particle dynamics. Coupling this with the mechanisms of collection and adhesion (complex in their own right) of a polydisperse fly ash and the task becomes intractable. Further, the main theme of this work is to perform fundamental tests leading as quickly as possible to invention of practical

systems and meaningful evaluation of feasible alternatives.

In this light we will now proceed to discuss the important features of the models presented and the results of a series of tests which confirm these predictions. The model predicts two important results. First is that a transient exists when a clean system is started up in which the collection efficiency adjusts to its steady-state value. This transient is characterized by the time τ_e as given in Eq. 5.14. τ_e is dependent on parameters such as T_{es} which are difficult to predict, so it was argued that it should be on the same order of magnitude as T_m, the time required to build up a monolayer of fly ash on the bed particles. For typical values, T_m was shown to be about 400 sec as in Eq. 5.29.

The second important finding was that the bed collection efficiency was the product of two terms, one the adhesion assured collection efficiency η_c and two the so-called adhesion efficiency η_a. The adhesion efficiency depends on the ratio of single particle collection and reentrainment rates. The latter is impossible now to predict due to the complexities of the adhesion and dislodging mechanisms.

It is expected that in the presence of a liquid adhesive agent the viscous liquid adhesive forces are dominant in fluidized beds. In fact, tests run on collection of fly ash in fluidized beds with no liquid adhesive showed essentially no collection efficiency for all particle sizes. No other mechanisms were capable of adhering the fly ash under the intense impulsive dislodging forces encountered in the fluidized bed. Adhesion of particles subject to impulsive forces resulting from impulsive forces have been shown to depend on the adhesion parameter S as given in Eq. 4.47. Further tests have shown that minimum oil thicknesses are required for fly ash to show performance described by this model. For fly ashes typically

encountered, this quantity corresponds to oil quantities of about 2% of the mass of the fly ash. It is expected that the reentrainment rate T_{es} should depend on the adhesive effectiveness. Specifically it should depend on the adhesion parameter S where U is the bed particle collision velocity. Several important parameters which are needed for the development of a model for predicting T_{es} from S are unspecified. Those include bed particle collision frequency, the spectrum of bed particle collision velocities, the number of adhered fly ash particles affected by a single bed particle collision, etc. We can postulate, though, that T_{es} should depend on S and several characteristics of the dependence can be described.

Experiments have shown that adhesion is good for $S < S_{crit}$ ($S_{crit} \approx 1.4$). Translated to terms of T_{es}, this would mean that $T_{es} << m_o \pi R^2 U C_t$ or equivalently $\eta_a \simeq 1$. In other words, we are stating that if enough oil is used, the adhesion will be good, reentrainment low, and thus adhesion efficiency will be near 100%. For $S > S_{crit}$ adhesion will not be good, i.e., some particles may become dislodged and the adhesion efficiency would be reduced. However, no prediction can be made as to the exact values of η_a for certain S. In fact we would not expect that there would be any one relationship as η_a depends on many more parameters than S. One other relationship can be predicted, though, that is η_a should be monotonically decreasing with increasing S for any one set of bed parameters (R, U, ℓ_o). In other words, adhesion should lose effectiveness as S increases, so T_{es} would decrease, resulting in decreased adhesion efficiency η_a.

These phenomena are the subject of a series of experiments on collection and reenetrainment of fly ash in fluidized beds. As well as validating some aspects of the models presented, these experiments are good small scale demonstrations of the concept of a fluidized bed with liquid additive as a

fly ash collector. As a result, experiments were run varying several parameters, especially the bed particle material. These feasibility experimental results will be summarized at the end of this chapter. These tests were performed for conventional fluidized beds without an electric field. The reason was twofold. It was convenient not to encumber the experiments with the additional complexities of charging the fly ash and imposing electric fields. More important, it was desired to test the modeling which resulted in Eq. 5.38, in which the bed collection efficiency is the product of an adhesion, assured collection efficiency η_c and an adhesion efficiency η_a. In electro-fluidized beds, η_c is very near 1 for all fly ash sizes and an adequate test of the theory is not provided. For fluidized beds, η_c can be quite low for submicron and micron sized fly ash, while it increases to near 1 for supermicron particles. Thus a range in η_c is tested. It is left to other experiments to study the importance of electrification.

It was desired to measure collection efficiencies of fluidized beds for a fly ash aerosol with liquid adhesive agents introduced. The best way to introduce liquid adhesive agents into the bed is by atomizing the liquid and then collecting it on the bed particles along with the fly ash. This method assured uniform distributions of liquid in the bed. Other methods, such as direct liquid injection can easily result in local wet spots which can defluidize the bed. Determination of the collection of the aerosol liquid is done in the same way as for the fly ash according to Chapter III.

2. Experimental Procedures

Two sets of experiments were run to determine collection and reentrainment data for fly ash with a liquid adhesive additive. The first set were run at room temperature, the second at a nominal temperature of 140°C. The

higher temperature tests were run for two reasons. 140°C is a temperature typical of stack gases at a conventional coal burning power plant. Also, the 140°C effectively reduced the liquid additive viscosity by about an order of magnitude, thus permitting a good range of viscosities to be tested. It is to the credit of the theory that both sets of data are correlated by the same theory. Details of the experimental apparatus and diagnostic equipment are goven in Appendix A.

Each experimental run was performed in the following sequence. The bed sections and channels were cleaned of any build-ups of fly ash resulting from previous experiments. A bed particle type was chosen and loaded in the bed, then the bed inserted into the test channel. Fluidization conditions were established and measured. In all cases a stable uniform fluidization was maintained because failure to do so resulted in irreproducible results. As a result, these fluidization velocities were always at least 2 to 3 times the minimum fluidization velocity. After stable fluidization was verified, the fly ash and oil additive were injected into the inlet gas system at predetermined controlled rates. Typically ten minutes were allowed for the system to achieve steady-state conditions. Measured amounts of gas were then sampled through the sampling

trains. Finally, the run was terminated.

In all, three types of bed particles were tested.

1) New Jersey No. 2 yellow sand of mean radius .4 mm.
2) Crushed and sifted bituminous coal, -7 + 14 U.S. standard mesh.
3) Sintered fly ash agglomerates, -7 +14 mesh, sintered at 2000°F for 30 minutes in air.

Corresponding fluidization velocities ranged from 1 to 3 m/sec.

3. Data Analysis

A certain amount of the meaningful data resulting from these experiments were obtained simply by observation. We will discuss those first as they help to place the more analytical data reductions in their proper perspectives.

The raw data of the experiments consisted of determinations of bed collection efficiency η_b vs. fly ash size a. These curves were easily reduced to plots of the adhesion efficiency η_a vs. a by using the adhesion assured collection efficiencies η_c found in Chapter III. With Eq. 5.38, now restated,

$$\eta_a(a) = \frac{\eta_b(a)}{\eta_c(a)} \tag{5.42}$$

The resulting plots for all tests are shown in Fig. 5.5.. A summary of the test parameters is given with each plot. These figures will be referred to subsequently.

Perhaps the most important empirical observation was that of the build-up of agglomerates of fly ash on the bed particles. This build-up was noted only for the cold flow runs with the larger amounts of oil additive (>2%). In these runs, after several tens of minutes, large round spheres

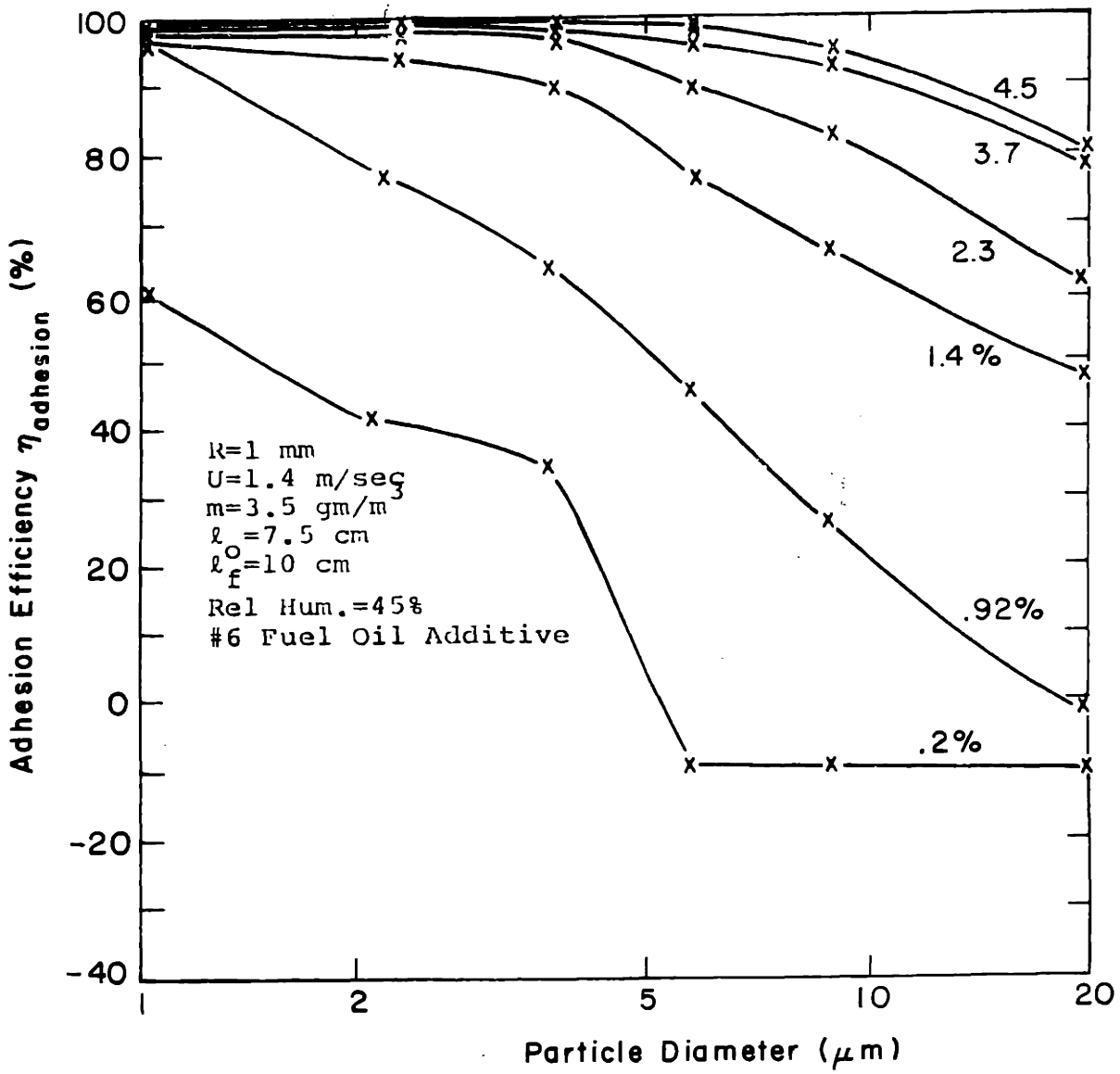

Figure 5.5 Data for fluidized bed collection and reentrainment of fly ash. Adhesion efficiency plotted vs. fly ash diameter. Test conditions as indicated.

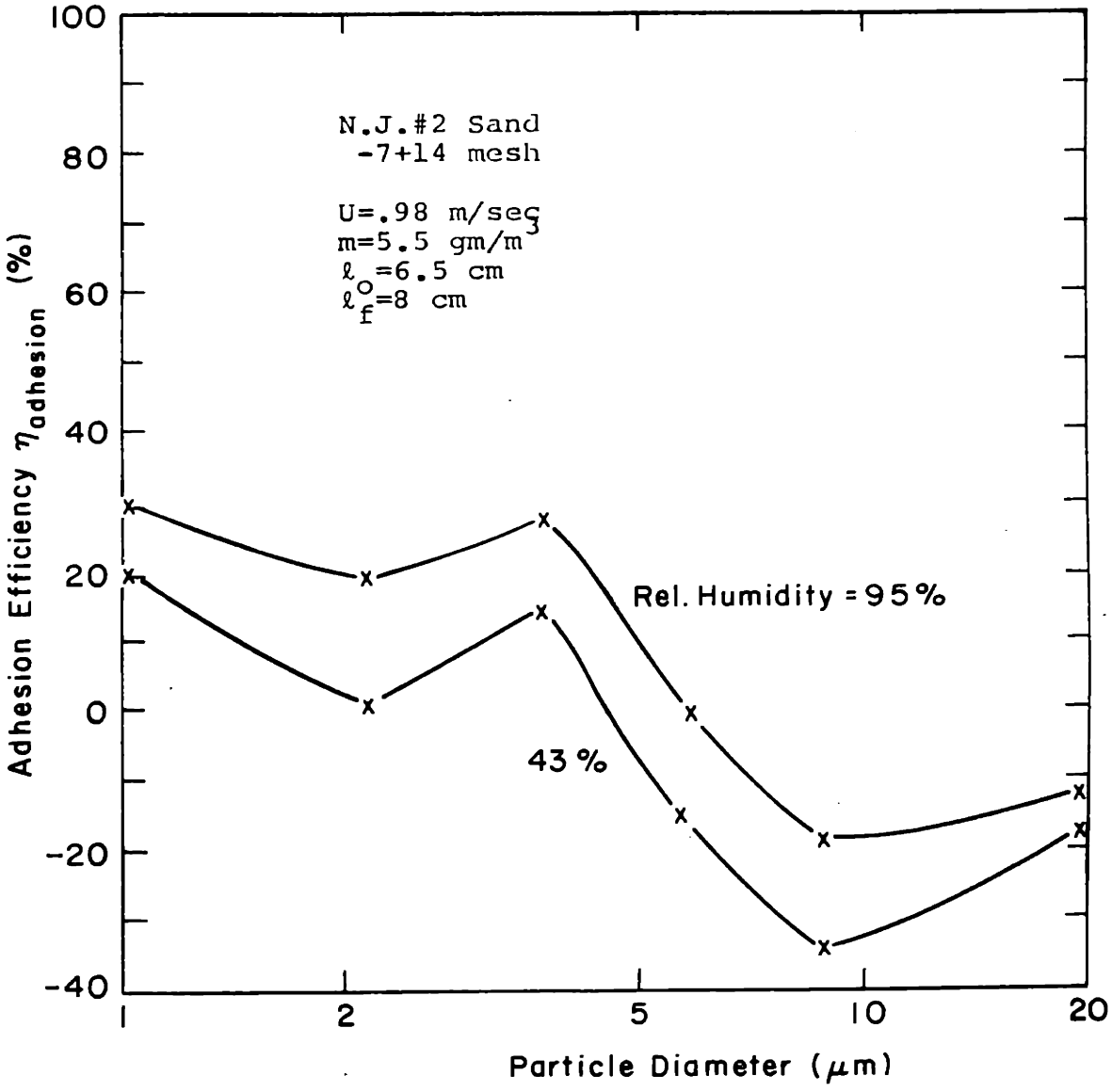
N.J.#2 Sand
-7+14 mesh
U=.98 m/sec
m=5.5 gm/m³
ℓo=6.5 cm
ℓf=8 cm
Rel. Humidity = 95%
43%
Adhesion Efficiency ηadhesion (%)
Particle Diameter (μm)
100
80
60
40
20
0
-20
-40
1
2
5
10
20

Figure 5.5

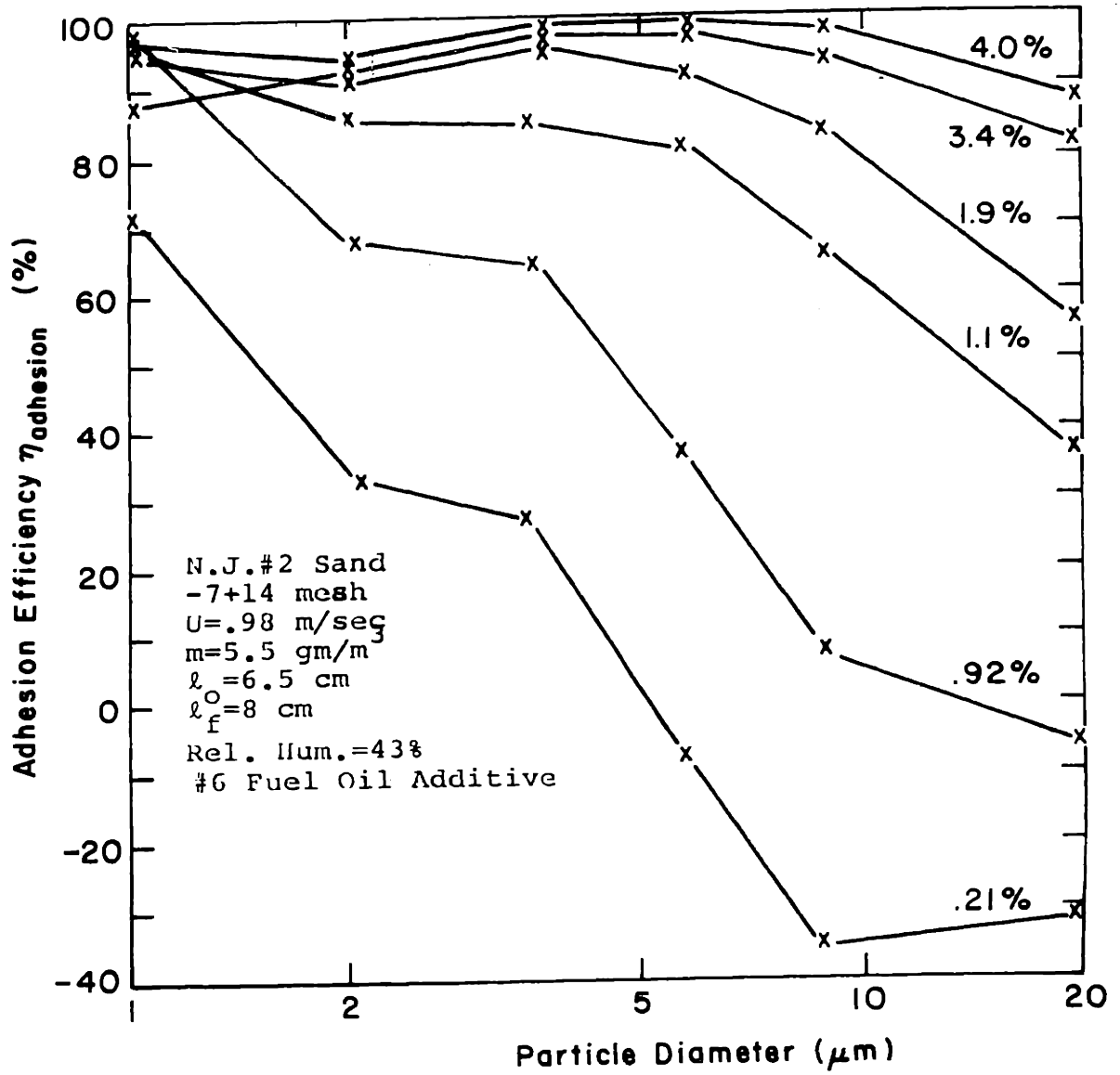
Adhesion Efficiency $\eta_{adhesion}$ (%)
100
80
60
40
20
0
-20
-40
1
2
5
10
20
Particle Diameter (μm)
4.0%
3.4%
1.9%
1.1%
.92%
.21%
N.J.#2 Sand
-7+14 mesh
U=.98 m/sec
m=5.5 gm/m^3
ℓ_o=6.5 cm
ℓ_f=8 cm
Rel. Hum.=43%
#6 Fuel Oil Additive

Figure 5.5

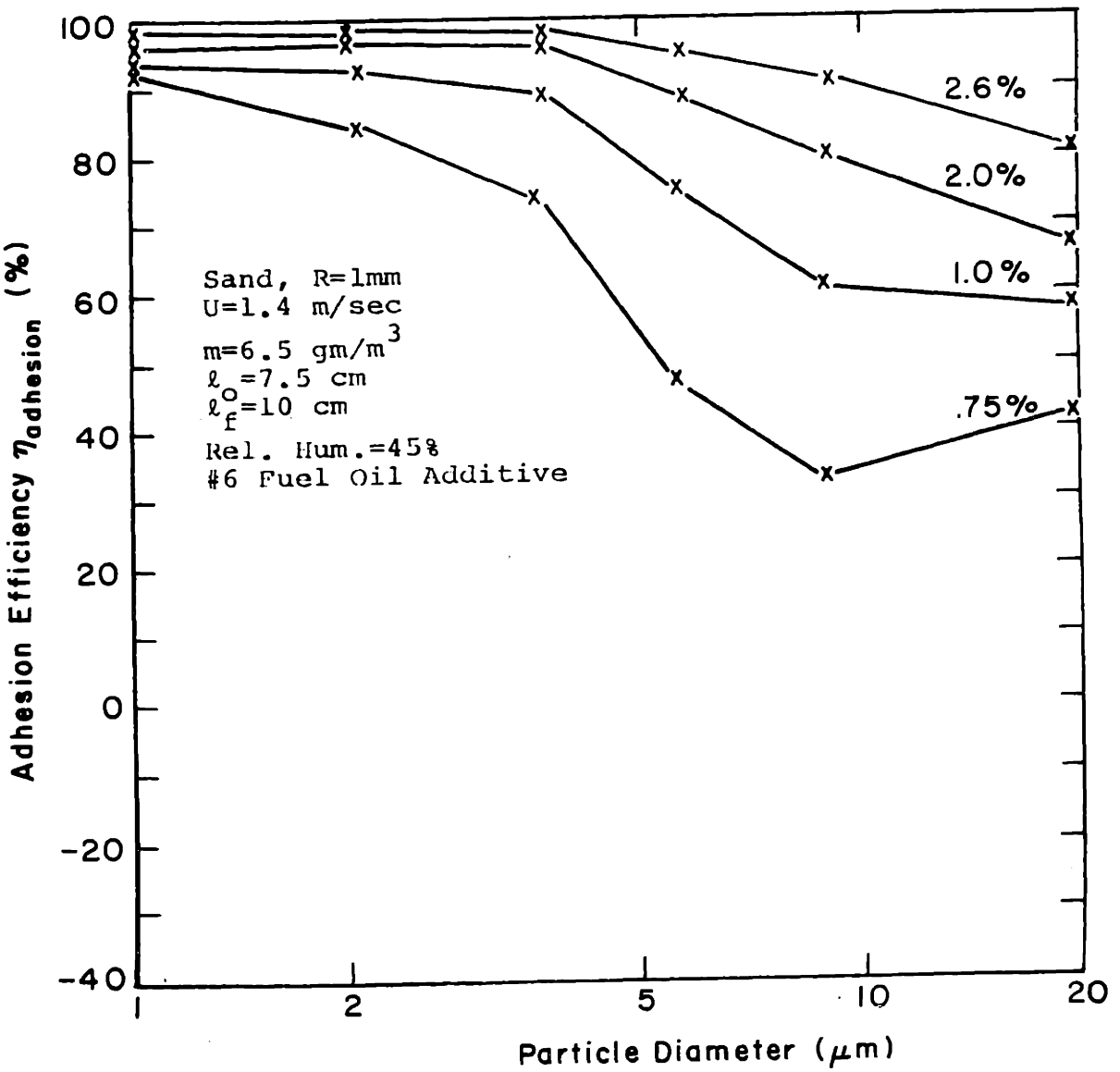
100
80
60
40
20
0
-20
-40
1
2
5
10
20
Adhesion Efficiency $\eta_{adhesion}$ (%)
Particle Diameter (μm)
Sand, R=1mm
U=1.4 m/sec
m=6.5 gm/m^3
ℓ_c=7.5 cm
ℓ_f^o=10 cm
Rel. Hum.=45%
#6 Fuel Oil Additive
2.6%
2.0%
1.0%
.75%

Figure 5.5

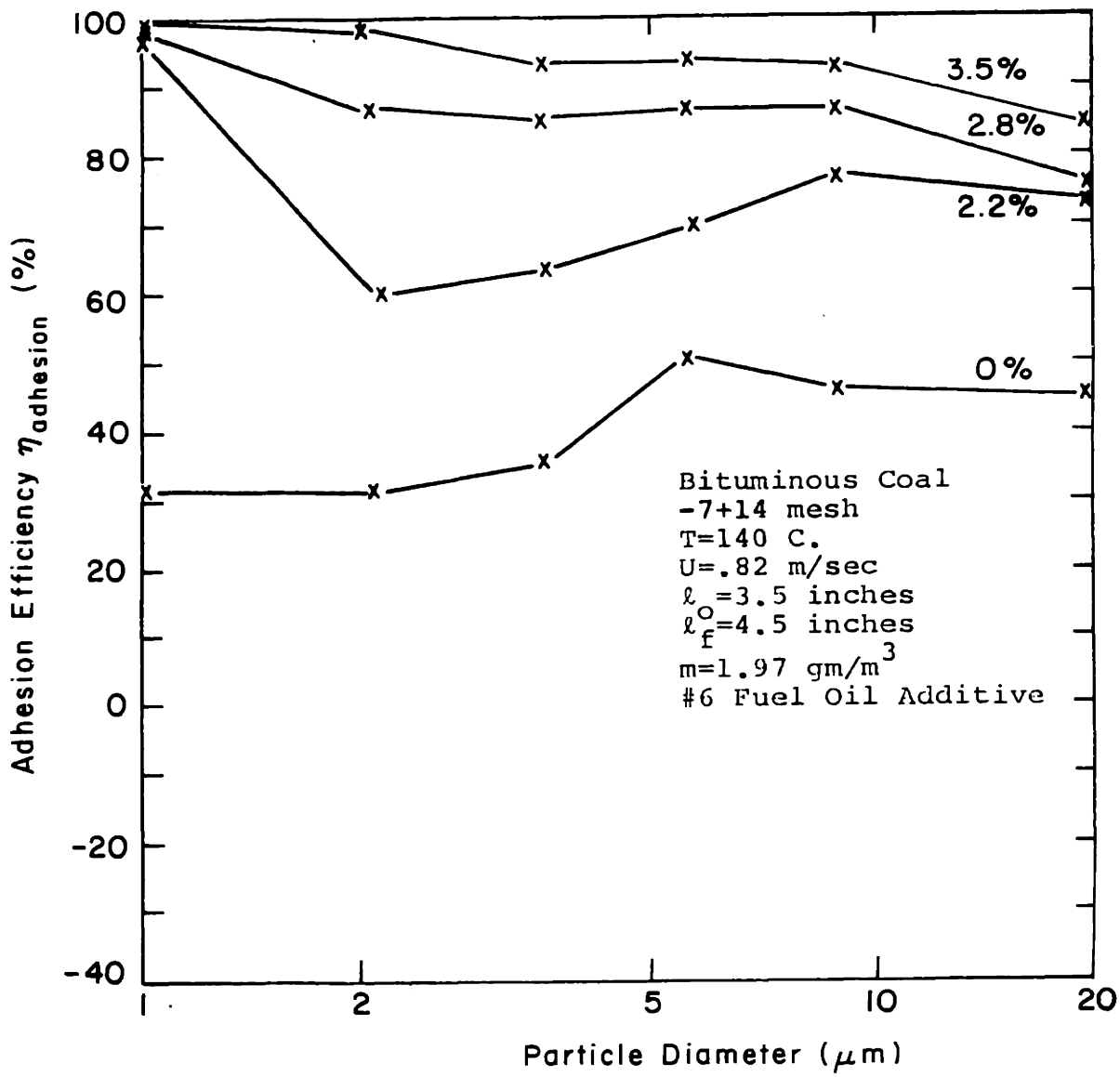
100
80
60
40
20
0
-20
-40
1
2
5
10
20
Adhesion Efficiency $\eta_{adhesion}$ (%)
Particle Diameter (μm)
3.5%
2.8%
2.2%
0%
Bituminous Coal
-7+14 mesh
T=140 C.
U=.82 m/sec
ℓ_o=3.5 inches
ℓ_f^o=4.5 inches
m=1.97 gm/m^3
#6 Fuel Oil Additive

Figure 5.5

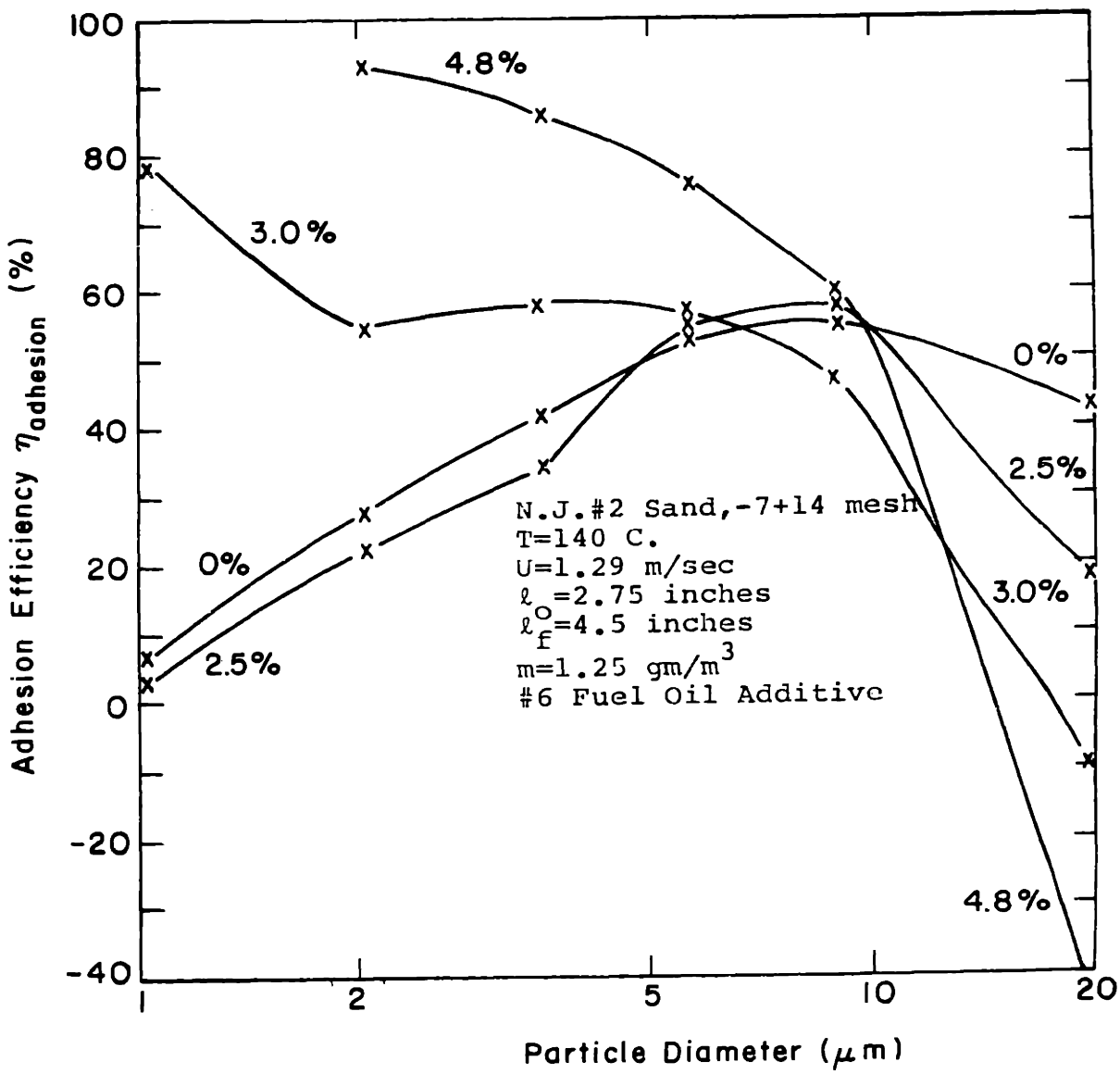
100
80
60
40
20
0
-20
-40
1
2
5
10
20
Adhesion Efficiency $\eta_{adhesion}$ (%)
Particle Diameter (μm)
4.8%
3.0%
0%
2.5%
N.J.#2 Sand,-7+14 mesh
T=140 C.
U=1.29 m/sec
ℓ_o=2.75 inches
ℓ_f^o=4.5 inches
m=1.25 gm/m^3
#6 Fuel Oil Additive

Figure 5.5

consisting of fly ash with a seed of the bed particle material were found near the bottom of the bed. Figure 5.6 is a photograph of a typical seeded agglomerate. Smaller seeded spheres were found throughout the bed. These were not found in the hot flow beds, or in the cold flow beds with smaller oil quantities. The transition to the growth of stable agglomerates was gradual and could not be quantized.

It is interesting though that even for these beds with little fly ash build-up, moderate collection efficiencies are reported. This seems contradictory as the collected fly ash must go somewhere. The resolution to the paradox lies in the sampling system capabilities. It was discovered that the sampling systems do not sample particulate matter much larger than about 20-30 μm in diameter. These large particles are impacted onto the sampling tube walls by inertial impaction at points were the tube curves, or simply by gravitational settling. Also, considerable amounts of fly ash were noted to collect on the flow channel walls above the bed. Thus our data can only be interpreted accurately up to $2a \approx 10$ μm.

In the bed then, smaller particles are collected on the bed particles, but are then reentrained as larger agglomerates of bed particles. The bed collection efficiency can be zero overall, even though it is positive for all sizes of fly ash with substantial loadings in the inlet. We have "created" new large particles by agglomeration. This causes a breakdown of our collection and reentrainment model formalism which treated particles individually. We might expect that the formalism would describe the data for the size ranges less than 10 μm, which do represent single fly ash particle collection and reentrainment. But the newly formed agglomerates cannot be analyzed in the same way. In fact, these observed phenomena were

Figure 5.6 Picture of fly ash agglomerates built-up on seed particles of bituminous coal. On left are two intact agglomerates, then a crushed agglomerate and finally a coal seed particle.

the basis of the invention of the agglomerator system and will be discussed in a subsequent section.

The presence of very large agglomerates at the bottom of the bed was predicted in Appendix F on solids mixing in fluidized beds. The theory presented there showed an instability in bed particle growth when the particles are grown by aerosol deposition. Briefly stated, this instability results because larger bed particles tend to spend more time near the bottom of the bed and because particulate deposition is also greatest near the bottom of the bed. This causes uneven bed particle growth and the growth of very large agglomerates near the bottom of the bed.

Another interesting observation was that of approach to steady state. While difficult to measure, it could be roughly noted from observations of the outlet gas opacity. Typically this time was in the range of three to five minutes and was the reason for choosing a ten-minute waiting time until sampling was commenced. This time corresponds to that predicted by Eq. 5.29, thus it corresponds to the time required to coat the bed particles with a few layers of fly ash.

The plots of raw data given in Fig. 5. 5 show several interesting characteristics. In nearly all cases the adhesion efficiency η_a is monotonically decreasing with increasing a and with decreasing oil quantity. This implies that it is valid to separate the overall efficiency η_b into η_a and η_c. For the micron sized particles, η_b was moderate and in most cases less than η_b for larger sized particulate. However, when η_c was divided out and η_a resulted, η_a was monotonically decreasing, as our theory predicts. This behavior lends credibility to the adhesion efficiency concept and to the proposed dependence of η_a on S.

Further these plots show that adhesion efficiencies can be made reasonably high, but that there are certain limitations. Since η_c can be made somewhat arbitrarily high for all sized particles, it is the properties of η_a which might limit the performance of a device. For the smaller particles studied (in the micron and submicron range), adhesion efficiencies in the range 95-99% could be obtained. As a matter of fact, these are as high as we could expect to measure with the inaccuracies of the experimental arrangement. However, the efficiencies in the larger size ranges (around 10 μm) were even in the best cases limited to about 90%. These unsatisfactory efficiencies resulted not only from insufficient single particle adhesion, but also the agglomeration effect. Apparently the breaking off of some larger particles and agglomerates of smaller particles is unavoidable in fluidized beds. This is the effect which ultimately restricts electro-fluidized bed fly ash collectors from achieving very high collection efficiencies ($\eta_b > 99\%$). It is the motivation for the two-stage collector which is described and demonstrated in the concluding chapter.

Analytically the most interesting analysis of the data results from plotting the experimentally determined adhesion efficiency η_a vs. the adhesion parameter S. S was calculated using Eq. 4.47 with the proper experimental parameters. The bed parameters are as in Figure 5.5 and Fig. 5.7 is the resulting plot. It should be remembered that this plot summarizes a host of different bed parameters, including both room temperature and hot flow tests.

For all points with S less than about 1, the adhesion efficiency is high ($\eta_a > 90\%$), while for $S > 1$, η_a shows considerable scatter and many very low values. Our theories predict that adhesion should be good for $S < S_{crit}$, where $S_{crit} \simeq 1.4$. Good adhesion should result in high adhesion

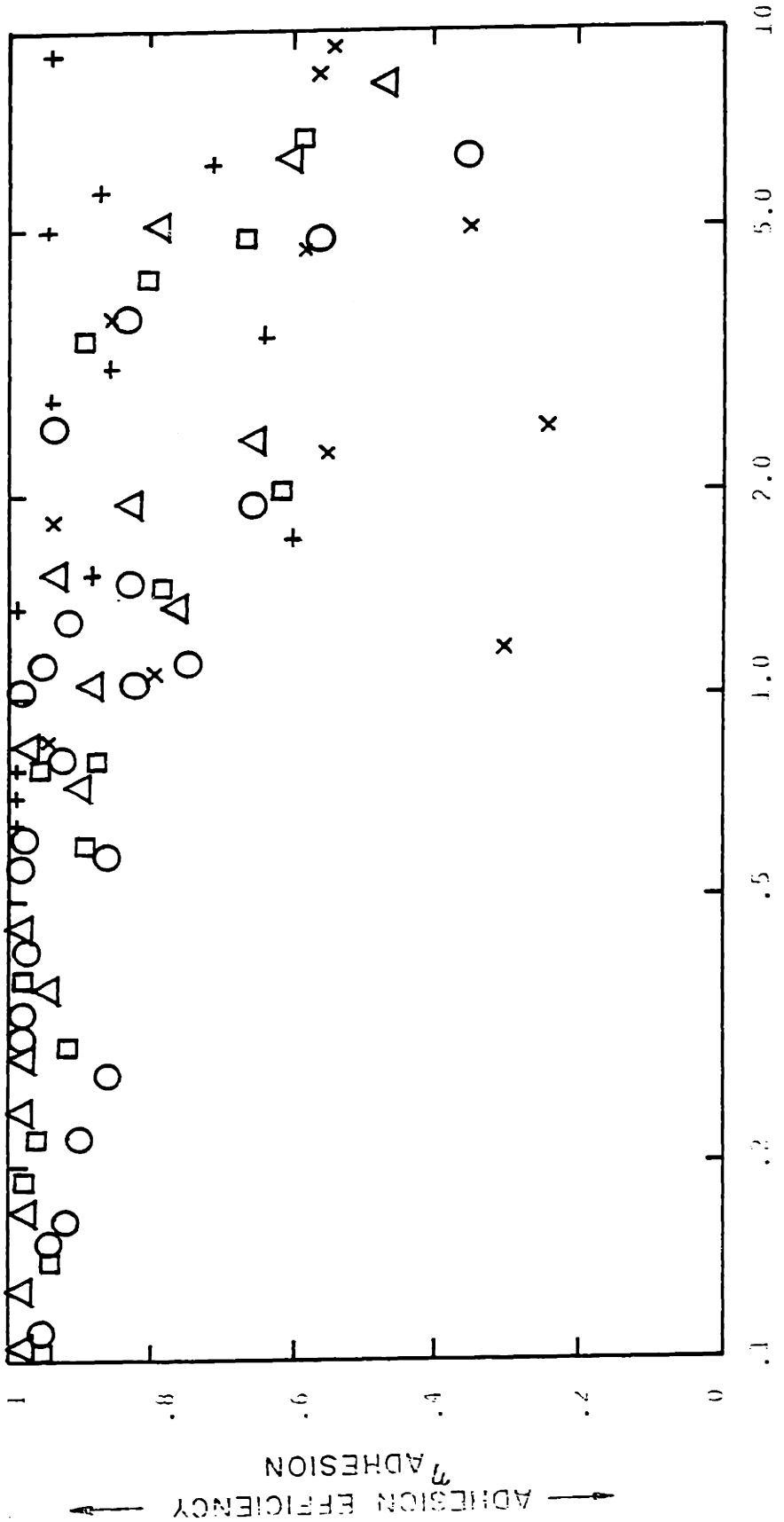

Figure 6.7 Experimentally measured adhesion efficiency plotted vs. adhesion parameter S for a variety of bed operating conditions

efficiencies. We feel that the correlations in Fig. 5.7 are important verifications of the viscous liquid adhesion theory proposed in Chapter IV.

The fact that the points for $S > 1$ show such wide scatter is not surprising. These data represent a wide range of bed parameters, oil additive quantity and viscosity, and operating temperatures. We in no way claim that adhesion efficiency should depend on S, only that it should be high for $S < 1.4$. The scatter in the experimental points for $S > 1$ is then just the result of the wide variety of beds and conditions tested.

Chapter VI Conclusions and Proposed Systems

The previous three chapters could be construed as the accumulation of the pieces of a puzzle. This chapter will fit them together. We will attempt here to design systems for fly ash control from coal burning technologies. To do so we must keep in mind the capabilities of fluidized and electrofluidized bed fly ash collectors, the control requirements, and the practicalities of fitting these collector systems into the coal burning technology under consideration.

Thes chapter will begin by reviewing and summarizing the important findings of Chapters III, IV and V with discussions of their practical implications. Then we will concentrate on electrofluidized bed (EFB) systems as collectors, that is where the EFB is the point of final fly ash removal from the effluent gas stream. Experimental demonstrations of these systems were set up and their performance will be discussed. Also, several practical aspects of full scale implementation will be considered. Finally, the EFB agglomerator systems will be treated in the same way.

A. Summary

1. Polydisperse Collection

Chapter III discussed the various collection mechanisms which come to play in fluidized bed collectros. The relative importance and aerosol collection effectiveness of each depend upon the parameters of the bed collection system being considered. We can make reasonable assumptions as to the parameter values, these assumptions being based on system practicalities. Typically, huge volumes of effluent gas are produced in coal combustion and must be treated. In order that the fly ash collection systems not be excessively large (and as a result expensive) the gas velocities must be on the order of 1 m/sec. For good fluidization, this requires bed particles of radius about 1 mm. Pressure drop through the bed must be kept reasonable, so bed depths can be at most on the order of 20 cm.

If these values are used with the theories of Chapter III the curve of Fig. 3.12 results, which shows collection efficiency vs. fly ash radius for a fluidized bed collector. A serious drop in collection efficiency is noted in the submicron range. In this range the fly ash is too small for inertial impaction or interception to be effective, while it is still too large for diffusion collection. This problem can be resolved by the introduction of electrostatic collection and is really the motivation for electrofluidized beds. EFB's can collect submicron particulate with very high efficiencies.

There is a limitation, though on maximum obtainable collection efficiencies that is independent of the collection mechanisms. Particulate can bypass the collecting bed particles by traveling in gas bubbles through the bed. For the system parameters under consideration here we might expect an upper bound of 95% collection efficiency for any particulate size. This will be seen to be

an important consideration for system design.

2. Ash Adhesion

The chapter on ash adhesion in fluidized beds pointed to a definite conclusion. Many typical adhesion forces were reviewed, but, over the temperature range 300-600 °F, found to be ineffective for ash adhesion in fluidized beds. The reason being that dislodging forces are impulsive in nature, thus of relatively high magnitude for a short duration. A force is needed which is rate dependent and can act at a distance, thereby retaining the fly ash particle which is effectively given a sudden initial velocity relative to the bed particle. The viscosity in liquid bridge forces was proposed and studied, theoretically and experimentally. Basically it was found that adhesion was good if the adhesion parameters S (as defined in Eq. 4.47) was less than a critical value, determined to be about 1. Thus, some sort of liquid additive is required for fly ash adhesion in fluidized bed collectors. It was further found that for fly ash, a "continuum limit" exists. That is, a minimum quantity of liquid additive of about 2% of the fly ash collected by mass is required to fill the surface irregularities. Little viscous adhesion is realized unless capillary bridges are formed, which occurs after the surface irregulartities are filled.

3. Collection and Reentrainment in Fluidized Beds

A model was developed in Chapter V to provide a formalism for fly ash collection and reentrainment processes in fluidized beds. It predicted that the bed collection efficiency η_b is the product of an adhesion assured collection efficiency η_c (i.e. that which would be for collection of a liquid aerosol) and an adhesion efficiency η_a which depends on the ratio of single particle

collection and reentrainment rates. Collection is well modeled in Chapter V. Chapter VI reduced to the study of η_a.

Several properties of η_a were predicted and observed. It is always less than 1. It is dependent on S, being near 1 for values of S less than the critical value and reduced for values above the critical value. These findings are important for predictive capacities and verification of the model.

In the course of these experiments it was found that for beds operated with S < Scrit for the smaller fly ash particles and S > Scrit for larger sizes, the beds acted as agglomerators. That is, the smaller particles were removed from the gas stream but reentrained in an agglomerate form which acted like a larger sized particle. In fact, all beds tested, even those with S < Scrit for all fly ash sizes, showed some reentrainment of very large sized agglomerates. Thus, it was natural to consider the possibility of using the electrofluidized bed as an agglomerator.

B. Electrofluidized Bed Fly Ash Collector

1. Proposed Systems

Based on the findings of the work reported here it was realized that the electrofluidized bed (EFB) collector is best utilized in a two stage collection scheme when applied to fly ash control. That is, used as a collector of coal ash, the EFB should be preceded by a stage of collection of some sort. Consider the reasons for this

1) Typically 95% or more (by mass) of the fly ash is supermicron and can be removed easily by other technologies.

2) The EFB is especially suited to the collection of submicron material.

3) It is difficult to charge high concentrations of fly ash with a short charger gas residence times.

4) EFB's are limited to about 95% collection efficiencies by mechanisms of bubble bypass and breakoff of large agglomerates. For submicron particles such efficiencies are outstanding. However, for the full spectrum of particles, higher efficiences are required for coal burning technologies.

The use of a liquid adhesive agent is required for an EFB fly ash collector. The most likely is #6 fuel oil such as the type used in electric power generating plants. The reasons for this are

1) Fuel oil is enough on an electrical insulator that the required electric fields can be applied to the EFB with minimal current drain.

2) Fuel oil is available at electric power plants. These plants are used to handling and atomizing fuel oil.

3) Fuel oil is inepxensive enough that it is economically feasible to use it for this purpose.

4) In some schemes, the ash agglomerate may be reinjected into the combustion region. In these cases, the heat value of the fuel oil additive would be utilized.

5) Fuel oil is fairly viscous, even at stack gas temperatures.

6) Fuel oil is relatively involatile at stack gas temperatures. Thus it does not evaporate away.

We will now describe the two most promising systems for two stage EFB fly ash collection with added #6 fuel oil.

a. Fluidized Bed-Electrofluidized Bed System (FB-EFB)

This system utilizes a fluidized bed (FB) collector as the first stage. It is attractive because it is a convenient "match" to the EFB second stage collector. This will become apparent during the following system description.

The proposed system is depicted schematically in Fig. 6.1. It consists of

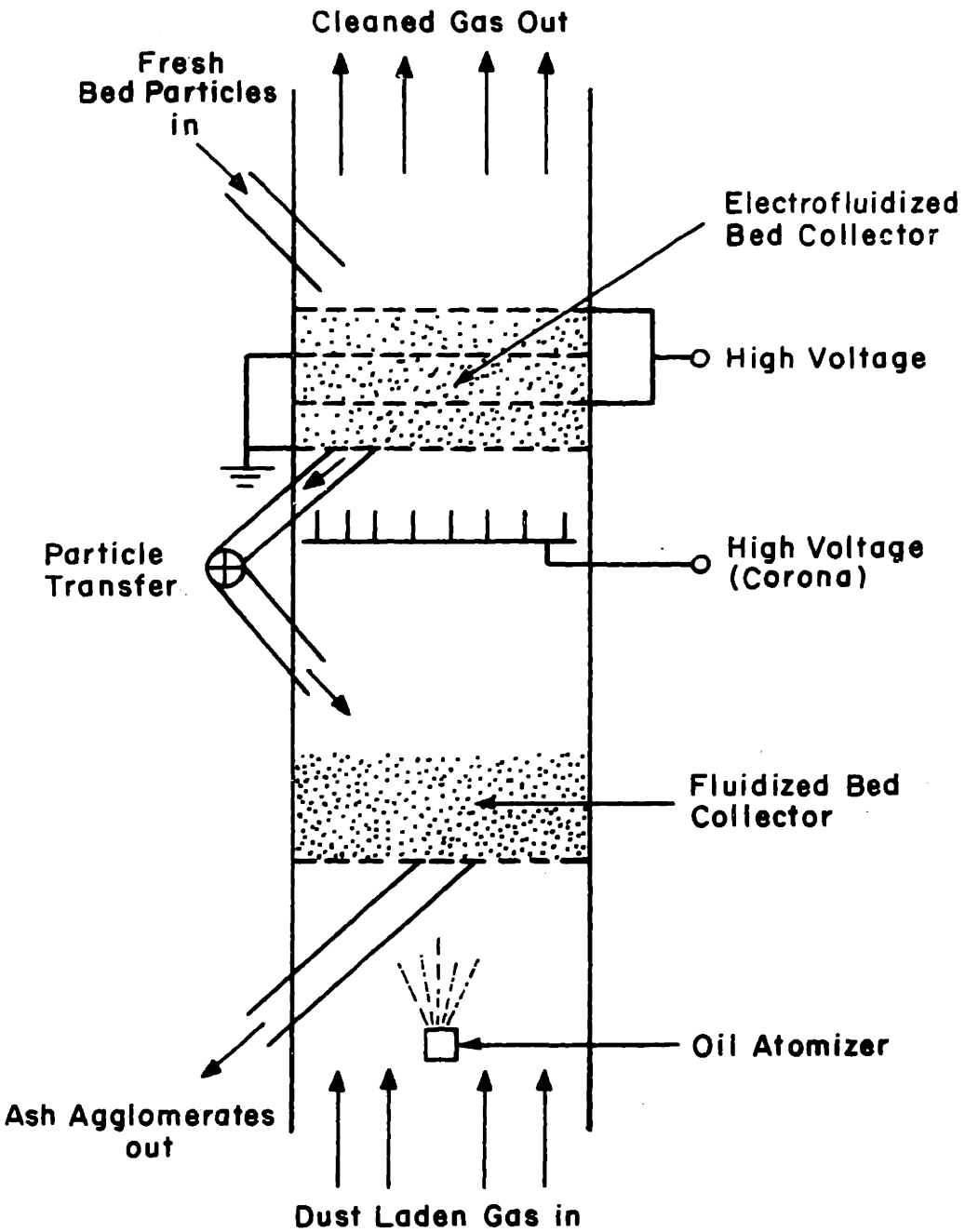

Figure 6.1 Schematic of proposed two stage FB-EFB fly ash collection system.

1) an atomizer to inject the fuel oil additive

2) a fluidized bed first stage coleector with a rapped distributor plate means for introduction and removal of bed particles

3) a corona charging section

4) an EFB stage collector with means for introduction and removal of bed particles

As was demonstrated, a fluidized bed collector is effective for supermicron particulate. This collection stage would then serve to remove the majority of fly ash (~95%) and leave the submicron fly ash in the gas stream. This submicron component of the fly ash, because of its greatly reduced loading, can now be effectively charged in a corona ionizer. Afterward, it is collected with about 95% efficiency in the EFB collector. Thus the overall collection efficiency of the system would be 99+%, and would be at least 95% for the submicron particulate.

The oil additive would be introduced by an atomizer below the first bed. It has been shown that atomization is the most effective means of introducing liquid additives. The first stage FB collector as well as the second stage EFB requires liquid additive for efficient fly ash collection. The relative amounts of oil collected in each stage would depend upon the size distribution of the oil aerosol and the bed parameters. Typically it would be desirable to match the size distribution of the oil aerosol to that of the fly ash. In this case the ratio of oil to fly ash collected in each bed would be identical, a desirable feature for optimum use of oil as an adhesive.

It should also be noted that in the preferred scheme, clean bed particles are introduced into the EFB stage. Particles removed from this stage are then introduced to the FB stage. Removal of the ash coated particles from the FB stage then constitutes final removal from the system. Because about 95% of

the fly ash is collected in the FB stage, the amount of ash on the bed particles in this stage is about 20 times that in the EFB stage. This has some important effects on the system's performance. Because the EFB stage is relatively "clean", there is little reentrainment of large agglomerates of fly ash. In fact, the feed and removal rates of bed particles could be chosen such that fly ash could not build up in the second stage to the point of reentrainment. Also, as previously described, the charger functions better with low fly ash loadings.

In this system the fate of the ash coated bed particles is as yet undetermined. This will be discussed later, along with the potential candidates for bed particle material in the section on system feasibility. These choices mainly depend on the economics of integrating the system into the application process.

b. Electrostatic Precipitator-Electrofluidized Bed System (ESP-EFB)

This system utilizes an electrostatic precipitator (ESP) as the first stage collector. Such a collector could be sized mush smaller than those designed for total fly ash collection because it only need be efficient for supermicron fly ash. The second stage EFB would werve to collect the submicron component. A reduction in ESP size could be as much as 10 times compared to conventional designs. A system of this type has several attractive features.

1) fuel oil additive is only needed for the submicron fly ash collected in the second stage EFB. Thus the total additive amounts can be drastically reduced (by as much as a factor of 20) compared to those required in the FB-EFB system.

2) this system could be retrofitted to installations where ESP's are already used. They would be used to upgrade performance, especially in the submicron range.

3) The ESP serves not only as the first stage supermicron particulate collector, but also as a charger for the submicron fly ash.

The proposed ESP-EFB system is depicted schematically in Fig. 6.2. The first stage ESP would most likely be of conventional design but would require a greatly reduced collection surface area. Operating conditions would also be those of conventional precipitators. The oil atomizer is now located between the two stages. The oil aerosol will be collected in the EFB by inertial impaction if the droplets are large enough, or if the droplets are submicron they must be charged and then collected by electrical forces.

2. Experimental Demonstrations

It was desired to demonstrate these proposed systems in configurations as near to a practical design as possible. The hot-flow test rig described in Appendix A and depicted schematically in Fig. A-3 was constructed for this purpose. For these tests, the diagnostics, fly ash redispersal and oil atomization systems were as described in Appendix A. The test rig was designed such that different plug-in test systems could be conveniently inserted.

A detailed drawing of the FB-EFB plug-in section is shown in Fig. 6.3. The first stage FB collector was supported by a 1/16" hole perforated steel plate. A pneumatic rapper located at the center of the plate providing timed impacts (every 30 secs.) from the spring returned piston in the rapper. The second stage EFB collector was supported on a similar distributor plate. Electrode screens of 1/2" mesh wire cloth were spaced 1 1/2" apart by ceramic insulators, thus providing the field imposing electrodes. The distributor plate also served as the ground electrode for the corona charger. An assemblage of needles was suspended below the plate from a ceramic insulator. A

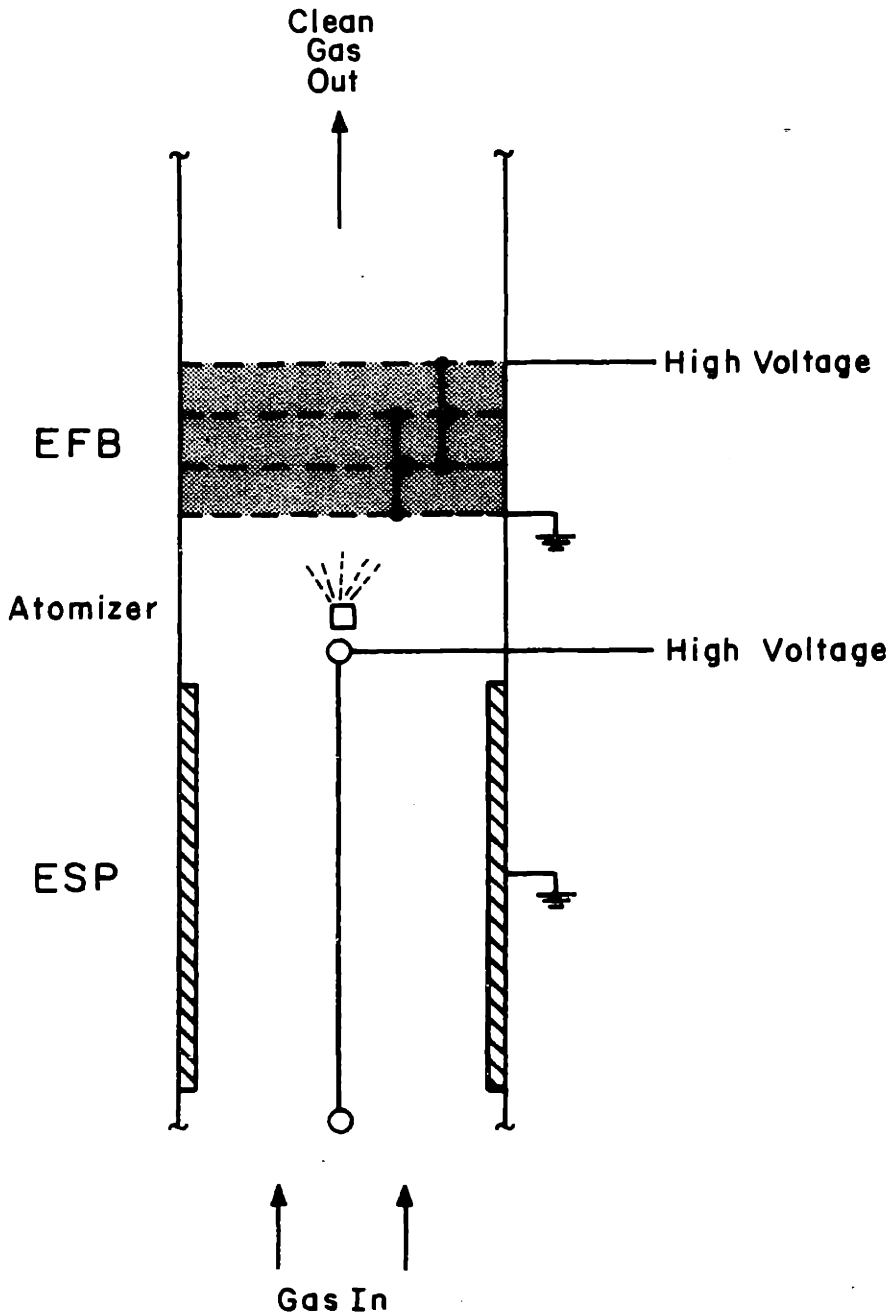

Figure 6.2 Schematic of proposed two stage ESP-EFB fly ash collection system.

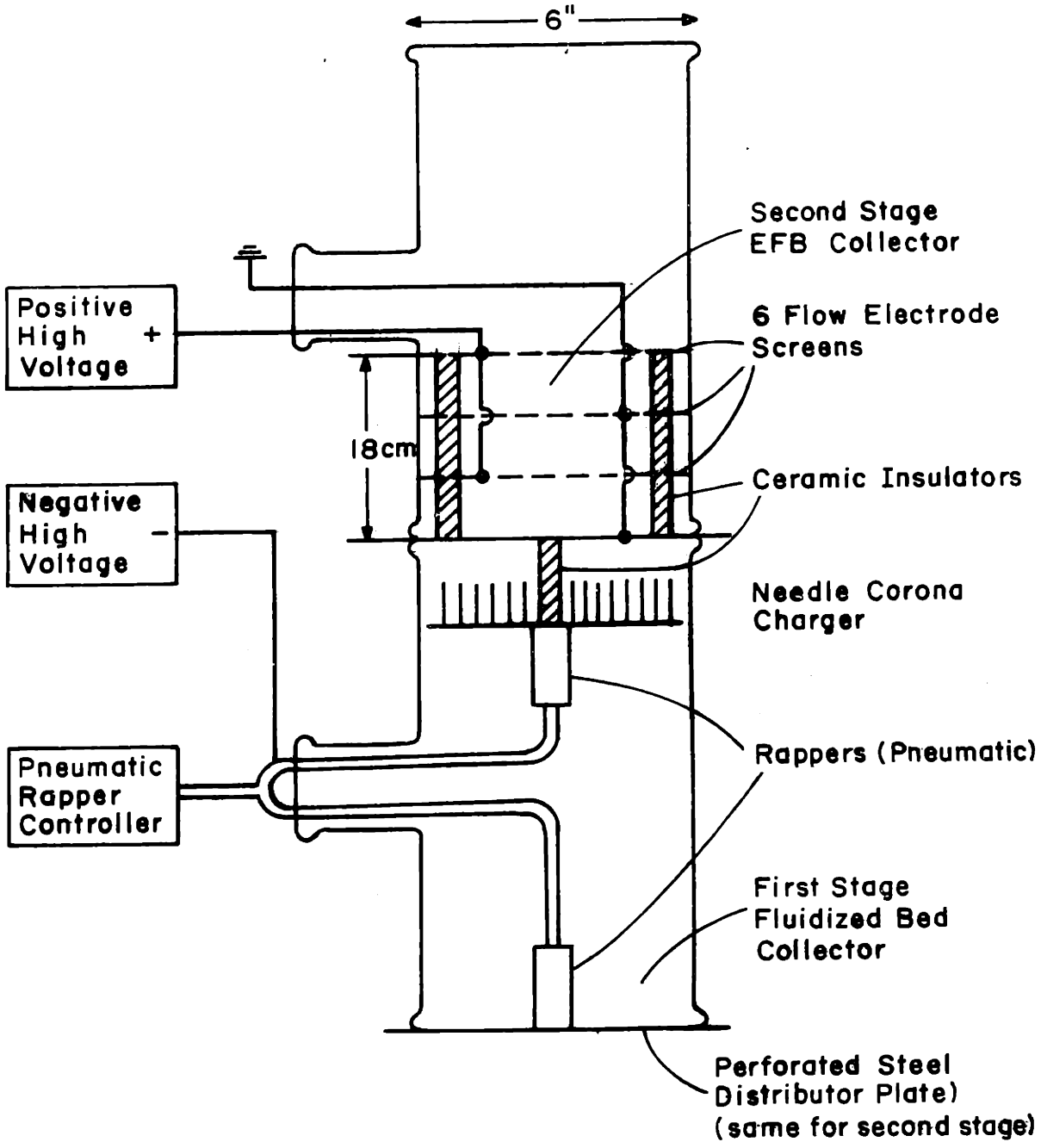

Figure 6.3 FB-EFB experimental plug in bed section.

pneumatic rapper was attached under the needle assemblage and served to dislodge fly ash from both the needles and distributor plate. Mechanical rapping was found to very adequate for the prevention of fly ash clogging in the distributor plate.

The electrical power and pneumatic lines were fed out of the system through the glass "T" sections as shown in the diagram. Electrical power was provided by two 30 KV, 3 mA DC high voltage power supplies with variable controls. Rapping intensity and frequency could be controlled by varying the rapping air pressure and the solenoid-valve timing unit.

This system was demonstrated in two modes of operation. In the first, the FB first stage was omitted, and the system was a demonstration of a single stage EFB collecter. In the second, the FB stage was used. In both cases, Bunker "C" #6 fuel oil was injected and the bed particles were the -7 +14 mesh crushed bituminous coal.

Fig. 6.4 shows the experimental results of the single stage EFB system. These results are reported as collection efficiency vs. fly ash particle diameter. The corresponding bed operating parameters are also shown in the figure. Runs were made at two different additive levels and the comparison can be seen. Because no means for particle removal and replacement were experimentally possible, the duration of each test was limited. Typically these tests were run for 30 min., at which time the build-up of fly ash on the bed particles was sufficient to defluidize the bed. It was felt that tests of this duration were adequate demonstrations of the steady state characteristics of the system. True achievement of steady state would be realized by simply removing the large built up bed particles (which migrate to the bottom of the bed) and introducing clean bed particles to replace them. Sampling for collection

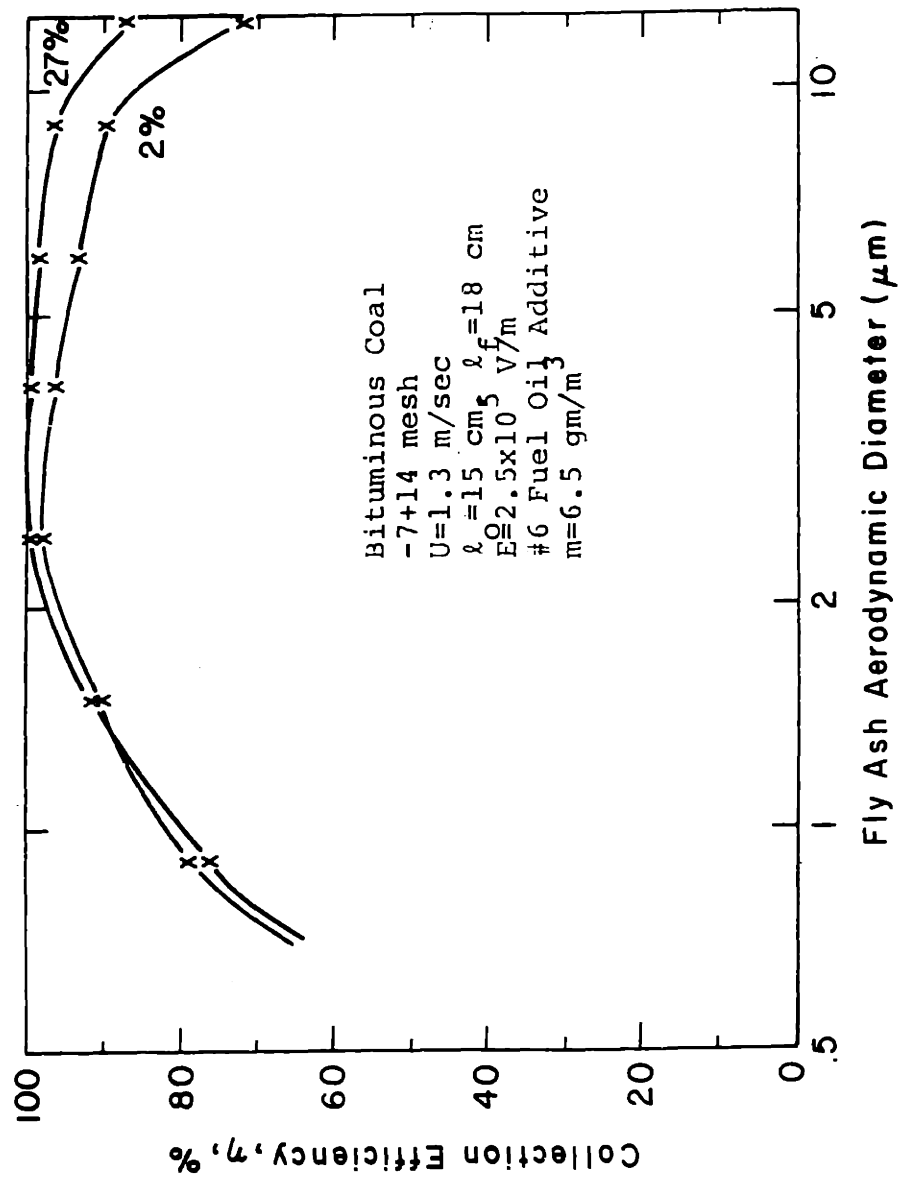

Figure 6.4 Experimental results of single stage EFB collection of fly ash.

efficiencies was performed twenty minutes after system startup so as to measure the steady state performance.

The performance of the single stage EFB was not adequate. The drop-offs in collection efficiency for large fly ash sizes was attributable to the breaking off of agglomerates, while the drop-off for the submicron sizes was due to ineffective performance of the charger. This was caused by the attempt to charge the high loading fly ash in a short residence time charger ($\tau_{res} \approx 10^{-2}$ sec). These results point to the necessity of two collection stages.

The FB-EFB two stage collector was tested with the same run procedures. Data for the tests are shown in Fig. 6.5 with the lower set of points showing performance of the system when electrical power was not applied. The necessity of electrifying the bed and charging the fly ash for submicron fly ash removal is clearly demonstrated. Overall collection efficiency of the system was 98%, and again there was some reentrainment of larger fly ash agglomerates as evidenced by the drop in efficiency for the larger sizes. The submicron fly ash was effectively collected, with about 95% efficiency. This is the upper limit we could expect to obtain in a bubbling bed, even with co-flow electrode screens to break up the bubbles.

Both of these systems, the FB and the FB-EFB, were tested here at room temperature. When tested at typical stack temperatures, the system performance changed drastically. At higher temperatures, the oil viscosity decreased by about an order of magnitude. Because 3% oil additive (by mass) is about the maximum amount that is economically feasible, the oil quantity added could not be increased accordingly to keep the adhesion parameter S at reasonably low levels. Large amounts of reentrainment of collected fly

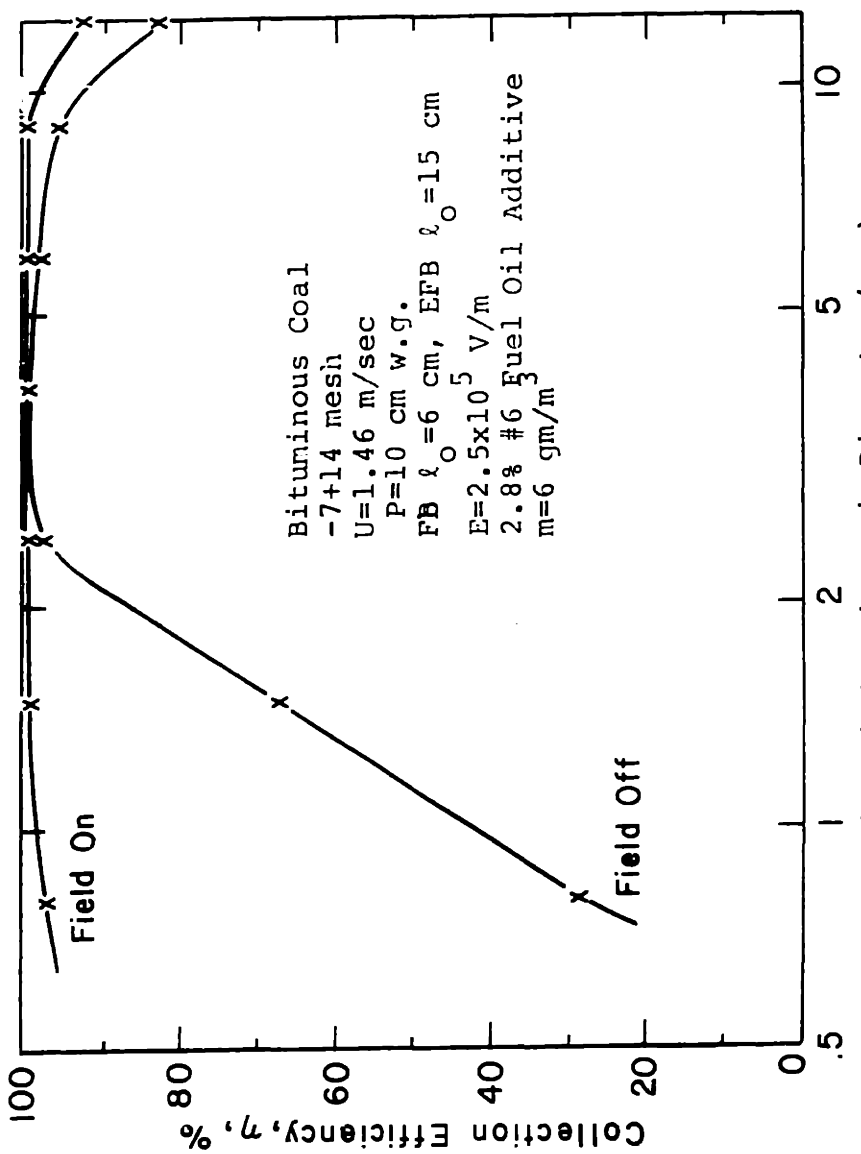

Figure 6.5 Experimental results of two stage FB-EFB collection of fly ash.

ash occurred. In fact, inspection of bed particles after long runs revealed little fly ash build-up on the particles. Also observed were large amounts of fly ash on the test channel walls above the beds. Apparently the fly ash was collected, but reentrained in agglomerates large enough to be impacted on the walls of the ducting. In fact, in this case the system was acting like a good agglomerator. We will describe experimental demonstrations of a system designed specifically to be an agglomerator in the latter part of this chapter.

The ESP-EFB plug in system is detailed in Fig. 6.6. The ESP stage was a 6" diameter brass tube, 1 foot long, with internal "tulip" baffles to provide for effective retention of fly ash rapped on the collecting plates. A .010 inch diameter steel wire was strung in the center of the tube and held at high voltage, thus providing the necessary corona current and precipitation electric fields. Rapping assemblies were external to the collecting tube. Immediately above the ESP was the same EFB unit as described and used for the FB-EFB system. In this case, though, no needle charger assembly was required, since the ESP also served as a chrager.

The ESP collection stage was first tested alone, that is, no bed particles were present in the EFB stage. Also, no oil additive was used. Fig. 6.7 shows the collection efficiency of the ESP vs. fly ash diameter. Efficiency is good for larger fly ash, but poor in the micron and submicron range. Still, the overall mass collection efficiency was 97%.

Fig. 6.8 shows the experimental data for the combined ESP-EFB system using -7 +14 mesh crushed bituminous coal as the bed particle. Again Bunker "C" #6 fuel oil was used as the adhesive additive. Since the oil was injected below the ESP, much of it was "wasted", that is needlessly collected in the ESP. In a practical system, much smaller quantities of oil would be added

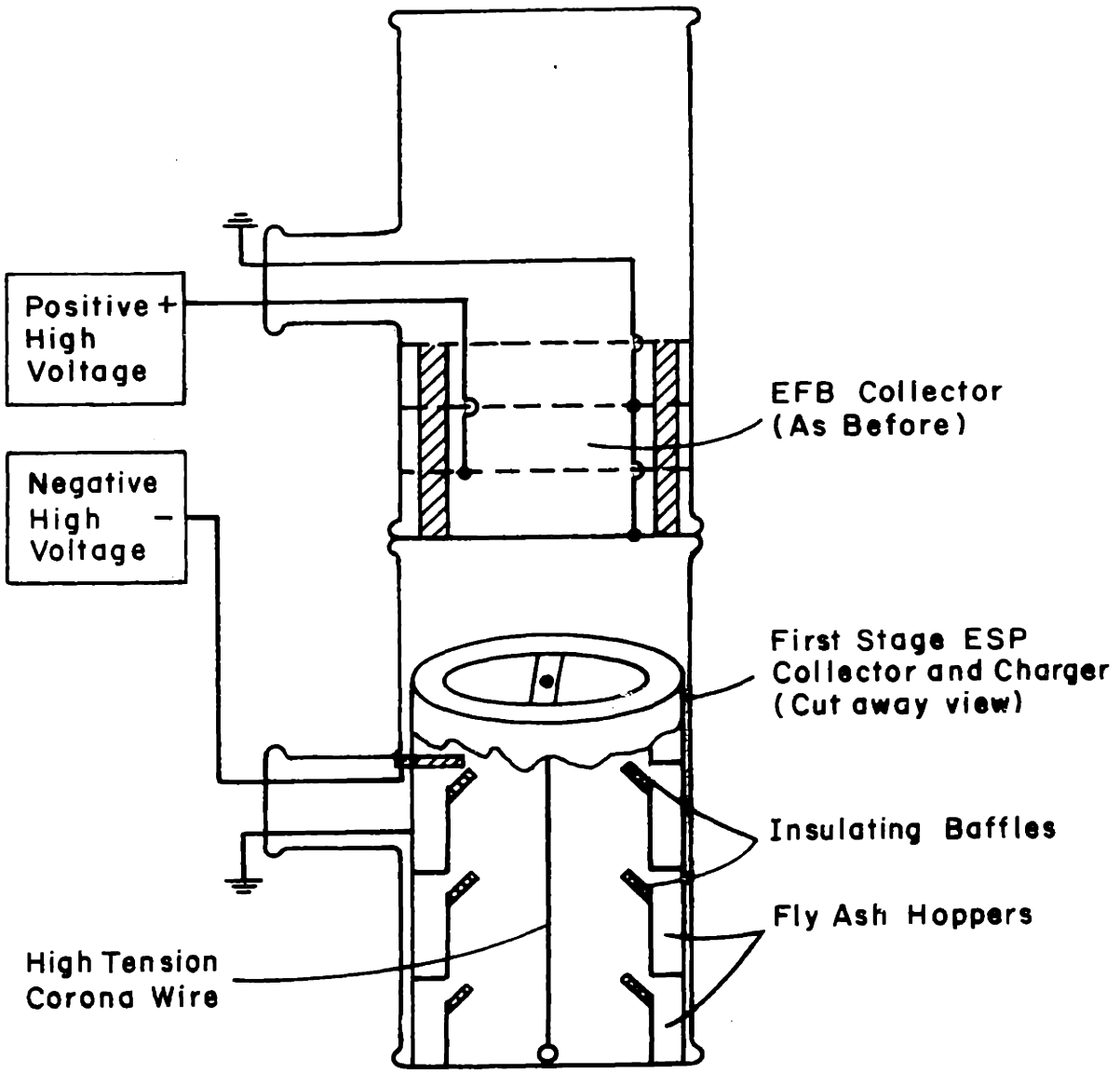

Figure 6.6 ESP-EFB experimental plug in bed section.

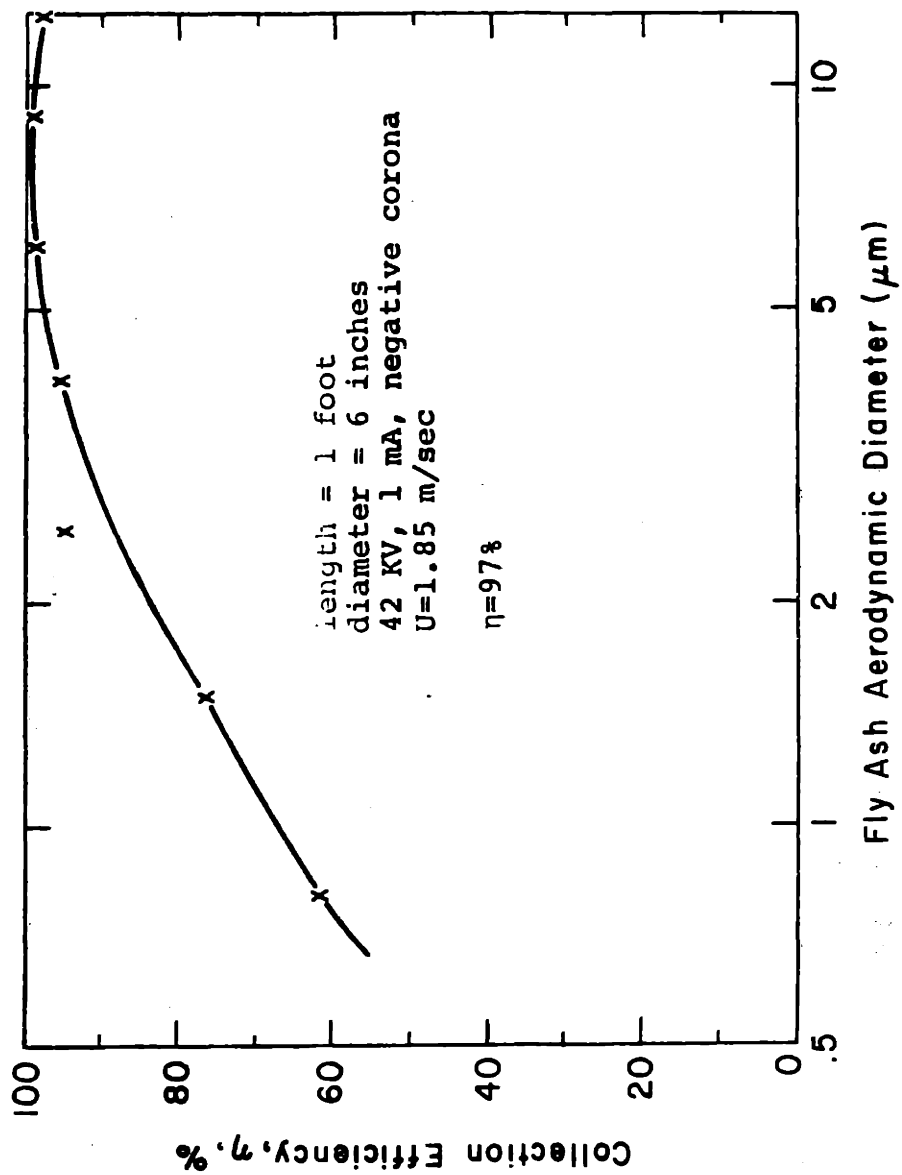

Figure 6.7 Measured performance of the ESP as a collector.

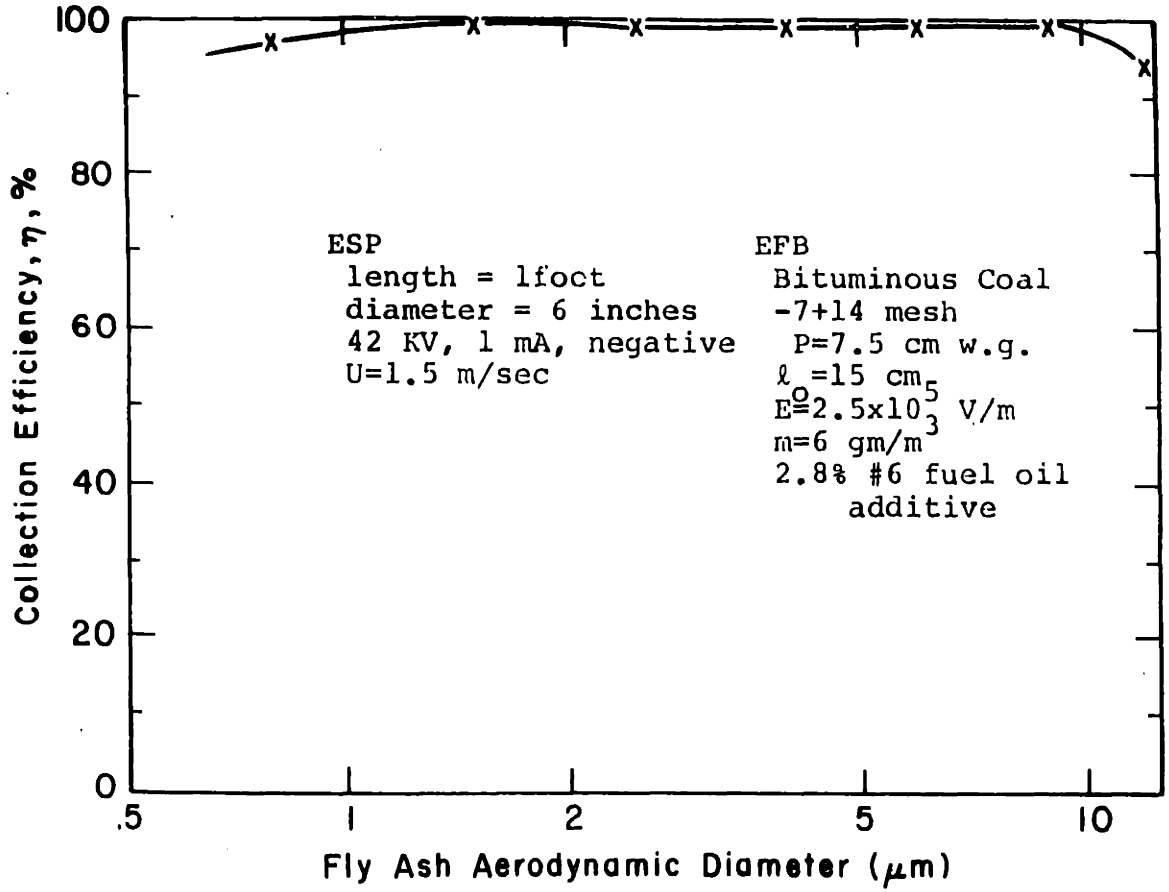

Figure 6.8 Experimental results of two stage ESP-EFB collection of fly ash.

between the two colelcting stages. Again, sampling was done after 20 min. of run time, so steady state operation is approximated.

The results of this test are similar to the two stage FB-EFB system. Good collection efficiency (~99%) is realized but still some reentrainment of large agglomerates exists. Submicron efficiency is again around 95%, consistent with a bubbling bed EFB.

This system was also taken to higher operating temperatures, specifically 140°C. Again the reentrainment of large agglomerates occurred and little fly ash build up in the bed was observed. Another important effect of the higher temperature was observed with operation of the ESP. As gas temperature increase, the gas electrical breakdown strength decreases. More important as gas temperature increases, fly ash resistivity increases. The operation at high current levels creates the well known back corona at the fly ash coated collecting electrode. As a results, the ESP operating voltage has to be drastically reduced. It is well known that in ESP technology that the ESP collection efficiency depends exponentially upon the square of the operating voltage. This is because both the changing and collecting mechanisms depend independently on the voltage. Thus, the higher temperature ESP collection efficiency was drastically reduced.

3. Feasibility of Systems

a. Operational Aspects

Several features must be considered when the scaling up to full scale is pondered. Of course structural and mechanical problems must be dealt with, but these are the tasks of specialized engineers and will not be discussed here. Rather we shall be concerned with some of the more fundamental concep-

tual problems of making a full scale system work.

Bed Particles

The first is the choice of bed particle material and the handling of such particles. Any mechanically sound, semi-insulating granular material with small fractions of fine particles is acceptable for the operation of the system. The optimum choice of bed particle, though, derives from consideration of the EFB as part of a larger system, namely the coal burning facility to which it is applied. Further discussion will be left to the following section on system integration.

One of the principal advantages of fluidized bed systems is their high particle mixing rates and ease of particle handling. Particles in the bed behave like a liquid and the literature is rich in related particle handling schemes (see for example Kunii and Levelspiel[1]). The most sure means for feeding and removing bed particles at controlled rates is the use of a rotary airlock, a device widely available in industry. Rotary airlocks basically consist of several vanes, mounted on a shaft and rotated inside of a cylinder. (See Fig. 6.9). Tolerances between the vane edges and the inner cylinder surface is quite small, preventing gas flow in either direction. Granular material is displaced by falling through a hole in the top of the cylinder into the space between two vanes. As the vanes turn, they carry the material to the bottom hole, where the material is dumped. Such devices permit positive transport of granular material regardless of the gas pressure in the system. It is envisioned that each bed unit would require two rotary airlocks, one to feed fresh bed material and one to removed fly ash coated particles. The airlocks would be activated intermittently to keep the bed at constant height and state of fluidization. The activation of the airlocks would be

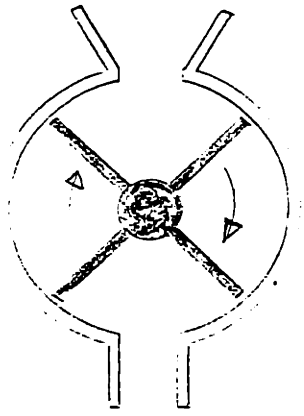

Figure 6.9 Schematic of a rotary airlock material handling system.

controlled by pressure sensors located above and below the bed. These sensors would signal a controller set for the range of acceptable pressure drops across the bed. If pressure drop fell below the range, the feeding airlock would activate and feed a certain amount of fresh bed material to the bed, thus increasing its pressure drop. If pressure drop exceeded the operating range, the removal feeder would activate to remove a specified amount of material and as a results decrease the pressure drop. Of course material would be removed from the bottom of the bed where the large ash coated bed particles migrate. Also, all angled transport pipes must be steeper than the granular material angle of repose which is about 35° from the horizontal.

The two-stage FB-EFB requires particle handling for both bed stages. It would be optimum to introduce fresh bed stages to the EFB stage. Then the particles fed to the FB stage are just those removed from the EFB stage. In this way, the EFB stage is kept relatively clean, there being only small amounts of fly ash build-up. The FB particles receive the bulk of the fly ash buildup. This scheme would keep reentrainment of large agglomerates from the EFB stage to a minimum.

The residence time of bed particles in the system is am important issue as it determines the bed particle usage rate and its related economics. If m_p is defined as the maximum loading tolerated on one bed particle (kg), m_0 the fly ash mass loading in the incident gas (kg m^3), ℓ_0 the combined unfluidized bed height (of the sum of the individual height of each stage) (m), ε_v the unfluidized bed fraction voids; R the bed particle radius (m), and U the superficial gas velocity (m/sec) the residence time is found directly to be

$$t_{res} = \frac{3\,\ell_0(1-\varepsilon_v)\,m_p}{4\pi R^3 U m_0} \quad \text{(sec)} \tag{6.1}$$

Typical values for the parameters could be

$\ell_0 = .2\text{m}$

$\varepsilon_0 = .4$

$m_p = 4/3\ \pi R^3 \rho_p$, [the mass of one bed particle]

$\rho_p = 10^3\ \text{kg/m}^3$

$R = 10^{-3}\ \text{m}$

$U = 1\ \text{m/sec}$

$m_0 = 10^{-2}\ \text{kg/m}^3$

for which

$$t_{res} = 12{,}000\ \text{sec} \quad \text{or} \quad = 200\ \text{min.} \tag{6.2}$$

These calculations were based on the maximum fly ash single particle loading about equal to the mass of a bed particle. In fact, fly ash loadings of as much as 5 times the bed aprticle mass before fluidization is seriously affected have been demonstrated. Thus our assumption appears to be on the safe side.

The total bed particle usage rate then derives directly from the amount of fly ash produced by the coal combustion. Since bed particles and fly ash

are removed from the system in a 1:1 ratio, the usage of bed particles just equals the amount of fly ash collected.

Thus

$$\text{Bed particle usage rate}, \frac{kg}{sec} = Q\, m_0 \tag{6.3}$$

where Q is the total plant effluent gas flow (m^3/sec) and m_0 is the fly ash loading in the effluent fas. For a typical power plant (with 10^6 cfm of stack gas)

$Q = 500\ m^3/sec$

$m_0 = 10^{-2}\ kg/m^3$

and the bed particle usage rate is

$$5\ kg/sec \tag{6.4}$$

This topic will be discussed further when economics are considered. For now let it suffice to say that handling equipment for 5 kg/sec of granular material is readily available industrially.

Liquid Additives

The choice of a good liquid additive is imperative. A good additive must satisfy many requirements. It must

1) be viscous enough at stack temperatures that small quantities (2-3% of fly ash mass) be sufficient for good adhesion
2) be readily available and inexpensive
3) be capable of being atomized
4) be an electrical insulator (conductivity $\approx 10^{-6}\ \frac{mho}{m}$)
5) be in the liquid phase at stack temperature
6) not produce objectionable odors

The most readily available naturally occurring liquid on earth, namely water, can be eliminated from consideration because it is an electrical conductor and it evaporates at stack gas conditions. In fact, stack gas temperatures are purposely kept above the dew point to prevent condensation of water and sulfuric acid which corrodes ducting.

The next obvious choice, fuel oil, is very attractive. While not being nearly as inexpensive as water, its cost is not prohibitive. All the other requirements are met by fuel oil, with some question reserved on viscosity. The fuel oils tested in the course of this study were typical of those used at oil burning power plants. Their viscosity at stack temperatures was found to be too low for use to promote collector adhesion. Further work needs to be done to identify possibly heavier grades of fuel oil which could be used. Our tests indicate that the oil viscosity at 140°C must be at least $1 \frac{kgm}{m\text{-}sec}$ for effective collector adhesion.

In other applications of EFB's to fly ash control, such as in combined cycle energy production schemes, the identification of a liquid additive is of first order importance. At the high temperatures of these schemes, even fuel oil is in the vapor phase. There is some indication that alkali salts are molten at these temperatures, in fact molten salt scrubbers have been proposed as high temperature gas cleanup devices. But molten salts should be highly conducting and thus are probably not applicable to EFB's. Identification of a suitable liquid additive remains a problem for high temperature applications.

b. System Integration

This section will discuss the issues involved in integrating the EFB fly ash collector into the overall operation of a coal burning plant. Much

of this discussion is the subject of a patent application "Fluidized Bed Particulate Collectors" which is included in this report as Appendix E. System integration really involved two important aspects, the geometry of the hardware and the source and disposal of bed particles and fly ash.

Hardware

Zahedi proposed a configuration for the application of EFB's to oil burning power plants in which the bed is arranged as a collar around the base of the stack. (See fig. 6.11). Similarly, this would appear to be optimum for coal burning plants using the FB-EFB system. Of course, a fluidized bed first stage collector would now be included. This would not really affect the size of the "collar", since its size is dominated by air plenums. This design is considered optimum because it places each bed stage in one plane which takes full advantage of the savings in active collector volume afforded by an EFB. Also, it eliminates the need for baffling of separate smaller bed modules and permits the use of relative little material handling equipment.

This design also appears optimum for ESP-EFB systems. In one envisioned case, a plant with an existing ESP would be looking to upgrade its collection performance. In such a retrofit application, a collar with enclosed EFB would be easy to install with virtually no interruption of plant operation. In new installations of ESP-EFB systems, the ESP stage would be placed in the collar below the EFB as in Fig. 6.12. This would require some additional collar height and width to afford space for the ESP, but only something on the order of 10 ft. The ESP hopper could be right below the ESP and removal of both bed particles and fly ash would be convenient.

Bed Material

Except for viscosity and atomization, the requirements for granular bed

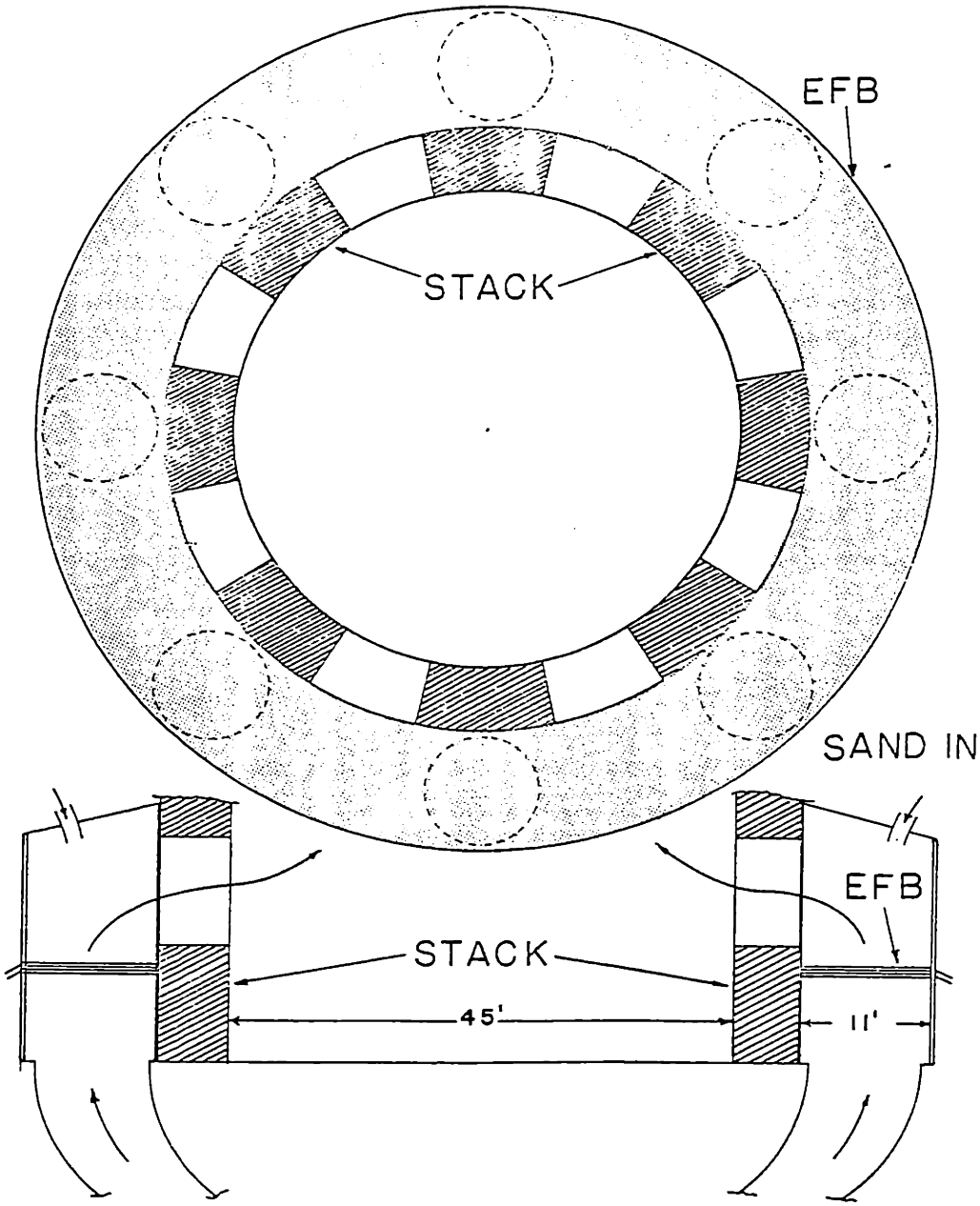

Figure 6.11 A 10^6 cfm EFB constructed around the base of a stack.

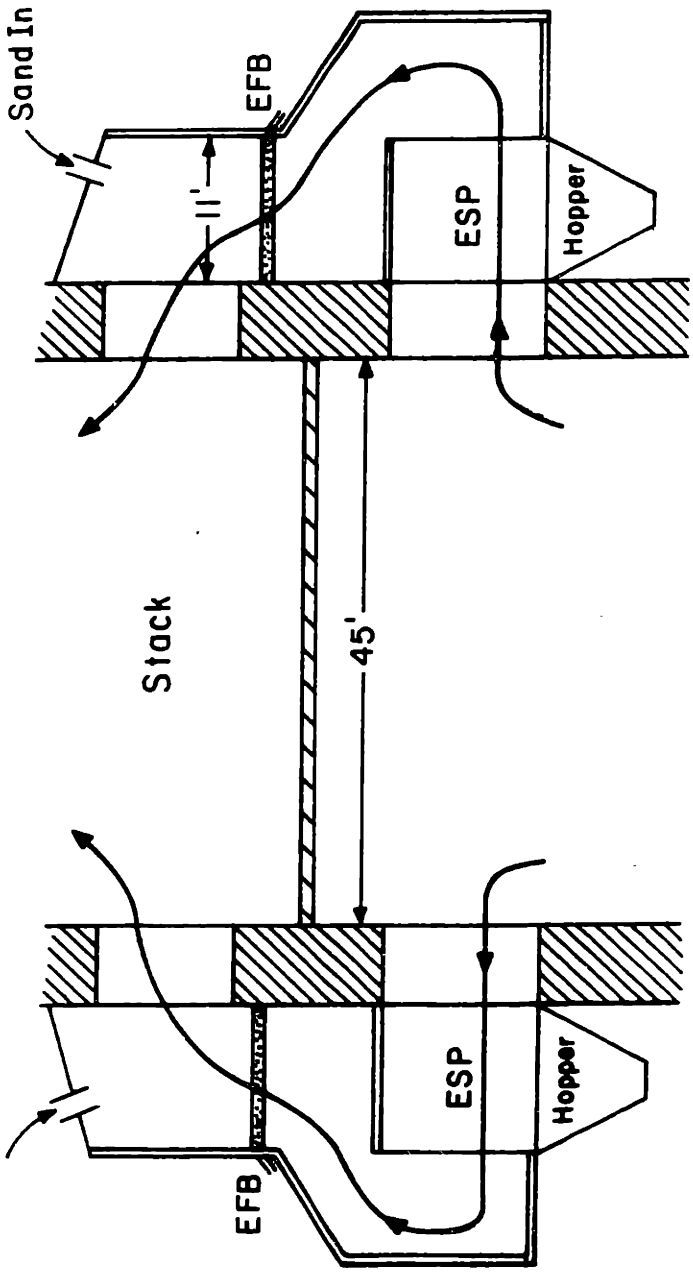

Figure 6.12 A 10^6 cfm two stage ESP-EFB constructed around the base of a stack.

materials is about the same as for the liquid additives. However, economics are emphasized because much greater amounts of bed material are required than liquid additive material. This leads the search for bed materials to those materials intrinsic to the coal burning process. Three schemes have been identified, the coal scheme, the sintering scheme and the throwaway scheme.

Coal Scheme

This scheme is well described in the patent of Appendix E. Basically it consists of using crushed and sieved coal particles as the bed particles. After being coated with fly ash and adhesive fuel oil, they are injected into the coal combustion region. Thus the heating value of the coal particles and even of the oil additive are utilized. Also, further burnout of residual carbon in the fly ash is realized.

When a typical bituminous coal particle is heated for combustion, 30-40% of its initial weight is driven off by thermal decomposition or de-volatilization. At a temperature above 650°C and in the presence of an oxidizing atmosphere these volatiles burn at a fast rate compared to their evolution. For mm sized coal particles this complete evolution and combustion time is on the order of a fraction of a second. It has been observed that if the coal particle is coated with fly ash, the evolution of volatiles causes the agglomerate to explode, thus freeing the coal particle. The combustion of the remaining char (fixed carbon) is a much slower process. For large char particles (greater than 50 μm) the diffusion of oxygen to the char particle surface is the controlling rate process. The reaction rates depend on the temperature and oxygen content of the gas, but roughly speaking the burn-out of a mm sized char particle is characterized by a time of 1 - 10 sec. (with excess air of about 20%). Such large particle may burn too slowly for complete combustion

in the furnace; so the re-injected coal-ash agglomerate may first have to be pulverized or may have to be burnt in a special separate combustor. (However, coal particles for fluidized bed combustion are just the size of those proposed for the EFB herein and then complete burnout is likely without further pulverization.)

The overall system performance for a system with ash-coal agglomerate recirculation can be analyzed from a knowledge of the ash retention (η_f) in the combustor and the collection efficiency (η_b) of the EFB system. It is possible that the recirculated ash is collected in the combustor with a different efficiency than the ash with the primary coal injection. The primary ash retention is termed η_{f1} in Fig. 6.13 and hereinafter and the secondary ash retention η_{f2}.

Two important parameters are defined in Fig. 6.13 to analyze the system. The ratio of the mass flow rate of ash exiting the combustor to that entering, with the primary pulverized coal, $\frac{m_f}{m_i}$, is a measure of dust loading in the gas incident to the EFB collector. Values in excess of one are to avoided as they indicate the necessity of repeated collection of the same ash and the associated expense (mainly for oil additive and material handling). The overall system ash collection efficiency $\eta_{overall}$, is derived from the ratio of ash mass flow rate up the stack to ash mass flow into the combustor with the primary pulverized coal, $\frac{m_s}{m_i}$, by

$$\eta_{overall} = 1 - \frac{m_s}{m_i} \tag{6.5}$$

The total ash removal efficiency by the entire system is measured by $\eta_{overall}$. If 100% of the ash collected in the EFB is recirculated to the

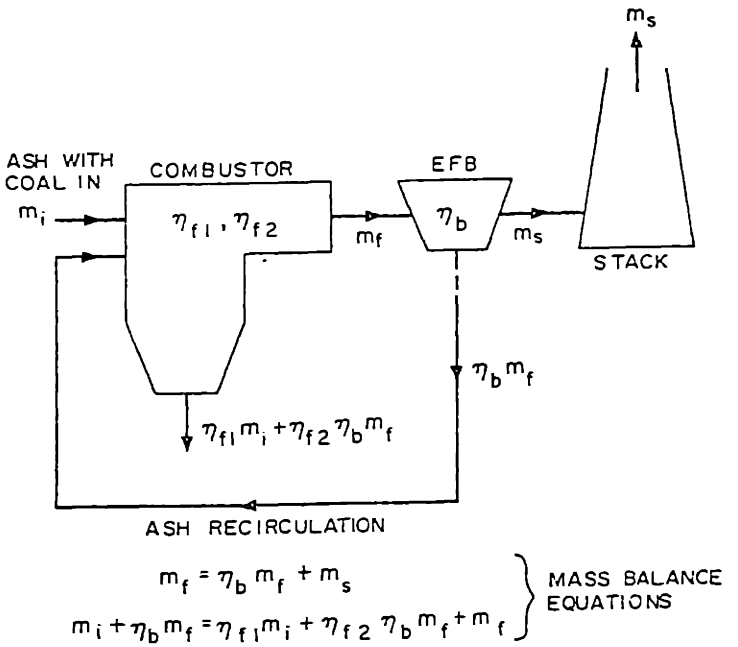

Figure 6.13 Block diagram of coal scheme EFB system with recirculation of coal-ash agglomerates.

furnace the steady state values of these parameters are determined from system mass conservation statements (see Fig. 6.13).

$$\frac{m_f}{m_i} = \frac{1 - \eta_{f1}}{1-\eta_b(1 - \eta_{f2})}$$

$$\frac{m_s}{m_i} = \frac{(1 - \eta_b)(1 - \eta_{f1})}{1 - \eta_b(1 - \eta_{f2})} \qquad (6.6)$$

When the coal ash agglomerated are recirculated directly, it is likely that $\eta_{f2} = 1$ since the recirculated ash will be in large agglomerates which will fuse in the furnace and assuredly drop to the bottom. In such a case:

$$\frac{m_f}{m_i} = (1 - \eta_{f1})$$

$$\eta_{overall} = 1-(1 - \eta_b)(1 - \eta_{f1}) \qquad (6.7)$$

The performance is then essentially that of two collectors in series. If the coal-ash agglomerate is pulverized before injection, it is likely that the secondary ash retention is equal to the primary ash retention or $\eta_{f1} = \eta_{f2} = \eta_f$. Figures 6.14 and 6.15 show plots of $\frac{m_f}{m_i}$ and $\eta_{overall}$ as functions of η_b with η_f as a parameter. It can be seen that to eliminate excessive dust loadings, the furnace ash retention should be at least 50%. In this range, high overall efficiencies are also achieved.

This analysis eliminates the use of the coal scheme for modern pulverized coal steam boilers from two standpoints. First, these furnaces are not de-

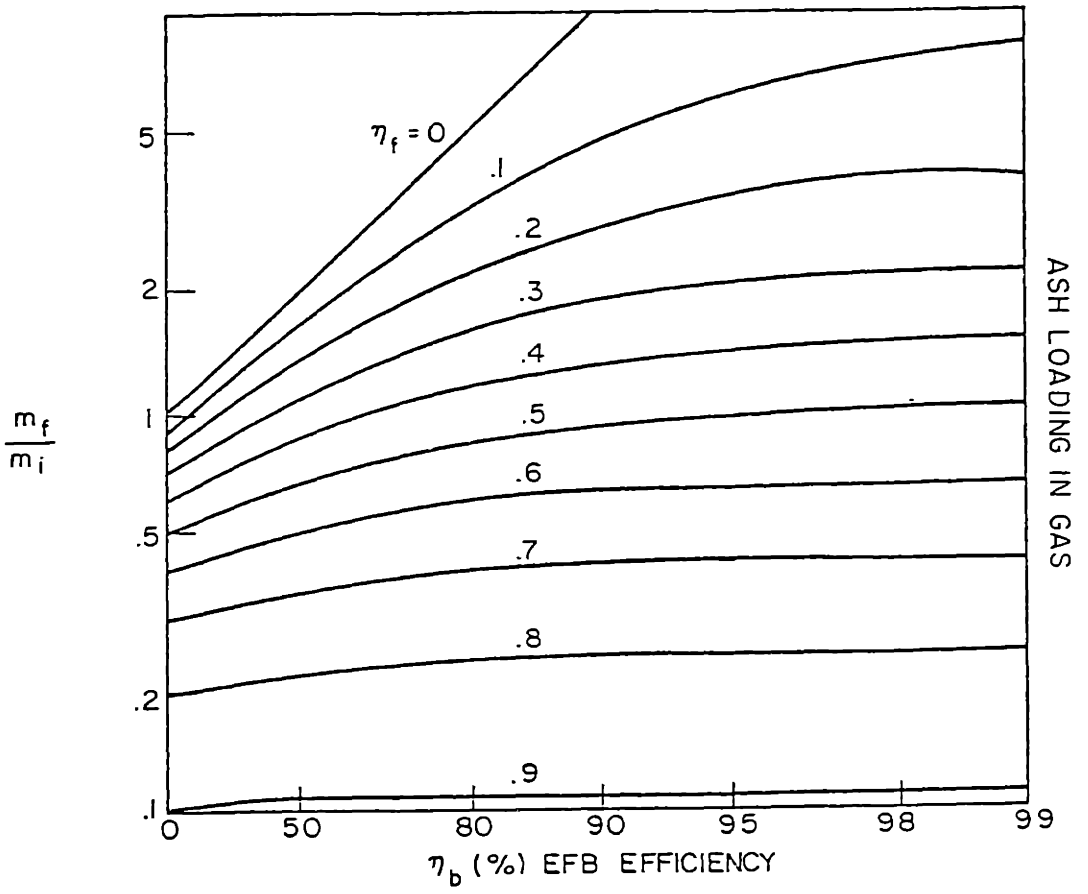

Figure 6.14 Fly ash loading at inlet of EFB system for various EFB collection efficiencies with furnace ash retention as a parameter.

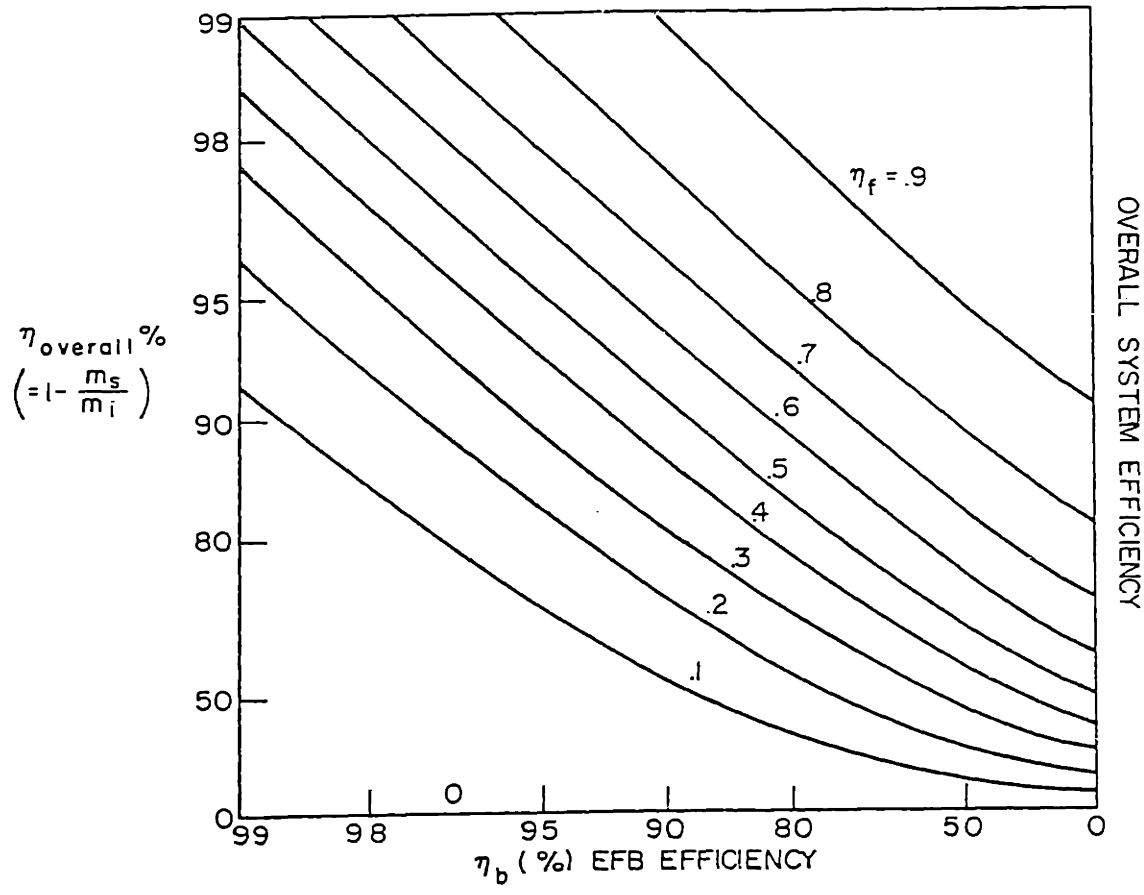

Figure 6.15 Overall fly ash removal efficiency for various EFB collection efficiencies with furnace ash retention as a parameter.

signed to burn out mm sized particles, but rather 50μm sized particles. Complete burn out of the coal ash agglomerates appears unlikely. Second, the furnace ash retention efficiencies for typical modern dry bottom furnaces are in the range of 10-20%. In fact they were designed to minimize ash retention. As a result excessive fly ash loadings would be built up from the continued recirculation of the fly ash.

However, the fluidized bed combustion (FBC) technolgoy is perfectly suited for this EFB coal scheme. FBC's typically burn coal particles in the mm size range. Further, ash retention efficiencies of up to 90% have been demonstrated[2]. This promising alternative requires further experimental and theoretical study.

Fly Ash Sintering Scheme

Another attractive alternative is that of sintering the agglomerated fly ash bed particles. Initially, the bed would be seeded with a bed material such as sand, fly ash would be grown on the seed particles and then removed from the bed. This agglomerate would be sintered according to available technology[3], then crushed and sieved to obtain a sintered fly ash pellet of suitable size for the fluidized bed. Eventually, the entire bed would consist of fly ash, some of it in sintered seed form and some in the form of the coating on the seed. Thus, no external bed particles would be introduced. The fly ash sifted away and not used in the bed would simply be discarded. In fact, the value of fly ash as a usable product has been shown to increase when in a sintered form. Sintered fly ash pellets are non-dusting, easily transportable and much better suited mechanically for landfill or use as aggregate in concret construction[4].

As part of the oil adhesion tests described in Cahpter V, sintered fly

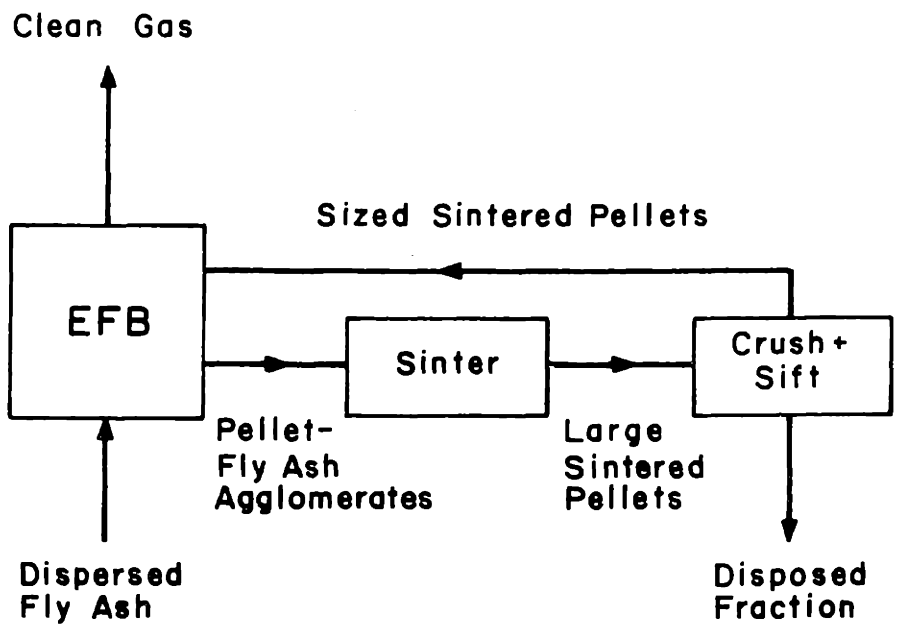

Figure 6.16 Block diagram of EFB sintering scheme.

ash pellets were used as seed bed material. After sufficient fly ash growth, the agglomerates were removed and sintered in an electric oven at 1900°F for 30 min. These larger pellets were then crushed and sieved, with the -7 +14 component being retained. This retained sintered fly ash was then used as new seed bed material to grow new agglomerates. This demonstration proved the feasibility of the Fly Ash Sintering Scheme.

Disposal Scheme

The easiest scheme to envision is that of disposal of the bed seed-ash agglomerate material. It is possible that the product may have a resale value as landfill of concrete or asphalt aggregate, but this value is dominated by the plant location and transportation costs to the nearest use site.

One of the most attractive disposal schemes uses dolomite or limestone from a fluidized bed combustor as the bed material. This material is used in the FBC as a sulfur absorbent and is usually in the form of -8 +16 mesh granules. After its usefulness as an absorbent is gone, the material is simply discarded or used as landfill. We propose simply running the material through the EFB system once, and then disposing of it. The seed bed material then has no effective cost to the overal process.

b. Economics

The ultimate deciding factors in the choice of a fly ash collection system is a result of the tradeoffs of cost with effectiveness. Any degree of emission control requirements could be satisfied is cost were no object.

The total cost of a system consists of three components:

1) The capital cost of the system amortized over the lifetime of the device

2) The operating cost of the system

3) The maintenance cost of the system

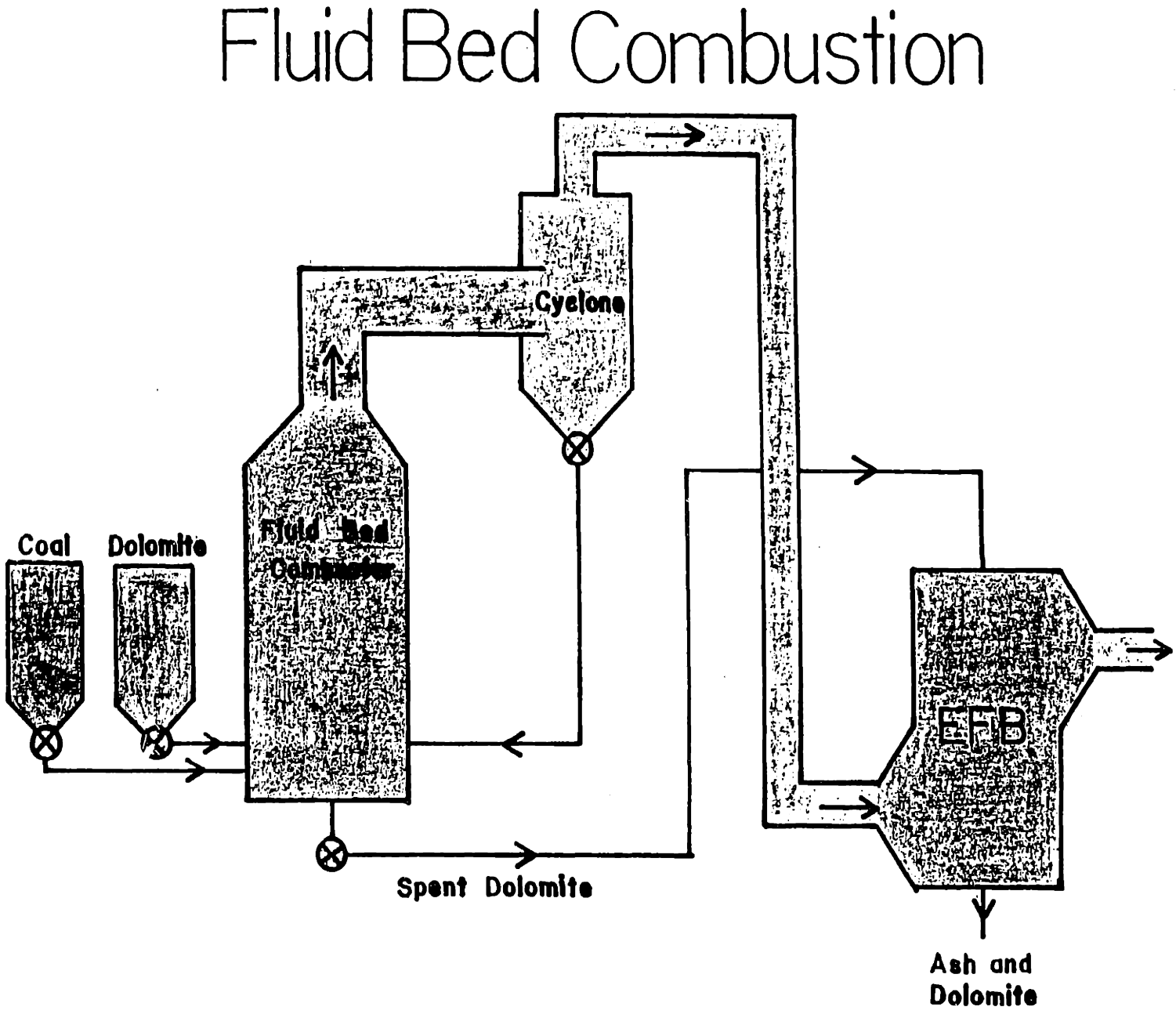

Figure 6.17 Block diagram of FFB dolomite scheme for fluid bed combustion applic ti

We will make a comparison of EFB systems with the current popular technology for fly ash control, the electrostatic precipitator.

Zahedi[5] compared capital costs based on theoretical active volumes. He assumed that at this stage of development it was not feasible to truly project the cost of a full scale EFB, and proceeded to argue that the cost should go roughly as the required theoretical active volume required to obtain the desired collection efficiency. His arguments showed that the ratio of active volumes is:

$$\frac{(\text{Volume})_{EFB}}{(\text{Volume})_{ESP}} \simeq 2.4 \times 10^{-2}$$

It is unlikely that an EFB system would cost 1/50 that of an ESP. As can be seen in Fig. 6.11, the active volume of an EFB is a relatively small fraction of the total system folume, especially if the peripheral material handling equipment is included. It is feasible though that because of reduced size the EFB could be less expensive than an ESP by some substantial fraction. With current prices of ESP systems ranging from $2 - 10 million, this saving is sizeable.

Zahedi also approximates the ratio of operation to be

$$\frac{P_{EFB}}{P_{ESP}} \simeq 2$$

The major component of the operating cost is to power the fan for the pressure drop experienced across the beds. For the collection of coal ash, though, there is an additional operating cost in the oil additive. Table 6.1 shows a summary of the expected operating costs of a two stage FB-EFB system.

Table 6.1

FB-EFB Operating Costs

	($¢/10^6$ cu.ft.)
Fan	32
1% oil additive	4
ESP Corona Power $\frac{120 \text{ watts}}{1000 \text{ cfm}}$	8

The calculations are based upon electricity costing 4¢/kw-hr and crude oil at 14$/barrel. The corona power required for a typically operated ESP is shown for comparison. Even if 2-3% oil is required, the oil costs are significantly less than the fan power. Two points should be made to emphasize the really low operating costs of the system. First, there is often enough "slop" in the pressure drop afforded by fans for the effluent gas in a power plant that the ≈ 6" w.g. pressured drop of the EFB would be unnoticed, and plants could operate with their esiting air moving equipment. Second, the operating costs of ESP's are usually considered negligible compared to the amortizing capital costs. EFB operating costs are on the same order as those for ESP's, so that they may be considered inconsequential, too.

C. Electrofluidized Bed Agglomerator Systems

1. Proposed System

The EFB Agglomerator System appears to be the most attractive of any of the schemes identified as a result of this reserach work. It uses the inherent advantages of an EFB, namely that of very short residence time collection of submicron particulate, while at the same time using the natural charac-

teristics of fluidized beds, Fluidized beds are very good at cleaning surfaces as a results of their violent and random bed particle collisions and abrasions. Witness even the eventual attrition of even very durable bed particles broken away by abrasion. The use of liquid additive permitted reasonable adhesion of fly ash to be affected, but still, some reentrainment of fly ash agglomerates resulted.

By suitably choosing liquid additive properties (specifically amount and viscosity) and EFB collector system can become an agglomerator. Such a system is shown schematically in Fig. 6.18 and is the subject of the patent application "Electrofluidized Bed Agglomerator" included in this report as Appendix F. The system consists of an oil atomizer which sprays appropriate amounts of of adhesive oil into the gas stream along with the fly ash. The fly ash and oil mist are then charge in a corona ionizer and then pass into a co-flow electrofluidized bed. In the electrofluidized bed, all the fly ash particles and oil droplets are transported to the bed particle surfaces by the various mechanical and electrical collection mechanisms as analyzed in Chapter III. The fly ash particles adhere by the action of the oil adhesive agent, but the oil properties are chosen such that the growth is limited to certain sized agglomerated which then break off and reentrain in the gas flow. In this way, a steady state is approached where the mass fluxes to and from any given bed particle are the same and the mass flux to and from the entire bed are the same.

Such a system requires no handling of bed particle material. Bed particles are placed in the system upon installation and remain there essentially indefinitely. Except for a slight initial build up of fly ash, the system is complete-self-cleaning.

The functional results of the agglomerator is simple. It transforms an

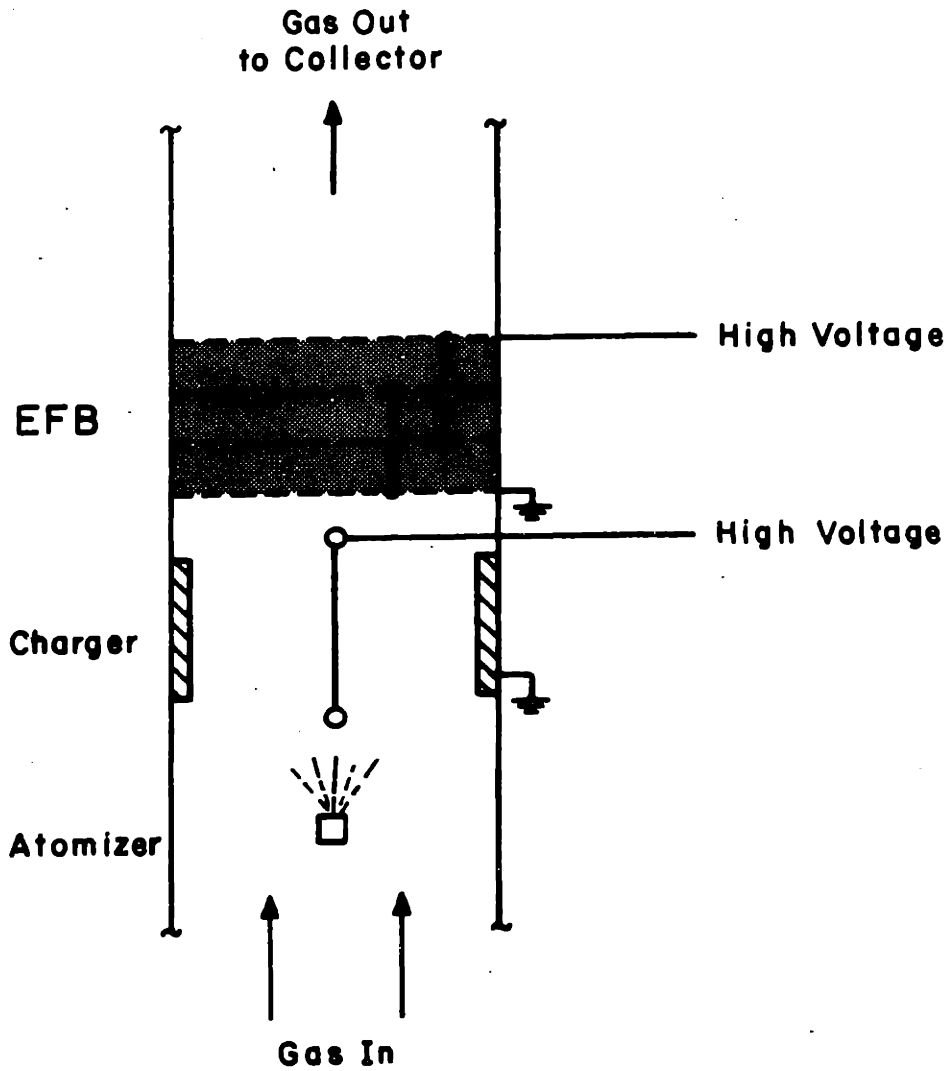

Figure 6.18 Schematic of proposed EFB fly ash agglomeration system

aerosol of fine fly ash into one of size distribution skewed to the larger sizes. The total mass loading remains unchanged. For most particulate removal devices, collection efficiency increase with increasing particulate size. Thus the agglomerator is intended to be used as a conditioning stage for some other collection device where the particulate is actually removed from the gas stream. This collector though does not have to be effective in the micron and submicron size range as most of these particles have been removed from the gas stream and reentrained as effectively larger agglomerates by the EFB.

2. Experimental Demonstration

A series of tests were run to determine the performance of the proposed agglomerator system. In these tests the hot flow test rig as described in Appendix A and Fig. A. was used with the ESP-EFB plug in unit described in this chapter and Fig. 6.6. The tests were performed at 140°C for which case the system with the oil quantities used acted as an agglomerator. The bed material was N.J. #2 sand with mean particle radius of .4 mm. The rest of the operating parameters are summarized in the plot of the data in Fig. 6.19. This plot shows the cumulative removal efficiency (CRE) defined in Appendix E for runs made with four different oil additive quantities. The plots do not show the CRE going to zero as $a \to \infty$ because out fly ash sampling measurements were only valid up to $a \approx 10$ μm (as described in Chapter V). However, in all cases the overall collection efficiency of the EFB was zero. There was no accumulation of fly ash on the bed. Further, the CRE for micron sized fly ash was only appreciable for the 3.0% and 4.8% oil additive quantities.

For the tests run at 3.0% and 4.8% oil additive the adhesion parameter passed through its critical value for aly ash diameters of 1-2 μm. Thus we

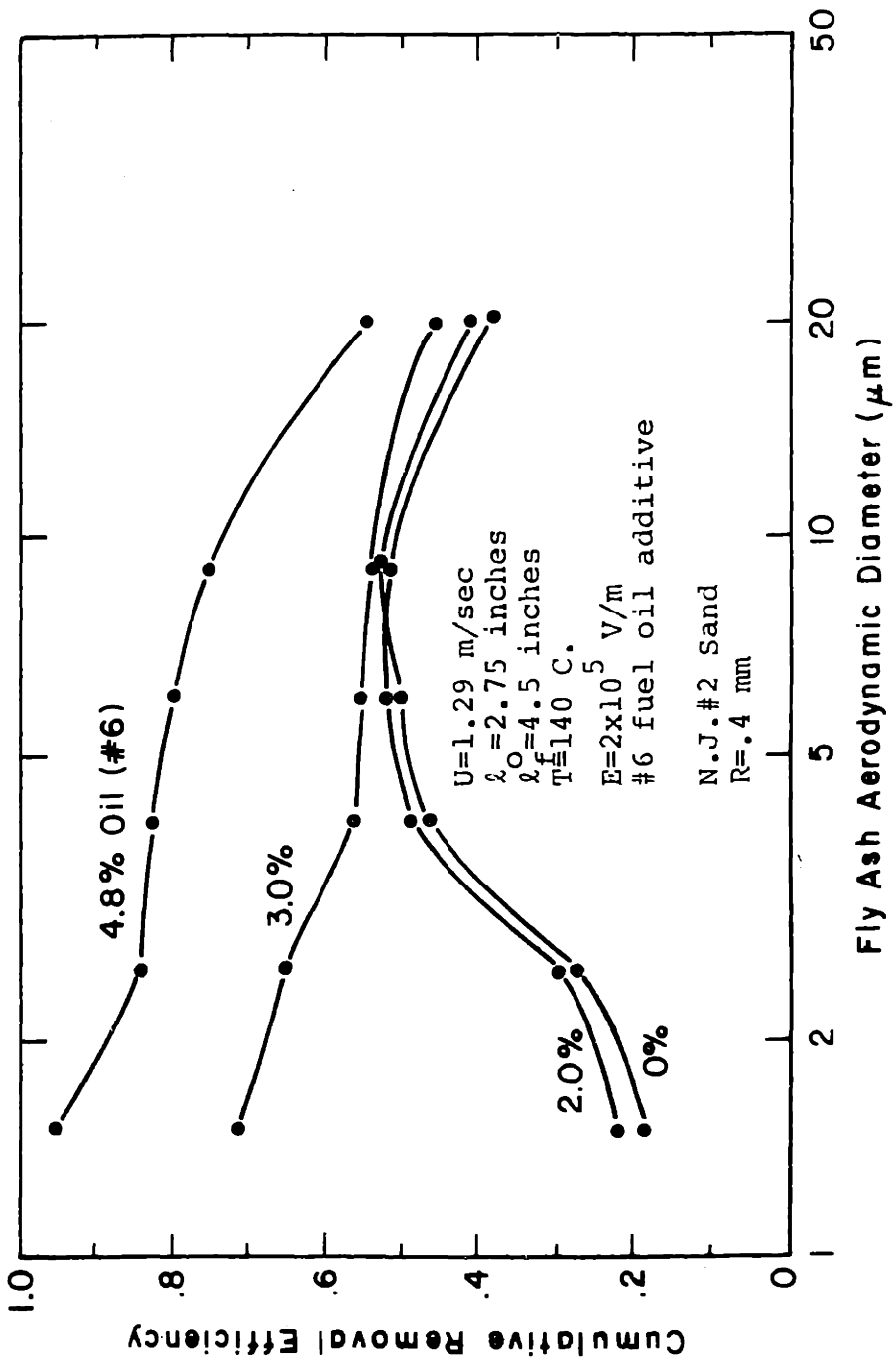

Figure 6.19 Experimentally measured cumulative removal efficiencies for the EFB fly ash agglomerator.

would expect fly ash or agglomerates of larger size to reentrain while those smaller would be effectively adhered until growth to the reentrainment size. The data is indeed clear evidence of this as the CRE begins to drop in these size ranges. For the cold flow tests where oil viscosity is higher reported earlier, the adhesion parameter passed through its critical value for 20-30 μm particles. This is why the cold flow tests acted as collectors while the hot flow act as agglomerators.

The analysis equipment used was not sensitive to the submicron component of the fly ash. Since we are really most concerned with the submicron removal efficiencies a series of tests were run to specifically determine this data. The same bed channel and plug in units were used, but the diagnostic sampling train was replaced with the one shown in Fig. A.13. With this sampling set up, super-micron fly ash particles are removed from the gas stream before measurements are made with the mass monitor. The sampled gas was first passed through a cyclone separator which had a cut diameter of 3 μm. The the gas passed through the 0-5 stages of the Anderson 2000 cascade impactor which removed all remaining particles greater than 1.1 μm diameter. Finally, after passage through a radioactive source charge neutralizer the submicron fly ash mass loading was measured with the mass monitor.

Two bed materials were tested with this set up, the N.J. #2 sand and -7 +14 mesh bituminous coal. Results are plotted in Figs. 6.20 and 6.21. They show the submicron removal efficiency of the bed vs. oil additive quantity with applied electric field as a parameter. The oil additive is seen to be critical, and quantities of about 2% are seen necessary for good submicron adhesion and thus removal. It is interesting to note that the applied electric field does not have much effect on the submicron removal, in the case

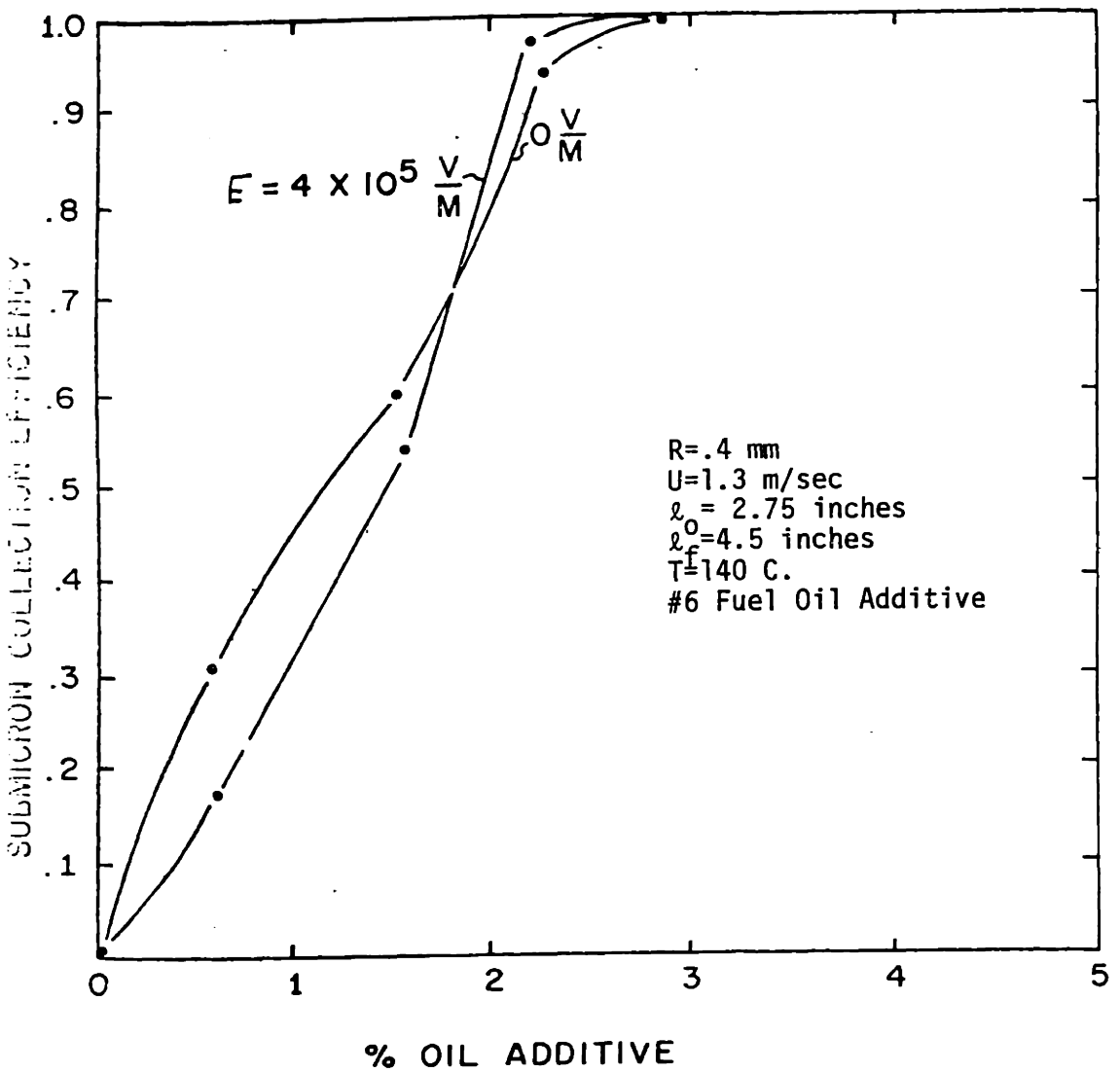

Figure 6.20 Experimental fly ash submicron removal efficiencies for the EFB agglomerator. N.J.#2 sand.

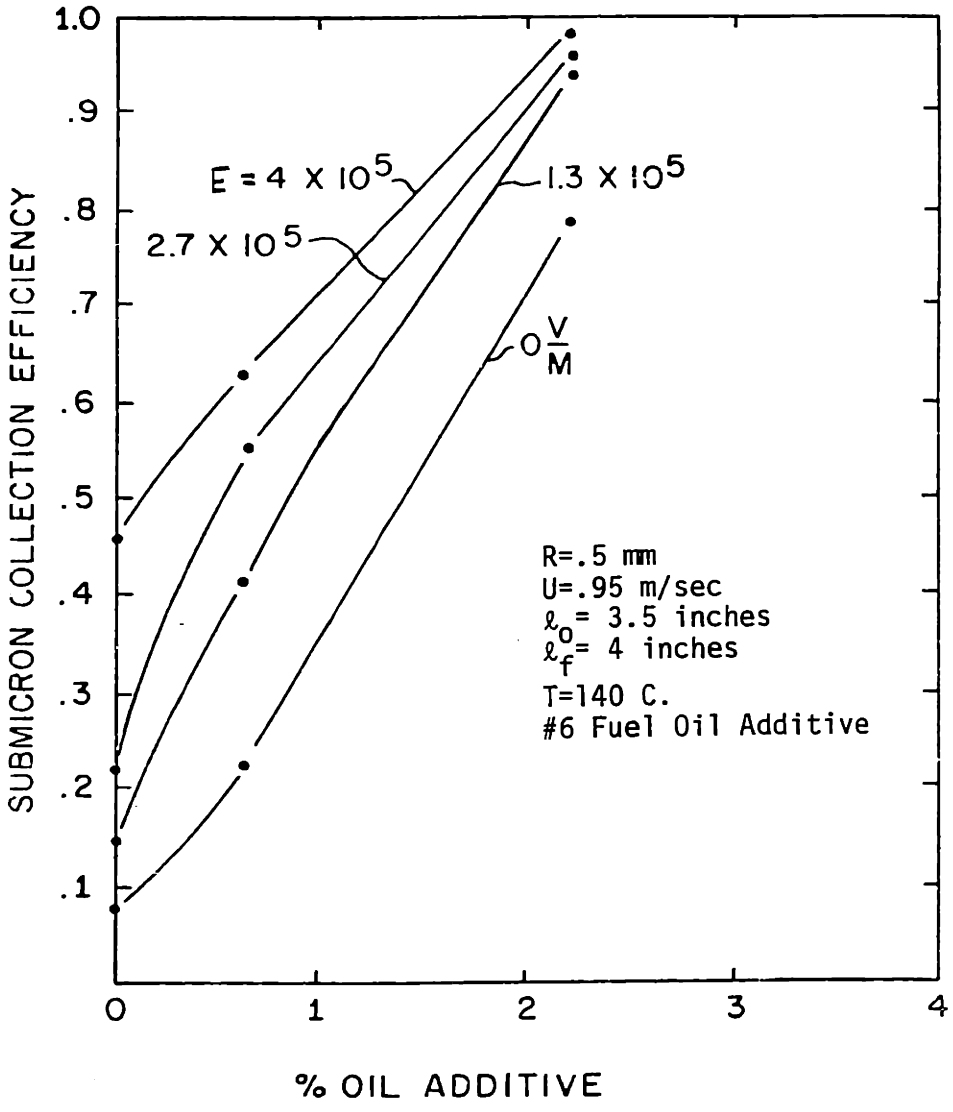

Figure 6.21 Experimental fly ash submicron removal efficiencies for the EFB agglomerator. Bituminous coal -7+14 mesh.

of the sand bed. This is because collection of the charged fly ash is achieved by micro-fields produced in the beds by frictionally induced charges which reside on the bed particles for long times because of their high resistiveness in the hot, dry gas.

These results are important. Submicron particles are the most difficult ones to collect in other types of control devices. Our tests here show that submicron removal efficiences on the order of 95-99% can be obtained in an EFB agglomerator.

a. Operational Aspects

The agglomerator system is very well suited for long term, trouble free operation. Because there are no buildups of fly ash in the system (the overall collection efficiency is zero), there is no need to incorporate equipment for feeding or removing material to or from the EFB. Fluidization can be kept at a relatively wild state, and in this mode a fluidized bed is very effective are keeping itself clean. The chraging section can utilize standard ESP rapping technology to keep clean and it has been demonstrated that pneumatic rappers are effective at keeping the distributor plate clear of fly ash buildups. Basically, it is expected that the system would be installed and could remain "untouched" of free of maintenance for an indefinite period of time.

Choice of bed material is not an economic issue for the agglomerator because the bed material need not be renewed. It is probable that something like sifted sand would be used. For high temperature applications, even expensive materials could be used, such as crushed ceramics.

A new technology is being developed by EPRI and Air Pollution[6] Systems Inc. for fly ash charging which would appear to match very nicely with the agglomerator system proposed here. This technology, called the high intensity

ionizer charges fly ash as it is accelerated with the gas flow through a venturi throat. Very little fly ash collection occurs in the throat, in fact secondary air is introduced at the corona collecting electrode as a further aid at keeping this area clear of fly ash. It is claimed that fly ash charging can be increased by 6 times compared to that in conventional ESP's. The charging even exceeds the calculated saturation charge. Also, because the corona collecting electrode is kept clean, it is claimed that the charger is immune to resistivity problems normally encountered in conventional ESP's. Fig. 6.22 shows a schematic of the ionizer and its proposed installation scheme with a conventional ESP. Each venturi throat in the array is designed for about 3000 cfm of gas flow.

b. System Integration

The geometry of installation for both new and retrofitted systems is best analyzed by considering installations along with a high intensity ionizer. It would be optimum for the EFB system to be in the form of a vertical sheet which could "slide" in front of an ESP. Further it would be ideal to modularize the EFB into bed section matched 1 to 1 with tne ionizer venturi throat. Thus each would handle about 3000 cfm. At a superficial velocity of 1 m/sec, this implies bed cross sectional area of 15 ft. Fig. 6.23 shows a schematic of what a combined system would look like, with dimensions. Each bed would be about 5 feet wide. Any flow capacity could be handled by adding any number of these 3,000 cfm modules. The total combined system could then be slid into place before a conventional ESP as in Fig. 6.22, making this design ideal for retrofit applications.

It is possible, too, that for many applications, the high intensity ionizer is not necessary. This might especially be true because the EFB is so

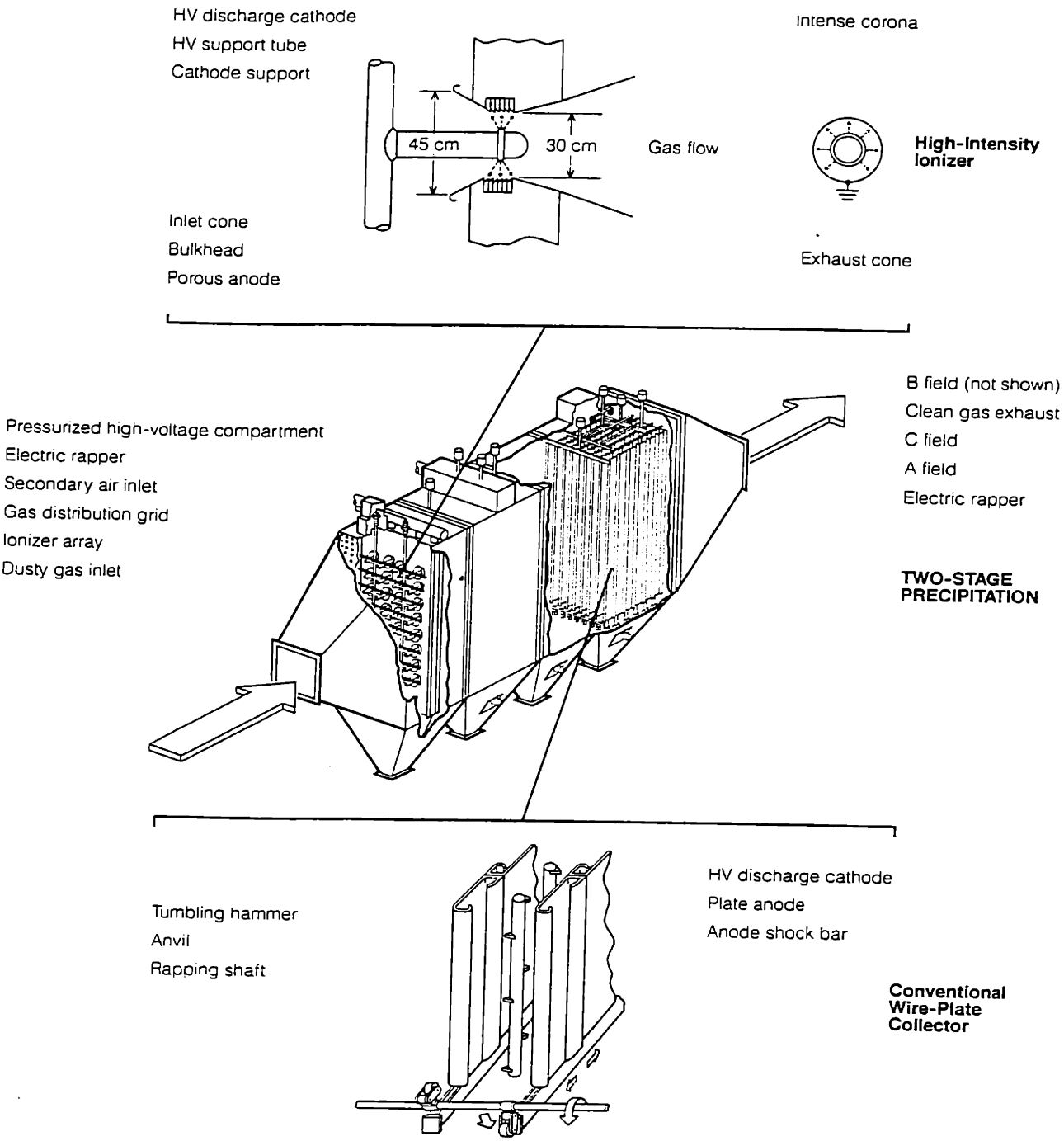

Figure 6.22 Schematic of high intensity ionizer proposed by EPRI.

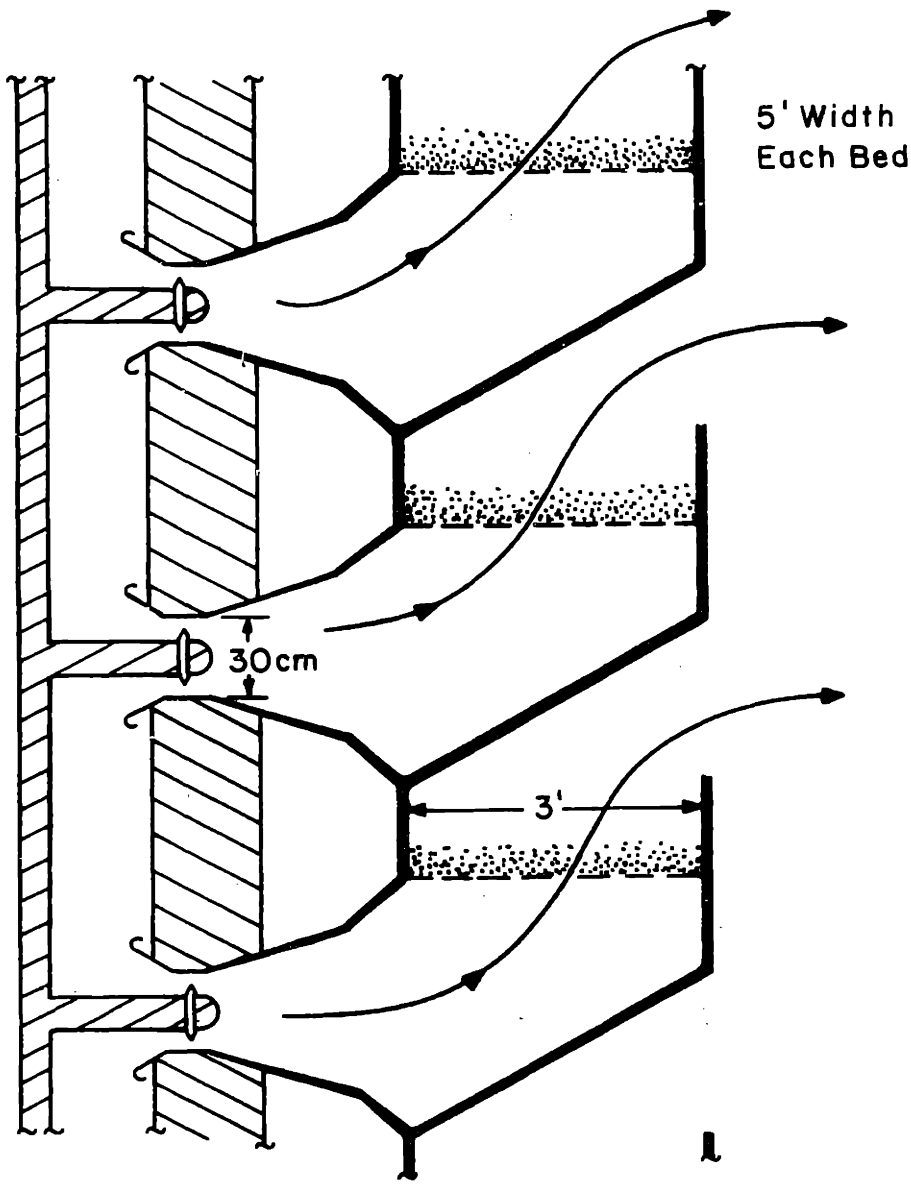

Figure 6.23 Schematic of proposed combined high intensity ionizer and EFB agglomerator system.

highly efficient for charged submicron fly ash. Thus, good charging is not as critical for an EFB as for an ESP. For this case, a conventional wire-tube or wire-plate charger would be sufficient and could reduce costs of the High Intensity Ionizer.

c. Economics

Since the system is very similar to the EFB fly ash collector, we expect the cost figures to be similar to those proposed earlier. However, substantial capital cost savings over the collector are expected because of the elimination of material handling equipment. Also, since only one bed stage is used, pressure drop would be less for the agglomerator. Oil additive quantities could also be less.

On the negative side is the fact that the agglomerator system must be followed by another collection device, usually an ESP. Although it could be designed for the collection of larger fly ash and thus be smaller and cheaper, it is expected that the system costs would be dominated by the final collector.

Economically, then, the agglomerator is perfect for a retrofit application where the performance of an installed ESP needs upgrading. It is expected that this situation will be encountered frequently in the near future as oil burning power plants with ESP's are forced to switch to burning coal. In these cases it will certainly be cheaper to retrofit an EFB agglomerator than to install a new high performance ESP.

REFERENCES

(1) Kunii, D. and O. Levenspiel, Fluidization Engineering (Wiley and Sons, New York, 1969).

(2) Goldberger, W.M., "Collection of Fly Ash in a Self-Agglomerating Fluidized-Bed Coal Burner", ASME Publication 67-WA/FU-3.

(3) Coxon, P., Power Engineering, 52, April (1968).

(4) Capp, J.P., Combustion, 36, February (1966).

(5) Zahedi, K., "Electrofluidized Bed Filtration: Fundamentals and Applications", Ph.D. Thesis, MIT, September, 1976.

Chapter VII Summary

The details of this thesis are well summarized at the beginning of Chapter VI. More general issues will be discussed here. First of all, the EFB has been shown to be very effective in the control of fly ash by the demonstrations presented. Several practical configurations have been identified. Especially important are two practical operational aspects.

1) Electric fields must be utilized to achieve good submicron efficiency. In some cases, frictionally induced bed microfields may exist, but these effects cannot be relied upon. To assure consistent operation, electric fields must be applied by suitable electrode means.

2) A liquid additive is necessary for effective fly ash adhesion in either collectors or agglomerators. Number 6 fuel oil was identified as a suitable candidate for conventional applications. One problem remains to be studied further. This is the production of odors by hydrocarbon volatilization from the atomized oil. In experiments run here, noticeable, but not objectional, odors were produced. The impact of this problem on system practicality is fundamental.

For high temperature - high pressure gas clean-up applications, the choice of a suitable liquid adhesive additive is also of fundamental importance. Further work should be done here.

Appendix A - Experimental Apparatus and Procedures

Two fluidized bed experimental rigs were used in the course of these studies, along with a considerable amount of diagnostic equipment. This appendix will describe each of the test rigs, the diagnostic equipment, much of which was common to both rigs, and some of the calibration experimental results.

Cold Flow Fluidized Bed

This rig consisted principally of a 4 inch square vertical plexiglass channel and was used for the room temperature experiments. The overall set-up with typical associated equipment is shown in fig. A.1.

The bed section was a "plug-in" unit for easy changing of beds. It is detailed in fig. A. 2. The horizontal co-flow screen electrodes were 1/2" mesh hardware cloth. These served as internal bed baffles, to promote bubble break up and help insure plug flow conditions. They also served as electrodes as indicated on the figure.

A roof fan and damper system, connected to the top outlet of the channel provided the necessary flow and flow control. At the bottom inlet section, a mixing chamber was included for good aerosol distribution. An inlet humidifier was needed because at low relative humitities, bed particles acquire charge frictionally. For basic studies, the associated "micro-field" collection of charged aerosol is undesirable. Such effects are eliminated when the fluidizing air is at relative humidities greater than about 90%, because water absorbed on the bed particle surfaces increases their conductivity and allows frictionally generated charge to leak off.

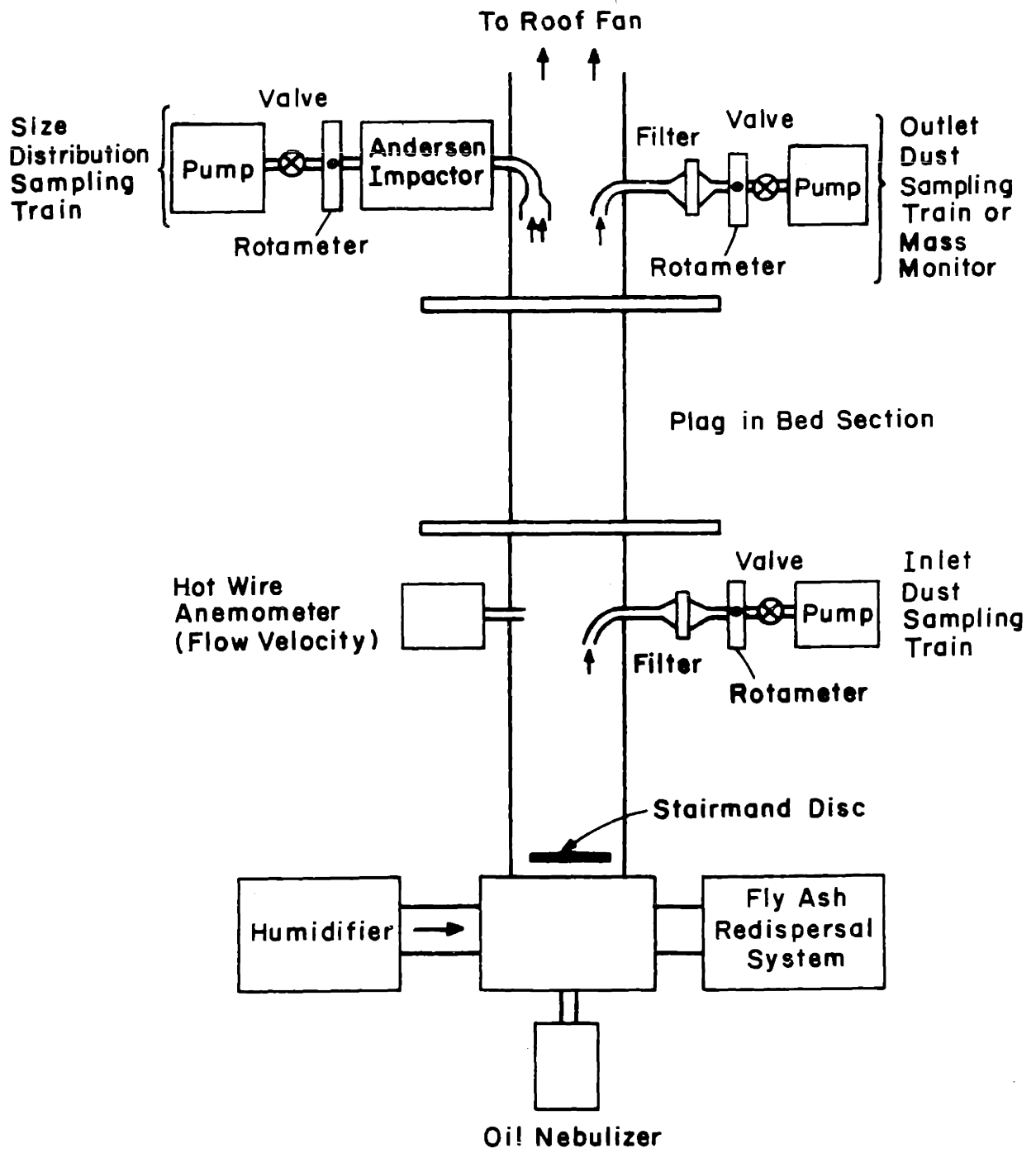

Figure A.1 Test facility for EFB collection DOP aerosol.

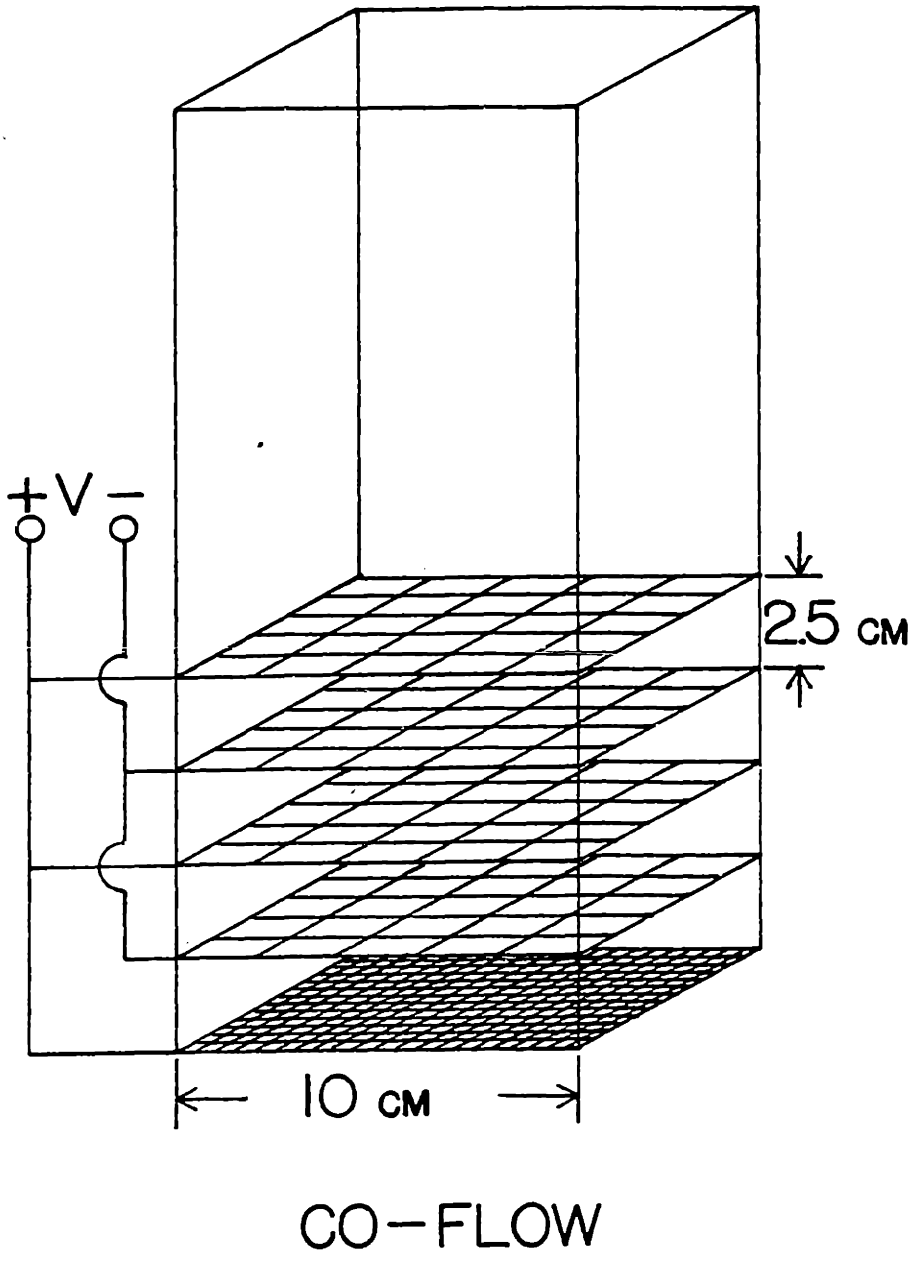

Figure A.2 Co-flow fluidized bed geometry

 (best copy available)

Hot Flow Fluidized Bed

This rig was designed for fluidized bed operation at controlled temperatures up to [illegible]°F. Schematically it is shown in Fig. [illegible].3. It consisted of a [illegible]" I.D. metalbestos thermally insulated chimney arrangement with provision for a [illegible] plug-in assembly.

[illegible] a roof fan and damper assembly provided the necessary flow and flow control. A mixing section with stainless [illegible] disc was provided at the aerosol inlet portions.

The air in the hot flow test channel was heated by a [illegible] kW electrical heating unit designed specifically for the experiments. Gas temperature was sensed by a thermocouple and controlled by an [illegible] power controller to the heating element. Figure [illegible] is a schematic of the system. Controlled temperatures up to [illegible]°F were obtainable.

The bed plug-in units consisted of two [illegible]" I.D. by 18" Corning Pyrex glass T's. Fluidized bed internals and electrodes were mounted as shown in Fig. [illegible], which depicts the basic EFB system tested. Function of the various bed components and alternative bed designs are presented in Chapter [illegible].

Aerosol Generation Equipment

The polydisperse [illegible] aerosols and fuel oil aerosols were produced with the atomizer-nebulizer depicted in Fig. [illegible]. In it a two stream atomizer (Spraying Systems Co., Conv. Atom - 1/[illegible]) injected a liquid spray into a [illegible] gal. can. The large liquid droplets were impacted at the bottom of the can while the remaining droplets exited via the outlet port. The resulting outlet mist was roughly [illegible]. Size distributions obtained with the Andersen [illegible] cascade impactor for the [illegible] and [illegible] fuel oil aerosol are shown in Figures [illegible] and [illegible] [illegible].

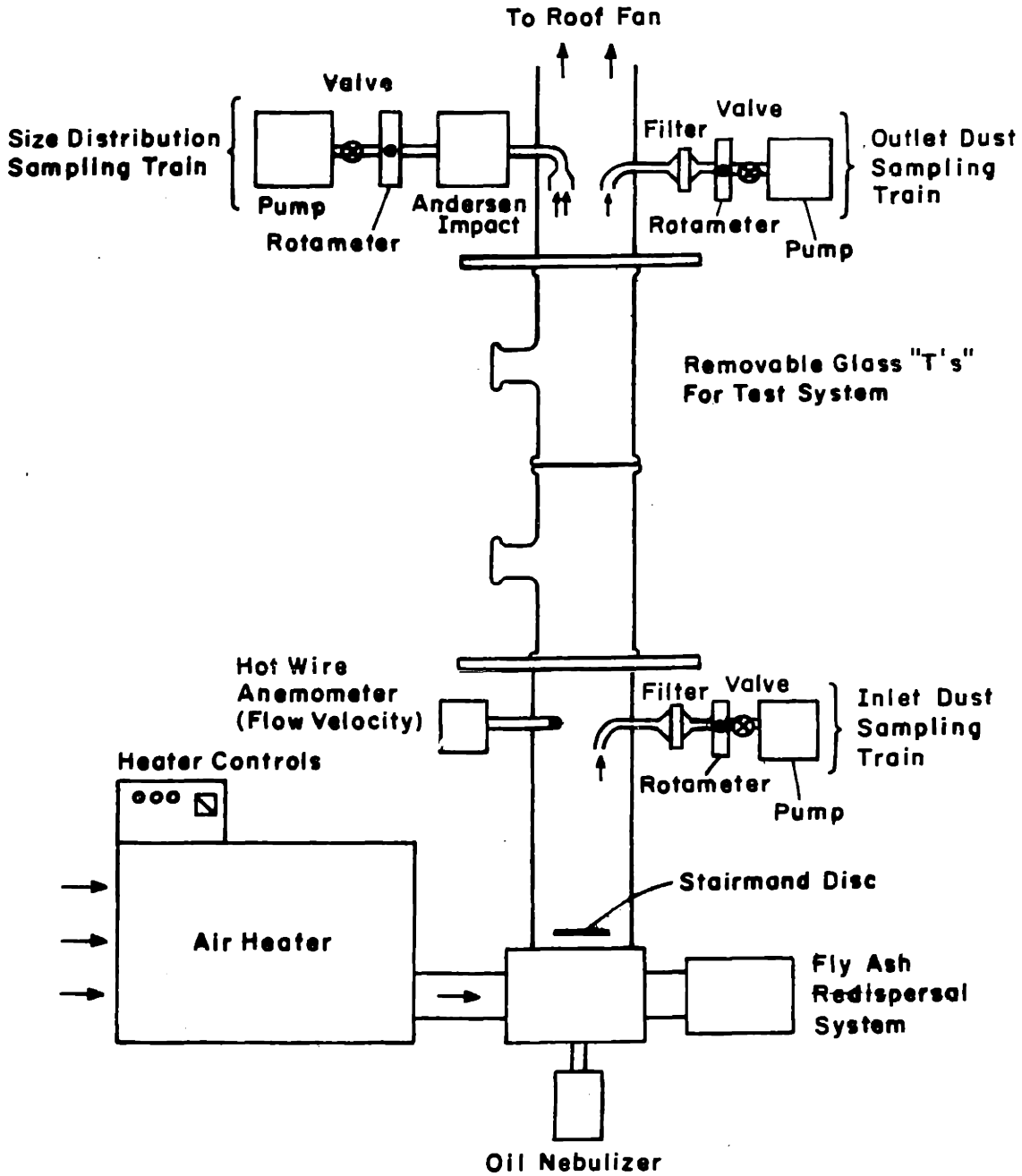

Figure A.3 Schematic of hot flow test facility. Capability to 100 cfm and 600 F.

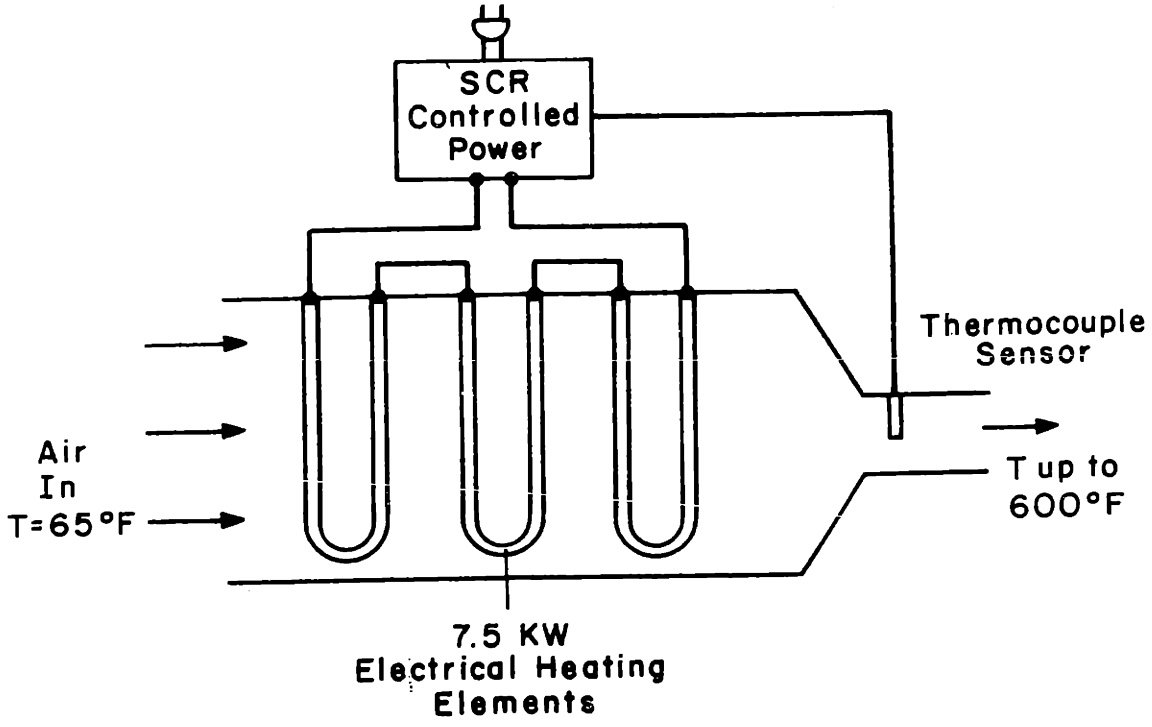

Figure A.4 Schematic of 100 cfm air heater with temperature control.

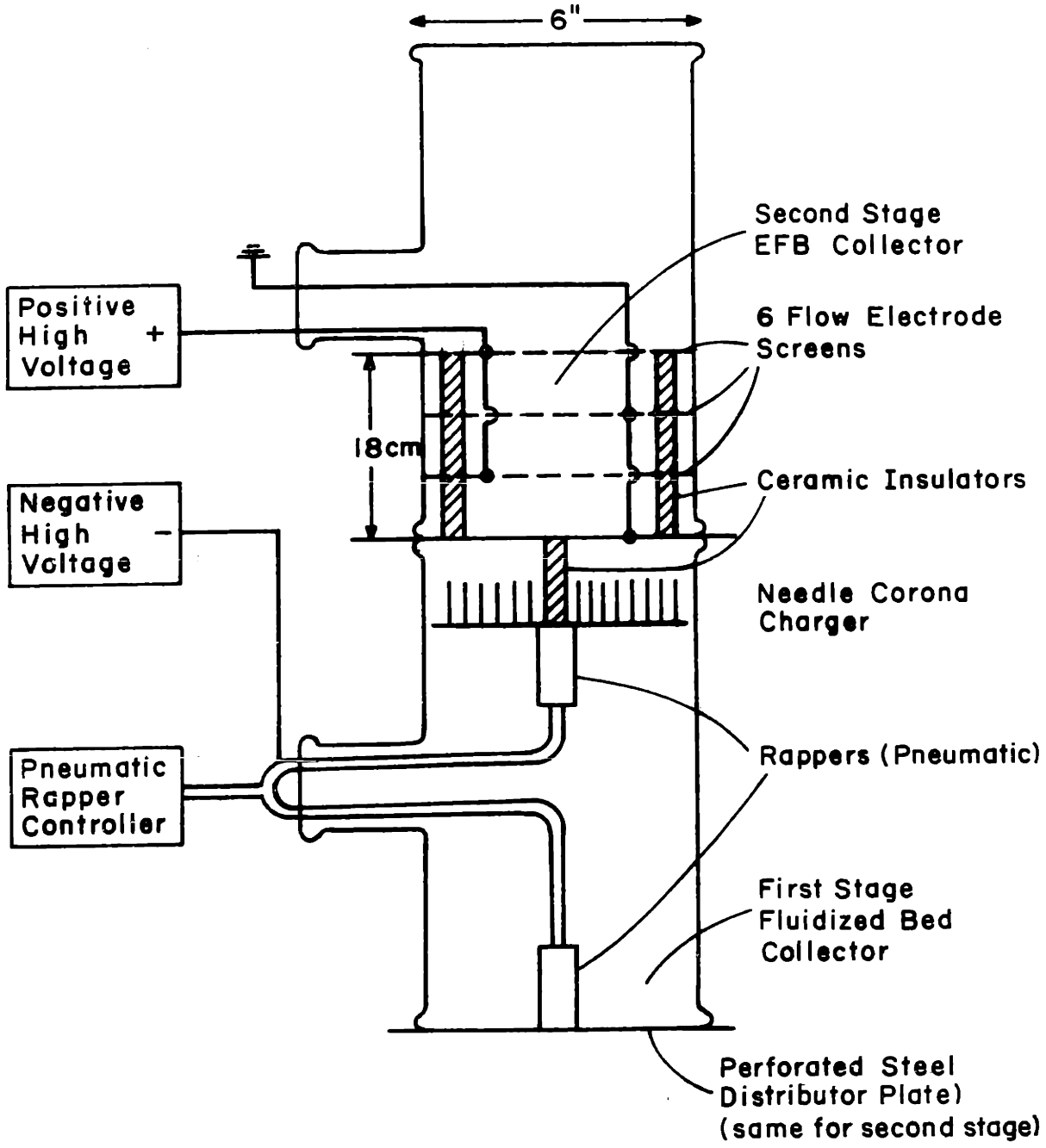

Figure A.5 Co-flow plug-in glass-T bed section.

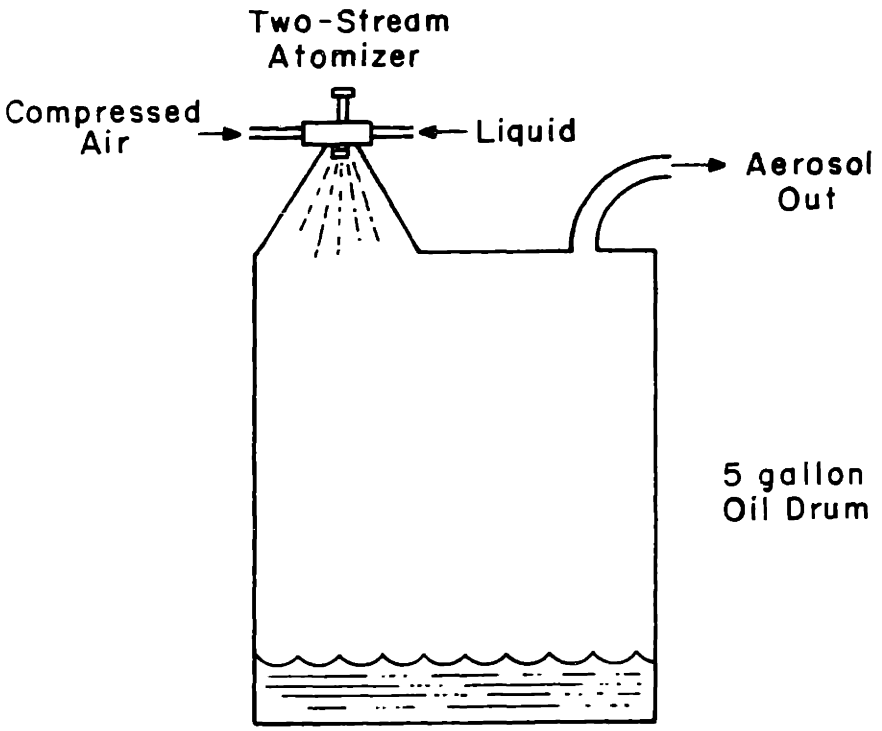

Figure A.6 Schematic of atomizer-nebulizer aerosol generator.

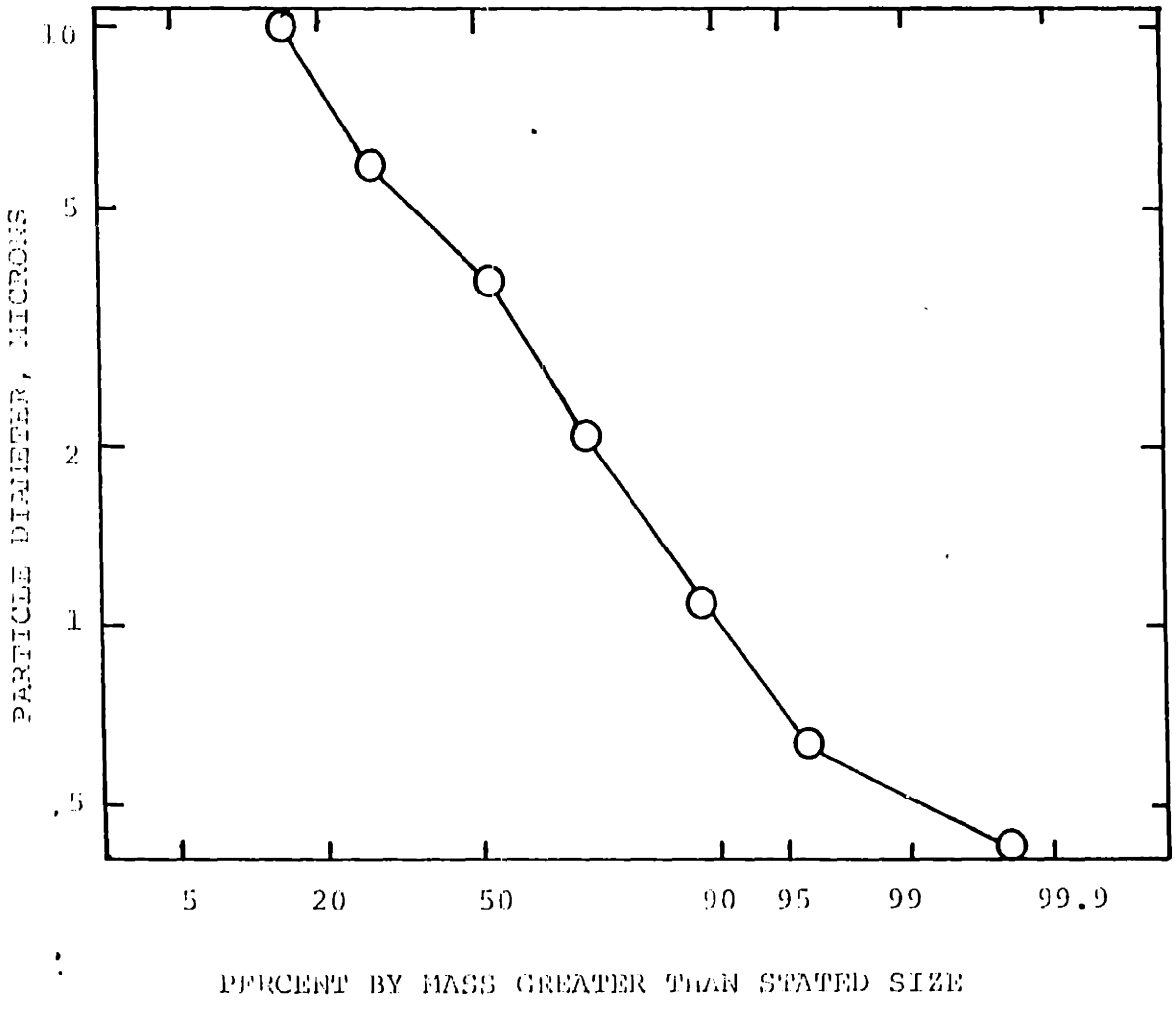

Figure A.7 Experimentally measured DOP size distribution

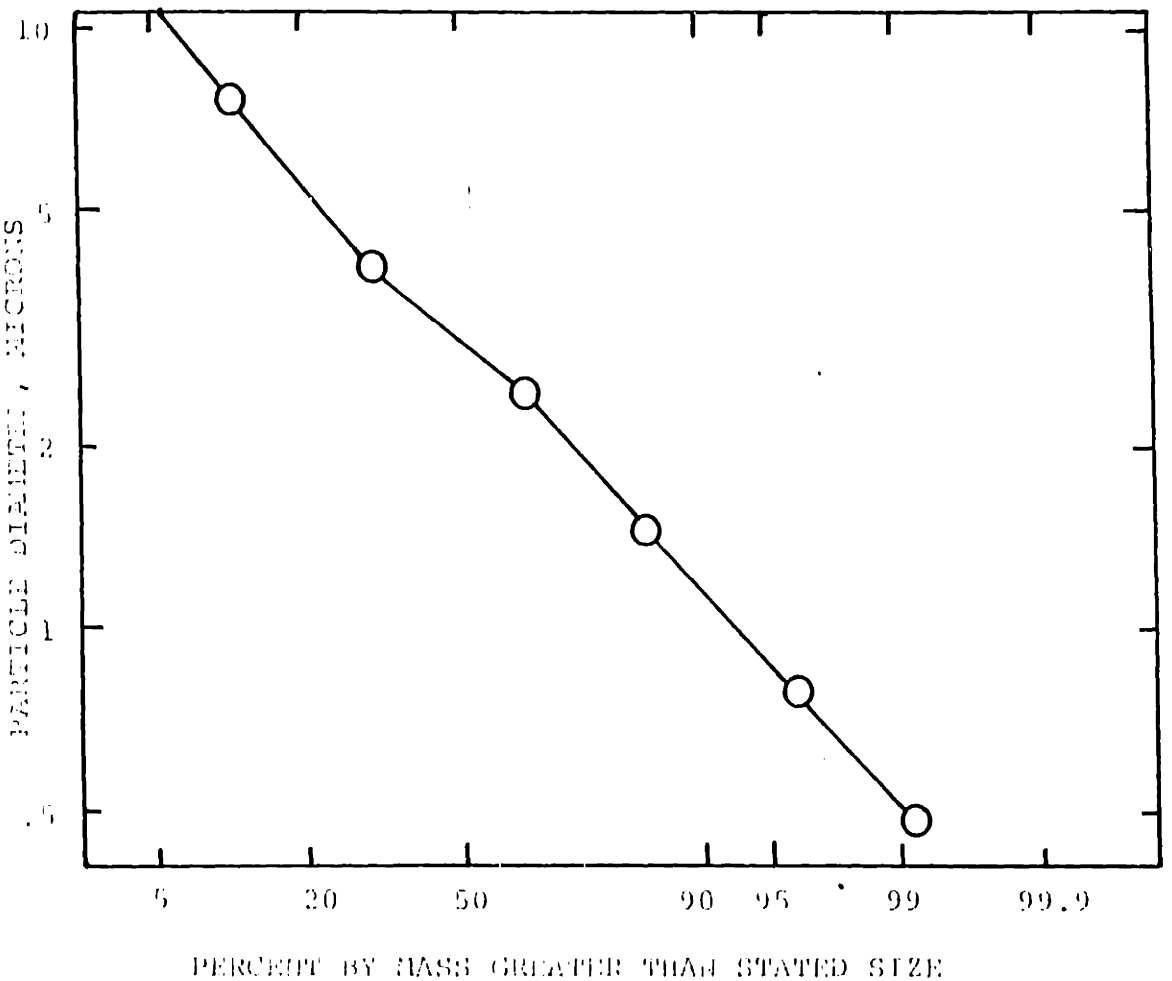

Figure 3.3 Experimentally measured #6 fuel oil aerosol size distribution

Table A.1 Low Viscosity #6
Fuel Oil Analysis

TEST	RESULT
Gravity, API @ 60° F	24.7
Flash Pojnt, pm/cc	200+°F
Viscosity, SSU @ 100° F	202
Pour Point	-20°F
Water & Sediment	0.1%
Sediment by Extraction	0.01%
Water by Distillation	0.05%
Btu's per pound	19,200
Btu's per gallon	144,845
LBS/US GAL.	7.544
Ash	0.02%
Carbon	86.44%
Hydrogen	12.82%
Nitrogen	0.19%
Oxygen	0.10%
Sulphur, ASTM:D1552	0.43%

Table A.2 High Viscosity #6
Fuel Oil Analysis

A N A L Y S I S - Composite of vessel's tanks - Lab. No. K-2979

Gravity, API @ 60°F	15.2	Sed. Extraction	0.03%
Flash Point, PM, CC	166°F	Water Distillation	0.1%
Vis. S.F. @ 122°F	166 sec.	B.T.U. per pound	18,607
Pour Point, ASTM	25°F	" " gallon	149,470
Carbon res. con.	9.82%	Ash	0.05%
Sulphur, ASTM	1.92%	Vanadium	210 PPM
Water & Sed.	0.5%	Sodium	26 PPM

Also, tables A.1 and A.2 show the chemical analyses of the two #6 fuel oils tested, on an as received basis. To insure good oil flow for the high viscosity oil, the atomizer nozzle was heated with electrical heating elements.

Reproducibility of this aerosol generator was good and several independent size distribution and aerosol mass loading tests were performed in the course of the experiments. Nominalmy, the compressed air was supplied at 40 psi and .4 cfm. Liquid was gravity fed, with the feed liquid reservoir level held at 6" above the atomizer.

The fly ash aerosol was generated by redispersal.

The fly used was obtained from a disposal pile at a Connecticut power plant. Its source coal was undetermined, since the plant has not burned coal in several years. Fly ash was received wet, broken into small pieces, dried in ambient air, then passed through a 140 mesh screen to remove very coarse fractions. A fine, freely flowing high dusting powder resulted. Dispersal of the fly ash was achieved using the "turntable" dust feeder shown schematically in fig. A.9.

In it a uniform stripe of fly ash is placed on the edge of a slowly rotating (1 rpm) flat disc by a vibratory feeder. The disc carries the fly ash to the intake of an air aspirator. The fly ash is then sucked up into the aspirator throat region where sonic velocities are maintained to break up any agglomerates of fly ash particles. The dispersed fly ash is then ejected from the aspirator into the fluidizing gas stream. With such a system, very uniform and reproducible fly ash injection rates were obtained, and the fly ash feed could be turned on or off instantaneously by starting or stopping the disc rotation. The fly ash size distribution as measured by an Andersen 2000 cascade impactor is shown in fig. A.10.

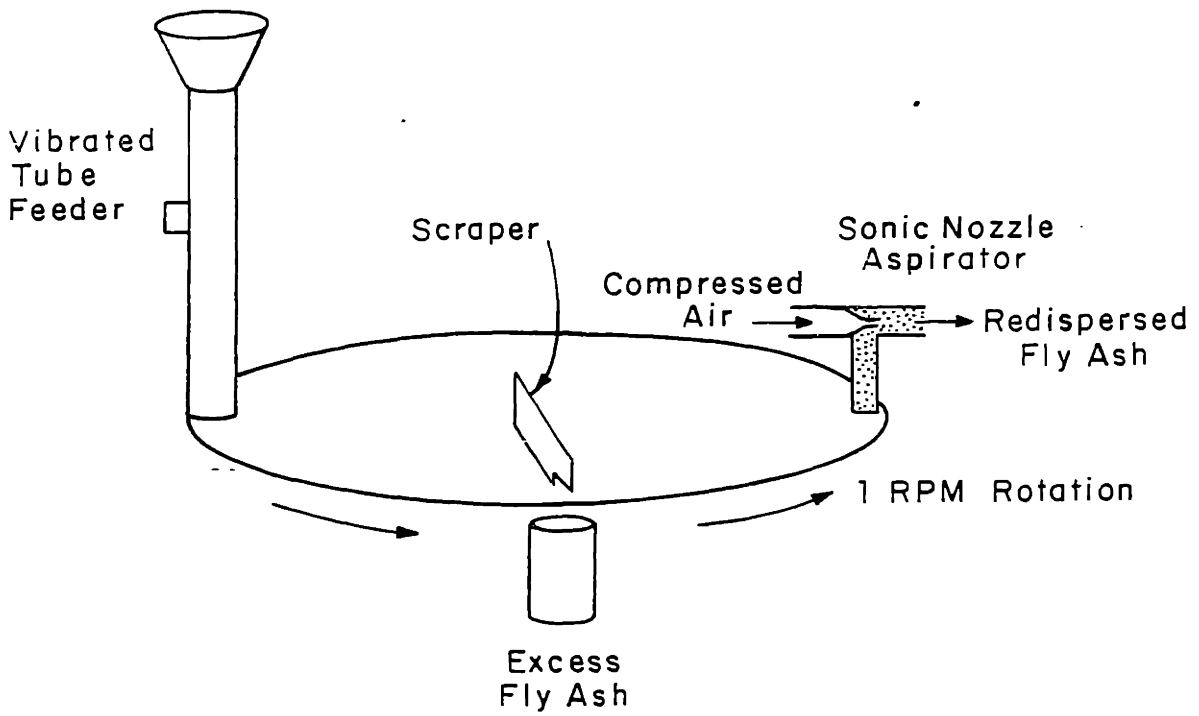

Figure A.9 Schematic of turntable fly ash redispersal apparatus.

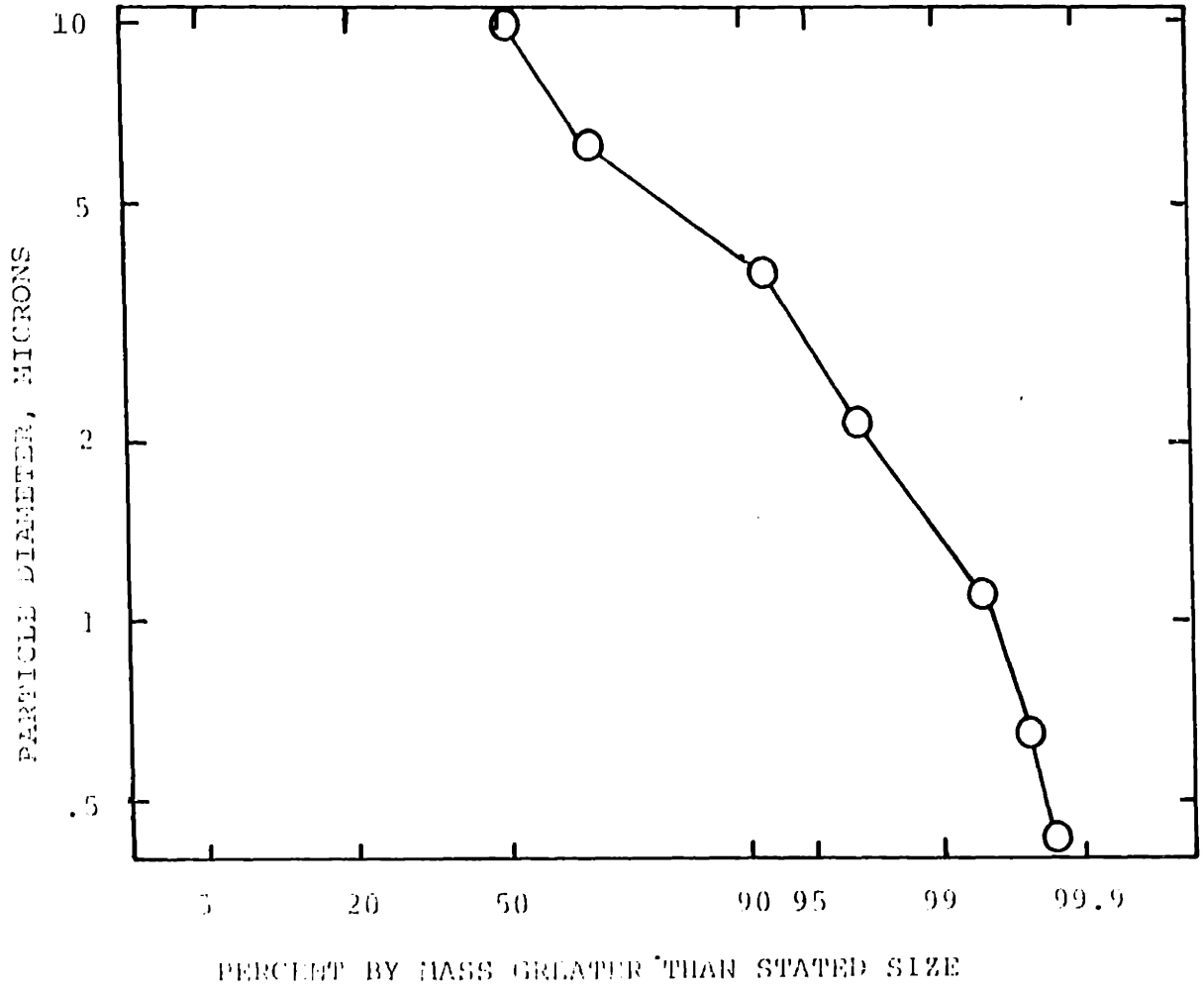

Figure A.10 Experimentally measured fly ash size distribution

Diagnostic Equipment

Three types of aerosol diagnostic equipment were used. The first, depicted in the schematics of figs. A.1 and A.3 was direct filtration. Gas samples were drawn from the test channels by isokinetically sized sampling tubes and passed through filter media. The 47 mm glass fiber Schleider and Schnell #25/47 filter media discs were held in sample holders in series with the tube, a gas flow measuring rotameter, value, and vacuum pump. Flow rates were set to isokinetic values, usually around 1 lpm with a 1/4" I.D. sampling probe. Change in mass on the filter substrates as measured by a Mettler micro balance for know has sample volumes permitted calculation of gas particulate mass concentrations. Sampling trains were placed both at the inlet and the outlet of the EFB for collection efficiency determinations. Size disbributions were obtained using the Andersen 2000 cascade impactor, also used with an isokinetic sampling probe. In the impactor, progressively smaller sizes of particulate are impacted on fiberglass media substrates in succeeding impactor stages. Weighing of the sutstrates allows determination of the size distribution. The impactor is designed for 1 cfm nominal flow sampling rates, which was controlled by a value and measured with a rotameter in series with the impactor. The impactor was only used to measure the outlet aerosol but fractional efficiencies were determined from the outlet cascade impactor data in the following way. First, the fly ash was sampled with no bed in place, with the inlet total mass loading m_{in} and the size distribution being determined. The impactor really only tells us the mass loading of fly ash particles of certain ranges of particulate size, each size range corresponding to a given impactor stage. For now let us term the mass loading of aerosol in the size range corresponding to the nth stage of the impactor as being m_n.

Now, with the bed in place and the expiment in progress, we measure the new inlet loading m_{in} and the new nth stage size range outlet loading m_n. We can assume that the inlet loading for this nth stage size range is

$$\frac{m_{in}'}{m_{in}} m_n \qquad \text{A.1}$$

because it should be proportional to that measured as a calibration. Thus, the co-lection efficiency of the nth stage size range fly ash n_{bn} is

$$n_{bn} = 1 - \frac{m_n'}{m_n} \frac{m_{in}}{m_{in}'} \qquad \text{A.2}$$

The calibration run is essential for the determination of n_{bn}' and was performed for all runs.

Manufacturer's calibrations of the impactor have been found to be incorrect by Rao[1]. New calibrations experimentally found by Rao were used in this study. Comparison of these with the manufactuer's calibrations are shown in Table. A.3.

The TSI inc mass monitor was used to measure aerosol concentrations for the monodisperse DOP tests, the real time Fly Ash breakthrough tests, and the agglomerator submicron efficiency tests.

The mass monitor is a device where particulate in a sample has stream is electrostatically desposited onto a quartz piezoelectric crystal. The crystal is driven electrically to its resonant frequency, and this frequency is in turn monitored electronically. As particulate is deposited onto the crystal, its resonant frequency shifts. From small particulate mass loadings on the crystal, the frequency shift is proportional to the deposited mass. By comparing this frequency to that of a reference crystal, these frequency shifts are then a direct measure of aerosol mass concentration:

$$C(\mu g/m^3) = \text{constant} \times \frac{\Delta f}{\Delta t} \qquad \text{A.3}$$

Table A.3

Stage Calibration For Anderson Impactor
1.0 cfm, 50% cut-off size

Stage #	Mftr. Calibration	Rao Calibration
0	11	-
1	7.0	11.0
2	4.7	6.1
3	3.2	4.0
4	2.6	2.35
5	1.1	1.11
6	0.65	0.69
7	0.43	-

where Δf is the change in crystal frequency in time Δt. The constant is dependent upon several parameters such as the crystal properties and gas flow rate through the mass monitor. The manufacturer (Thermo-Systems, Inc.) gives 333 as the constant for a 1 lpm sample flow rate. A somewhat higher value, 400, has been found when the mass monitor readings are checked against those of highly efficient filters.

For the monodisperse DOP tests, isokinetic gas samples were simply passed through a radioactive source charge neutralizer before going to the mass monitor. Direct aerosol concentrations were obtained for the real time fly-ash breakthrough experiments. An isokinetic probe mounted in the channel above the bed drew the gas sample which then was passed through the dilution system shown in fig. A. 11. With this system dilutions of 10:1 were obtainable and controllable. The diluted gas was then passed on to the mass monitor with compatible aerosol concentrations.

The electrical output of the mass monitor is a 1-volt square wave whose frequency is the difference of frequencies between the reference and measuring crystal. For typical operation with well-matched crystals, this square wave varied in frequency from 300 to about 5000 Hz. The linear region of operation (Δf with Δm) was a frequency band of 3000 Hz, starting from the clean crystal value. A signal processor was built that converted this digital signal to an analog signal. The analog voltage was proportional to the frequency of the square wave. The circuit schematic of this D/A converter is presented in fig. A. 12. This signal was then applied to a strip chart recorder whose output was then a continuous measure of outlet fly ash mass loading vs. time.

The response time of the mass monitor is related to the crystal resonant frequency which is in the MHz range. That of the D/A converter is related to the crystal difference frequency whose smallest value is 300 Hz. The longest response time is the gas residence time in the sampling tubes, which was minimized to be about 0.1 sec.

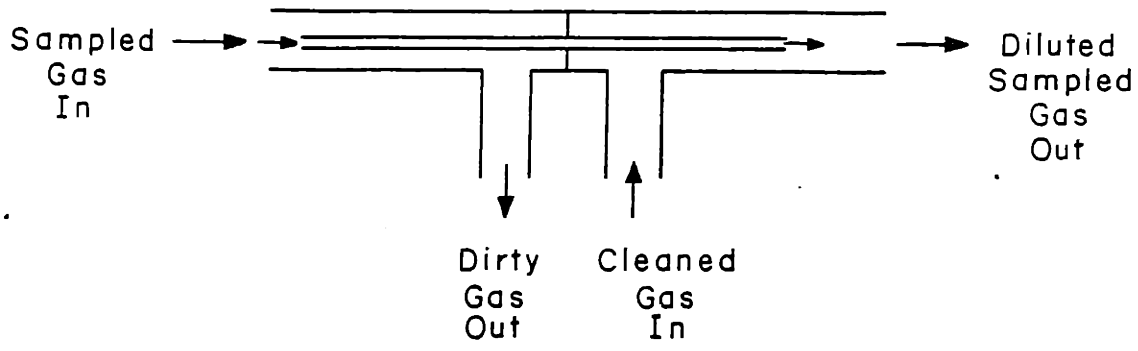

Figure A.11 Schematic of isokinetic dilution apparatus.

The entire sampling system is depicted schematically in fig. A.13.

For the agglomerator submicron removal efficiency tests, the diagnostic sampling train was the one shown in fig. A.14. With this sampling set up, supermicron fly ash particles were removed from the gas stream before measurements were made with the mass monitor. The sampled gas was first passed through a cyclone separator which had a cut diameter of 3μm. Then the gas passed through the 0-5 stages of the Andersen 2000 cascade impactor, which removed all remaining particles greater than 1.1μm diameter. Finally, after passage through a radioactive source charge neutralizer, the submicron fly ash mass loading was measured with the mass monitor.

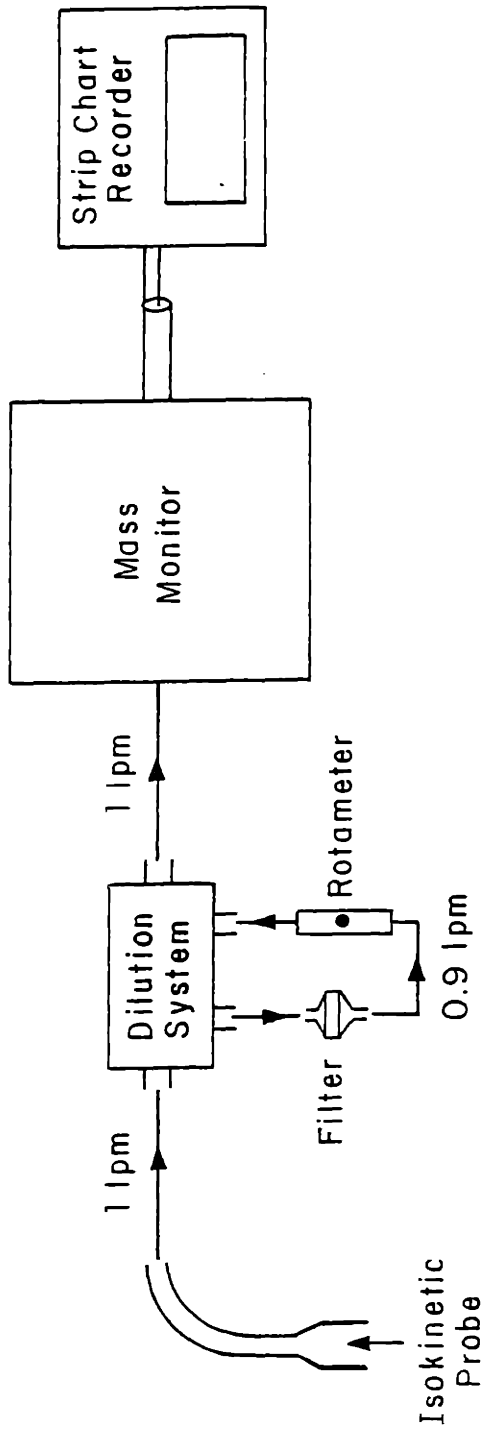

Figure A.13 Schematic of fly ash sampling system for real time determination of fly ash mass in outlet gas.

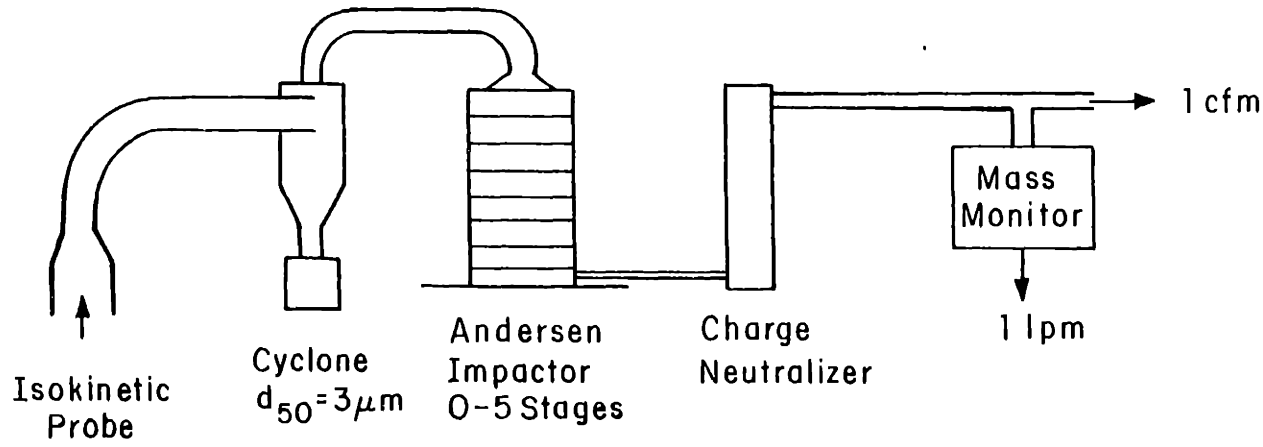

Figure A.14 Schematic of fly ash sampling train for determination of submicron removal efficiencies.

Appendix B - Fly Ash Collection in Electropacked Beds

The experimental apparatus for hot flow studies, as described in Appendix A lent itself to the convenient study of electropacked beds (EPB). The experiments run are only preliminary and are meant to indicate the potential for future studies. No attempt is made to correlate any of the collection or adhesion models of the thesis, but they certainly may be used to discuss the results.

In the tests, packed beds of N.J. #2 sand were used to collect redispersed fly ash. Bed depths, flow veolcities, operating temperatures, and applied electric fields were varied. Collection efficiencies were measured using the direct filter sampling trains of fig. A.1.Initially the beds were clean of fly ash and proper test conditions were established and measured. Simultaneously, the fly ash redispersal system and sampling system were turned on. After an appropriate length of time the sampling system was turned off and filter papers removed. Clean papers were reloaded and sampling was resumed. In such a way measurements of collection efficiency vs. time were recorded. During the test, pressure drop across the bed was held constant.

The raw data are shown in fig. B.1 in which overall bed collection efficiency is plotted vs. run time. The width of each data "bar" indicates the filter sample run time, while the height of each bar indicates the measurement error of the filter papers.

The parameters of each bed tested are shown in the data plots. Careful examination of the data leads to several important conclusions.

1) Air flow velocity is important to operational longevity of the bed. Degradation of performance is chiefly due to fly ash "blow through" whereby once collected fly ash is reentrained into the air flow. At "low" air velocities as in fig. B. 1b

collection efficiency actually increases with time. This results in eventual plugging of the bed and reduction of air flow. At "medium" and "high" velocities, collection efficiency degraded with time.

2) Applied field is important for both initial collection and operational longevity. Initially the field is responsible for collection of the submicron component of the fly ash. This observation is noted in all the tests. The field is also effective for retention of efficiency, although as the air velocity is increased the field effect is all but eliminated. In this case blow through dominates. The electric field probably affects the fly ash adhesion via the stringing forces discussed in Chapter IV.

3) Temperature, and equivalently fly ash resistivity had little effect in these tests. It is expected, however, that this will be important to the "stringing" forces and warrants further study.

An important conclusion is that by proper choice of conditions, namely low air velocity to prevent blow through and high electric fields to enhance fly ash adhesion and collect submicron particulate, electropacked beds can achieve ultra high collection efficiencies of 99+%. However, under these conditions, plugging of the bed especially at the inlet, occurs and means to prevent this must be realized. This could be accomplished by periodic replacement of the beds.

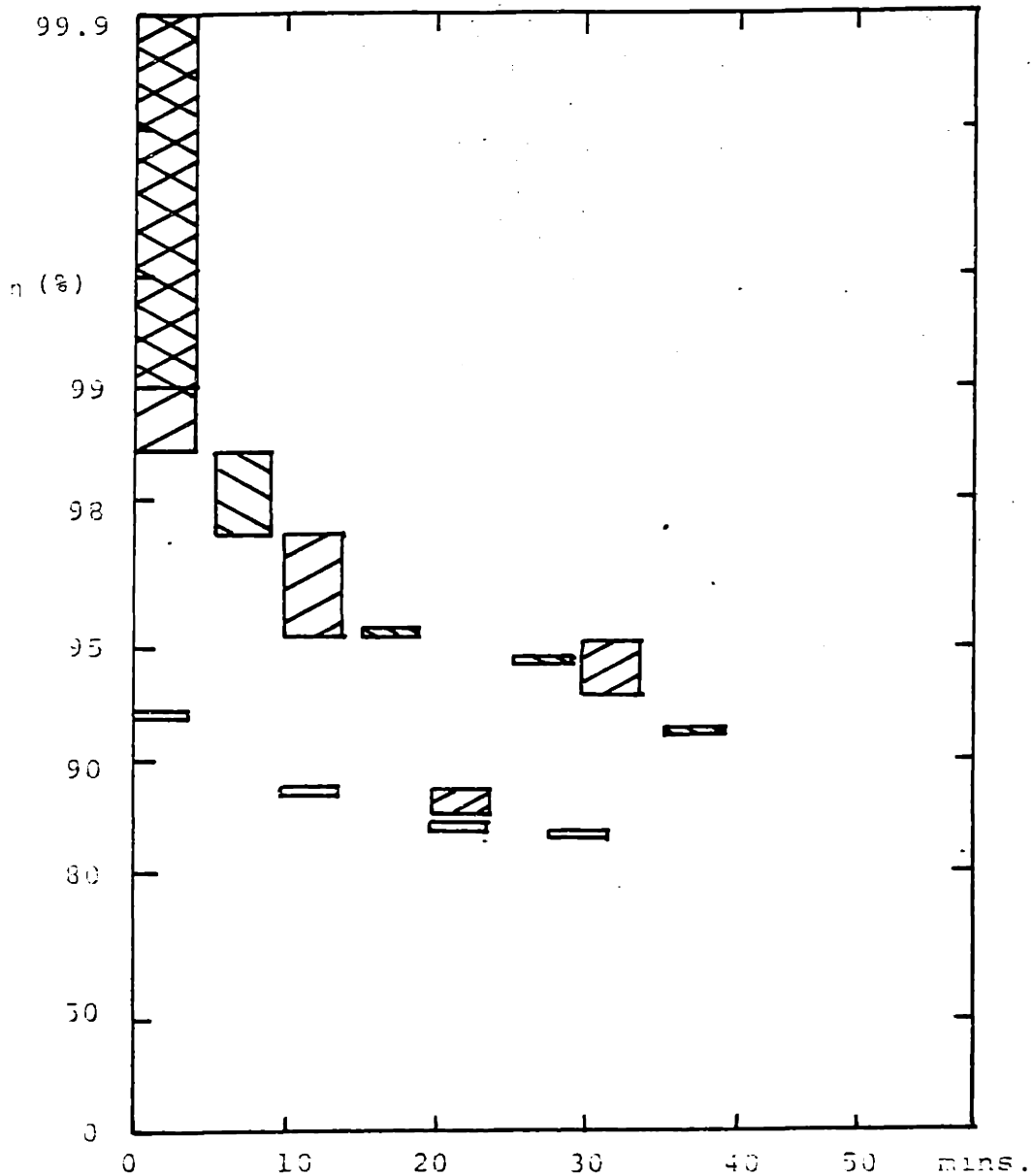

Figure B.1a Electropacked Bed fly ash collection efficiency vs. time -- Medium Velocity

U = .56 m/sec, $l_0 = 1^5/_8$", R =.5 mm
T = 270°F, fly ash resistivity = 2 x10" Ω-m
E = 3.6 x 10^5 V/m
E = 1.8 x 10^5 V/m
E = 0

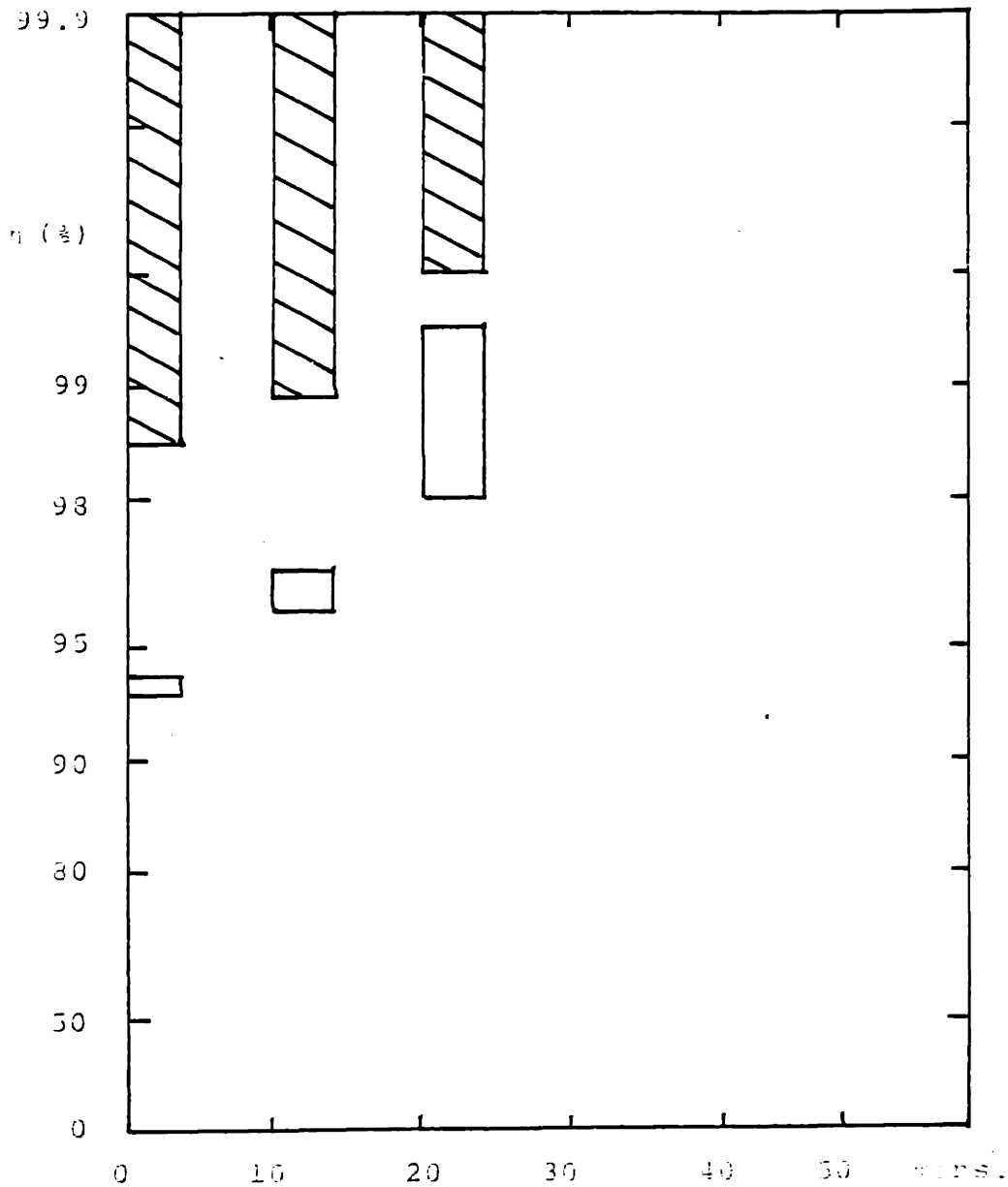

Figure B.1b Electropacked Bed fly ash collection efficiency vs. time -- Low Velocity

U = .28 m/sec, l_0 = $1^{5/8}$", R = .5 mm
T = 270°F, fly ash resistivity = 2 x 10" Ω-m
▨ E = 3.6 x 10^5 V/m
□ E = 0

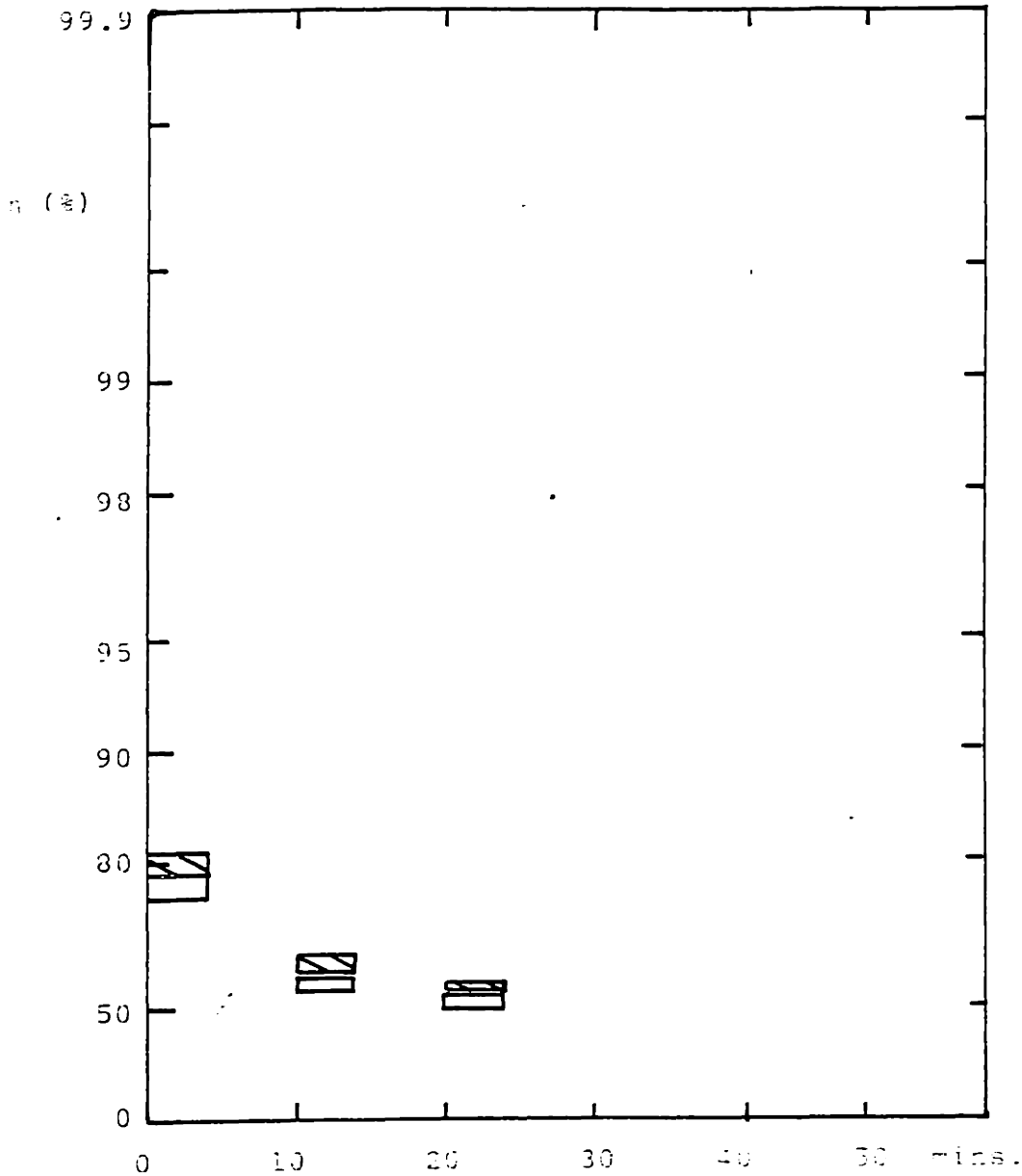

Figure B.1c Electropacked Bed fly ash collection efficiency vs. time -- High Velocity

U = .75 m/sec, $l_0 = 1^{5/8}$", R = .5 mm
T = 270°F, fly ash resisitivity = 2 x 10^{11} Ω-m
E = 3.6 x 10^5 V/m
E = 0

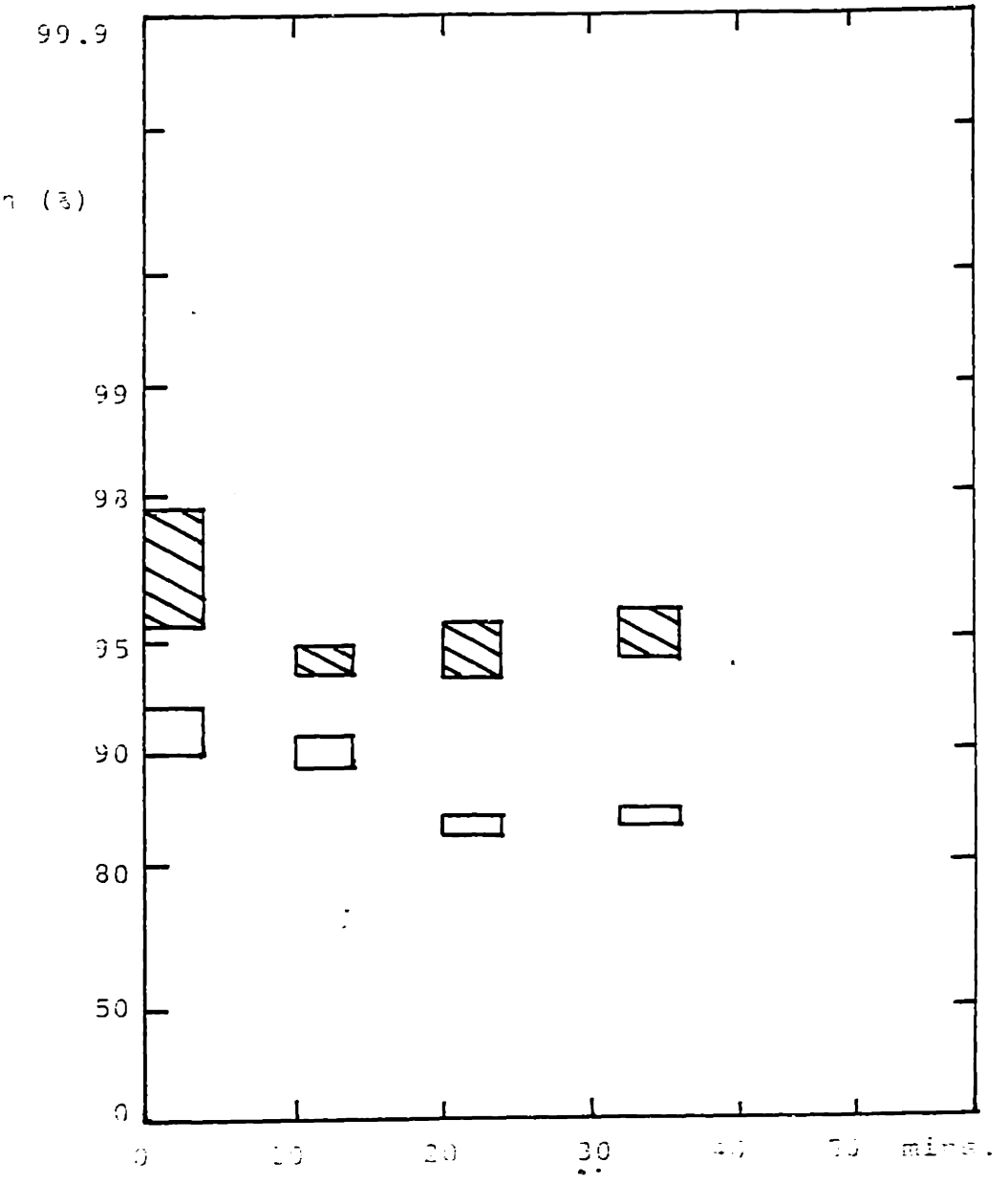

Figure B.1d Electrpacked Bed fly ash collection efficiency vs. time -- Low Temperature

U = .56 m/sec, $l_0 = 1\frac{5}{8}$", R = .5 mm
T = 70°F, fly ash resistivity = 2×10^8 Ω-m
▨ E = 3.6×10^5 V/m
□ E = 0

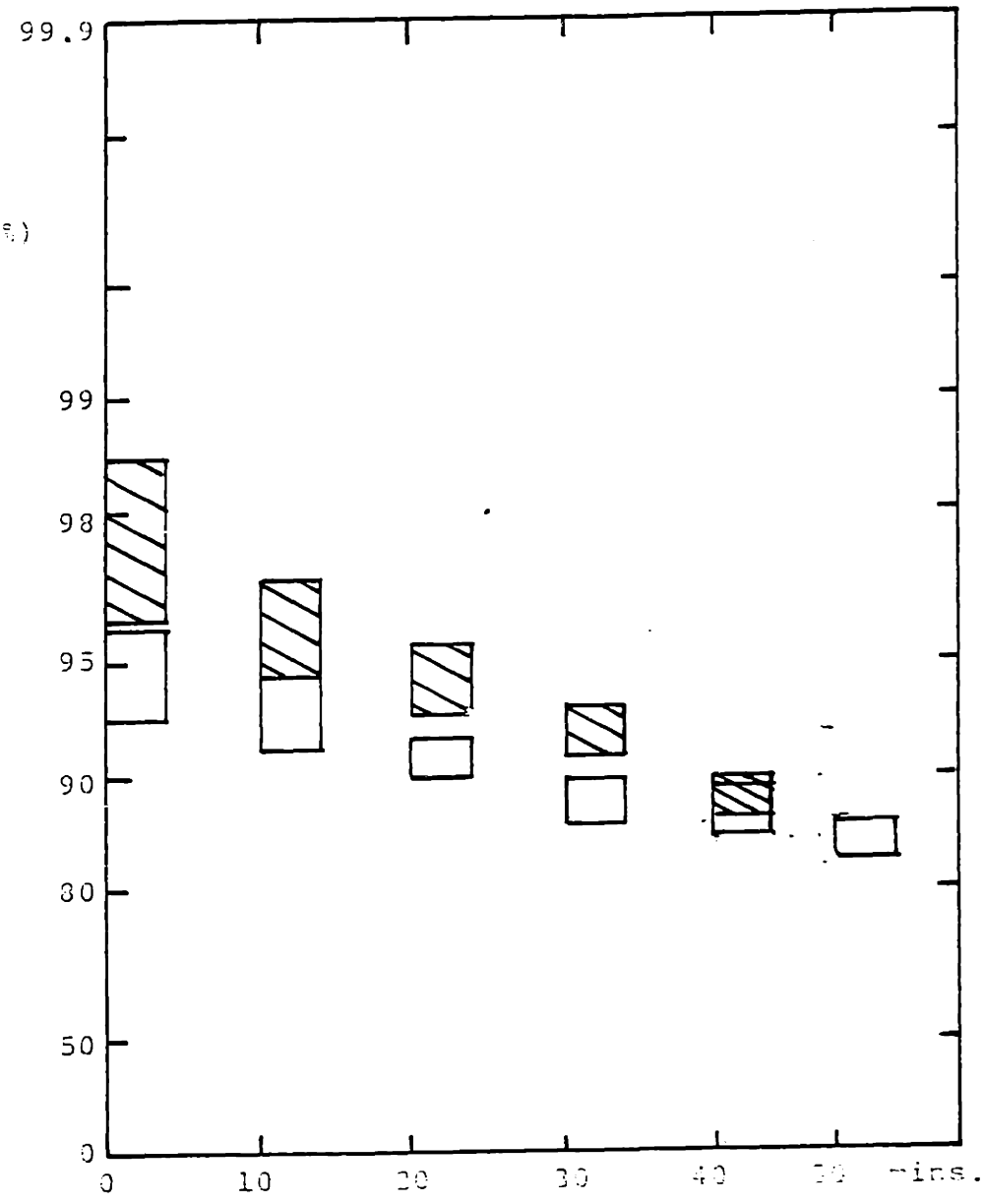

Figure B.1e Electropacked Bed fly ash collection efficiency vs. time -- Deep Bed

U = .75 m/sec, $l_0 = 3\,1/4$", R = .5 mm
T = 70°F, fly ash resistivity = 2 x 10" Ω-m
▨ E = 3.6 x 10^5 V/m
□ E = 0

APPENDIX C

FLUIDIZED BED PARTICULATE COLLECTORS

Abstract of the Disclosure

A fluidized bed, particulate collector system wherein, in one embodiment, the bed particles have applied thereto at the surface thereof, an additive that serves to adhere particulate, once collected, to the bed particles. The bed particles and/or additive may be combustible or may be incombustible. In one embodiment, the system includes two fluidized beds, in tandem, the first of which collects particulate mostly in the supermicron sizes and the second of which is an electrofluidized bed that collects particulate mostly in the submicron sizes.

The present invention relates to fluidized bed collectors that may be employed, by way of illustration, to remove fly ash, smoke and/or dust and the like from combustion gases.

By way of background, attention is called to applications for Letters Patent S.N. 516, 056 (Melcher et al), filed October 18, 1974 and S.N. 516,057 (Melcher et al), filed October 18, 1974, as well as to the prior art referred to in the two applications.

No detailed discussion is necessary at this time, the Winter of 1976-1977, to emphasize the importance of providing systems suited to remove particulate from a gas -- particularly in view of the emphasis being placed on coal as an increasingly important fuel. The more conventional electrostatic precipitators (ESP) that have served so well for so long are proving uneconomical in removing submicron and other particulate. The electrofluidized bed (EFB) in said S.N. 516,057, is particularly suited to removal of the submicron fly ash, smoke, and/or dust from gases, whether the effluent be from oil or coal, but in the EFB system there can arise the problem of disposing of the bed particles plus the collected particulate. A very important object of the present invention addresses that problem by providing as bed particles for the EFB, combustible particles, which, together with collected particulate, are burned in a combustor and collected as solid ash in the combustor.

It has been found by the present inventors that pulverized coal can be employed as particles of a fluidized bed and that retention of particulate, once collected upon the bed particles of the fluidized bed, is greatly enhanced by a liquid film upon the surface of the particles. Accordingly, another object of the invention is to provide a surface film as a liquid additive to the bed particles of a fluidized bed collector whether electrofluidized or simply fluidized.

The EFB of said S.N. 516,057 does a remarkable job in removing particulate, supermicron as well as submicron in size, from the gaseous effluent, but there is a tendency for the electric field mechanism used to charge particulate prior to entry into the bed region, to be fouled by the large particulate. It is still another object, therefore, to provide a fluidized bed collector

system wherein the supermicron sizes of particulate are removed from a gaseous effluent prior to entry into a charging region.

These and still further objects are addressed hereinafter.

The foregoing objects are achieved in a fluidized bed collection system that includes at least one bed of particles through which a gaseous medium is passed with a vertical component of flow to effect fluidization of the particles. The particles may be, and in an important aspect of the invention are, combustible; and in a very important aspect there is applied to the surface of the particles an additive to enhance adherence of the particulate, once collected, to the particles. The particles of the bed may be placed in an electric field, to provide an EFB, and the particulate is charged prior to entry into the bed region. In such case, it has been found to be advantageous to place a fluidized bed upstream of the EFB to collect supermicron sizes of particulate prior to entry into the region wherein the particulate is charged.

The invention is hereinafter described with reference to the accompanying drawing in which:

Fig. 1 is a representation, in block diagram form, of a system that includes a fluidized bed particulate collector of the present invention;

Fig. 2 is a diagrammatic representation showing two fluidized beds within a vertically oriented, cylindrical housing, the housing being cutaway to show the inner active elements which are shown in schematic form;

Fig. 3 is a representation in block diagram form showing a feedback scheme;

Fig. 4 is a theoretical plot of relative dust mass loading to the fluidized bed particulate collector of Fig. 3 as a function of the bed collection efficiency and combustor retention efficiency;

Fig. 5 is a theoretical plot of the overall system collection efficiency of the system shown in Fig. 3 as a function of the bed collection efficiency and combustor retention efficiency;

Fig. 6 is a photograph showing two particles of fly ash, a third particle of fly ash which has been crushed, and a particle of coal, all of the particles being enlarged in the photograph; and

Fig. 7 is an experimental plot of typical EFB collection efficiency as a function of particulate diameter and applied electric field.

It should be apparent that the present disclosure is multi- aspects of the particulate collectors herein disclosed apply to e (EFB) collectors, but some aspects are not so limited. In the de description hereinafter the various ramifications are taken up ir but first there follows a general discussion to place the collect invention in proper context; the general discussion applies mostl burning systems wherein a fluidized bed collection system serves fly ash from stack gases.

Many types of coal-fired combustors exist or are proposed an able that the optimal design of an effective EFB particulate cont depend on the type of combustor with which it is to be used. For furnaces, two of the most important boiler /distinctions are those of dry bottom vs. wet bottom units retention of the furnace. Wet bottom units are operated such that wall temperatures are above the melting point of the ash; thus, as on the walls is molten and runs to the bottom as a liquid (calle Dry bottom units are just the opposite; the ash remains solid, eve bottom of the furnace, whence it is removed. In general, wet botto have higher ash retention than dry bottom units, ash retention be retentio fraction of total ash retained in the furnace. Highest ash/(up t is exhibited in so-called cyclone furnaces, while for dry bottom ash retention is as low as 10-20%. Of potential future use are f coal combustors; such combustors have shown ash retentions compar- cyclone furnaces.

The unique problems for control of fly ash from coal combust from the variability of coal compositions and the high ash content to oil) of the coal. Typical gas loadings of fly ash range from 5 and for typical 1000 mw power plants many tons of ash are produced To make matters worse, a significant portion of this fly ash is in micron range, rendering it very difficult to collect in convention systems. Expensive electrostatic precipitators (ESP) have been use varying degrees of success in the collection of coal fly ash. The economical, though, in collecting the highly resistive fly ash whi from the combustion of low sulfur coal.

It is expected that an EFB control system would not be hindered by the same ash resistivity problems typical of an ESP. However, the state of the prior art in EFB technology leaves open several vital operational questions in the collection of fly ash. An efficient charging system for dusts of such high loading, prior to the present teaching, has not been demonstrated. Such a system must charge all the dust particles, and be able to operate indefinitely in time. The retention (or adhesion) of the dry particulate, once collected, must be assured, and the removal of the high quantities of collected ash must be done efficiently (and in a steady state mode of operation). The collection system herein disclosed offers solutions to these problems.

Turning now to Fig. 1, the overall system labeled 101 includes a combustor 105 to burn a fuel such as, for example, a solid fuel such as coal from a solid fuel supply 103. The coal, in the system 101, is reduced to particles by a pulverizer 104 and conveyed to the combustor 105. A small amount of the coal particles is blown or otherwise delivered to a bed in a fluidized bed collector 102 to provide bed particles, as later discussed. Smoke from the combustor 105 is drawn by natural draft and/or fluidizing means 107 (which may be a fan or blower or the like) through the collector 102 wherein particulate is removed from the smoke by particles in the fluidized bed, and cleansed air is delivered to a stack 108. In a preferred embodiment of the present system, fuel oil or some other additive is continuously deposited as a liquid film, in situ, upon the bed particles; the film, as later discussed, serves to adhere the particulate to the bed particles. In a preferred system, the combustible particles, with combustible liquid thereon and including particulate collected upon the combustible bed particles, are fed back directly to the combustor/or, indirectly, through the pulverizer 104. In an operating system, the fluidized bed collector 102 can be incorporated in the stack or, preferably, it can be located as a separate unit ahead of the stack in the way shown in Fig. 1.

105

Previous mention is made of a problem in electrofluidized beds, in that the mechanism that charges particulate in the smoke or dust laden gas is rendered inoperative by supermicron size particulate after some period of operation. The fluidized bed collector shown at 102A in Fig. 2 is adapted to address the contamination problem.

The collector 102A consists of a first fluidized bed 1 that serves to collect dust or other particulate 19, mostly in the supermicron size range, from a dust laden gas that is delivered at the lower end marked 10 of a vertically oriented cylindrical housing 9 that contains the first bed 1 and a second fluidized bed 2, the latter being an electrofluidized bed of the type designated coflow in said application S.N. 516,057 and described in great detail therein. While the bed 2 can remove supermicron size particulate from the gas, it is particularly well adapted to remove submicron particulate, a fact which is gone into in depth in the earlier application.

In the two-bed or two-stage collector system,beds 1 and 2 are disposed in tandem or series such that incoming gas containing entrained particulate moves as a fluid stream (having a vertical component in the region occupied by the two beds) through the first bed 1 and then through the second bed 2 to effect fluidization of the particles shown at 3 of the first particle bed and the second particle bed. The hot gas effluent from the combustor, then, not only delivers the gas (containing entrained particulate) to the collector 102A, it also effects fluidization of the bed particles 3 to create a fluidized bed. As previously noted, the bed 1 removes a high percentage of the supermicron particulate in the fluid stream and the removal process is mostly mechanical.

Charging means comprising a corona charging grid 4, disposed between the first particle bed 1 and the second particle bed 2, and a source of high voltage 5, acts to electrify that particulate remaining in the gas after passage through the first particle bed (typically at least 95% of the particulate is removed by the first bed 1 and almost all the supermicron size). Means for imposing an electric field comprising grids 6A-6D and a source of high voltage 7 act to polarize the particles 3 of the second particle bed 2 to create an electrofluidized bed (EFB) collector. The lowermost grid

6D performs a distributor plate function, that is, it supports the bed particles within the region of the bed (interacting, in this connection, with the walls of the housing 9), and the apertured plate marked 8 performs the same function for the bed 1 (see said application S.N. 516,056 for details on distributor plates). The particles 3 of both beds 1 and 2 now being discussed are coal particles; this aspect of the invention is described in greater detail in the next few paragraphs.

Fresh bed particles, which in the system discussed at this juncture are coal particles, are introduced through a chute 11 to the second bed 2 (or second stage of the two-stage system shown). The particles that form a fluidized bed are levitated by the fluidizing gas and move about with motions that are analogous to those of a boiling liquid.

Typically, the coal particles are sifted to introduce particle sizes of about 2 mm or less to the bed 2, the particles 3 being large enough so as not to elutriate from the bed and small enough to permit levitation thereof without excessive vertical gas movement; as is shown in the earlier application, S.N. 516,057, the higher the velocity of the levitating gas, the greater the tendency of collected particulate to be dislodged from the collecting particles or not to be collected at all. (Levitation is related also to particle density.) The heaviest particles gradually migrate to the bottom of the bed 2 whence they are conveyed by a duct 12, through a variable-opening valve 13 and a further duct 14 to the bed 1. Eventually, the largest particles (i.e., the bed particles with aggregated particulate attached thereto) are removed through a duct 15 and transported, say, to the combustor 105 or to some other combustor. Rappers 16 and 17 dislodge particles that may become attached to the distributor plates 6D and 8, respectively.

To assure adhesion of the dry fly ash, a mist of oil droplets 18A is introduced into the gas stream by an oil atomizer 18. Only very small amounts of oil are necessary (on the order of 1% of the ash collected by weight), but its presence is vital to the operation. The oil is collected on the bed particles 3 of both beds and acts as a binding agent for the ash.

An important feature of the system, as above discussed, is the use of coal particles as the bed seed materials. Typically mm sized particles will be used and will be obtained from crushing and sifting the coal to be combusted. The electrical conductivity of coal varies, But, for most U.S. coals, the conductivity is well within the ranges of practical EFB operation. Fresh coal particles, as above indicated, are fed in at the top of the second stage EFB. They are removed from the bottom and then introduced to the top of the first stage. Finally, when the particles are coated with enough ash that the agglomerates are too large to remain fluidized, they are removed from the bottom of the first stage. This size classification is performed naturally in a fluidized bed, with larger particles settling to the bottom, but may be aided by making the bed cross sectional area smaller at the bottom of the bed. Such size classification has been performed successfully by other workers.

The coal seeded ash agglomerates thus formed are then introduced into the combustion zone where the coal seed and the oil adhesive are combusted, and for the most part, the ash is dropped to the bottom of the combustor. As a result, no net expense is incurred by the use of the coal seed particles and the oil additive, as their heating values are utilized in the combustor. Also, any unburnt combustibles in the ash have another chance to be combusted; thus, the thermal efficiency of the boiler may improve.

Naturally occurring coal tars may be utilized as the adhesive agent. For that matter, any liquid may be injected for adhesive purposes. Water might be an alternative for the first stage collector 1, but would tend to short out the EFB collector 2.

The EFB stage may be in either the co-flow (as shown in Fig. 2) or the cross flow configuration discussed in said application S.N. 516,057. Also, alternating (ac) or direct (dc) fields may be used in the bed 2 and/or charging sections. Further, electromechanical effects (produced by electric field forces on the bed particles) may be utilized to influence collection dynamics (via bubble breakup) or solids mixing for particle flow control in either (or both) stage(s) of the system.

The conductivities of bed components or particles 3 are fundamental issues to effective EFB operation. The conductivity of coal depends on the presence of low molecular weight compounds which act as insulators between carbon units of low resistivity. Upon thermal decomposition these low-molecular weight components are volatilized, allowing the solid residue to become semiconducting. Typical bituminous coals have resistivities around $10^{12}\Omega$-m (as measured for a powdered coal) at 25°C.

Ash resistivity has been studied in some depth as a result of its importance to ESP operation. The expected resistivities of both coal and ash are high enough that electric current dissipation in the EFB is negligible. The exact values of resistivity are important, however, when electromechanical effects need to be considered.

The use of modest to high electric fields in fluidized beds of semi-insulating particles can radically alter the mechanical nature of the bed. In cross flow beds, as the applied field is increased, strings of particles form across the bed. These strings can cut right through bubbles and destroy their structure. Since mixing the bed particles depends upon particle transport via the wake region of the bubble, the axial mixing of the bed particles can be all but stopped. Beds, once fluidized, can even be "frozen" in their expanded states. Very often, though, channel formation accompanies these mechanical effects resulting in poor collection performance.

The collection of particulate 10 in a fluidized bed can be analyzed by first determining collection on a single bed particle. The separate mechanisms of diffusion, interception, impaction and electrostatic attraction are considered to act in a flow modeled to account for the effect of surrounding particles. When these efficiencies are used in a plug flow model of the bed, overall bed collection efficiencies can be determined. Experimental results of particulate collection efficiencies for a typical EFB collector are shown in Fig. 7. It should be noted that with no electric field applied, the beds act as an efficient collector only for supermicron particulate. With field applied, all particle sizes can be collected with high efficiencies.

Adhesion of the collected particulate to the bed particle is assured here.

Naturally occurring adhesion forces, such as electrostatic attraction and Van der Walls forces, are often not sufficient to hold the collected ash to the bed particle under strain of dislodging forces resulting from particle collisions in the bed. It has been shown by the present inventors that small amounts of liquid aerosol (which is collected in the bed) act as an adhesive agent. The liquid, once collected, is drawn to the contact points of the collected ash, thus forming bridges at these points. The removal of ash particulate necessitates the elongation of these bridges, an action opposed by the viscosity of the liquid. Capillary forces tend to pull the ash particulate back towards the contact point, thus retaining the particulate. The amount of liquid (usually an oil) additive necessary for assured adhesion depends on the ash particulate size, the intensity of collisions in the bed, and the viscosity of the liquid. It has been found experimentally that oil in quantities as little as 1% of the mass of the ash collected can assure adhesion in typical beds. This number is roughly supported theoretically. It is important that the injected oil be deposited between the two stages in quantities proportional to the respective quantities of ash collected. To such an end, the size spectrum of the injected oil (i.e., the droplets 18A in Fig. 2) can be chosen correctly, with supermicron droplets collected in the first stage and submicron in the second stage. It is simplest just to match the size distribution of the injected oil to that of the ash.

The build-up of coal ash agglomerates is the most important issue disclosed here. With 1% oil additive, agglomerates about twice the original coal particle diameter have been built up, as shown in Fig. 6. The only limitation to appear has been the defluidization of the bed due to the increase in particle size. Such a criterion can be used to judge the particle residence time in the system for a single particle. As a benchmark, one can find the time it takes for a bed to collect its own weight in ash. Given a bed with an overall depth of ten cm (sum of the two beds) with the bed mass density of 10^6 $gm/_{m^3}$, a fluidizing flow velocity of 1 m/sec. and a

typical ash loading of $10gm/m^3$, this time is on the order of two to three hours. Thus each coal particle can be expected to reside in the system for a couple of hours before it would grow to twice its original mass.

When a typical bituminous coal particle is heated for combustion, 30-40% of its initial weight is driven off by thermal decomposition or de-volatilization. At a temperature above 660°C and in the presence of an oxidizing atmosphere these volatiles burn at a fast rate compared to their evolution. For mm sized coal particles this complete evolution and combustion time is on the order of a fraction of a second. It has been observed that if the coal particle is coated with fly ash, the evolution of volatiles causes the agglomerate to explode, thus freeing the coal particle. The combustion of the remaining char (fixed carbon) is a much slower process. For large char particles (greater than 50 μm) the diffusion of oxygen to the char particle surface is the controlling rate process. The reaction rates depend on the temperature and oxygen content of the gas, but roughly speaking the burn-out of a mm sized char particle is characterized by a time of 1-10 sec. (with excess air of about 20%). Such large particles may burn too slowly for complete combustion in the furnace; so the re-injected coal-ash agglomerate may first have to be pulverized or may have to be burnt in a special separate combustor. (However, coal particles for fluidized bed combustion are just the size of those proposed for the EFB system herein and then complete burnout is likely without further pulverization.) In Fig. 6 there are shown particles $3A_1$, $3A_2$ and $3A_3$ which are agglomerates, that is, bed particles 3 with fly ash adhered thereto; the particle $3A_3$ has been crushed. The particle labeled $3A_4$ is, in fact, a coal particle which serves as seed for the fluidized bed.

The overall system performance for a system with ash-coal agglomerate recirculation can be analyzed from a knowledge of the ash retention (η_f) in the combustor and the collection efficiency (η_b) of the EFB system. It is possible that the recirculated ash is collected in the combustor with a different efficiency than the ash with the primary coal injection. The primary ash retention is termed η_{f1} in Fig. 3 and hereinafter and the secondary ash retention η_{f2}.

Two important parameters are defined in Fig. 3 to analyze the system. of the mass
The ratio/flow rate of ash exiting the combustor to that entering, with

the primary pulverized coal, $\frac{m_f}{m_i}$, is a measure of dust loading in the gas incident to the EFB collector. Values in excess of one are to be avoided as they indicate the necessity of repeated collection of the same ash and the associated expense (mainly for oil additive and material handling). The overall system ash collection efficiency $\eta_{overall}$, is derived from the ratio of ash mass flow rate up the stack to ash mass flow into the combustor with the primary pulverized coal, $\frac{m_s}{m_i}$, by

$$\eta_{overall} = 1 - \frac{m_s}{m_i}$$

The total ash removal efficiency by the entire system is measured by $\eta_{overall}$ If 100% of the ash collected in the EFB is recirculated to the furnace the steady state values of these parameters are determined from system mass conservation statements (see Fig. 3).

$$\frac{m_f}{m_i} = \frac{1 - \eta_{f1}}{1 - \eta_b(1 - \eta_{f2})}$$

$$\frac{m_s}{m_i} = \frac{(1 - \eta_b)(1 - \eta_{f1})}{1 - \eta_b(1 - \eta_{f2})}$$

When the coal ash agglomerates are recirculated directly, it is likely that $\eta_{f2} = 1$ since the recirculated ash will be in large agglomerates which will fuse in the furnace and assuredly drop to the bottom. In such a case:

$$\frac{m_f}{m_i} = (1 - \eta_{f1})$$

$$\eta_{overall} = 1-(1- \eta_b)(1 - \eta_{f1})$$

The performance is then essentially that of two collectors in series. If the coal-ash agglomerate is pulverized before injection, it is likely that the secondary ash retention is equal to the primary ash retention or

$\eta_{f1} = \eta_{f2} = \eta_f$. Figures 4 and 5 show plots of $\frac{m_f}{m_i}$ and $\eta_{overall}$ as functions of η_b with η_f as a parameter. It can be seen that to eliminate excessive dust loadings, the furnace ash retention should be at least 50%. In this range, high overall efficiencies are also achieved.

The fly ash control system above presented herein offers two principal advantages over the ESP. First, is its effectiveness of operation whatever the nature of the ash. For low sulfur Western coals with reduced sulfur oxide emissions, ESPs have failed in collecting the high resistivity fly ash that results. Further, the EFB offers improved ease of handling of the collected particulate. Many ash handling operations are aimed at pelletizing the ash. A major problem of ESPs is the removal of collected ash from the plates, which may be difficult if the ash is sticky, or may lead to re-entrainment upon rapping, neither of which is a problem in the EFB.

Second, the EFB offers potential economic advantages over ESPs and other alternatives such as bag filters. Gas residence times in EFBs are more than an order of magnitude less than for ESPs of equivalent theoretical collection efficiencies. Since residence time is a rough measure of device size and device size is a rough measure of device capital cost, the advantage here is obvious. Since the system proposed here requires no net expense for operating materials (the coal seed particles and the oil additive are eventually combusted, so their cost is not attributable to the EFB collection system), and may even slightly improve thermal efficiencies (by complete burn-out of combustibles from the recirculated ash), these operating expenses appear negligible. The expenses for the greater pressure losses of an EFB and the probably more sophisticated ash handling facilities do not appear to be excessive.

The flexibility of the proposed system, as indicated in the many permutations suggested, indicates that the EFB system may be tailor-fitted to a specific requirement, and the system may have many uses outside the steam boiler ash collection use indicated herein.

Although coal can be used as the seed material in the beds 1 and 2, sand, granulated slag, or other incombustible materials may be used, and the resulting agglomerate may be introduced to the furnace or other combustor 105 or treated separately (e.g., by sintering or melting in the treatment system labeled 109 in Fig. 1), or the particles removed from the bed may be simply disposed of. Alternatively, the agglomerate formed in the bed 1 may be removed, fused, crushed and/or sized in the treatment system 109 and then be returned to the beds 1 and 2 as seed; or some or all of the treated agglomerate may be delivered to refuse or waste.

The above and still further modifications of the invention herein disclosed will occur to persons skilled in the art and all such modifications are deemed to be within the scope of the invention as defined by the appended claims.

What is claimed is:

1. An electrofluidized bed particulate collection system that comprises, in combination: a bed of combustible particles; means to effect fluidization of the bed particles using a hot gas from which said particulate is to be collected as an ash agglomerate upon the particles; means providing an electric field in the region occupied by the bed to effectively polarize the bed particles; electric field means positioned to electrify the particulate prior to introducing the particulate to the bed region; means continuously depositing a combustible insulating liquid film in situ upon the bed particles, said liquid film serving to effect adherence of the particulate to the bed particles; and means to feed back said combustible bed particles with combustible liquid thereon and including particulate collected upon said combustible bed particles to a combustor for combustion thereof, said hot gas including at least in part combustion effuents from said combustion; said combustor having a reasonable retention for that part of the ash introduced to the combustor from the fluidizing bed.

2. An electrofluidized bed particulate collection system as claimed in claim 1 wherein the combustible particles are coal particles.

3. An electrofluidized bed particulate collection system as claimed in claim 2 wherein the combustible liquid is fuel oil.

4. An electrofluidized bed particulate collection system as claimed in claim 3 wherein said means continuously depositing is operable to introduce the fuel oil to the bed as an aerosol comprising fuel oil droplets.

5. An electrofluidized bed particulate collection system as claimed in claim 1 wherein the combustor is a fluidized bed combustor.

6. A particulate collection system that includes an electrofluidized bed as claimed in claim 1 as the second bed of a two-bed or two-stage, tandem system wherein the first bed is a fluidized bed collector that serves to collect particulate mostly in the supermicron range and in which the second bed serves to collect particulate mostly in the submicron range, the electric field means being disposed in the region between the first bed and the second bed to electrify the particulate prior to introducing the particulate to the second bed.

7. A fluidized bed, particulate collection system that comprises a plurality of fluidized beds acting in combination, said system including a first particle bed and a second particle bed, in tandem; means to introduce a gas through the first bed and then through the second bed as a fluid stream having a vertical component in the regions occupied by the two beds to effect fluidization of the particles of the first particle bed and the particles of the second particle bed, said gas containing the particulate to be collected as entrained particulate therein, the first particle bed serving to collect particulate mostly in the supermicron range and the second particle bed serving to collect particulate mostly in the submicron range; means disposed between the first particle bed and the second particle bed to electrify that particulate remaining in the gas after passage through the first particle bed; and means to electrify the particles of the second particle bed to create an electrofluidized bed collector to collect particulate mostly in the submicron range.

8. A fluidized bed, particulate collection system as claimed in claim 7 wherein the bed particles are combustible particles.

9. A fluidized bed, particulate collection system as claimed in claim 7 wherein the bed particles are incombustible particles.

10. An electrofluidized bed particulate collection system that comprises, in combination: a bed of particles; means to effect fluidization of the bed particles using a gas from which said particulate is to be collected as an ash agglomerate upon the particles; means providing an electric field in the region occupied by the bed to electrify the bed particles; and means depositing a liquid film upon the bed particles, said liquid film serving to effect adherence of the particulate to the bed particles.

11. In a fluidized bed system operable to collect particulate from a fluidizing gas, particle bed means, means passing a fluidizing gas through the particle bed means to effect fluidization of the particles of the bed, and means introducing a liquid additive to said particles to promote adhesion of the particulate to the bed particles.

12. A fluidized bed system as claimed in claim 11 wherein said particles are combustible.

13. A fluidized bed system as claimed in claim 12 wherein said particles are incombustible.

14. A fluidized bed system as claimed in claim 11 that includes a treatment system, the bed particles with particulate adhered thereto to form, thereby, an agglomerate being removed from the fluidized bed and delivered to the treatment system to be processed therein and returned to the fluidized bed as bed particles.

15. A fluidized bed system as claimed in claim 14 wherein said treatment system is operable to fuse the agglomerate and crush the same, the crushed agglomerate being returned to the fluidized bed as bed particles.

16. A fluidized bed system as claimed in claim 14 wherein said treatment system is operable to crush the agglomerate, the crushed agglomerate being returned to the fluidized bed as bed particles

17. A fluidized bed system as claimed in claim 14 that includes means to electrify the bed particles to produce thereby an electrofluidized bed.

18. A method of collecting particulate, that comprises, forming a bed of particles, directing a gas containing said particulate entrained therein through the bed with a vertical component to fluidize said particles and provide a fluidized bed, and introducing a liquid into the bed region in the form of droplets, the droplets being collected upon the particles of the bed and effecting adherence of particulate collected on bed particles to the collecting particle.

JOINT

DECLARATION, POWER OF ATTORNEY, AND PETITION

We, James R. Melcher, Jeffrey C. Alexander and Karim Zahedi declare that we are citizens of United States of America residing at Lexington, Massachusetts and of United States of America residing at Somerville, Massachusetts and of Iran residing at Watertown, Massachusetts and of _____ residing at _____ respectively; that we have read the foregoing specification and claims and we verily believe we are the original, first, and joint inventors of the invention in Fluidized Bed Particulate Collectors

described and claimed therein; that we do not know and do not believe that this invention was ever known or used in the United States before our invention thereof; or patented or described in any printed publication in any country before our invention thereof, or more than one year prior to the date of this application; or in public use or on sale in the United States more than one year prior to the date of this application; that this invention has not been patented or made the subject of an inventor's certificate in any country foreign to the United States on an application filed by us or our legal representatives or assigns more than twelve months prior to the date of this application; and that no application for patent or inventor's certificate on this invention has been filed be us or our legal representatives or assigns in any country foreign to the United States, except as follows:

And we hereby appoint Arthur A. Smith, Jr., Registration No. 24,178, Room E19-722, Massachusetts Institute of Technology, Cambridge, Massachusetts 02139; Martin A. Santa, Registration No. 20,920, and Robert Shaw, Registration No. 20,440

our attorneys (or agent) to prosecute this application and to transact all business in the Patent Office connected therewith.

Wherefore we pray that Letters Patent be granted to us for the invention or discovery described and claimed in the foregoing specification and claims, and we hereby subscribe our names to the foregoing specification and claims, declaration, power of attorney, and this petition.

The undersigned petitioners declare further that all statements made herein of their own knowledge are true and that all statements made on information and belief are believed to be true; and further that these statements were made with the knowledge that willful false statements and the like so made are punishable by fine or imprisonment, or both, under section 1001 of Titled 18 of the United States Code and that such willful false statements may jeopardize the validity of the application or any patent issuing thereon.

Date: _____ Inventor _____

Post Office Address 29 Fairlawn Lane
Lexington, Massachusetts 02173

Date: _____ Inventor _____

Post Office Address 88 Beacon Street, Apartment 13
Somerville, Massachusetts 02143

Date: _____ Inventor _____

Post Office Address 805 Mt. Auburn Street, Apartment 44
Watertown, Massachusetts 02172

Date: _____ Inventor _____

Post Office Address _____

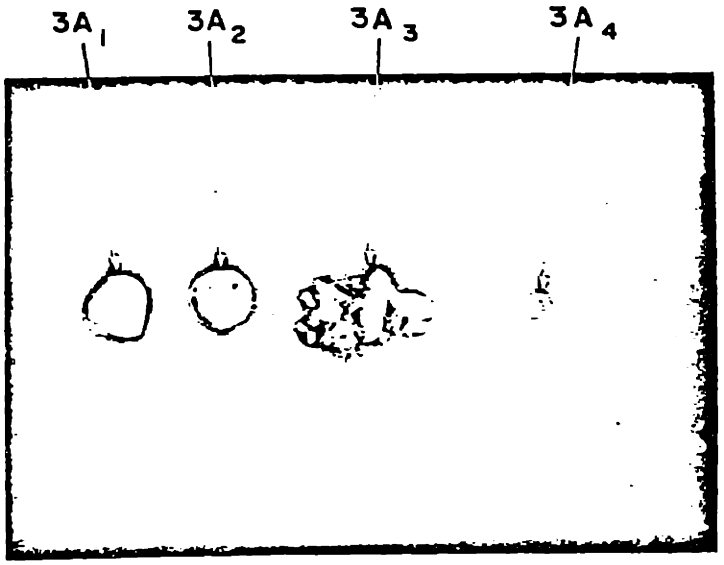
3A1
3A2
3A3
3A4

FIG. 6

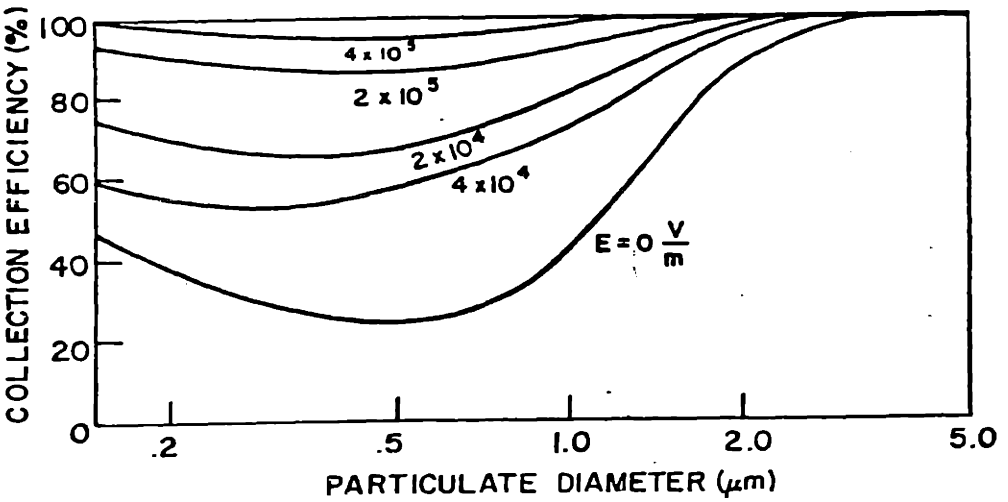
COLLECTION EFFICIENCY (%)
100
80
60
40
20
0
4 x 10^5
2 x 10^5
2 x 10^4
4 x 10^4
E = 0 V/m
.2
.5
1.0
2.0
5.0
PARTICULATE DIAMETER (μm)

FIG. 7

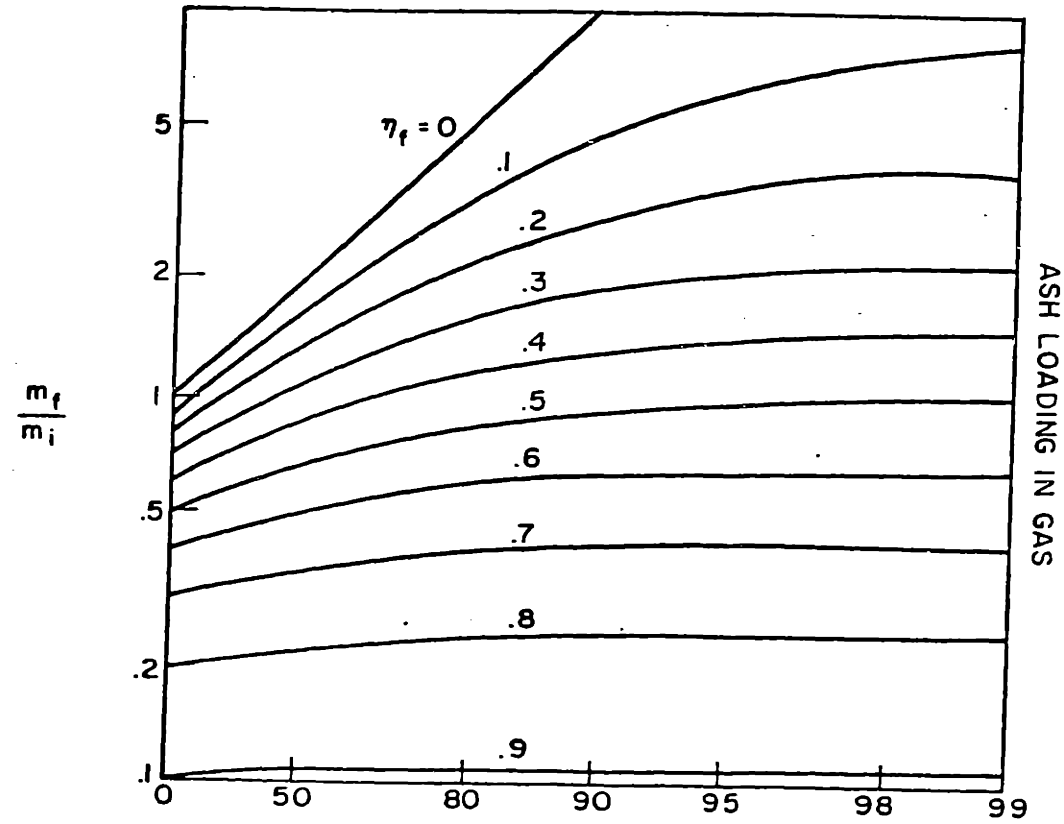
$\frac{m_f}{m_i}$
5
2
1
.5
.2
.1
$\eta_f = 0$
.1
.2
.3
.4
.5
.6
.7
.8
.9
0
50
80
90
95
98
99
η_b (%) EFB EFFICIENCY
ASH LOADING IN GAS

FIG. 4

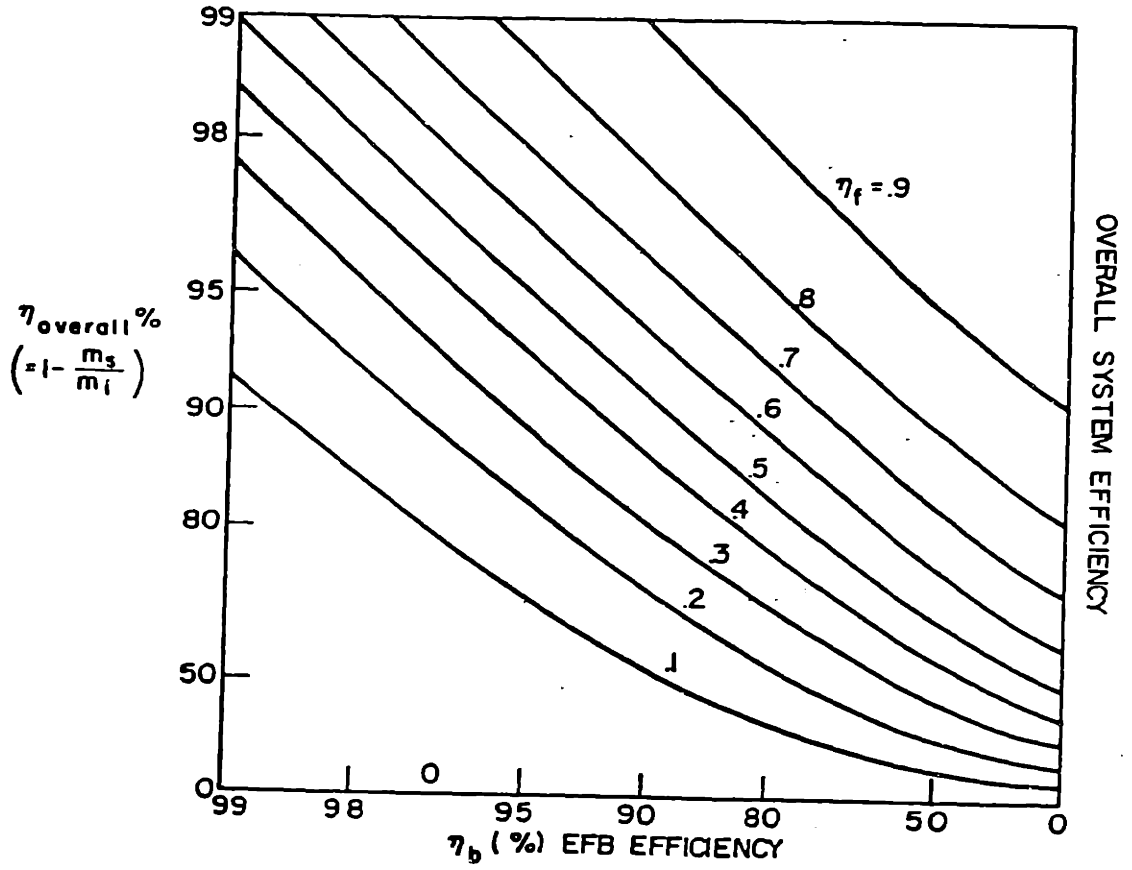
$\eta_{overall}$ %
$\left(=1-\frac{m_s}{m_i}\right)$
99
98
95
90
80
50
0
$\eta_f = .9$
.8
.7
.6
.5
.4
.3
.2
.1
0
99
98
95
90
80
50
0
η_b (%) EFB EFFICIENCY
OVERALL SYSTEM EFFICIENCY

FIG. 5

APPENDIX D

ELECTROFLUIDIZED BED AGGLOMERATOR

Abstract of the Disclosure

An electrofluidized bed agglomerator which serves to agglomerate submicron (and/or supermicron) particulates and a liquid, said liquid acting as a bond between particulates of the agglomerate thus formed to maintain the integrity thereof.

The present invention relates to agglomerators which serve to agglomerate particulates in the submicron and supermicron size ranges.

Attention is called to United States Letters Patents 3,755,122 (Melcher et al), 4,038,049 (Melcher et al), and 4,038,052 and an application for Letters Patent, S.N. 781,599, filed March 28, 1977 (Melcher et al).

The removal of submicron particulates from the effluent of stacks associated with coal burning and the like is an existing and increasingly important consideration in the energy-conscious world today. Although the system herein described is useful for removal as supermicron particulates, it makes its greatest contribution with regard to submicron size smoke, since the latter cannot economically now be removed by scrubbers, conventional precipitators and like systems--although supermicron smoke can. The present system provides a mechanism whereby particulates, submicron and supermicron in size, in the gaseous effluent from a combustion or other system, is combined or agglomerated to form an agglomerate which can be economically removed from the gaseous effluent by scrubbers, conventional precipitators and the like.

Accordingly, it is an object of the invention to provide a system to effect agglomeration of submicron particulates as well as a system to effect agglomeration of supermicron particulates.

Another object is to provide an agglomerate whose integrity is maintained so that collection thereof can be effected in conventional collectors or precipitators.

Another object is to provide a system of the foregoing type, which can be retrofitted into existing collection systems.

These and still further objects are addressed hereinafter.

The foregoing objects are achieved, generally, in a system for agglomerating particulates in a gas stream that further includes entrained liquid droplets. Means is provided for charging the particulates and the liquid droplets in the stream; and means is provided for moving the thusly charged particulates and liquid droplets in the gas stream through a bed of charged particles with a vertical component to fluidize the particles of the bed and create an electrofludized/bed, both

the particulates and the liquid droplets being collected upon the surface of the bed particles forming on said surface agglomerates of particulates with liquid bonds therebetween. The agglomerates eventually achieve a size at which the combined effects of collisions between particles and turbulent effect of the gas moving thereby serve to dislodge the agglomerates which entrain in the gas stream and are carried by the gas stream from the bed. The liquid serves as a bond between particulates of the agglomerates to maintain the integrity thereof upon leaving the bed. The flow rate of the gas stream, the amount of liquid and an applied electric field serve to control the size of the agglomerates thus formed.

The invention is hereinafter described with reference to the accompanying drawing in which:

Fig. 1 is a diagrammatic representation of a system that includes an agglomerator adapted to agglomerate particulates such as fly ash and the like in a fluidized particle bed;

Fig. 2 is a visualization of the collection of particulates (greatly enlarged) upon a single-bed particle (greatly enlarged) to form agglomerates and the entrainment of the agglomerates (greatly enlarged) from the bed particle;

Fig. 3 is a plot of experimental results showing the elsewhere defined bed adhesion efficiency vs. the elsewhere defined adhesion parameter;

Fig. 4 is a plot of experimental results showing adhesion efficiency vs. particulate diameter for a fluidized bed collecting fly ash with varying amounts of No. 6 fuel oil additive, the bed being operated at room temperature and acting as a collector;

Fig. 5 is a plot of experimental results showing adhesion efficiency vs. particulate diameter for a fluidized bed agglomerating fly ash with varying amounts of No. 6 fuel oil additive, the bed being operated at 140°C and acting as an agglomerator;

Fig. 6 is a plot of experimental results showing submicron particulate removal efficiency by an electrofluidized bed of N. J. No. 2 sand with No. 6 fuel oil additive with applied electric field as a variable; and

Fig. 7 is a plot of experimental results showing submicron particulate removal efficiency by an electrofluidized bed of crushed bituminous coal with No. 6 fuel oil additive with applied electric field as a variable.

Before discussing the invention with reference to the figures, a few comments of a general nature are in order. The present inventors have found and disclose herein a novel mechanism for efficiently agglomerating particulates, especially submicron particulates, and for maintaining the integrity of the agglomerate thus formed. It is not merely sufficient for present purposes, as is clear in the explanation, merely to efficiently bring particulates together in the form of an agglomerate; it is necessary, as well, that the integrity of the agglomerate, thus formed, be maintained. Toward that end, the inventors provide liquid bonding between the particulates of the agglomerate. The particulate of interest is in and around the micrometer-size range (i.e., submicron and supermicron), and the liquid serves to bond particulate to particulate in the agglomerate. Throughout this explanation the term "particle" is used to denote the constituents of a bed or a fluidized bed and "particulate" is used to designate the solid constituents such as fly ash to be removed from a gaseous effluent. Whereas the particles are typically about two millimeters in average cross dimensions, the particulates are typically micrometers or less in cross dimensions.

Turning now to Fig. 1, there is shown at 101 an electrofluidized bed agglomerator system to effect agglomeration of particulates 1. The agglomerator or agglomerator portion of the system 101 is labeled 102. The function of the agglomerator 102 is to process the particulates 1 from a source 2 of fly ash or the like to form agglomerates 3 which can then be collected by a collector 4. A blower 5 serves to provide a controllable flow rate for the gas in the system 101.

The agglomerator 102 includes a bed 6 of particles 7. The bed particles 7 are electrified by screen-like electrodes 8A, 8B, 8C and 8D that are energized by a source of high voltage 9; the electric field in the region occupied by the bed is maintained sufficiently high to effect collisions of the particulates and the liquid droplets with the particles but sufficiently low that the bed particles are not frozen by virtue of the electric field effect and sufficiently low that the agglomerates, thus formed, can escape from the bed. (Typically $\sim$ 10 k-volts between, say, the electrode 8A and the electrode 8B which are spaced vertically from one another about 3 centimeters.) The lowermost electrode 8D acts also as a distributor plate which acts in concert with the

housing designated 10 to keep the particles 7 within the bed region 6. A rapper 17 is used to dislodge materials that adhere to the electrode 8D.

The agglomerator 102 can be retrofitted to existing systems wherein the source 1 may be the combustor of an electric power plant and the collector 4 a conventional Cottrel precipitator or a scrubber which, in the absence of agglomeration of submicron particulates, is not capable, within economic constraints of such systems, of removing submicron sizes of particulates. In Fig. 1 the arrow shown at A is intended to denote gas flow vertically upward. The entrained fly ash from the source 2 moves upward in housing 10 past a source 11 of liquid droplets in the form of a spray represented by the broken lines 12. The gas moves through the charging section labeled 15 as a gas stream in which the particulares 1 and liquid droplets 12 are entrained. The charging section can take various forms known from the arts of electrostatic precipitation. In the embodiment of Fig. 1 includes the charger shown /a center electrode 13, a wall electrode or electrodes 14 and a source of high voltage 18; the wall electrode might be circular (although not so shown in Fig. 16)so that the electric field marked E is a radial field in the region 15 within the circular cylindrical housing 10. or semi-insulating The thusly charged particulates 1 and insulating/liquid droplets 12 that emerge from the charging section 15 are moved in the gas stream into the bed 6 with a vertically upward component of gas flow (the gas flow is in fact vertically upward in Fig. 1) to fluidize the bed particles 7. While in or semi-insulating the bed region, the particulates 1 and the insulating/liquid droplets 12 are deposited upon the surface of the particles 7, as now explained with reference to Fig. 2 which shows greatly enlarged representations of a particle 7, etc.

In the region below the particle 7 in Fig. 2, there are shown particulates 1 and liquid droplets 12 which deposit on the bed particle 7, as shown, to form agglomerates. The motion of bed particles in a fluidized bed is somewhat similar to rapidly boiling water, that is, there is a great deal of turbulence within the bed and, hence, the bed particles collide with one another tending to dislodge the particulates and liquid from the surface thereof. As is explained in detail hereinafter with supporting experimental evidence, this happens mostly when the agglomerates reach some critical size corresponding to a critical adhesion parameter called S_{crit} hereinafter.

Thus, eventually, the agglomerates achieve a size at which the combined effects of collisions between bed particles and the turbulent effect of the gas moving therethrough serve to dislodge them from the particle surface; the thusly dislodged agglomerates 3 in Fig. 2 are entrained in the gas stream and carried from the bed 6, as shown in Fig. 1. The agglomerates 3 consist of particulates and liquid, the liquid serving as a bond between particulates of the agglomerate to maintain the integrity thereof upon leaving the bed 6. The agglomerates which may be, say, 10 microns in average cross dimensions, can now be collected by a conventional collector. It will be appreciated on the basis of the foregoing explanation and what follows, that the size of the agglomerates 3 will be somewhat related to the flow rate of the gas stream and the quantity and type of liquid introduced into the stream. A more detailed explanation of the agglomerating process now follows.

An agglomerator, as above indicated, is a device which increases the size distribution of an aerosol without appreciably altering its total mass concentration. Most pollution control devices are more effective for larger sized particulates than for smaller sizes, thus agglomerators serve to improve the performance of other devices. Especially difficult to collect are submicron particulates. The electrofluidized bed has been demonstrated to collect submicron liquid particulates very efficiently (see said patent 4,038,049). With the addition of liquid additives it has been shown to also collect dry particulates (fly ash). Operating as an agglomerator, the electrofluidized bed collects particulates only as a transient followed by a steady-state in which the total mass leaving the bed is equal to the total mass entering it. Liquid additives are necessary to effect agglomeration, which takes place on a bed particle surface, but in quantities small enough that agglomerates retained in the bed reach a limiting size.

Fundamental to a determination of optimum liquid additive quantities is the present inventors' work on the adhesion of spheres to surfaces by liquid bridge forces under the dislodging action of impulsive types of forces. These impulsive forces impart an initial velocity U to a sphere simulating the particulate as it adheres to a flat surface (the bed particle); whether or not the sphere remains adhered to the surface depends on the inertia of the sphere (radius a, mass density ρ_p) and the viscosity η and thickness d of the liquid bridge. An adhesion parameter S was defined

$$S = \frac{U\rho_p a^{3/2}}{\eta d^{1/2}}$$

and its critical value, $S_{crit} = 0.7$, was discovered by fundamental experiments. For values of S greater than about S_{crit}, the sphere is dislodged, while it is not for values less than S_{crit}.

The electrofluidized bed agglomerator necessarily involves the collection of particulates and re-entrainment of such particulates in the form of agglomerates. A model of such a process predicts the collection efficiency of any one size bed particle to be

$$\eta(a) = \eta_{collection} \times \eta_{adhesion}$$

The agglomeration efficiency for any one size particulate is the product of the collection efficiency with adhesion assured $\eta_{collection}$, which depends on the parameters contributing to the bed efficiency when it is operated as a collector, and an adhesion efficiency which is the relation between the single bed particle collection and re-entrainment rates. The adhesion efficiency has been shown to correlate with the adhesion parameter, namely for $S > S_{crit}$, $\eta_{adhesion}$ is reduced.

Experiments were run in which fluidized beds of N.J. No. 2 sand, Bituminous coal (-7 + 14 mesh), and sintered fly ask (-7 + 14 mesh) collected re-dispersed fly ash (geometric mean diameter of 4.7 μm, geometric standard deviation 1.9) with an oil mist (Bunker "C" No. 6 fuel oil) added. Fractional efficiencies by particle size were measured by an Anderson 2000 cascade impactor. For very small quantities of oil additive (< 1% of the fly ash by mass) erratic results were obtained. For greater quantities of oil additive, the results are summarized in Fig. 3 hereof, where adhesion efficiency vs. adhesion parameter is plotted. The data represent a range of fluidization velocities typical for proposed application. Additive viscosity was changed by varying the temperature of the gas from room temperature to 140°C, which varies the viscosity by about an order of magnitude. As can be seen, for $S \lesssim 0.7$ adhesion is good while for $S \gtrsim 0.7$ it decreases. The parameter S correlates the critical condition for entrainment of agglomerates and not the adhesion efficiency for values of S exceeding this value.

These tests tend to support the basic model for adhesion of the particulates, which can then be used to design an agglomerator system. Additive quanitites should be chosen so that the adhesion parameter for the desired outlet mean particulate size is about 0.7. Particulates less than this size will tend to be converted to entrained agglomerates greater than this size. If too much additive is used, say an amount greater than that required to adhere the largest particulate sizes, the bed will act as a collector until bed particles reach sufficient dimensions to establish steady-state. This may imply defluidization. An agglomerator operates with zero overall collection efficiency, but it will have positive fractional efficiencies for the smaller sizes and negative fractional efficiencies for the larger sizes.

For the No. 6 fuel oil used, at room temperature, the beds acted principally as a collector for quantities of 2-4%, while at 140°C (when the viscosity is an order of magnitude less) they act as agglomerators. Fig. 4 shows adhesion efficiencies as a function of particulate size for beds at room temperature, with additive amount as a parameter. Fig. 5 shows the same

at 140°C. Measurement equipment sensitivity limits the results to the range 1.5 μm < 2a < 20 μm, but the effect of additive is clear.

Primary concern here is with the agglomeration of the submicron particulates. Before agglomeration can occur, the particulates must be transferred from the gas to the bed particle surface. For a supermicron particulate this can be done purely by mechanical collection mechanisms, but submicron particulate must be charged and then collected in a bed with either an imposed electric field or fields generated between bed particles by frictional electrification. Experiments were done in which just the submicron efficiencies were monitored. Re-dispersed fly ash was injected into the inlet gas stream along with an oil mist. Submicron concentrations were determined by passing a sample of the gas through a small cyclone with cut diameter of about 3 μm, then through several cascade impactor stages to remove all particulates greater than 1.1 μm in size. The gas then was run through a TSI mass monitor to determine the submicron concentration. The fly ash upon re-dispersal is highly charged; so no further charging is needed. Also, the beds, especially the sand beds, develop internal fields by frictional electrification. Still, the imposed field was varied.

Figs. 6 and 7 show the submicron collection efficiencies vs. oil additive quantities with applied field as a parameter for beds of N.J. No. 2 sand and crushed bituminous coal. These tests were done at 140°C. It can be seen that about a 2% additive of this oil is sufficient for very good submicron efficiency. Fig. 6 illustrates the frictional electrification of operation whereas Fig. 7 shows the imposed field mode.

It has been demonstrated for present purposes that electrofluidized beds can serve as effective agglomerators, especially in the submicron range. What is required is the transfer of the particulates to the bed particle surface, which is achieved by the electrofluidized bed high electrical collection performance and a liquid additive to promote adhesion between the particulates. Amounts of liquid additive are generally predicted by the adhesion parameter S based on fundamental models and experiments, but the complexity of the problem prevents exact specifications. Effective removal of submicron

particulates has been demonstrated with agglomeration to sizes greater than 10 μm.

The experimental work has focused on a scheme where the liquid additive is added to the system externally, but depending on the application, liquids may exist in the gas stream to be controlled and such processes may require no external additives.

Modifications of the invention herein disclosed will occur to persons skilled in the art and all such modifications are deemed to be within the scope of the invention as defined by the appended claims.

What is claimed is:

1. An electrofluidized bed agglomerator system to effect agglomeration of particulates and having, in combination: a bed of particles; means to provide an electric field in the region occupied by the bed to electrify the bed particles; a source of liquid in the form of insulating droplets; charging means to charge the particulate and the droplets; means directing a gas as a gas stream in which the particulates are entrained past said charging means to charge the particulates and then through the bed with a vertically upward component to fluidize the particles therein, said gas stream being directed, as well, past the source of liquid droplets so that said droplets being deposited upon the surface of bed particles forming on said surface agglomerates of particulates with liquid bonds therebetween, which agglomerates eventually achieve a size at which the combined effects of collisions between the bed particles and the turbulent effect of the gas moving thereby serve to dislodge the agglomerates carried by the gas stream from the bed, said liquid serving as a bond between the particulates of the agglomerates to maintain the integrity thereof upon leaving the bed.

2. Apparatus as claimed in claim 1 wherein the means to provide an electric field in the region occupied by the bed provides a field whose intensity is maintained sufficiently high to effect collisions of the particulates and liquid droplets with bed particles but sufficiently low that the bed particles are not frozen by virtue of electric field effect and sufficiently low that said agglomerates can escape from the bed.

3. Apparatus as claimed in claim 1 wherein the amount of liquid droplets introduced to the gas stream is sufficient to provide liquid bridges between particulates of the agglomerates but insufficient to allow the bed particles to build up to the point of defluidization.

4. Apparatus as claimed in claim 4 wherein adhesion between particulates by virtue of the liquid bridge therebetween is in accordance with an adhesion parameter S wherein

$$S = \frac{U\rho_p a^{3/2}}{\eta d^{1/2}}$$

wherein U denotes maximum initial velocity expected due to impulse forces upon an agglomerate formed in the system a is the cross dimension of the largest sized particulate to be agglomerated, η is the viscosity of the liquid, and d is the thickness of the liquid bridge between particulates.

5. Apparatus as claimed in claim 1 and that further includes means to collect the agglomerates.

6. Apparatus as claimed in claim 1 wherein the combination of bed thickness, amount of liquid introduced, the electric field in the bed and the flow rate through the bed are adjusted and maintained at levels at which the agglomerate sizes leaving the bed in a steady-state system operation are at a desired size range.

7. A method of agglomerating particulates in a gas stream that further includes entrained liquid droplets that comprises: charging the particulates and the liquid droplets in the stream; moving the thusly charged particulates and liquid droplets in the gas stream through a bed of particles with a vertical component to fluidize the particles of the bed and create a fluidized bed, both the particulates and the liquid droplets being deposited upon the surface of the bed particles forming on said surface agglomerates of particulates with liquid bonds therebetween, which agglomerates eventually achieve a size at which the combined effects of collisions between the particles and turbulent effect of the gas moving thereby serve to dislodge the agglomerates which entrain in the gas stream and are carried by the gas stream from the bed, said liquid serving as a bond between particulates of the agglomerates to maintain the integrity thereof upon leaving the bed.

8. Apparatus for agglomerating particulates in a gas stream that electrified particle bed means; further includes entrained liquid droplets, that comprises: /means for charging the particulates and the liquid droplets in the stream; means for moving the thusly charged particulates and liquid droplets in the gas stream, the through / bed of particles with a vertical component to fluidize the particles electrofluidized of the bed and create an / bed, both the particulates and the liquid droplets being deposited upon the surface of the bed particles forming on which said surface agglomerates /eventually achieve a size at which the combined effects of collisions between particles and turbulent effect of the gas moving thereby serve to dislodge the agglomerates which entrain in the gas stream and are carried by the gas stream from the bed, said liquid serving as a bond between particulates of the agglomerates to maintain the integrity thereof upon leaving the bed.

9. Apparatus as claimed in claim 8 wherein electrification of the particle bed means is effected by frictional electrification of the bed particles of the particle bed means.

10. Apparatus as claimed in claim 8 that includes electrodes and a source of high voltage connected thereto, said electrodes being appropriately placed to electrify the particles of the particle bed means.

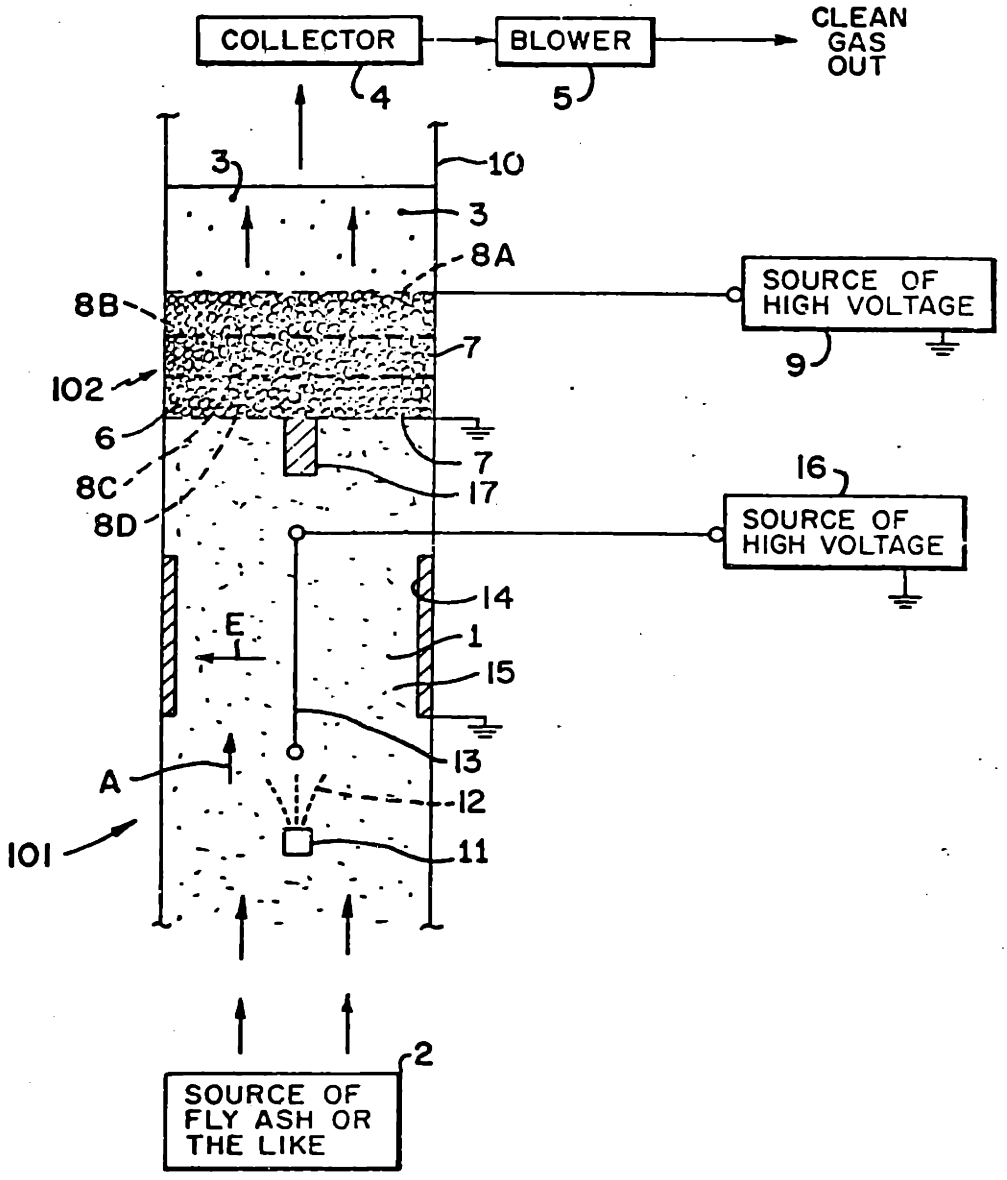
COLLECTOR
BLOWER
CLEAN GAS OUT
4
5
3
10
3
8A
8B
SOURCE OF HIGH VOLTAGE
9
7
102
6
7
8C
17
16
8D
SOURCE OF HIGH VOLTAGE
14
E
1
15
13
A
12
101
11
2
SOURCE OF FLY ASH OR THE LIKE

FIG. 1

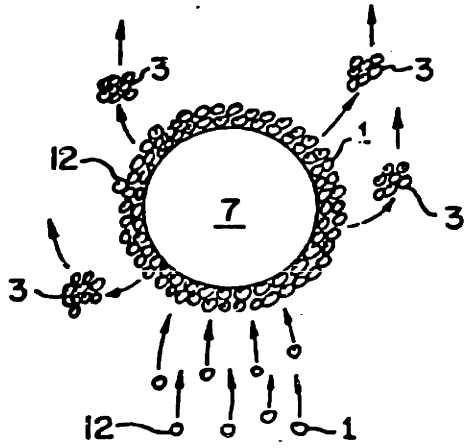
3
3
1
12
7
3
3
12
1

FIG. 2

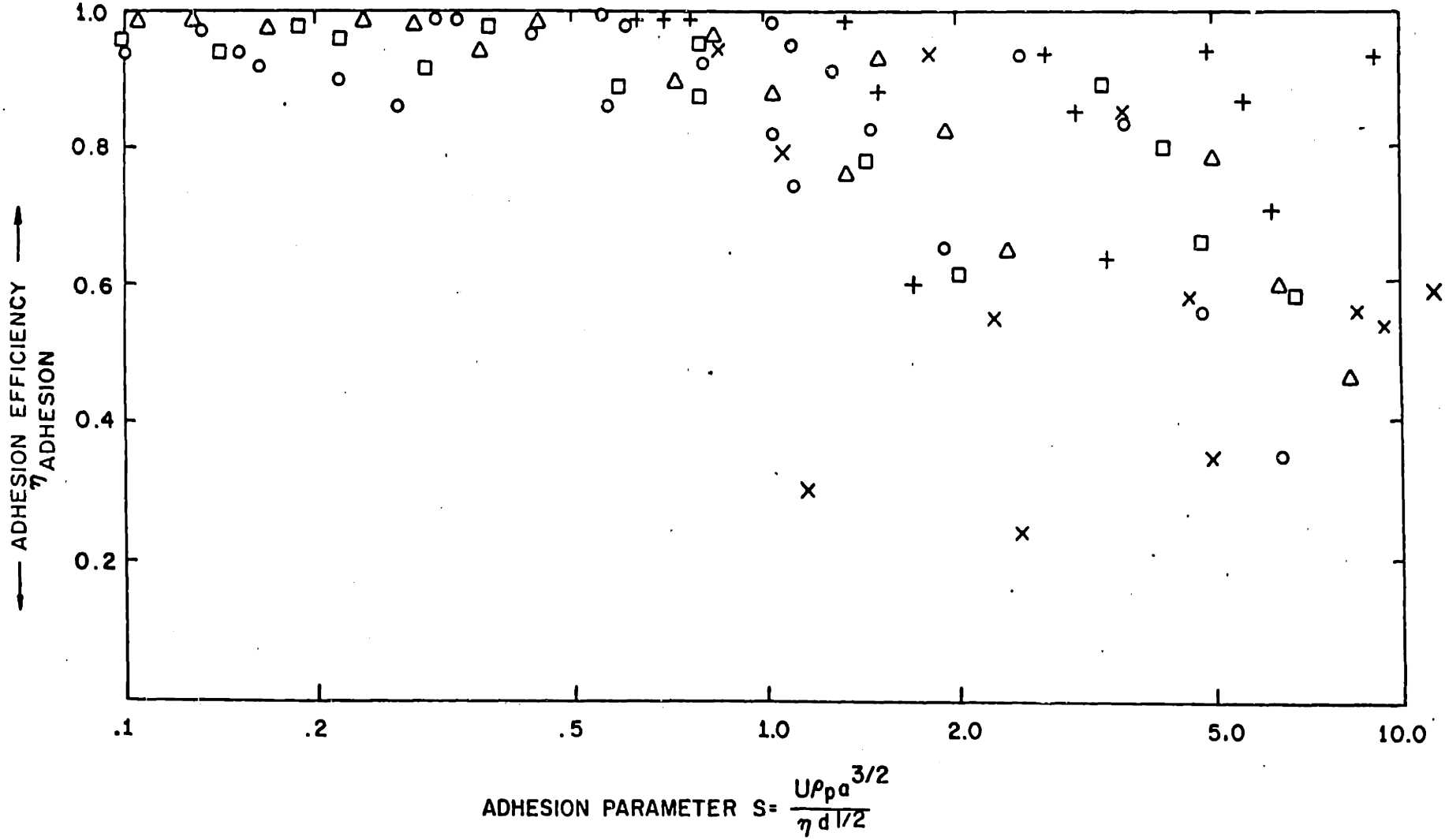
1.0
0.8
0.6
0.4
0.2
— ADHESION EFFICIENCY
$\eta_{ADHESION}$
.1
.2
.5
1.0
2.0
5.0
10.0
ADHESION PARAMETER $S = \frac{U\rho_p a^{3/2}}{\eta d^{1/2}}$

FIG. 3

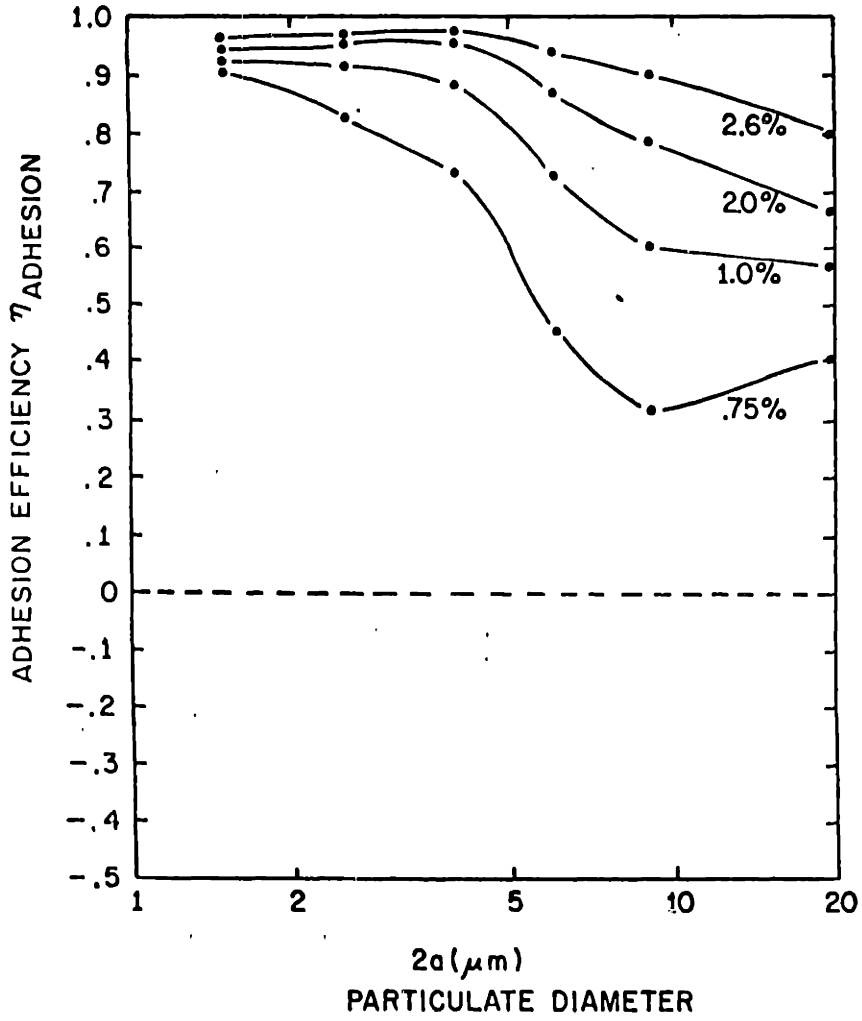
ADHESION EFFICIENCY $\eta_{ADHESION}$
1.0
.9
.8
.7
.6
.5
.4
.3
.2
.1
0
-.1
-.2
-.3
-.4
-.5
1
2
5
10
20
2.6%
2.0%
1.0%
.75%
2a(μm)
PARTICULATE DIAMETER

FIG. 4

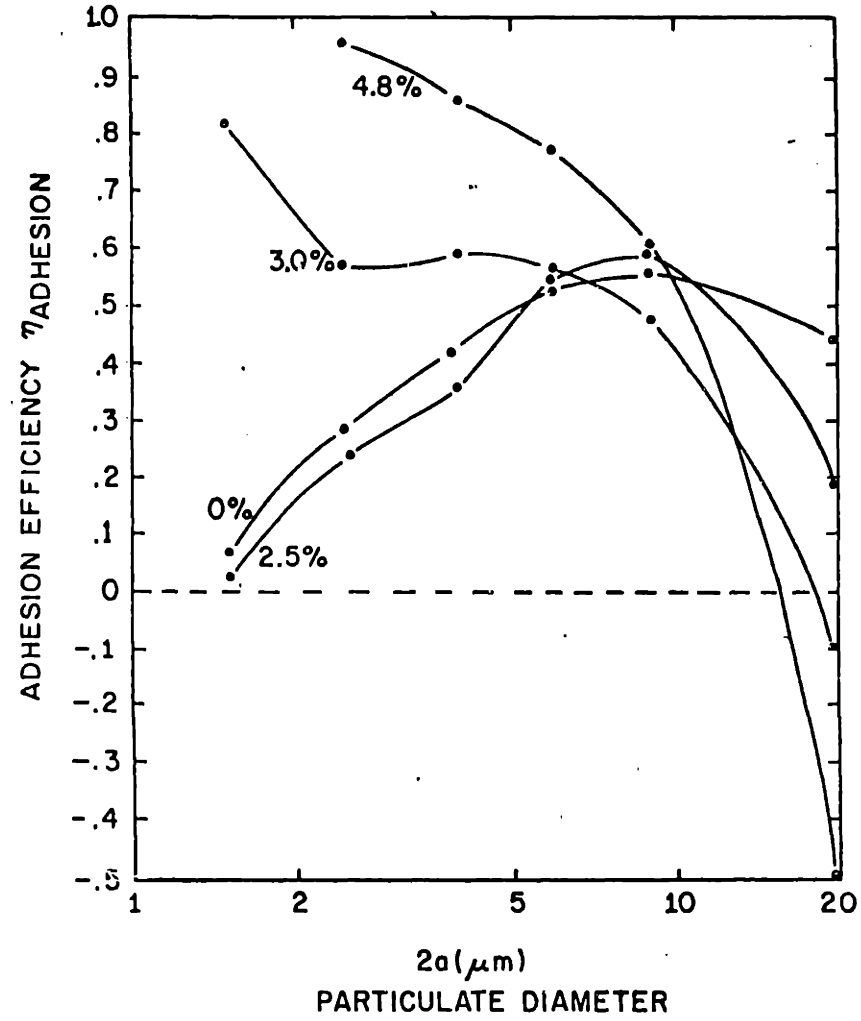
ADHESION EFFICIENCY $\eta_{ADHESION}$
1.0
.9
.8
.7
.6
.5
.4
.3
.2
.1
0
-.1
-.2
-.3
-.4
-.5
1
2
5
10
20
4.8%
3.0%
0%
2.5%
2a(μm)
PARTICULATE DIAMETER

FIG. 5

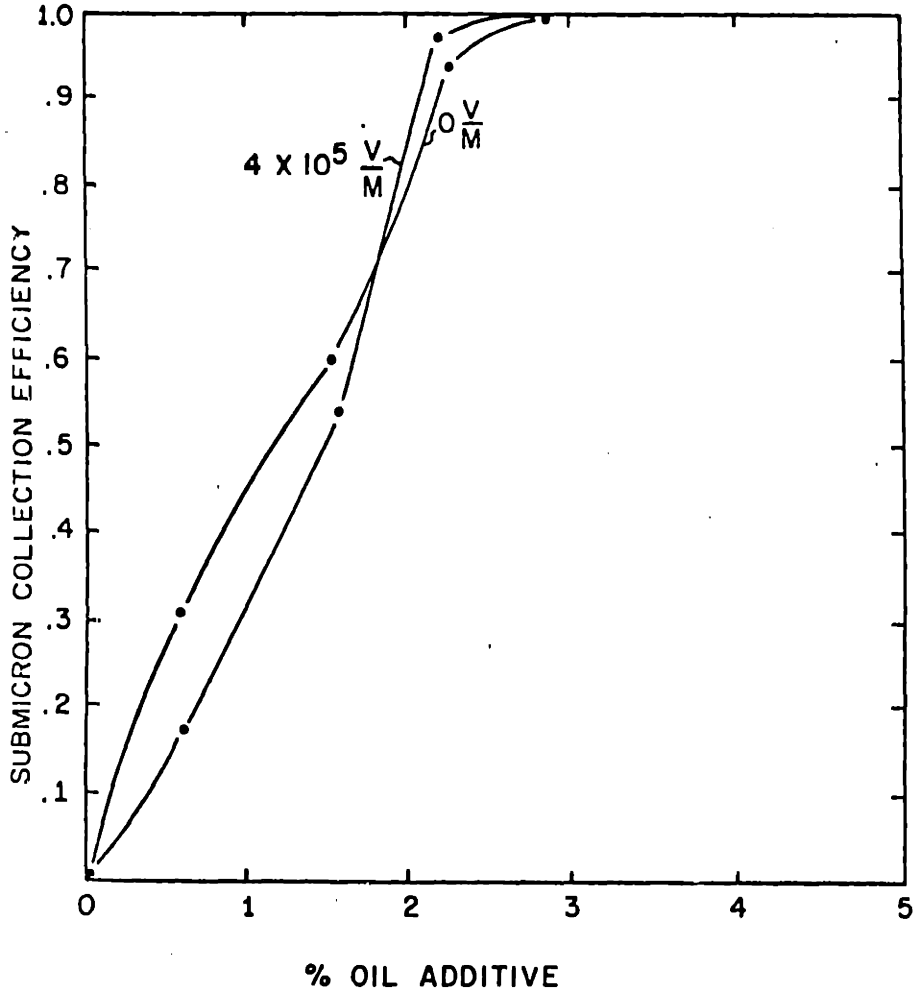
1.0
.9
.8
.7
.6
.5
.4
.3
.2
.1
SUBMICRON COLLECTION EFFICIENCY
4 X 10^5 V/M
0 V/M
0
1
2
3
4
5
% OIL ADDITIVE

FIG. 6

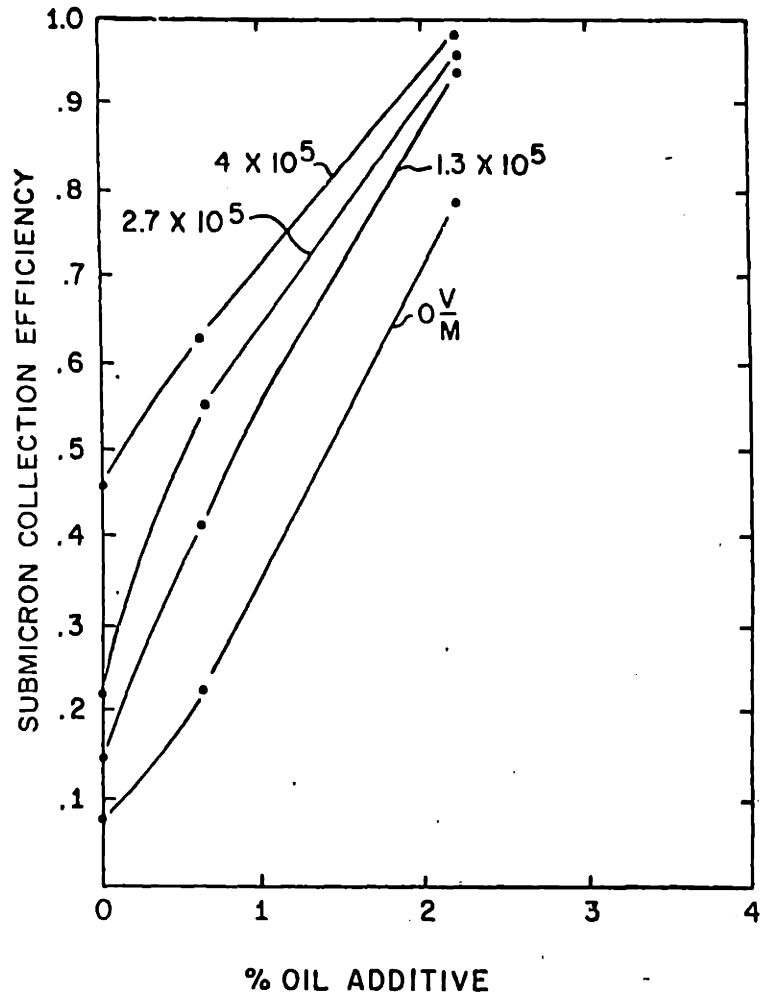
1.0
.9
.8
.7
.6
.5
.4
.3
.2
.1
SUBMICRON COLLECTION EFFICIENCY
4 X 10^5
1.3 X 10^5
2.7 X 10^5
0 V/M
0
1
2
3
4
% OIL ADDITIVE

FIG. 7

APPENDIX E

Mathematical Formalism for Description of Agglomerator Performance

We will now present a model for discussing the agglomeration phenomenon which was noted in the experiments of Chapter IV. It is shown here merely to provide a formalism for describing the performance of agglomerators and will be used in the concluding chapter's discussion and demonstration of fly ash agglomerators.

The derivations in the previous two section assumed that reentrained particulate was not agglomerates of smaller particulate. As a result, the steady-state collection and adhesion effeciencies are all well defined functions varying vetween 0 and 1. It is quite likely and has been shown that agglomeration does occur under suitable conditions. In this case, agglomerates of small particles can exit the fluidized bed collector and effectively act like larger particles. Thus the mass loading of a certain sized aerosol in the outlet gas can be greater than that in the inlet. Such a "negative" collection efficiency confuses the issues in the previous collection and reentrainment models. For these "agglomerator" systems we will now describe a formalism, the cumulative removal efficiency, which is more meaningful.

An agglomerator can be considered as a system where the total bed collection efficiency is zero. The usefulness of an agglomerator derives from its ability to alter the size distribution function of the inlet aerosol; usually for air pollution control, the desired shift is to larger particle sizes. The transition of a system from a collection (where $\eta_b \approx 1$) to an agglomerator (where $\eta_b \approx 0$) is not clearly defined and many transition states exist. The following formalism will provide a structure for distinguishing the two.

For particulate control devices it is convenient to describe performance in terms of removal efficiencies of particles. In general this takes the form of

$$\eta = 1 - \frac{m_f}{m_o} \qquad \text{E.1}$$

where m_f is a mass concentration leaving the system and m_o is a mass concentration entering the system. For polydisperse systems the mass is distributed over a range of a parameter describing the particulate, usually its size or radius. For systems acting as collectors, an overall mass removal efficiency is meaningful but not complete, as the collector may selectively remove certain sized particulate. A complete specification of outlet sizes and concentrations related to inlet dizes and concentrations is desired. This is especially true for systems acting as agglomerators where the total mass leaving the system is equalt to the total mass entering it.

For the following model we will assume that the collecting or agglomerating system is in the steady state, that is, any inlet particulate cannot be further subdivided into smaller sized constituents. This implies that for any given particulate size, the steady-state outlet mass concentration of particulate smaller than that size cannot exceed the same steady-state inlet mass concentration.

As a useful measure of system performance, we now define a removal efficiency H(a) for particles of radius less than a given radius a as being

$$H(a) = 1 - \frac{\int_0^a m_f \gamma_f(a')da'}{\int_0^a m_0 \gamma_i(a')da'} \tag{E.2}$$

where $\gamma_f(a')$ and $\gamma_i(a')$ are the usual normalized distribution functions. Because of the perfect dispersal assumption,

$$\int_0^a m_f \gamma_f(a')da' < \int_0^a m_0 \gamma_i(a')da' \tag{E.3}$$

and thus H(a) varies between

$$0 < H(a) < 1 \tag{E.4}$$

In this way H(a) is a measure of the performance of the collector/agglomerator system. The limiting value of H(a), that is, $H(a \to \infty)$ is just the overall mass collection efficiency of the system, as can be seen by taking the limit $a \to \infty$ of Eq. E.2:

$$H(a \to \infty) = 1 - \frac{m_f}{m_0} = \eta_b \tag{E.5}$$

For a system acting as a collector, this number is very important and should be very near 1. For effective agglomerator systems, this number can (and probably should) be very near 0. In this case it is the dependence of H(a) on a which is important, and its relationship to the inlet size distribution $\gamma_i(a)$.

In order to understand the cumulative removal efficiency and the characteristics of it which indicate the quality of the agglomerator it describes, it is useful to look at some examples of its use.

A cumulative removal efficiency function for a good agglomeration might look something like Fig. E.1. Simultaneously plotted is the inlet size distribution function. For small particulate radius a the cumulative removal efficiency H(a) is high, while as $a \to \infty$, $H(a) \to 0$, so there is no significant mass buildup in the system. a_{50} is defined as the radius at which 50% of the particulate smaller than a_{50} is removed from the gas, Eq. E.6. This radius roughly marks the transition of H(a) from high to low values. For a good agglomerator, a_{50} should be sufficiently greater than the inlet particulate mean radius $\bar{a}_i$ that a significant increase in mean size has occured.

$$H(a_{50}) = .5 = 1 - \frac{\int_0^{a_{50}} m_f \gamma_f(a')da'}{\int_0^{a_{50}} m_o \gamma_f(a')da'} \tag{E.6}$$

In general then, a good agglomerator defined as one where small particles are effectively agglomerated into larger particles is characterized by the following requirements:

(1) A monotonically decreasing H(a) - this insures that there are no "special" particle sizes which are not effectively agglomerated.

(2) For $a < a_{50}$, $H(a) = 1$ - this insures that the small particles are removed from the gas stream with a high removal efficiency.

(3) For $a \to \infty$, $H(a) \to 0$ - this insures that the overall collection efficiency of the system is zero, thus there is no build up of collected particulate.

(4) $a_{50} > \bar{a}_i$ - this insures that a significant partion of the inlet small particles have been agglomerated.

An interesting relationship is seen to result if a_{50} is much greater than the inlet mean radius $\bar{a}_i$. If $a_{50} >> \bar{a}_i$, then

$$\int_0^{a_{50}} \gamma_i(a')d(a') \simeq 1 \tag{E.7}$$

Then using Eq. (E.6) for a perfect agglomerator ($m_f = m_o$)

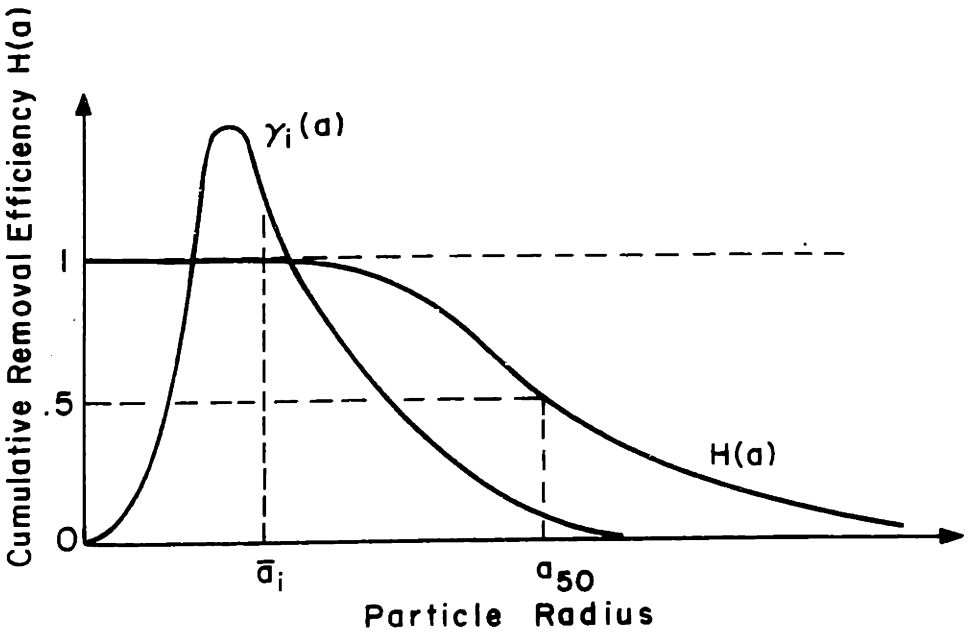

Figure E.1 Typical cumulative removal efficiency function and inlet size distribution.

$$\int_0^{a_{50}} \gamma_f(a')da' = .5 \quad \int_0^{a_{50}} \gamma_i(a')da' \cong .5 \tag{E.8}$$

Since, by definition

$$\int_0^{\bar{a}_o} \gamma_f(a')da' = .5 \tag{E.9}$$

then,

$$\bar{a}_f = a_{50} \tag{E.10}$$

Eq. E.10 is important since it states that for a good agglomerator ($a_{50} >> \bar{a}_i$) the cummulative removal efficiency is a good measure of the outlet size distribution mean.

Some theoretical special cases of inlet and outlet size distributions are now presented:

Case I Monodisperse inlet

Supporse we are dealing with a monodisperse inlet particulate. Then $\gamma_i(a) = u_o(a_m)$ where u_o is the usually defined impulse function and a_m is the particulate radius.

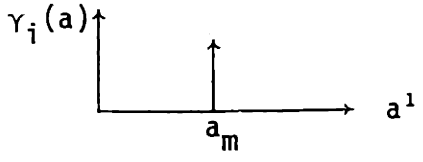

(Fig. E.2)

The outlet concentration will then in general, be $\gamma_f(a^1)$ with the condition that

$$\gamma_f(a^1) = 0 \quad \text{for } a^1 < a_m \tag{E.11}$$

It might look like this

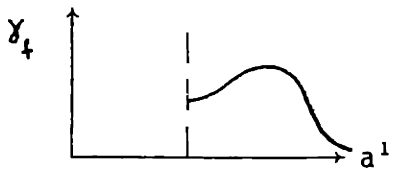

Fig E.2

H(a) is then

$$0 < a \leq a_m \quad H(a) \overset{\Delta}{=} 1 \tag{E.12}$$

$$a_m < a < \infty \quad H(a) = 1 - \int_{a_m}^{a} m_f \gamma_f(a^1)\, da = 1 - \int_{a_m}^{a} m_f \gamma_f(a^1) da^1$$

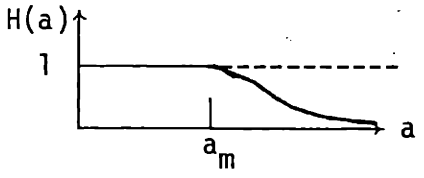

Fig. E.2

Note that H(a) may or may not go to zero depending on whether m_o is greater than or is equal to $\int_o^\infty m_f \gamma_f(a^1)\, da^1$.

H(a) was defined as being 1 for $a < a_m$ because $\gamma_i(a<a_m)=0$ and $\gamma_f(a<a_m)=0$, resulting in an ambiguous result if the formula for H(a) is strictly applied. Since there is no particulate in this size range either in the inles or the outlet, it really doesn't matter how we define it. Choosing the value 1 has esthetic advantages for comparison with other cases.

Case II Log Normal Distributions

This case is more realistic of actual situations which may be encountered. It is assumed that both the inlet and outlet size distributions are log normal. Most naturally formed aerosols (by condensation or grinding operations) have been found to be very closely log normal with some skewing in the tails of the distribution, thus the approximation is good for the inlet particulate. For similar reasons we might expect the outlet distribution to be log normal, but due to the complexities of the collection and

adhesion mechanisms no general statement can be made.

It is easiest to handle this case mathematically if we define

$$u = \log a \tag{E.13}$$

The log normal sized distributions are then

$$\gamma_i(u) = \frac{1}{\sqrt{2\pi}\,\delta_{ui}}\, e^{-(u - \bar{u}_i)^2/2\delta^2_{ui}} \tag{E.14}$$

$$\gamma_{o_f}(u) = \frac{1}{\sqrt{2\pi}\,\sigma_{u_{o_f}}}$$

where

$$\begin{aligned} \sigma_{ui} &= \log \sigma_{gi} \\ \sigma_{uof} &= \log \sigma_{gf} \\ \bar{u}_i &= \log \bar{a}_i \\ \bar{u}_f &= \log \bar{a}_f \end{aligned} \tag{E.15}$$

then

$$H(u) = 1 - \frac{\int_{-\infty}^{u} m_{o_f}\gamma_{o_f}(u')du'}{\int_{-\infty}^{u} m_o\gamma_i(u')du'} \tag{E.16}$$

For simplicity, let us analyze the case of a perfect agglomorator. ($m_o = m_i$) where the geometric standard deviations of the inlet and outlet distributions are the same.

$$\sigma_{ui} = \sigma_{u.f} \overset{\Delta}{=} \sigma_u \tag{E.17}$$

Figure E.4 is a normalized plot of the cummulative removal efficiency as a function of $\frac{u-\bar{u}_i}{\sigma_u}$ with $\frac{\bar{u}_d}{\sigma_u}$ as a parameter. $\frac{\bar{u}_d}{\sigma_u}$ is a measure of the size difference between the inlet and outlet size distributions as defined below and illustrated in figure E.4.

$$\bar{u}_d = \bar{u}_f - \bar{u}_i = \log \bar{a}_f - \log \bar{a}_{fi} \qquad (E.18)$$

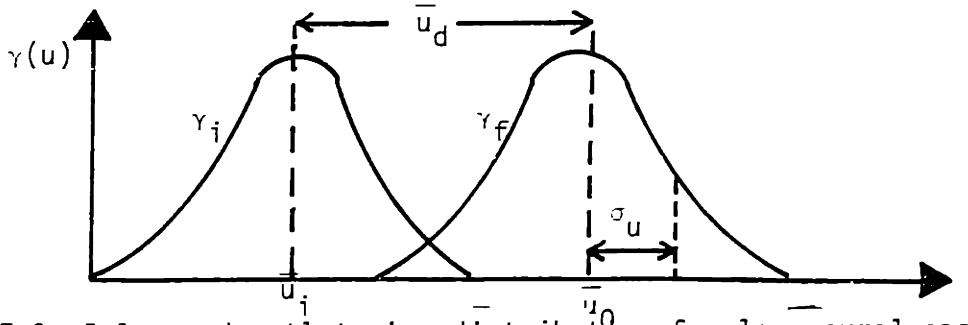

Fig. E.3 Inlet and outlet size distribution for log-normal case

This example shows how H(u) can be used as a good measure of agglomerator preformance. Several important features in H(u) are apparent.

(1) For all $\bar{u}_d$ (note $\bar{u}_d > 0$ by the perfect dispersal assumption) as $u \to \infty$, $H(u) \to 0$ according to the perfect agglomerator assumption.

(2) As $\bar{u}_f \geq \bar{u}_i$ ($\bar{u}_d \geq 0$) u_{50} ($=\log a_{50}$) $\tilde{=} \bar{u}_f$

(3) For good agglomerators, ($\frac{\bar{u}_d}{\sigma_u} > Z$) $H(u) \to 1$, for $\frac{u-\bar{u}_i}{\sigma_u} < 0$. This means that nearly all particles smaller than the inlet mean size are removed from the gas stream and re-entrained as larger agglomerates.

(4) As $\bar{u}_d \to 0$, (i.e., the system is not changing the particulate size distribution) $H(u) \to 0$ for all u.

Analysis of Fig. E.4 reveals how the criterion for good agglomerators is applied.

(1) For all $\bar{u}_d$, as $u \to \infty$, $H(u) \to 0$ according to the perfect agglomerator assumption. Further, all H(u) functions are monotomically decreasing with u.

(2) As $\bar{u}_f$ becomes much greater than $\bar{u}_i$ (or $\bar{u}_d >> 0$), then $u_{50} \tilde{=} \bar{u}_f$.

(3) For good agglomerators ($\frac{\bar{u}_d}{\sigma_u} \gtrsim 2$), $H(u) \rightarrow 1$ when $\frac{u-\bar{u}_i}{\sigma_u} < 0$. Thus, nearly all of the particles smaller than the inlet mean size are removed from the gas stream and re-entrained as larger agglomerates.

(4) As $\bar{u}_d \rightarrow 0$ (the system is becoming a poor agglomerator) than $H(u) \rightarrow 0$ for all u.

An interesting relationship results in this case when $\frac{\bar{u}_d}{\sigma_u} \gtrsim 2$ (or the system is a good agglomerator). In this case, when $\frac{u-\bar{u}_i}{\sigma_u} \gtrsim 2$

$$\int_{-\infty}^{u} \gamma_i(u')du' \approx 1 \tag{E.19}$$

then by Eq. (5.58)

$$H(u) \cong 1 - \int_{-\infty}^{u} \gamma_f(u')du' \tag{E.20}$$

and H(u) is a direct measure of $\gamma_f(u)$, the outlet size distribution.

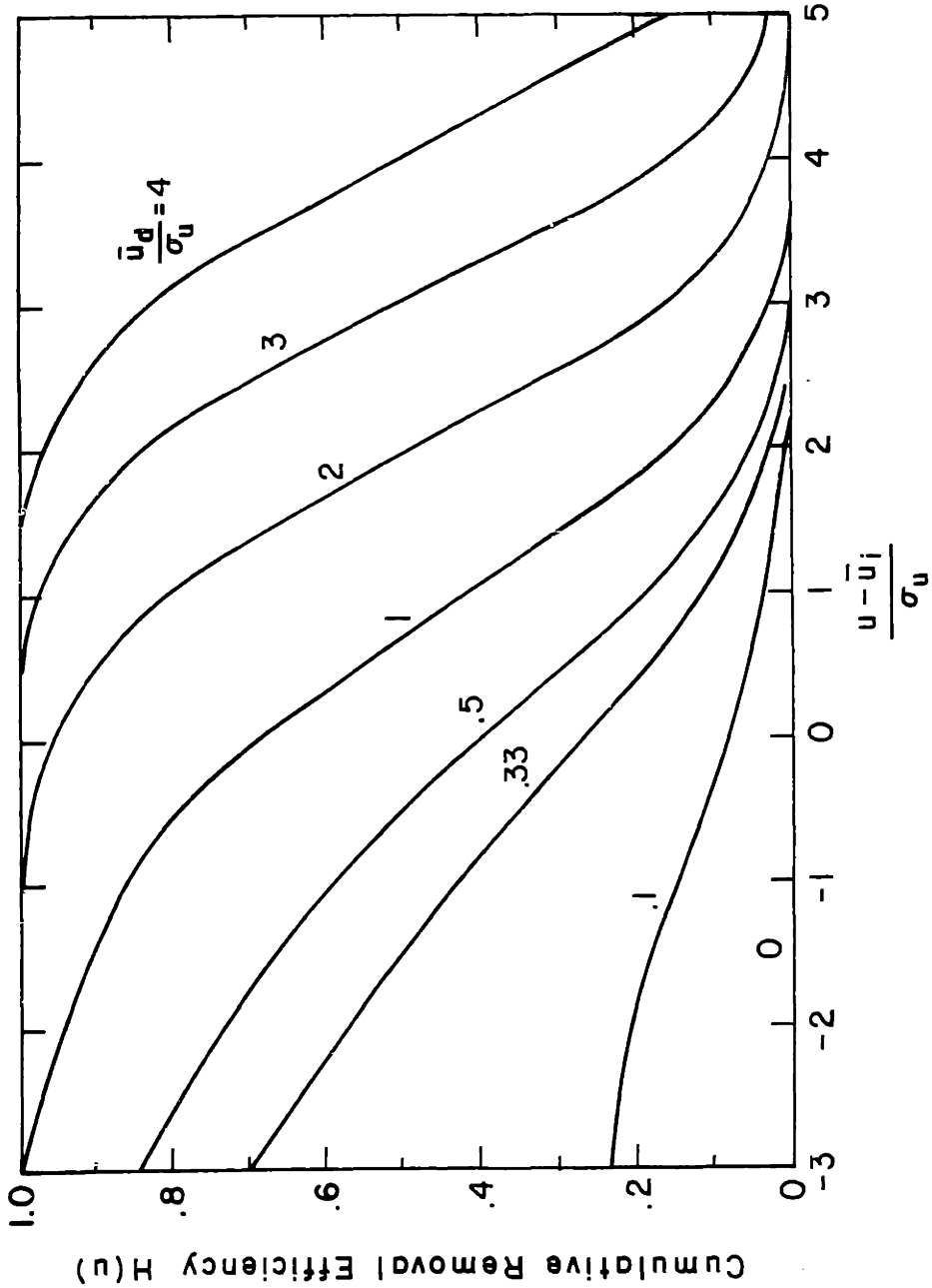

Figure E.4 Cumulative removal efficiencies for the log-normal case.

Biographical Note

The author was born in Skokie, Illinois on February 18, 1952. He graduated from Niles East High School in Skokie in 1970 and began his undergraduate education at MIT.

At MIT, he majored in Electrical Engineering and was elected to Eta Kappa Nu, Tau Beta Pi, and Sigma Xi honorary fraternities.

He began graduate studies at MIT in 1974 under the award of the Schlumberger Foundation Fellowship and received his M.S. degree in 1975 with a thesis entitled "Frequency Characteristics of Electrofluidized Beds in the Collection of Submicron Particulate." Also in 1975, he was awarded a National Science Foundation Energy Traineeship to carry on the research which is the topic of this thesis.

He is the author of the following papers:

"Excitation of Thin Elastic Membranes by Momentum of Laser Light" (with A.V. Nurmikko), Optics Communications,9,4,404 (1973).

"Alternating Field Electrofluidized Beds in the Collection of Submicron Aerosols" (with J.R. Melcher), I&EC Fundamentals,16,311 (1977).


OF FILM
REWIND